Flow beneath inland navigation vessels

Master Thesis

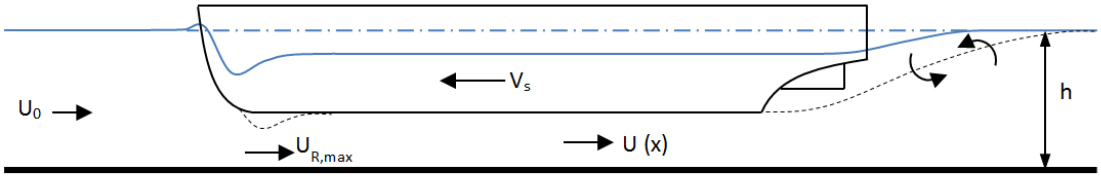

T. Robijns

Delft, 31 December 2014

Deltares
Enabling Delta Life

TU Delft Delft University of Technology

Final version

Delft, December 31, 2014

Author
Thijs Robijns

Master Thesis Committee

Prof.ir. T. Vellinga	Delft University of Technology, section Ports and Waterways
Ir. H.J. Verheij	Deltares & Delft University of Technology, section Ports and Waterways
Dr.ir. H.J. de Koning Gans	Delft University of Technology, section Maritime Engineering
Dr.ir. A. Sieben	Rijkswaterstaat

Preface

In front of you lies the final part of my master in Hydraulic Engineering at Delft University of Technology: my master thesis. The goal of this master thesis was to develop a model, which is able to predict flow velocities underneath sailing inland navigation vessels. After a year of hard work, it is finally finished.

Last year has been a turbulent year, and it has not always been easy. There were a lot of struggles, but I have pulled through. I must also admit, I had hoped to achieve more, and am not completely satisfied with the results. Although always more research can be done, at some point it is enough and time to let go. My knowledge has increased significantly in the last year, and I hope it will help me for the rest of my life.

During my thesis, a lot of people were actively involved in guiding, helping and teaching me. My thanks first of all go out to my committee members: prof. ir. T. Vellinga, ir. H.J. Verheij, dr. ir. H.J. de Koning Gans and dr. ir. A. Sieben. I want to thank you for your contributions, sharp comments, insights and guidance throughout this thesis. Especially to Henk Verheij, thanks for all the time you made available for me. I also would like to thank Marcel Busink and Marcel Grootenboer, without whom I could not have performed the experiments at Deltares.

Secondly, I would like to thank my parents. Thank you for the opportunity to study, for your everlasting support and your encouragements. Without your support I would not be standing here. Also many thanks go out to all of my friends, who have helped me through my struggles (both personal and professional) during this year, and kept believing in me, even when I did not. But above all I want to thank God, for His everlasting love, patience and guidance through the toughest times during this year, I dedicate my work to Him. Thank You Father!

Thijs Robijns

Delft, December 2014

Summary

Growing transportation rates and the subsequent growth in inland waterway transport have led to an increase in inland vessel sizes and draught. Due to the fluctuating water levels on rivers and these increasing draughts, the distance between the river bed and the ships are decreasing. Rijkswaterstaat wants to know the effects of sailing at these small underkeel clearances on river beds and ship manoeuvrability. In order to quantify these effects, more knowledge about the flow field beneath sailing vessels is required, as well as the effect of the flow field on erosion of bed material. The goal of this master thesis is to investigate these topics and develop a prediction model for the velocities underneath the keel.

Currently no methods exist to determine the flow field beneath vessels, only a few formulations for a single maximum velocity value are available, but these are not applicable at small underkeel clearances ($h / T < 1.25$). Also the effect on the river bed is fairly unknown.

To quantify the different effects of small underkeel clearances on the flow field physical model tests (with a length scale of 30) have been performed at Deltares. During these experiments a ship was towed through the flume, and flow velocities and pressures on the bed were measured, as well as forces on the ship. Additional experiments have been performed to investigate the effect on a moveable bed with different bed forms.

From the experiments, it was found that the most important parameters that influence the flow field beneath the keel are the bow shape and the underkeel clearance. Barge bows force more flow underneath the keel than conventional bows, and this results in higher bed velocities. Decreasing keel clearances also result in significantly higher velocities at the bed.

However, for very small underkeel clearances the boundary layer on the ship will interact with the boundary layer on the bed. This results in flow blockage underneath the keel. As a result, the flow needs to divert to the sides, and the velocities underneath the keel decrease. The diversion of the flow to the sides is also known as the fanning-out effect. This effect has definitely been proved by the measurements from the experiments. The effect (transverse velocities) increases with decreasing keel clearance (due to boundary layer interaction) and also increases with increasing ship widths.

During the experiments, erosion of bed material was clearly observed, and its effect increased with decreasing keel clearance. However, the underkeel clearance needs to be very small ($h /UKC < 1.1$) to give significant bed erosion. Due to the fanning-out effect and turbulence fluctuations, most sediment transport occurred immediately alongside the vessel, rather than underneath the keel. With bed forms such as dunes the erosion increased, due to erosion at the dune tops and deposition in the troughs (10 passages of a conventional vessel over a dune resulted in a decrease in dune height of 20%). For the removal of small shoals this might be interesting, although a small underkeel clearance is necessary. Barges are preferred over conventional vessels due to the higher velocities and increased turbulence intensity.

From the measured velocities during the physical model tests a model has been developed to predict the flow field underneath sailing inland navigation vessels. There are separate models for conventional vessels and for barges. The model is able to accurately predict maximum velocities (in sailing direction as well as in transverse direction), as well as a transverse velocity distribution. Compared to the previous prediction methods, the newly developed model is preferable. The results are more accurate, and the model is more extensive, due to the inclusion of transverse velocities and velocity distributions. More validation is required however, due to the lack of other data sets.

Contents

List of symbols

Latin characters

Symbol	Description	Unit
A_C	Cross-sectional area waterway	[m^2]
A_S	Cross-sectional area ship	[m^2]
A_τ	Mixing coefficient	[kg/ms]
a	Height weir crest	[m]
B	Width of waterway/flume	[m]
B_S	Beam width	[m]
C	Chèzy coefficient	[$m^{½}$/s]
C_B	Block coefficient	[-]
C_D	1. Resistance coefficient (for headwater height)	[-]
	2. Drag coefficient (on a sediment particle)	[-]
d_{50}	Median particle diameter	[m]
d_{90}	90-percentile diameter of sediment sample	[m]
Fr	Froude number	[-]
Fr_h	Froude depth number	[-]
g	Acceleration of gravity	[m/s^2]
h	1. Water depth	[m]
	2. Distance between walls (Couette flow)	[m]
h_0	Undisturbed water depth	[m]
h_k	Water depth above weir crest	[m]
k	Source term (Navier-Stokes equation)	[N/m]
k_s	Roughness height	[m]
L	Length	[m]
L_{PP}	Ship length (length between perpendiculars)	[m]
L_S	Ship length	[m]
n_X	Scale factor of parameter X	[-]
P	Perimeter	[m]
p	Pressure	[N/m^2]
Q	Discharge	[m^3/s]
R	Hydraulic radius	[m]
R^2	Coefficient of determination	[-]
$RMSE$	Root mean square error	[varying]
Re	Reynolds number	[-]
Re_H	Reynolds number for Couette flow	[-]
Re_x	Local Reynolds number	[-]
Re_*	Particle Reynolds number	[-]

Symbol	Description	Unit
r	Turbulence intensity	[-]
S_b	Squat (at bow)	[m]
s	Sediment transport rate (bed + suspended load)	[m^2/s]
s_b	Bed load transport rate	[m^2/s]
T	Draught of ship	[m]
T_{bow}	Draught at the bow (including headwater)	[m]
t	Time	[s]
U	Velocity of moving wall (Couette flow)	[m/s]
U_0	Ambient flow velocity	[m/s]
U_R	Return flow velocity	[m/s]
$U_{R,max}$	Maximum return flow velocity (underneath the keel)	[m/s]
U_{max}	Maximum absolute velocity underneath the keel	[m/s]
$U_{X,max}$	Maximum x-velocity (against sailing direction) underneath the keel	[m/s]
$U_{X,max}(y)$	Maximum x-velocity underneath the keel, dependent on transversal y-coordinate	[m/s]
$U_{X,bow,max}(y)$	Maximum x-velocity (in sailing direction) of velocity in front of bow, dependent on transversal y-coordinate	[m/s]
$U_{Y,max}$	Maximum y-velocity (perpendicular to sailing direction) underneath the keel	[m/s]
$U_{Y,max}(y)$	Maximum y-velocity underneath the keel, dependent on transversal y-coordinate	[m/s]
$U_{stern,max}$	Maximum x-velocity at the stern, just before the propellers	[m/s]
u	Flow velocity	[m/s]
$\bar{u}$	Mean velocity component	[m/s]
u'	Fluctuating velocity component	[m/s]
u_*	Shear velocity	[m/s]
$u_{*,cr}$	Critical shear velocity	[m/s]
UKC	Underkeel clearance	[m]
V_A	Absolute sailing speed ($V_S - U_0$)	[m/s]
V_{lim}	Ship limit velocity	[m/s]
V_S	Ship velocity	[m/s]
w_S	Fall velocity sediment particle	[m/s]
x	Distance from leading edge	[m]
z	Water level/ship drawdown	[m]

Greek characters

Symbol	Description	Unit
α	Ship's relative cross-sectional area (A_S / A_C)	[-]
β	Relative sailing speed (V_S / U_0)	[-]
γ	1. Bow shape coefficient	[-]
	2. Relative keel clearance	[-]
Δ	Relative density ($\rho_s - \rho_w$) / ρ_w	[-]
δ	1. Boundary layer thickness	[m]
	2. Relative draught (h / T)	[-]
ζ	Mid-ship shape coefficient	[-]
η	1. Headwater height	[m]
	2. Dynamic viscosity	[kg/ms]
θ	Mobility parameter (Shields number)	[-]
θ_{cr}	Critical mobility parameter	[-]
κ	Dimensionless keel clearance (while sailing)	[-]
κ_0	Non-sailing dimensionless keel clearance	[-]
μ	Contraction coefficient	[-]
ν	Kinematic viscosity	[m^2/s]
ξ_i	Energy loss coefficient	[-]
ρ_s	Specific weight sediment	[kg/m^3]
ρ_w	Density water	[kg/m^3]
τ	Shear stress	[N/m^2]
τ_b	Bed shear stress	[N/m^2]
$\tau_{pk,bow}$	Peak bed shear stress at bow	[N/m^2]
τ_v	Viscous shear stress	[N/m^2]
τ_t	Turbulent shear stress	[N/m^2]
∇	Water displacement	[m^3]

1. Introduction

1.1 Background

For many generations humans are using waterways, such as rivers and seas, for transportation of persons and goods. Since the Industrial Revolution the waterway network has been improved by the construction of canals, extending the reach of transport over water. For the Netherlands the main waterways are maintained and facilitated by Rijkswaterstaat.

Due to the ever growing world trade, also the transportation of goods over water has been growing in the last centuries, and even more in the last decades as a result of technological progress. This is especially true for intercontinental transport rates, in which the use of large sea-going vessels is essential, but it also applies to the inland transport rates.

For container transport at the Port of Rotterdam, the inland transport increased from 6.579.000 TEU (**T**wenty feet **E**quivalent **U**nit, standardized unit for container transport) in 2009 to 7.405.000 TEU in 2012, see Port of Rotterdam (2012). During this period, the growth of inland waterway transport increased from 2.200.000 TEU to 2.613.000 TEU, an increase of 18.7%. The modal split (distribution of transport volumes over the transport methods, such as water, rail and road) increased from 33.4% to 35.3% for inland waterway transport. The future task is to increase this percentage up to 45%.

With ever growing transport rates, also the size of vessels is increasing. For sea-going vessels this is not really a problem, due to the unrestricted nature of the waterway. Inland waterways however do have restricted dimensions, and therefore the growth of the vessel size is limited. The maximum length, width and draught of inland waterway vessels are determined by the dimensions of the navigation locks in the rivers and canals. For canals only an increase in draught or an increase in traffic intensity is leading to increased transport volumes. On open waterways (rivers), without locks, also the vessel size can increase.

The increased transportation has indeed led to larger vessel draughts in rivers. As a result, keel clearances between fairway beds and ships are decreasing. The question arises which keel clearance still guarantees a safe navigation. For the design of canals a waterdepth/draught ratio (h/T) of 1.4 is often applied, but for rivers such guidelines do not exist since it are natural systems with fluctuating discharges and water levels.

For the rivers Rijkswaterstaat usually guarantees a minimal navigable depth, and gives day-to-day information about the water levels. Shippers determine their load capacity based on this information. From an economical point of view, a larger draught results in larger transport volumes and therefore a larger profit. In fact, sometimes shippers load their ships lower than the least measured depth, and they navigate their ship through the river by avoiding the shoals. Nevertheless, this results in very small underkeel clearances, sometimes even smaller than 0.3 m.

Rijkswaterstaat, as the responsible authority for waterways, is concerned with the safety of navigation and the changes in waterway bathymetry. Since the river bed is dynamic and has different bedforms, the passing of a ship can change the bathymetry, especially at small underkeel clearances. On the other hand, bedforms can influence the manoeuvrability of the sailing vessels. The safety and manoeuvrability of navigation must be ensured and therefore Rijkswaterstaat wants to know what the interaction between the river bed and navigation is at these small underkeel clearances. The goal is to make substantiated guidelines for the maintenance of the fairways, and increase knowledge about safe ship maneuvering in these conditions.

This research will be done by Deltares, on behalf of Rijkswaterstaat, for the long-term program known as ‘Duurzame Vaarweg’ (‘Sustainable Fairways’). In order to understand the interaction between the dynamic riverbed and navigation, first the flow field between the ship’s keel and the

river bed needs to be determined, as well as the influence (erosion and deposition of sediments) of the flow field on the river bed. This master thesis will focus on this part of the research.

1.2 Problem description

Inland navigation vessels and their fairways have a complex relation in which they both influence one another. The size of the waterway (and locks) determines for instance the dimensions of ships, their sailing velocity and the traffic intensity. On the other hand, sailing vessels introduce water motions in the waterway, which in turn can affect the banks and bed of the waterway.

The most visible effects of the sailing vessels on the waterway are the water level drawdown with return flow and the ship waves. These water motions, as well as screw race, can erode the bed and banks of the waterway. Besides erosion, these water motions also influence other navigation. To predict these effects, many models have been developed to determine the return current and water level drawdown, from simple analytical models (for instance the method of Schijf or Bouwmeester) to advanced computer simulations (for instance FINEL2D or RAPID).

Despite the amount of available methods and models to determine flow circumstances around sailing vessels, it appears hardly any of them can predict flow velocities beneath a ship, i.e. between its hull and the river/canal bed. As a result, it proves difficult to predict velocities beneath vessels, and thereby the influence of the return current on erosion of the bed, especially at these small underkeel clearances.

Flow description

From previous researches with barge combinations (WL|Delft Hydraulics (1987), Maynord (1990), Rodriquez et al. (2002)) it is known that there is an increased return velocity beneath a sailing vessel just after passage of the bow, probably due to contraction of the flow lines by separation at the bow (this has not been proven yet), see Figure 1.

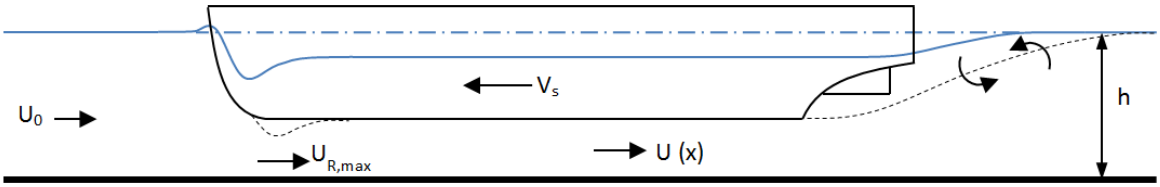

Figure 1: Flow field beneath a sailing ship

In a ship-based coordinate system, the water streaming to the bow will be diverted besides and beneath the ship. The fraction of the flow which passes under the bow is mainly determined by the bow shape and draught of the ship. Part of the water at the bow is forced down and will separate from the hull just after passing the bow. As a result, contraction will occur (comparable to flow under a weir) and the velocity will increase. This effect depends on the shape of the bow of the ship; more streamlined bows reduce the contraction. After the contraction at the bow, flow velocities will decrease and boundary layers on the ship and bed will start to develop. From bow to stern these boundary layers will grow in thickness, reducing the effective underkeel clearance, and consequently the velocities should increase or the discharge under the keel should decrease. The only way the discharge can decrease is if water is flowing away to the sides of the ship. This flow process is called fanning out. At the stern, the rotating propeller will induce an area of low pressure in front of the propeller. Therefore, the flow will be directed upward towards that area. Immediately after passage of the vessel the flow will be mainly determined by the influence of the propeller jet.

Figure 2 shows the vector plot of the measured velocities of a performed experiment, which clearly shows the fanning-out effect and the reduction of flow velocities due to boundary layer development.

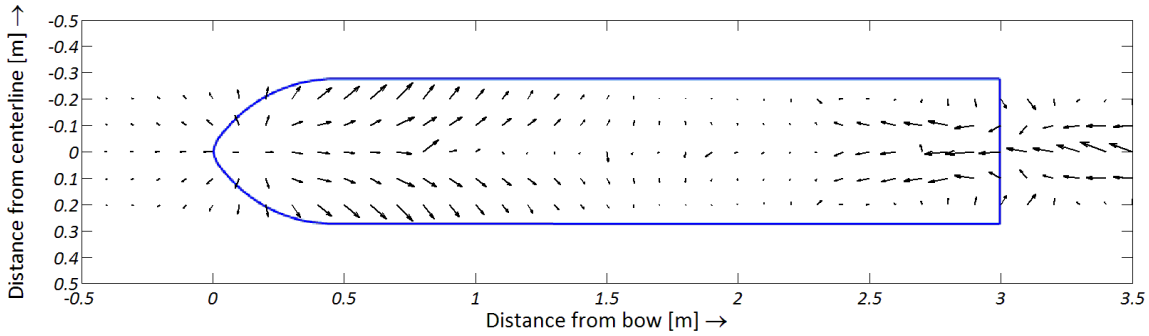

Figure 2: Vector plot of experiment 13

Previous research

Velocities

Previous research into the effects on the bed and flow underneath the keel of sailing vessels has been carried out by WL|Delft Hydraulics in 1986. During model tests they discovered that the maximum occurring return current on the bed ($U_{R,max}$) was situated under the vessel, immediately after passage of the bow. This resulted in a simple equation, based on the one-dimensional return current U_R, as calculated by Schijf, see equation [1.1].

$$U_{R,max} = (1.5 \text{ to } 2) \cdot U_R \qquad [1.1]$$

Later on, Stolker et al. (2006) suggested to change the coefficient into 1 to 5 times the return current, and recent investigations by Lenselink (2011) revealed a factor of 1.46 (although these velocities were not measured at the bed, but halfway between the bed and the ship's keel). So, although the equation is rather easy, the large spread severely reduces accuracy.

In 1990, Maynord did experiments to research the effects of sailing barges on the Mississippi. He found a different relation, based on the relative draught h/T and the relative channel blockage A_S/A_C. His equation is given in § 2.2.

Finally, three new methods have been developed by Stolker et al. (2006). They changed the equation of Maynord and introduced two new methods, all of which are given in § 2.2. Their research significantly improved the accuracy of the prediction of the maximum velocity underneath the keel.

However, all of the methods described above only apply to the maximum velocity, measured in the centerline of the vessel. This is not very strange, usually only the velocities here were measured, and mostly only velocities in the sailing direction were considered or measured. This single value does however not represent the entire flow field underneath the keel, and therefore more research and experiments are necessary to determine the entire flow field, so both velocities (in the sailing direction and normal to the sailing direction) and the distribution over the bed of these velocities. By studying the transverse velocities also the fanning-out effect can be investigated: the tendency of flow underneath the keel of a ship to divert to the sides. It is widely accepted that this occurs, but it has never been measured accurately.

Also the application range of the current prediction methods is limited. They are valid for h / T > 1.25, so not at the smallest underkeel clearances. It might be expected that at these small underkeel clearances the effect on the bed (possible erosion) will be greatest. This can also be seen in the experiments done by Bots (2011). Bots researched the possibility to use deep draught barges to dredge dunes in the river. He concluded that a decrease in keel clearance would lead to more erosion at the top of dunes, which indicates that the velocities (or turbulence) are increasing with smaller keel clearances.

Shear stresses

Besides research into flow velocities beneath ships, also research into shear stresses on the bed beneath sailing barges has been executed, for instance by Rodríguez et al. (2002). Their research

focused on determining the role of barges in resuspension of sediment. In model tests, one-dimensional shear stress sensors were used to measure shear stresses beneath sailing barges, both parallel and perpendicular to the sailing direction. This is much more effective for determining the erosion due to passage of a ship, since shear stresses can immediately be coupled to sediment transport, while this is more difficult for velocities.

The passage of a barge tow results in two regions with high shear stresses. The first region is associated with the bow of the vessel, and the other is located at the stern of the vessel, due to the propeller jet forces on the bed. For the bow, the shear stress distribution was approximately constant across the bow, while for the stern the peaks were located on the line of the propellers. For decreasing water depth, the magnitude of the shear stresses on the bottom increased (with same vessel draught). For a given depth, the upbound tests (sailing against the ambient flow) resulted in higher shear stresses than the downbound tests.

Scaling up of the model shows that shear stress in prototype situations can reach peak values of approximately 100 N/m^2. This sudden perturbation can entrain a lot of sediment. However, since the time period for this perturbation is very short, it might be expected that the entrained sediment will redeposit fast, preventing large bed scour. However, this research does indicate that shear stresses (and thus velocity gradients) are increased beneath sailing barges, especially when the keel clearance decreases. For the clearance of small shoals in the river this could be interesting.

Erosion

Only two experiments have ever been performed in which the erosion of the bed was measured after the passage of a vessel. They were performed by Lenselink (2011) and Bots (2011). They measured bed levels before and after passage of a (strongly simplified) vessel. They both concluded that the erosion was not very large. Bots estimated 5% of the dune top was eroded due to the passing of a vessel, and Lenselink concluded that the use of barges for the removal of shoals was not very effective. According to these experiments the effect of a passing vessel on the bed is limited.

However, their experiments were conducted with a relative draught (h/T) of 1.5, which is rather large. This means the effects at small underkeel clearances on erosion have not been studied. Since inland navigation vessels nowadays often sail very close to the bed (due to economic reasons or limited water depths), more insight into erosion at these small underkeel clearances is desirable.

1.3 Research objectives

As shown, it remains difficult to determine flow velocities beneath inland navigation vessels. Some simple formulae exist to calculate a maximum velocity, but the effect of this velocity on bed erosion remains unclear. Also these formulae only give a maximum velocity, rather than a complete flow field, which might be of importance for the erosion of bed material and ship manoeuvrability. As a result, more knowledge about the flow field between the river bed and the ship's hull is desirable.

Therefore, the goal of this research is **to develop an analytical model which is able to predict the flow velocities between the keel of an inland navigation vessel, sailing at small underkeel clearance, and the bed of the waterway.**

The research goal can be interpreted as developing a completely new model, or improving/extending the current models.

Research questions

Following from this research goal, the main research question will be:

What are the properties (direction and magnitude) of the flow field between the hull of an inland navigation vessel, sailing with small underkeel clearance, and the bottom of the waterway, and how does this affect the bed of the waterway?

From the main research question, the following (sub-) research questions are defined:

- What are the governing parameters that determine the flow beneath a sailing vessel?
- How do the governing parameters influence the flow field beneath a sailing vessel?
- On what properties does the fanning out effect depend, and how does it influence the flow field?
- What happens with the flow beneath vessels at very small underkeel clearances?
- What is the influence of the flow beneath sailing vessels on erosion of the bed?

Desired result

The desired result will be to have a practical (empirical) model (or formula) which can be used to compute flow velocities beneath sailing vessels, depending on the governing parameters.

If possible, the model will be presented in formulas which are usable for fast calculations, if necessary with for instance a script in Matlab. However, it is explicitly not the intention to create a numerical model to compute the flow beneath sailing vessels.

1.4 Research boundaries

The goal of this research is to investigate the flow beneath inland navigation vessels. Therefore, no research is done in the flow beside the sailing vessel (unless it was of importance for the flow beneath the vessel), and also not in the flow after the vessel passes. This is an important boundary, because in this zone the effect of the propeller jet becomes important, especially for sediment transports. The effect of the propeller is not taken into account.

Furthermore, the research into erosion/sedimentation patterns was only applied to non-cohesive sediments. Dependent on the location along a river, for instance the Waal, different sediment compositions can be found. Near Rotterdam river beds consist for a large part of cohesive sediments (clay/silt), while more upstream the sediment diameter increases and the sediment is mainly non-cohesive. In this research, only non-cohesive sediments were studied.

Also, the research specifically is about vessels sailing near the river bed, with a small underkeel clearance ($h/T < 1.4$). Sailing vessels with a larger underkeel clearance are not taken into account, since the interaction between the river bed and the ships is minimal in that case.

It might be good to point out that this master thesis was carried out in the framework of a larger project, which was done by Deltares for Rijkswaterstaat. However, the goal of this project is not the same as the objective of this thesis. The goal of the project is to gain more insight in the interaction between sailing vessels and river bedforms/banks, and study the effects of this interaction on ship movements and bed deformations, possibly leading to quicker and safer fairway maintenance. For more information about this project, reference is made to the work plan by Talmon et al. (2014). During this master thesis the physical experiments of this project were carried out and part of the data was used. Although a lot more data was gathered during the physical experiments (for instance on ship forces, and sailing above different river profiles), these aspects were not worked out in this thesis.

1.5 Approach

To realize the goal of this research, a good approach is necessary. For this research, the approach was divided into five phases, which are further elaborated in this chapter:

1. Literature research
2. Physical testing
3. Analysis of results

4. Model development
5. Model calibration and validation

Literature research

At first, all known relevant knowledge on topics important for this research was studied, during the literature research. The following topics were studied:

- Ship hydrodynamics: velocities occurring in return currents (Schijf, Bouwmeester), squat, results of previous experiments (WL|Delft Hydraulics, Maynord)
- Fluid dynamics: boundary layer theory (Schlichting) and Couette flow
- Sediment transport: bed erosion, initiation of motion (Shields)

Besides these main topics, literature on available datasets and scaling were also part of the literature research. The goal of this phase is to obtain all the available knowledge needed for this research.

Physical testing

For the research Deltares is performing for Rijkswaterstaat, about the interaction between navigation and the (dynamic) riverbed, physical model test were planned in the 'Water-Grond Goot' at Deltares. A model ship was towed through the flume, with a fixed underkeel clearance (no vertical movement possible), while pressure sensors and velocity meters measured the flow- and pressure field around the sailing ship. This happened for different configurations, with different water depths, underkeel clearances, ambient flow velocities and sailing velocities. During the experiments forces on the ship were measured, so the expected ship movements could be calculated later. Also experiments with a moveable bed (sediments) were done to see the effects of passing ships on the riverbed.

More information about the model tests can be found in Chapter 3.

Analysis of results

After the experiments, the results were analyzed. The aim was to find relations between the observed flow fields and the different parameters. This was done for all the parameters which had different values during the experiments. For simplicity the velocities are split up in longitudinal and perpendicular components (x and y directions) and analyzed separately.

Furthermore sedimentation/erosion patterns due to vessel passage are qualitatively analyzed, to describe to effect of vessel passage on a moveable bed.

Model development

From the analysis of the results and the literature research it was tried to develop a model that can predict flow velocities beneath sailing vessels. The aim was to develop an empirical model/formulation, comparable with the already existing formulas. This gives insight into the contribution of the different parameters on the flow field.

Model calibration and validation

Finally, both models need to be calibrated and validated. Calibration was done against the results of the physical model tests, while validation was done on the already existing datasets. Known existing datasets are:

- WL|Delft Hydraulics (1987)
- Maynord (1990)
- VBD (2003)

For more information on these datasets, see Stolker et al. (2006). Literature research was done to search for more useable datasets.

2. Literature study

This chapter covers the most important aspects of the studied literature for this research. Research has been done into ship hydrodynamics, fluid mechanics, sediment transport and previous experiments/prediction methods.

2.1 Ship hydrodynamics

An important dimensionless number for ship hydrodynamics is the Froude number (Fr), given by [2.1].

$$Fr = \frac{u}{\sqrt{g \cdot h}} \qquad [2.1]$$

In which: u = flow velocity [m/s] g = gravitational acceleration [m/s^2]
h = water depth [m]

The Froude number represents the ratio between the inertia of the water and the static weight of the water. It gives an indication for the type of flow (supercritical/subcritical), but is also very important for geometric equality of models. For representing flow conditions in models according to the flow in prototype, the Froude number should remain equal.

Ship characteristics

The main dimensions of ships are given in Figure 3.

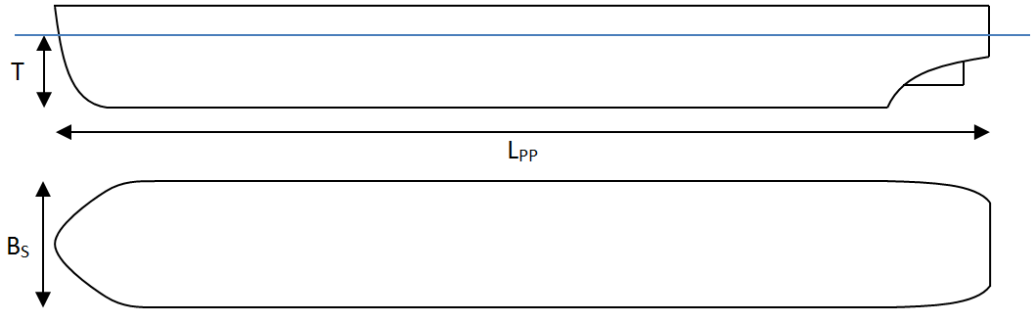

Figure 3: Ship dimensions

The volume of the water displaced by the ship is called the water displacement (∇), given by [2.2].

$$\nabla = C_B \cdot L_{PP} \cdot B_S \cdot T \qquad [2.2]$$

In which: C_B = block coefficient [-] L_{PP} = length between perpendiculars [m]
B_S = ship (beam) width [m] T = draught [m]

The block coefficient determines the slimness of the ship (the deviation of the volume of the ship from a rectangular box with dimensions L_{PP}, B_S and T). Another important parameter is the cross-sectional area of the ship (A_S), see [2.3]. The midkeel coefficient ζ gives the deviation of the largest cross-section of the ship from a rectangle (with dimensions B_S and T).

$$A_S = \zeta \cdot B_S \cdot T \qquad [2.3]$$

Ship-induced water movements

Ships sailing in canals or rivers generate water motions in these waterways. Generally, these water motions are divided in primary and secondary water movements. The primary water movements are

the motions related to the water displacement by the ship, so the water level depression and the return current, while the secondary water movements consist of the generated waves by the sailing ships. Besides these also propeller jets are a significant source of navigation induced water motions.

Primary water movements

The primary water movements can be divided in the water level depression and the return current. Very simplified one can state that the water volume at the bow of the vessel, where the vessel is headed, must flow back to the stern of the vessel, where the vessel is leaving. This creates a return flow alongside the vessel. Since flow velocities increase the velocity head ($u^2/2g$) will increase. With stating that energy must be preserved, the water level must be lowered in this area, resulting in water level drawdown.

Various methods have been developed to calculate these effects, from simple one-dimensional methods to advanced computer models, and from methods based on physics to purely empirical formulas. Here, the method of Schijf (based on energy conservation) and Bouwmeester (based on momentum conservation) are shortly discussed.

Method of Schijf

Schijf (1949) and Jansen et al. (1953) developed a method for determining the primary water movements based on preservation of energy. In his method, Schijf not only found expressions for water-level depression and return current, but he also found a natural limit sailing speed for self-propelled vessels. In his method, the limit speed is reached when the accompanying return current becomes critical, i.e. Fr = 1. If the vessel speed would increase further, the water movement next to the ship will become supercritical, leading to a strong decrease in water depth and, as a result, an increase in flow velocity. As a result, water will accumulate in front of the bow, and self-propelled ships are not able to overcome this accumulation. Even if the vessel has enough power to overcome this accumulation, it would be uneconomic to sail at such speeds, due to very high fuel consumption.

The method is based on preservation of energy (theorem of Bernoulli) and continuity (mass conservation). Applying these, in a ship-fixed co-ordinate system (axis moving along with the ship), between an undisturbed cross-section without ship (subscript 0) and the cross-section in the middle of the ship, results in equations [2.4] and [2.5] respectively (also see Figure 4).

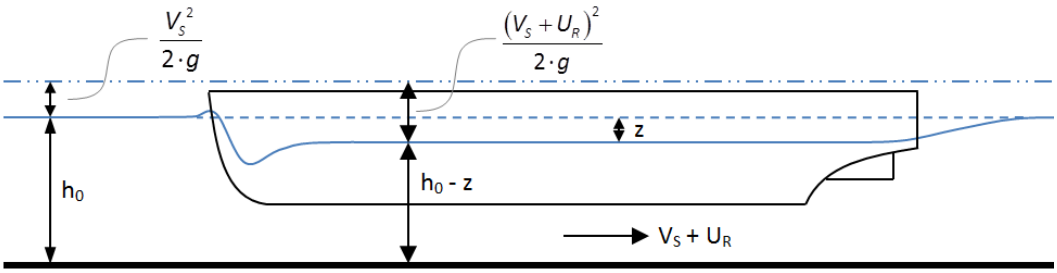

Figure 4: Method of Schijf

$$h_0 + \frac{(V_S - U_0)^2}{2 \cdot g} = (h_0 - z) + \frac{(V_S - U_0 + U_R)^2}{2 \cdot g} \qquad [2.4]$$

$$Q = (V_S - U_0) \cdot A_C = (V_S - U_0 + U_R) \cdot (A_C - A_S - B \cdot z) \qquad [2.5]$$

In which:

Q	=	discharge	[m^3/s]	V_S	=	sailing velocity	[m/s]
U_0	=	ambient flow velocity	[m/s]	U_R	=	return current	[m/s]
A_C	=	channel cross-sectional area	[m^2]	A_S	=	ship cross-sectional area	[m^2]
h_0	=	undisturbed water depth	[m]	z	=	water level depression	[m]

Combining these equations, applying Fr = 1 and rearranging results in a formula for the limit speed V_{lim} (which can be found by iteration of equation [2.6]).

$$1-\frac{A_S}{A_C}+\frac{1}{2}\cdot\left(\frac{V_{\lim}}{\sqrt{g\cdot h}}\right)^2-\frac{3}{2}\cdot\left(\frac{V_{\lim}}{\sqrt{g\cdot h}}\right)^{2/3}=0 \qquad [2.6]$$

Subsequently the solutions for the return current and water level depression are found (equations [2.7] and [2.8]), which also need to be solved iteratively.

$$\frac{\alpha\cdot\left(V_S-U_0+U_R\right)^2-\left(V_S-U_0\right)^2}{2\cdot g\cdot h}-\frac{U_R}{\left(V_S-U_0\right)+U_R}+\frac{A_S}{A_C}=0 \qquad [2.7]$$

$$z=\alpha\cdot\frac{\left(V_S-U_0+U_R\right)^2}{2\cdot g}-\frac{\left(V_S-U_0\right)^2}{2\cdot g} \qquad [2.8]$$

In equations [2.7] and [2.8], α is a correction factor for the non-uniform distribution of the return current and water level depression over the channel, based on measurements done by Delft Hydraulics in 1953. The factor can be found by applying equation [2.9].

$$\alpha=1.4-0.4\cdot\frac{V_S}{V_{\lim}} \qquad [2.9]$$

Besides these formulations, dimensionless forms are formulated by Schijf in order to develop diagrams, in which the limit speed, return current and water level depression can be estimated graphically. More detailed derivations, as well as made assumptions can be found in Schijf (1949), Schijf et al. (1953) or Verheij et al. (2008).

Method of Bouwmeester

In 1977, Bouwmeester et al. (1977) developed a new method for determining the water-level depression and the return current around sailing vessels. His method is based on the preservation of momentum, in which the forces acting on the vessel are in equilibrium with the momentum of the flow. Full formulations, derivations and assumptions can be found in Bouwmeester et al. (1977) or Verheij et al. (2008). Although the method gives good results, it is less frequently used than the method of Schijf.

For determining the hydrostatic pressure force on the ship at the bow, an equation for the generated headwater (η) at the bow is derived from experiments. It can be calculated by equations [2.10] and [2.11]. These equations are used later on to determine the maximal draught during the experiments.

$$\eta=C_D\cdot\frac{\left(V_S-U_0\right)}{2\cdot g} \qquad [2.10]$$

$$C_D=\gamma\cdot\left(\frac{T}{h}\right)^2 \qquad [2.11]$$

In which: C_D = resistance coefficient [-] γ = shape coefficient (here set to 1) [-]

Propeller jets

Besides the primary and secondary water movements, the propulsion system of a ship also induces important water motions in the channel. Most (modern) inland navigation ships have at least two types of propulsion systems: main propeller(s), responsible for the forward thrust, and bow and/or stern thruster(s), mainly for the manoeuvrability of the vessel. These propeller jets can induce very large flow velocities, which can result in severe bed erosion, especially with a limited distance between the bed and the propeller. Although the effect of propellers and thrusters is beyond the scope of this research, it is important to remember their possible influence on the flow field and bed erosion. More information on outflow velocities and distribution can be found in Verheij et al. (2008), and information about erosion by propulsion systems can be found in Schiereck et al. (2012).

Ship motions

Moving vessels do not only induce water motions, the water (and wind) also induces ship motions. Different loads like wind gusts, waves and currents result in different movements of the ship. Even the ship-induced water motions cause related ship motions. Dependent on the type of load, the ship can translate (move) and/or rotate in a certain direction. The translations and rotations can happen in three directions: longitudinal, transversal and vertical to the ship's original position. This means there are six degrees of freedom. The most important ship motion is called squat, a combination of longitudinal rotation and vertical translation. Other ship motions are unimportant for this research.

Squat

Due to the water level drawdown around the ship and since the water displacement of the ship should remain equal (law of Archimedes), the ship experiences a sinkage. However, the sinkage may be somewhat larger at one end (bow or stern) of the ship. Then the vessel is tilting a little bit in longitudinal direction, which is called trim. The combined action of sinkage and trim of the vessel is called squat. Squat is important for determining the underkeel clearance (distance between the ship's hull and the bed) and can cause grounding of deep draught ships in shallow water.

In one-dimensional primary water movement methods such as Schijf and Bouwmeester, the squat is assumed to be equal to the water level drawdown. Although this gives a relatively good first approximation of the sinkage, it disregards the effects of trim and the three-dimensional nature of the water level drawdown. Therefore, other methods have been developed to predict sinkage and trim or maximum squat (at bow or stern), based on empirical relations and/or based on physics. An overview of the available methods and their restrictions is given by PIANC (1997). Based on the overview, the most suitable methods for restricted waterways are Barrass II, Huuska/Guliev and Romisch. Accuracy investigations by Blaauw et al. (1983) and Ijsebaert (2010) revealed that the method of Huuska/Guliev is preferred.

Huuska/Guliev

The method of Huuska/Guliev, developed in 1976, is based on the fundamental slender body theory of Tuck. It was originally a method by Huuska, but is has been extended to be suitable for canals by using investigations of Guliev. It is given by equation [2.12].

$$S_b = 2.4 \frac{\nabla}{L_{pp}^{\ 2}} \frac{Fr_h^{\ 2}}{\sqrt{1 - Fr_h^{\ 2}}} \left(7.45 \left(\frac{A_S}{A_C} \right) + 0.76 \right) \qquad [2.12]$$

In which:

S_b	=	squat at bow	[m]	Fr_h	=	depth Froude number	[-]
∇	=	water displacement	[m^3]	L_{PP}	=	length between perpendiculars	[m]
A_C	=	channel cross-sectional area	[m^2]	A_S	=	ship cross-sectional area	[m^2]

This method is applicable for $1.1 \leq \frac{h}{T} \leq 2.0$ and $Fr_h \leq 0.7$, in which Fr_h is given by [2.13].

$$Fr_h = \frac{V_S - U_0}{\sqrt{gh}} \qquad [2.13]$$

The formulations of Barrass II and Romisch can be found in PIANC (1997).

Some remarks on these methods have to be made: it is important to realize that none of these methods calculate trim and sinkage separately, but rather calculate the maximum squat or the squat at the bow. In unrestricted waterways the squat at the bow is usually larger than the squat at the stern. However, in very narrow waterways with large block coefficients the maximum squat may occur at the stern. This may very well be the case in inland waterways.

Besides these relative simple formulations, nowadays even more complex squat prediction methods exist (for instance Ankudinov, see Lenselink (2011)), as well as advanced computermodels capable of predicting squat for sailing vessels. For this research however, squat is of minor importance and therefore these simple models will suffice.

2.2 Flow beneath ship's hull

Although many methods exist to predict return flow velocities and water level drawdown around the ship, only a few methods exist to calculate the flow between the hull of the ship and the bottom of the waterway. One-dimensional approaches such as Schijf and Bouwmeester assume a uniform return flow velocity in the waterway cross-section. This would imply the velocity beneath the vessel is equal to the velocity besides the ship. In reality however, return flow is highly three-dimensional, and will be affected by hull shape, waterway dimensions, boundary layers (on ship, bed and banks), ship dimensions, etcetera. Although it is almost impossible to incorporate all these aspects, a simple one-dimensional approach will not suffice for the flow beneath sailing vessels.

Moreover, also two- and three-dimensional (numerical) models are not capable of predicting the flow velocities beneath the vessel. Only a few simple methods exist to calculate the maximum flow velocity beneath sailing vessels, usually at the bow. As a result, it proves difficult to determine flow velocities beneath a moving ship, and thereby the influence of the flow on the bed beneath a sailing ship.

Flow description

From measurements with barge combinations (WL|Delft Hydraulics (1987), Maynord (1990), Rodriquez et al. (2002)) it is known that there is an increased return velocity beneath a sailing vessel just after passage of the bow, due to contraction of the flow lines by separation (see Figure 5).

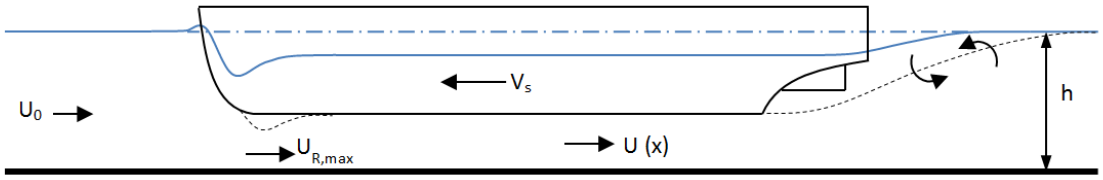

Figure 5: Flow field beneath a sailing ship

In a ship-frame coordinate system the water streaming to the bow will be diverted besides and beneath the ship. The fraction of the flow which passes under the bow is mainly determined by the bow shape and draught of the ship. Part of the water at the bow is forced down and will separate from the hull just after passing the bow. As a result, contraction will occur (comparable to flow under a weir) and the velocity will increase. This effect depends on the shape of the bow of the ship; more streamlined bows reduce the contraction. After the contraction at the bow, flow velocities will decrease and boundary layers on the ship and bed will start to develop. From bow to stern these boundary layers will grow in thickness, reducing the effective underkeel clearance, and consequently the velocities should increase or the discharge should decrease. The only way the discharge can decrease is if water is flowing away to the sides of the ship. This flow process is called fanning out. Figure 6 shows the vector plot of the measured velocities of a performed experiment, which clearly shows the fanning-out effect and the reduction of flow velocities due to boundary layer development.

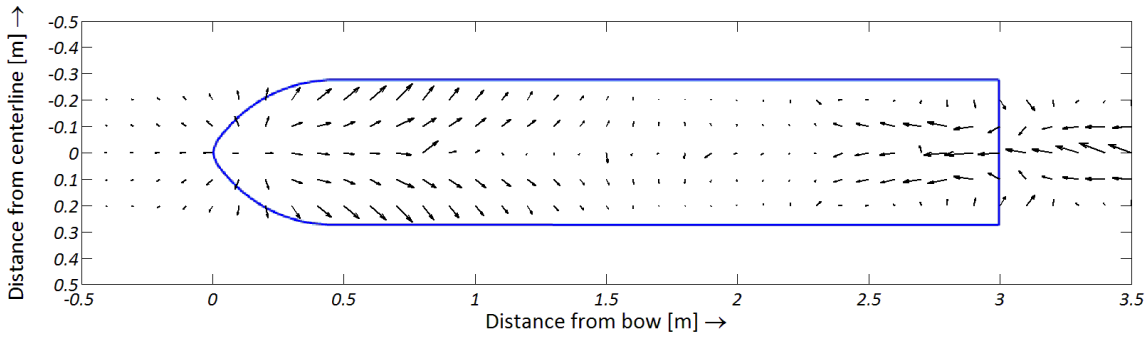

Figure 6: Vector plot of experiment 13

At the stern, the rotating propeller will induce an area of low pressure in front of the propeller. Therefore, the flow will be directed upward towards that area. Immediately after passage of the vessel the flow will be mainly determined by the influence of the propeller jet, which shall not be considered here.

Prediction methods

In their paper for the 31th International Navigation Congress of PIANC, Stolker et al. (2006) presented their findings on ship-induced water motions beneath the hull. Their survey showed that, although a lot of models exist to predict water motions around the ship, hardly any of them can predict the flow velocities beneath the ship accurately. Two empirical relations were found; the equation of Maynord (see Maynord (1990)) and the WL|Delft Hydraulics (1987) formula. In their paper three new methods are described: a model based on physics, a functional relation and a modified version of the formula of Maynord. These equations predict only the maximum flow velocity beneath the ship, depicted by $U_{R,max}$ (near the contraction at the bow). Besides these methods an additional equation to determine return flow velocity beneath ships developed by Führer and Römisch was found in the literature study of Maynord (1990).

WL|Delft Hydraulics formula (1987)

Measurements done by WL|Delft Hydraulics during the M1115 research resulted in a simple relation [2.14] for the maximum return current velocity near the bow, see WL|Delft Hydraulics (1987).

$$U_{R,max} = (1.5 \text{ to } 2) \cdot U_R \qquad [2.14]$$

In which: U_R = cross-sectional averaged return current (as calculated by Schijf) [m/s]

For this research, when the WL|Delft Hydraulics equation is used, coefficient $\alpha = 1.75$.

Maynord (1990)

Based on model research (scale 1:20) on push-tow units, Maynord (1990) developed an equation for the return current velocity beneath sailing barges. He found that the velocity magnitude is mainly dependent on water depth, draught beam width and sailing speed. Also, the velocity beneath the vessel seems to be relatively independent of channel size and return current velocity. The formula [2.15] is created by a regression analysis of the physical model data on dimensionless ratios.

$$\frac{U_{R,max}}{V_S} = 0.16 \cdot \left(\frac{B_S}{h}\right)^{0.54} \cdot \left(\frac{T}{h}\right)^{0.68} \qquad [2.15]$$

This formula is restricted by $\frac{h}{T} \geq 1.6$ and $\frac{A_C}{A_S} \geq 6$.

Physically based model (2006)

Based on unpublished work of Rigter in 1989, a new, physically based method is formulated by Stolker et al. (2006). In this method, the flow velocity beneath the bow depends on the sailing speed, ambient flow velocity, the underkeel clearance and the contraction at the bow, see [2.16].

$$U_{R,max} = \left| (V_S - U_R) \cdot \left(\frac{1 - \mu \cdot \kappa}{\mu \cdot \kappa}\right) - U_R \right| \qquad [2.16]$$

In which: κ = dimensionless keel clearance [-] μ = contraction coefficient [-]

The dimensionless keel clearance can be determined iteratively by equations [2.17] to [2.19]. The contraction coefficient is given by formula [2.20], which is empirically calibrated from the datasets.

$$\kappa = \kappa_0 - \frac{(U_R - V_S)^2}{2 \cdot g \cdot h_0} \left(\frac{\xi_i + 1 + \kappa^2}{\kappa^2}\right) \qquad [2.17]$$

$$\kappa_0 = \frac{A_c - A_s}{A_c} \qquad [2.18]$$

$$\xi_i = \left(\frac{1-\mu}{\mu} \right)^2 \qquad [2.19]$$

$$\mu = 1 - 0.54 \left(\frac{h}{T} \right)^{-1.5} \left(V_S - U_R \right)^{-0.18} \qquad [2.20]$$

In which: κ_0 = non-sailing dimensionless keel clearance [-] ξ_i = energy loss coefficient [-]

A more detailed derivation, as well as possible extensions of the model to include multiple layers or friction forces on the bed and the hull, can be found in Verheij et al. (2004).

Functional relation (2006)

A second new approach by Stolker et al. (2006) is a parameter analysis, resulting in a functional relation [2.21] for the flow velocity beneath a bow, based on the governing parameters.

$$U_{R,max} = U_R \cdot \left(1 + \alpha \left(\frac{h-T}{h} \right)^{\beta} \cdot \left(\frac{V_S - U_R}{\sqrt{g \cdot (h-T)}} \right)^{\gamma} \cdot \left(\frac{A_C}{A_S} \right)^{\delta} \right) \qquad [2.21]$$

After calibration with the dataset, a fit procedure resulted in the following values for the coefficients:

$$\alpha = 0.041 \,,\ \beta = -1.52 \,,\ \gamma = -1.07 \,,\ \delta = 0.81$$

Modified Maynord (2006)

The Maynord equation was calibrated only on its own dataset. Stolker et al. (2006) recalibrated the formula against other datasets to obtain a modified Maynord equation, see [2.22].

$$\frac{U_{R,max}}{V_S} = 1.07 \cdot \left(\frac{B_S}{h} \right)^{0.08} \cdot \left(\frac{T}{h} \right)^{1.82} \qquad [2.22]$$

Führer and Römisch (1977)

Besides these methods, Führer and Römisch developed equation [2.23] for the return velocity beneath the vessel, as found in Maynord (1990).

$$\frac{U_{R,\max}}{V_S} = \frac{h-T}{h-T-z} \left(1.11 + 5.25 \left(\frac{A_S}{A_C} \right)^{2.2} \right) - 1 \qquad [2.23]$$

In which: z = water level depression [m]

All methods described above are only applicable for push-tow barges, and not for other inland navigation vessels. Furthermore, the following restrictions hold for these methods (except Maynord):

$$\frac{h}{T} > 1.25 \quad \text{and} \quad \frac{A_C}{A_S} > 6$$

Calibration and validation of the methods (with the exception of the method of Führer and Römisch) was done by Stolker et al. (2006) against data sets of model tests by WL|Delft Hydraulics (1987), Maynord (1990) and VBD (2003). Based on these data sets, both the WL|Delft Hydraulics formula and the Maynord equation tend to underestimate the maximum flow velocities beneath the ship's hull. The functional relation gives a better prediction, although it still slightly underestimates the velocities. The best methods are, based on accuracy, the physical model and the modified Maynord

equation. This could be expected, since both methods are calibrated (completely or partially) on these data sets. Of these two methods, the physical model is preferred above the (empirical) modified Maynord equation, since it is based on real physics. However, the modified Maynord equation is easier in use and slightly more accurate than the physical model, and is therefore the most suitable method for predicting the velocities beneath sailing barges.

Important phenomena

In this paragraph some information is given about important phenomena that occur when a ship sails over a bed, especially when the distance between the keel and the bed is very small.

Boundary layers

A sailing ship will create a boundary layer along its hull. Gourlay (2006) made some investigations in this part. He found that on a sea-going vessel of 300 m, a boundary layer with a thickness of approximately 2.3 m could form. For an inland navigation vessel of 120 m, this could easily be 1.2 m (with a sailing speed of 3 m/s). It can also be expected that for inland vessels this effect occurs sooner than for sea-going vessels, due to the different keel shapes: an inland vessel usually has a very flat keel, resembling a smooth flat plate.

This means that at small underkeel clearances the boundary layer on the keel will interact with the bed, which will effectively block a large part of the flow underneath the keel. Due to the bed and its no-slip condition, the boundary layer cannot grow continuously. This will cause a very different type of flow between the hull and river bed. Apart from the moving ship, the flow has similarities with inflow in a pipe, where the boundary layers on the walls grow and merge into a fully developed flow. For flow beneath a ship however less longitudinal pressure gradient is present, causing much of the flow to divert around the sides rather than underneath the ship. As a result, flow is mainly governed by the no-slip conditions, leading to a faster fully developed flow (compared to pipe flow). With small underkeel clearances, this means flow will be almost uniform beneath the ship

Resemblance with Couette flow

The flow pattern beneath the hull will resemble Couette flow (flow between two plates, of which one is moving). The flow will be turbulent and there is a longitudinal pressure gradient, leading to a specific velocity profile (see Gourlay (2006)). Note that at model scale, the flow beneath the hull might be laminar.

In absence of a pressure gradient, the flow will be antisymmetric, with a mean velocity of $V_S/2$. Higher velocities can only be reached if a pressure difference is present. This can be feasible for sailing vessels, due to the high-pressure stagnation area near the bow and the flow separation near the stern, as well as the propeller effect (decreases pressure ahead of propeller). Insight into the importance of the pressure gradient may be obtained by estimating the drop over the ship in a ‘zero net flow’ case (zero net flow relative to sea floor). It turns out the required pressure differential for this case is significant. In reality, the flow will therefore resemble Couette-Poussieulle flow with a positive pressure gradient (see Figure 12). For more information reference is given to Gourlay (2006).

Boundary layers and Couette flow can therefore be used to describe the flow beneath the keel. More information on these subjects is given in § 2.3.

Fanning out

The flow beneath a ship, which is a combination of ambient flow (if present) and return current, usually has the tendency to divert to the sides of the ship, see Figure 7. This phenomenon is called fanning out, and it mainly depends on the occurring flow velocities, the shape of the hull and potential differences between the flow beneath the ship and the flow alongside the ship.

Since there is limited knowledge on the flow field beneath a ship in restricted waterways, also the knowledge on the fanning out effect is limited. None of the methods to determine maximum flow velocity beneath a ship mention this effect or refer to it. So, it is clear that there is not a lot of data on the fanning out effect.

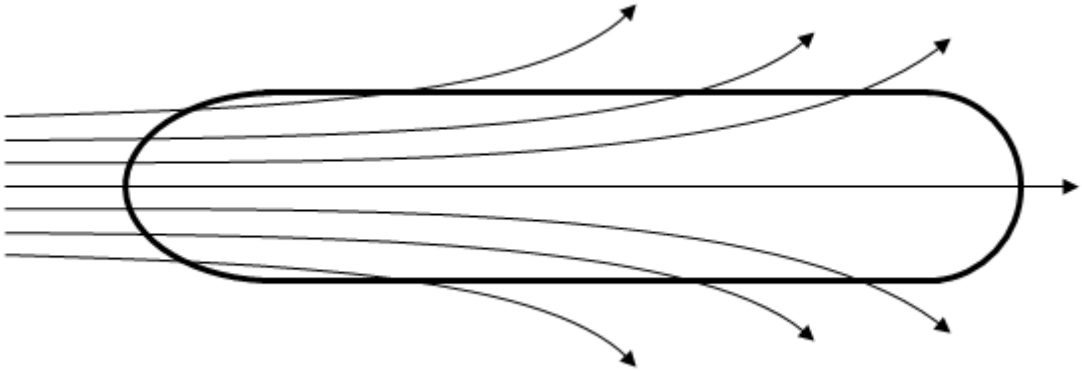

Figure 7: Fanning out effect

In his thesis, Lenselink (2011) found that the velocity beneath a ship decreases with increasing distance from the bow. This can only happen in case the discharge beneath the hull decreases, proving the fanning out effect. In his experiments, it seems the effect decreases with increasing flow velocities. However, Lenselink based his conclusions on the decrease of specific discharge in x-direction in the centerline of the ship (since his measurements were done at that location). This does not give information about transverse velocities, and no data is found which includes these velocities. Therefore, more research into the fanning-out effect is necessary.

2.3 Fluid dynamics

In § 2.2 it was stated that the flow beneath the keel of a ship can be described by Couette flow and with boundary layers. These topics, as well as turbulence effects, belong to the field of fluid dynamics. This paragraph gives an overview of the important aspects of fluid dynamics for this research.

Equations of motion

The motion of fluids can be described by the equations of motion. They are based on the principle of conservation of certain properties, in this case the conservation of mass and the conservation of momentum. The conservation of mass results in the continuity equation (see [2.24]) and the conservation of momentum leads to the Navier-Stokes equations (see [2.25]).

$$\frac{\partial u}{\partial x}+\frac{\partial v}{\partial y}+\frac{\partial w}{\partial z}=0 \qquad [2.24]$$

$$\frac{d}{dt}\left(\rho u_j\right)+\nabla_i\left(\rho u_i u_j\right)=-\nabla_j p+\eta\nabla_i{}^2 u_j+k_j \qquad [2.25]$$

In which:

x,y,z	=	length in specific (orthogonal) direction	[m]				
u,v,w	=	velocity in specific direction	[m/s]	t	=	time	[s]
ρ	=	density	[kg/m^3]	p	=	pressure	[N/m^2]
η	=	dynamic viscosity	[kg/ms]	k	=	source term	[N/m]
∇	=	gradient	[m^{-1}]	i,j	=	specific direction (x,y,z)	[-]

More information and derivations for the continuity equation and the Navier-Stokes equations can be found in (for instance) Schlichting (1968) or Uijttewaal (2013).

The combination of the continuity equation and the Navier-Stokes equations form a complete set of equations to describe a flow. When proper boundary conditions are chosen, there is enough information present to solve the equations. However, due to non-linear advection terms, the Navier-Stokes equations are also non-linear. Because of the non-linearity of the equations, there are no analytical solutions for these equations until the present day. Only for some particular cases (in which certain terms can be neglected) simple solutions can be found. Otherwise numerical models need to be used, but this usually requires brute computational force.

Turbulence

Although exact solutions to the Navier-Stokes equations are not available, still a very important distinction in flow can be made, namely the difference between laminar and turbulent flow. Laminar flow can be described as smooth flow, while turbulent flow is irregular, consisting of 3D vorticity and velocity fluctuations.

Reynolds number

Whether a flow is laminar or turbulent is expressed by the Reynolds number (Re), see [2.26].

$$Re = \frac{u \cdot L}{\nu} \qquad [2.26]$$

In which: u = velocity of fluid [m/s] L = length scale [m]
v = kinematic viscosity [m^2/s]

For Re < 2300 a flow is usually considered laminar, while a flow is turbulent if Re > 4000. An exact transition point cannot be given, since the transition is dependent on instability of the flow, which is very sensitive to small (immeasurable) influences. It can be shown that the Reynolds number is a measure for the ratio between the inertia effects and viscosity effects on the flow, see [2.27].

$$\frac{\text{Inertia effects}}{\text{Viscosity effects}} = \frac{\text{Advection}}{\text{Diffusion}} = \frac{\rho u \frac{du}{dx}}{\eta \frac{\partial^2 u}{\partial y^2}} \propto \frac{\frac{\rho u^2}{L}}{\frac{\eta u}{L^2}} = \frac{\rho u L}{\eta} = \frac{uL}{\nu} = Re \qquad [2.27]$$

In case of large Reynolds numbers, the (non-linear) advection terms dominates the fluid motions, resulting in non-linear, turbulent behaviour. At small Reynolds numbers the viscous effects are able to suppress the instabilities through diffusion (by shear stresses), i.e. the instabilities are 'damped'. However, at large Reynolds numbers the viscous effects are too small, and the instabilities are not damped sufficiently, leading to turbulent motion.

In most civil engineering circumstances the Reynolds number is in the order of 10^5 to 10^6. This means that the flow usually is turbulent, so laminar flow will not be considered here further.

Reynolds averaging

As stated above, no exact solutions exist for the Navier-Stokes equations, due to the non-linear behavior, especially in turbulent flow (high Reynolds numbers). A possible method to obtain proper solutions would be to numerically solve the NS-equations. This is possible, although brute computational force is already needed for simple flow situations. Another method is to simplify the NS-equations by means of Reynolds averaging. In this method the NS-equations are averaged, after decomposing the velocity and pressure vectors in a mean and a fluctuating component:

$$u = \bar{u} + u' \; ; \; v = \bar{v} + v' \; ; \; w = \bar{w} + w'$$

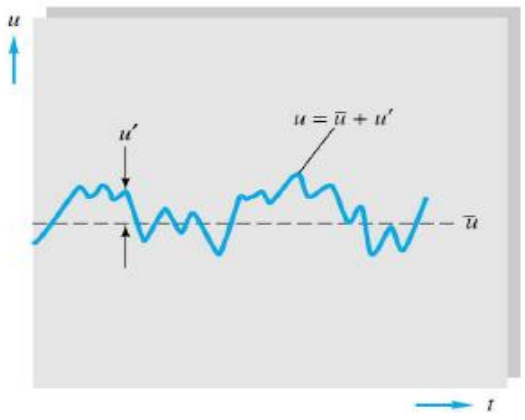

Figure 8: Reynolds averaging method (source: Lenselink (2011))

In which ū is the mean component and u' is the fluctuating component. The averaging operators are:

$$\overline{u'} = 0 \;;\; \bar{\bar{u}} = \bar{u} \;;\; \overline{uv} = \bar{u}\bar{v} + \overline{u'v'}$$

Applying this to the NS-equation results in the Reynolds Averaged Navier-Stokes equations:

$$\frac{d}{dt}\left(\rho\overline{u_j}\right) + \nabla_i\left(\rho\overline{u_i}\,\overline{u_j}\right) + \nabla_i\left(\rho\overline{u_i'u_j'}\right) = -\nabla_j\bar{p} + \eta\nabla_i{}^2\overline{u_j} + \overline{k_j} \qquad [2.28]$$

Compared to [2.25] an extra term is found, namely the correlation between velocity fluctuations u_i' and u_j'. These extra terms are apparent stresses, also referred to as Reynolds stresses (or turbulent stresses):

$$\overline{\rho v_i' v_j'} = q_{ij}$$

For i = j these are normal stresses, while for i ≠ j it are shear stresses. They show the effect of the fluctuating components on the mean motion of the flow, and cause the different flow behavior of turbulent and laminar flow. Due to the turbulent shear stresses (q_{ij}, with i ≠ j), momentum is diffused ('mixed') over the flow geometry. So, in fact they are similar to the viscous shear stresses. At high Reynolds numbers the turbulent shear stresses are far more effective than the viscous shear stresses.

Due to the diffusion of momentum, the Reynolds stresses redistribute energy from the mean motion towards the turbulent fluctuations. This transfer of energy keeps on continuing to increasingly smaller fluctuation scales (large scale turbulent motion 'feeds' smaller scale turbulent motion). The increasingly smaller scales result in large velocity gradients, until at some scale the viscous effects will dominate again. At this scale the energy will be dissipated through the viscous effects. A more thorough explanation, as well as derivations, can be found in Uijttewaal (2013).

Boundary layers

Most theoretical investigations in fluid dynamics are based on a perfect fluid, i.e. a fluid which is frictionless and incompressible. During motion this means that two contacting layers of fluid do not exert tangential forces (shear stresses) on each other, but only act on each other with normal forces (pressures). In many cases this theory gives a satisfactory description of real fluid motions.

In reality however, intermolecular attractions cause fluid layers to exert tangential forces (shear stresses) on each other. The property of the fluid that is connected to these shear stresses is called the viscosity. It is customary to relate these shear stresses (τ) to velocity gradients, see [2.29].

$$\tau = \eta\frac{du}{dz} \qquad [2.29]$$

The constant of proportionality η is called the (dynamic) viscosity. Due to these shear stresses, inertia is interchanged between fluid layers with different velocities. For fluid motions in which frictional and inertial forces interact, the ratio between the viscosity and the density of the fluid is important. This ratio is called the kinematic viscosity ν (= η / ρ).

Since water is a fluid with a very small viscosity, in many cases it agrees very well to the motions of a perfect fluid, because in most cases shearing stresses are very small. However, at and near boundaries (for instance near a wall) this is completely different. Absence of frictional forces would imply that there would be slip, i.e. no interaction between the flow and the wall (difference in relative velocities). In reality, there is a no-slip condition: due to adherence of the particles to the wall there is (almost) no motion at the boundary (so $u = 0$); frictional forces (shear stress) retard the motion of the fluid.

This happens in a thin layer near the boundary. In that thin layer the velocity of the fluid increases from zero (due to the no-slip condition at the wall) to its full value (which corresponds to frictionless flow). This thin layer is called the boundary layer. In this layer, fluid particles close to the boundary are decelerated due to the stagnant boundary. These fluid particles will decelerate particles even further away from the boundary due to shear stresses (caused by differences in velocity and the viscosity of the fluid, see equation [2.29]), and so on. Even at very small viscosities the shear stresses

are significant due to the large velocity gradients in the boundary layer. In this process, the boundary layer will grow, i.e. the boundary layer thickness increases.

Boundary layer development

Objects in the flow, such as walls, beds, but also ships, will create these boundary layers, which will grow with increasing distance from its leading edge, see Figure 9. There are two type of boundary layers: laminar and turbulent, and they grow at different rates.

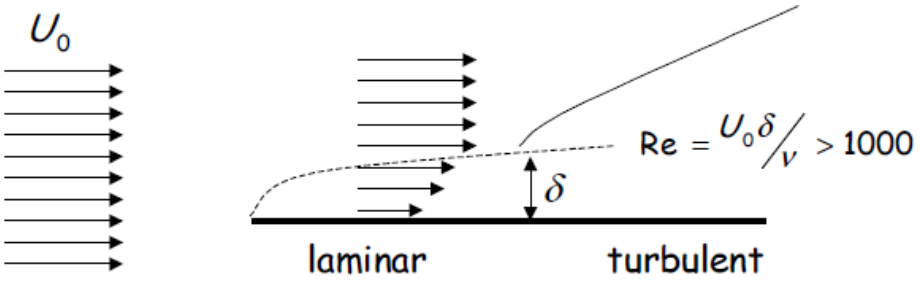

Figure 9: Boundary layer development on a smooth flat plate (source: Uijttewaal (2013))

The transition between a laminar and turbulent boundary layer is approximately at Re = 1000, in which the length scale is now the boundary layer thickness, as in Figure 9. However, this requires iteration, and therefore frequently instead the local Reynolds number Re_X is used, given by [2.30].

$$Re_x = \frac{u \cdot x}{\nu} \qquad [2.30]$$

In which: u = flow velocity [m/s] x = distance from leading edge [m]
v = kinematic viscosity [m^2/s]

For a smooth flat plate he transition point lies approximately at $Re_X = 5 \cdot 10^5$. The boundary layer thickness δ can then be calculated with the equation of Blasius [2.31] for laminar boundary layers and equation [2.32] for turbulent boundary layers.

$$\delta = 5\sqrt{\frac{\nu \cdot x}{u}} \qquad [2.31]$$

$$\delta = \frac{0.16 \cdot x}{Re_x^{1/7}} \qquad [2.32]$$

Besides these equations there are more methods to calculate the boundary layer thickness, but all amount to approximately the same thickness. Multiple methods exist since the equations are empirically derived from experiment data. This can also be explained by the fact that it is difficult to determine the end of the boundary layer. According to White (2008), this is at 99% of the external velocity U. When the boundary layer reaches over the entire water column (h for open channel flow, R for tubes) a flow is considered to be fully developed.

The equations above do not consider roughness of the wall itself. A rough wall probably will increase the boundary layer development at the beginning, and perhaps also quicken the transition to a turbulent boundary layer. At a certain thickness the roughness does not matter anymore, since the roughness is covered within the boundary layer. Some methods exist to include the roughness in the boundary layer development, but these will not be addressed here.

More information on boundary layers and boundary layer development can be found in Schlichting (1968), Uijttewaal (2013) and White (2008).

Couette flow

Couette flow is the flow between two plates, of which one is at rest and one is moving at a constant velocity U. Due to the no-slip boundary condition, the fluid adheres to the plate. Therefore, the

velocity of the fluid at the stationary plate is 0, while the velocity of the fluid at the moving plate is equal to U. In case of laminar flow, the velocity distribution is linear between the two plates, as shown in Figure 10. Since the friction (shear stress) is proportional to the gradient of the velocity in z-direction (see [2.29]), this implies that the shear stress is uniform between the two plates.

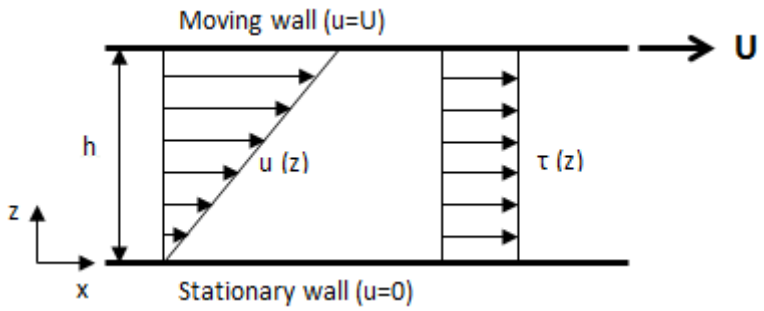

Figure 10: Couette flow in laminar flow

In this case the velocity distribution can be written as:

$$u(z) = \frac{z}{h} \cdot U \qquad [2.33]$$

In which: U = velocity of moving wall [m/s] h = distance between walls [m]

The velocity distribution is only valid for laminar flow, and when there is no longitudinal pressure gradient present.

Turbulent flow

However, in most cases a flow will not be laminar, but turbulent. Whether Couette flow is laminar or turbulent is determined by another Reynolds number, see [2.34].

$$Re_H = \frac{U \cdot h}{\nu} \qquad [2.34]$$

Many experiments (physical and experimental) have been undertaken to determine the Reynolds number in which transition from laminar to turbulent flow occurs. In fact, when Couette did his experiments in 1890 to determine the viscosity of water, he already found an increase in the viscosity around a Reynolds number of approximately 480. This can be explained by the transition from laminar to turbulent flow, see equation [2.35].

Further research into the transition to turbulence in Couette flow was done by Reichardt in 1954, see Schlichting (1968). He found a transition from laminar to turbulent Couette flow around $Re_H \approx 3000$. This is a so-called critical Reynolds number, which denotes the lowest Reynolds number at which an infinitesimal disturbance grows exponentially. Tillmark et al. (1992) have done experiments to determine the transitional Reynolds number, i.e. the Reynolds number at which transition to turbulence occurs if a large enough disturbance is applied. They found a transitional Reynolds number of $Re_H=1440 \pm 40$, and their experiments seem to agree well to numerical simulations by Lundbladh and Johansson (1991), who found an transitional Re_H of approximately 1500.

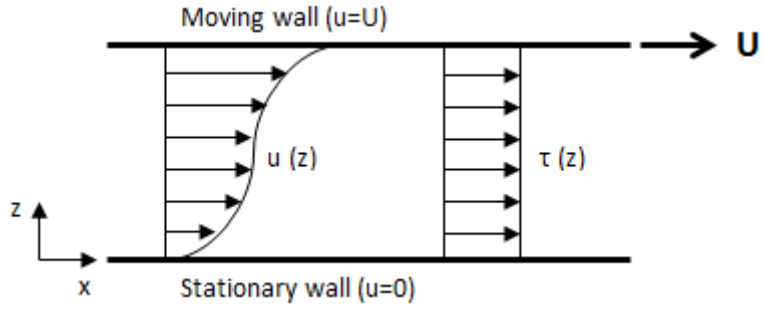

Figure 11: Turbulent Couette flow

When the flow becomes turbulent, also the velocity profile changes; see Figure 11. Due to the turbulent mixing of momentum in the flow, the velocity profile is very flat near the center and becomes very steep near the walls. This happens because the shear stress consists of a viscous contribution and contribution due to turbulent mixing:

$$\tau = \tau_v + \tau_t = \eta \frac{du}{dz} + A_\tau \frac{du}{dz} \qquad [2.35]$$

In which: τ_v = viscous shear stress [N/m^2] τ_t = turbulent shear stress [N/m^2]
η = dynamic viscosity [kg/ms] A_τ = mixing coefficient [kg/ms]

The mixing coefficient A_τ increases from zero at the wall to a maximum value at the center of the channel. Therefore, there is more mixing in the center and the velocity profile will flatten here, while it will steepen at the wall since there is only very little mixing here. With increasing turbulence (increasing Reynolds numbers), the turbulent mixing increases and hence the velocity profile will flatten (in the center) and steepen (at the walls) even more. Even in turbulent flow, the shear stress distribution in the channel remains approximately uniform. More information can be found in Schlichting (1968).

Influence of pressure gradient

Up until now Couette flow has been considered without a longitudinal pressure gradient. Flow in a pipe or channel under the influence of a pressure gradient is called Poiseuille flow. The combination hence is called Couette-Poiseuille flow.

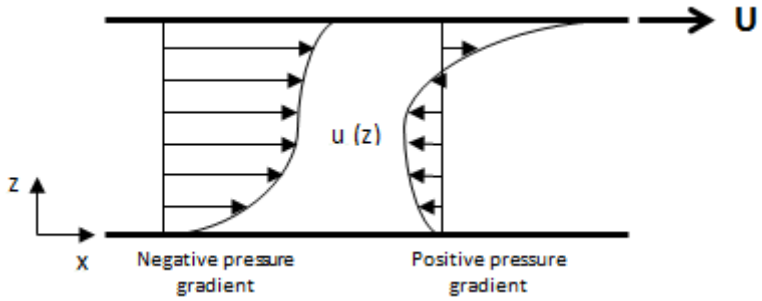

Figure 12: Couette flow with pressure gradients (also called Couette-Poiseuille flow)

The influence of a pressure gradient is given graphically in Figure 12. A negative pressure gradient in the direction of the moving plate will increase the flow velocities, especially in the middle part of the flow. A positive pressure gradient however will decrease and even reverse the flow over a large part of the area. More information can be found in Schlichting (1968).

When a vessel is moving over the bed, a positive pressure gradient is created from bow to stern, due to the headwater at the bow and the low pressure region in front of the propeller near the stern. This positive pressure gradient also drives a part of the flow underneath the keel. The (vertical) velocity profile underneath the keel should therefore result in approximately the profile from Figure 12.

2.4 Sediment transport

Initiation of motion

Before erosion is possible, sediment must become mobile, i.e. there must be initiation of motion. Whether or not a particle will move depends on several forces: the force exerted by the flow on the particle (lift force, drag force and shear force) and the gravity force due to the weight of the particle. Besides these forces also turbulence plays an important role, this can significantly increase the forces on the grain. Also the protrusion of the grain is of importance: deeply logged grains will be less mobile than grains at the top of the bed.

The most common method to determine initiation of motion is with the method of Shields (1936). He determined that whether or not a sediment grain is picked up depends on a dimensionless number, the Shields number θ (see [2.36]). The Shields number gives the ratio between the exerted shear stress on the particle and the submerged weight of the particle.

$$\theta = \frac{\tau_b}{(\rho_s - \rho_w) \cdot g \cdot d_{50}} \qquad [2.36]$$

In which: τ_b = bed shear stress [N/m^2] ρ_s = specific weight sediment [kg/m^3]
ρ_w = density water [kg/m^3] d_{50} = median sediment diameter [m]

The Shields number at which motion is initiated is called the critical Shields number, θ_{cr}, and its subsequent shear stress is known as the critical shear stress τ_{cr}. The shear stress can be coupled to the velocity by means of equation [2.37].

$$\tau = \rho_w \cdot |u_*| \cdot u_* \qquad [2.37]$$

In which: u_* = shear velocity [m/s]

The shear velocity is not an actual velocity, but it can be translated to the actual velocity with equation [2.38].

$$u_* = \frac{\bar{u} \cdot \sqrt{g}}{C} \qquad [2.38]$$

In which: ū = mean velocity [m/s] C = Chèzy coefficient [m^{½}/s]

In this manner, the velocity can be expressed in a shear stress, which in turn can be translated to the Shields number. The critical Shields number depends on the grain size, and it's value is determined by the particle Reynolds number Re_*, see [2.39]. From Figure 13 the critical Shields number can then be calculated.

$$Re_* = \frac{u_{*,cr} \cdot d_{50}}{\nu} \qquad [2.39]$$

In which: $u_{*,cr}$ = critical shear velocity [m/s] ν = kinematic viscosity [m^2/s]

Usually, the sediment diameter is known. Then the critical velocity at which initiation of motion will occur can be iteratively determined with equations [2.36] - [2.39] and Figure 13.

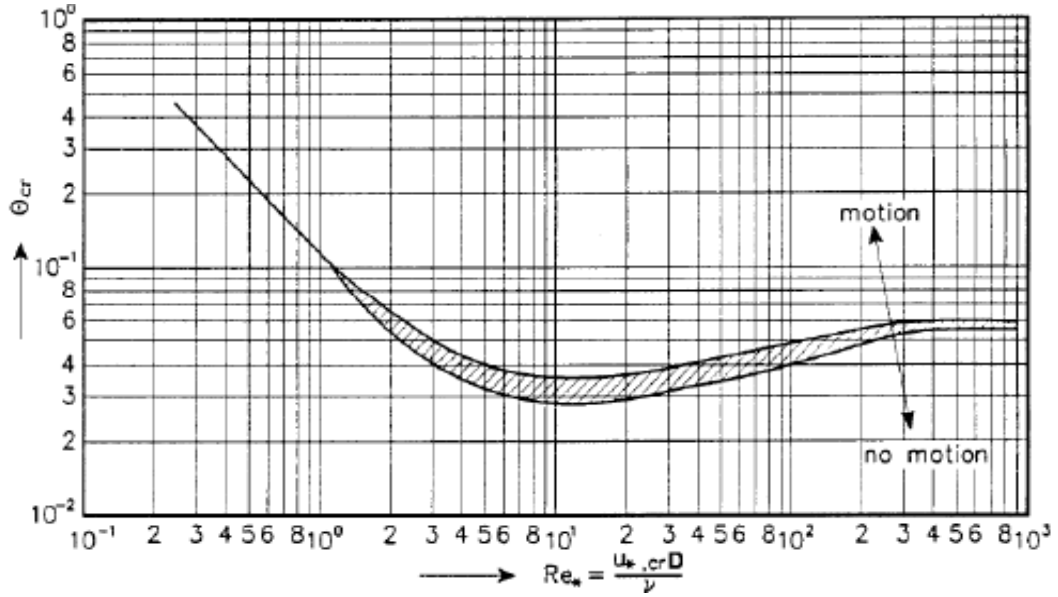

Figure 13: Shields diagram

Due to the passing of a vessel, the velocities at the bed will increase. As a result, the shear stresses will increase, and thus also the likelihood of initiation of motion. A passing vessel thus increases the pick-up of sediment, and consequently also the sediment transport. This effect may assumed to be greatest underneath the keel, where velocities are highest.

The pick-up of sediment is however also largely affected by turbulence. In fact, according to Schiereck et al. (2012) the turbulence intensity r, given by [2.40], should weigh for a factor 3 compared to a factor 1 for the mean velocity ū. This means velocity fluctuations are very important for pick-up of sediment and thus on erosion. More information about the influence of turbulence on initiation of motion is given in Schiereck et al. (2012).

$$r = \frac{\sqrt{\overline{u'^2}}}{\bar{u}} \qquad [2.40]$$

Sediment transport

When initiation of motion is achieved, three types of sediment transport can be distinguished:

- Bed transport: transport of sediment over the bed
- Suspended transport: transport of sediment suspended in the water column
- Wash load: transport of very fine particles, which will only settle without currents

Sediment transport is a highly empirical science which is still not exactly understood. As a consequence a lot of sediment transport formulae exist. The type of formula also depends on the type of transport. During the passage of a vessel the sediment underneath the vessel will come into motion, which results in both bed and suspended transport. Two frequently used sediment transport formulae are given here:

- Engelund-Hansen (1967)
- Meyer-Peter-Muller (1948)

For the validity of both equations the fall velocity of grains is important. The fall velocity (w_S) describes the velocity of a grain in still water, and is given by equation [2.41]. Coefficient C_D depends on the grain size.

$$w_S = \sqrt{\frac{4 \cdot (\Delta - 1) \cdot g \cdot d_{50}}{3 \cdot C_D}} \qquad [2.41]$$

In which: Δ = relative density ($(\rho_s - \rho_w) / \rho_w$) [-] C_D = drag coefficient [-]

Meyer-Peter-Muller

The Meyer-Peter-Muller equation [2.42] is applicable to bed transport (s_b), and can be used for sediment diameters larger than 0.4 mm, and when $w_S / u_* > 1$.

$$s_b = \frac{8 \cdot (\theta - 0.047)^{3/2}}{\sqrt{\Delta \cdot g \cdot d_{50}}} \qquad [2.42]$$

In which: d_{50} = median sediment diameter [m] θ = Shields number [-]

Engelund-Hansen

The equation of Engelund-Hansen [2.43] is an equation for the total sediment transport s (bed + suspended load). It was originally derived for bed transport but proved very good for relative fine material, i.e. for $w_S / u_* < 1$. It can be applied for $0.07 < \theta < 6$, with 0.19 mm < d_{50} < 0.93 mm.

$$s = \frac{0.05 \cdot \bar{u}^{-5}}{\sqrt{g} \cdot C^3 \cdot \Delta^2 \cdot d_{50}} \qquad [2.43]$$

In which: C = Chèzy coefficient [$m^{½}/s$] ū = mean velocity [m/s]

Above equations and theory can be found in more detail in Schiereck et al. (2012) and Vriend et al. (2010).

Erosion underneath vessels

Shear stress experiments

Multiple studies have been performed to determine the flow field underneath inland navigation vessels, and their role in the resuspension of sediment. The main focus of these studies was the velocity distribution and the sediment concentration measurements, and they have provided little information about the associated bed shear stresses.

Therefore, experiments have been conducted by Rodriguez et al. (2002) on a 1:25 Froude scale in which barges in a flume sailed over three shear stress sensors in the bed. The barge could be adjusted transversally, so different positions of the sensors beneath and besides the barge could be achieved. The sensors are one-dimensional, meaning they only give the shear stress in the streamwise direction. All results are ensemble-averaged. Shear stresses are measured on one side of the barge tow centerline only, under the assumption that the shear stress distribution can be mirrored over the tow centerline. Figure 14 shows an obtained shear stress footprint.

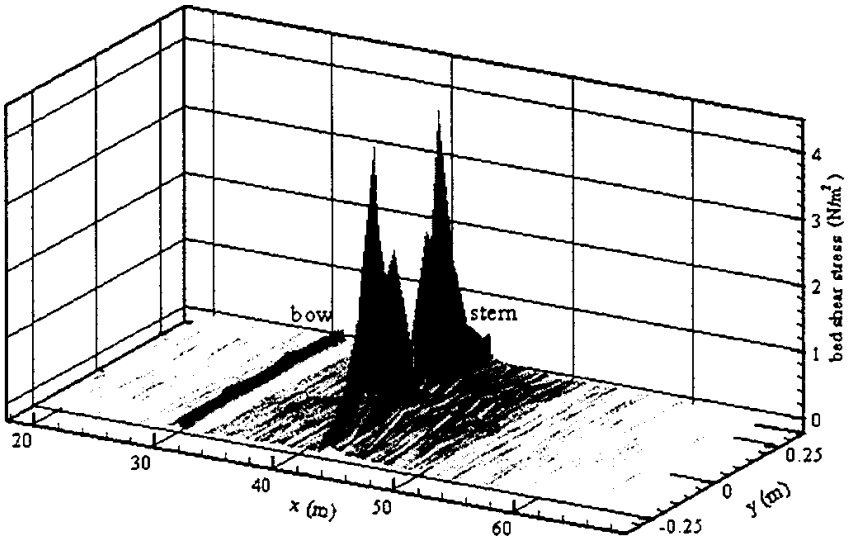

Figure 14: Three-dimensional reconstruction of shear stress footprint (see Rodriguez et al. (2002))

Due to the passage of a barge tow, two regions of high shear stresses are produced: one due to the arrival of the bow and another due to the arrival of the stern (due to the propellers). For the shear stress caused by the bow, the distribution was nearly constant across the entire bow width. The magnitude of the peak shear stress decreased as the flow depth increased. Also, the peak corresponding to the upbound tests (against the ambient flow direction) was higher than that of the downbound test (sailing direction). Tests also showed that the bow shear stress distribution is quite smooth; there is little variation between the distributions for different test conditions.

For the stern region the shear stress was highest immediately behind the propellers, with highest peak shear stresses for the lowest flow depths. The region after the passage of the stern is extremely turbulent, with significant differences in shear stress distribution between different runs with equal test conditions. The peak shear stresses at the stern are much higher than the peak shear stresses at the bow.

For the dimensionless peak shear stresses at the bow equation [2.44] is found. These equations show the large dependence on the distance between the keel and the bed, as well as the large difference in sailing up- or downbound.

$$\text{Downbound:}\quad \frac{\langle \tau_{pk,bow} \rangle}{\rho\left(\langle V_s \rangle - \langle U_0 \rangle\right)^2} = 4 \cdot 10^{-5} \cdot \exp\left(4.80 \cdot \left(\frac{T}{h}\right)\right)$$

$$\text{Upbound:}\quad \frac{\langle \tau_{pk,\text{bow}} \rangle}{\rho\left(\langle V_s \rangle - \langle U_0 \rangle\right)^2} = 20 \cdot 10^{-5} \cdot \exp\left(3.96 \cdot \left(\frac{T}{h}\right)\right) \qquad [2.44]$$

Scaling up the model values showed that navigation-induced shear stresses can reach peak values in the order of 100 N/m^2, which is seldom reached on rivers (even during floods). These high stresses act during a short time period, and this sudden perturbation can entrain a considerable amount of sediment instantaneously. However, the flow rapidly returns to its original conditions, resulting in a redeposition of most of the entrained sediment in a relatively short time. This prevents the development of important bed scour.

Bots, 2011

For his master thesis, Bots (2011) studied the dredging methods currently applied in the river Waal in the Netherlands. His thesis consisted of some new, innovative techniques for maintenance of the Dutch fairways. For all these new techniques he performed experiments. One of them was to use a deep draught barge to clear out small shoals and dunes in the river bed. This method was based on the increased flow velocities beneath the hull, resulting in additional sediment transport.

He found that flow velocities increase beneath the ship (compared to the return flow sideways of the ship), but they decrease with increasing distance from the bow. This confirms the fanning-out effect, in which flow beneath the vessel has the tendency to 'fan out' from underneath the barge, reducing the specific discharge (and thus the flow velocity) along the length of the ship. With a keel clearance of 25% of the waterdepth, he found a minor increase in sediment transport (approximately 5% of a dune was eroded). However, at increasing sailing speed an increase in sediment transport was found: sailing at the limit speed (model dimensions) – determined by Schijf – revealed an erosion of 10% of the dune. Furthermore, it appears that the results have a large dependence on the keel clearance. Decreasing the keel clearance might induce more sediment transport. However, this was not researched further.

2.5 Previous experiments

Lenselink (2011)

Lenselink (2011) specifically studied the interaction between loaded barges and bed material in his master thesis. He partly used the same experiments as Bots, but extended them to gain more insight in the specific velocity profile beneath a barge and its effect on the bed.

For the determination of a velocity profile a static condition was used, in which the vessel is at rest and the water is flowing around it. Velocity measurements were done by three EMS-devices beneath the barge, of which two could be adjusted in depth (up to minimal 8 cm from the bed, closer resulted in interference with the bed). It turns out, that with increasing flow velocities the fanning out effect seems to decrease. However, still approximately 45% of the specific discharge is diverging to the sides of the barge. Furthermore, when decreasing the keel clearance, the flow velocities beneath the vessel significantly increase. The maximum velocity beneath the barge can be found under the bow, measurements suggest a maximum of 1.46 times the return flow velocity as calculated with Schijf (1949). The minimal underkeel clearance was 0.15 m with a water depth of 0.46 m, which results in h / T ≈ 1.5. Besides experiments, also a potential flow model was used, leading to more or less the same conclusions.

The measurements of the maximum flow velocities were compared to the few existing (empirical) formulae, and the modified Maynord equation predicted the flow velocities very well. Although increasing flow velocities beneath a barge were measured, the short time-span over which the

increase takes place is not long enough to induce serious sediment transport differences. Therefore, the use of barges to remove dunes and small shoals does not seem to be very effective.

WL|Delft Hydraulics (1984, 1986, 1987)

WL|Delft Hydraulics (1984, 1986, 1987) did a lot of research into the effects of navigation on channels, including wave attack on the channel banks, wave height measurements, squat predictions and return current measurements. During the experiments for this research, a propeller meter was installed beneath the path of a sailing vessel (conventional vessels and tows). Eventually the measurements with this research have led to the WL|Delft Hydraulics equation ([2.14]).

They found that in most cases the extreme velocities and pressure differences occurred at the bed underneath the ship, rather than to the sides of the ship. They already established that the length of the push-tow combination is important for the influence of boundary layers, which decreases the velocity underneath the ship. The position of the ship in the channel is also important. When the ship sails in the centreline of the channel the occurring velocities underneath the keel are largest. Unfortunately only one velocity meter was placed underneath the ship, which only gives the magnitude in the sailing line. Nevertheless, they observed the increase of velocity directly after the bow.

Maynord (1990, 2000)

Maynord (1990, 2000) did research to determine the physical forces in the region near and beneath barges. The physical forces were used to determine scour, sediment suspension and effects on aquatic life. Although his research consisted of many different experiments and measurements, only the part on velocities beneath the keel is shortly discusses here. For extended details on his experiment setup, reference is made to Maynord (1990) and Maynord (2000).

Part of his experiments consisted of a 1:20 physical model investigation of bed velocities near the path of a moving tow. These experiments also resulted in the Maynord equation ([2.15]). The range of his experiments were: $1.67 \leq h/T \leq 3.33$

The most important conclusions from his research were:

- Maximum centreline velocities were only slightly less than maximum propeller-jet velocities.
- At equal water depths, the centreline velocities were relatively unaffected by channel cross-sections.

From his research the maximum centreline velocities could be obtained, which can be used for eventual validation of new prediction methods.

VBD

VBD (Versuchsanstalt für Binnenschiffbau e.V., Duisburg) has done experiments in 2003 with self-propelled barge trains for Stichting Projecten Binnenvaart, to check the effects of enlarged barge trains on the Rhine river.

More information can be found in VBD (2003). During these experiments three different barge trains were used in different settings. Water levels and draughts corresponded with navigation conditions on the Rhine. The range covered during these experiments is: $1.38 \leq h/T \leq 2.08$

During the experiments the following measurements were done:

- Force measurements on ship motions and manoeuvrability
- Bottom pressure distributions
- Axial bottom currents
- Wave measurements by means of wave gauges

For both the velocity and pressure measurements at 5 different positions in the cross-section instruments were placed. For the velocity measurements 5 pitot tubes (static and dynamic) were used, which means only x-velocities were measured. For more information about placement of the different instruments, barge train combinations and flume/ship dimensions, reference is made to

VBD (2003). The report itself does not give conclusions, just the model setup and the data is given there.

The output of the experiments is given in graphs, such as the one in Figure 15. The results in the graphs are translated to prototype circumstances. These graphs can be used to obtain maximum occurring velocities underneath barges, as well as provide control for the longitudinal velocity profile beneath barges.

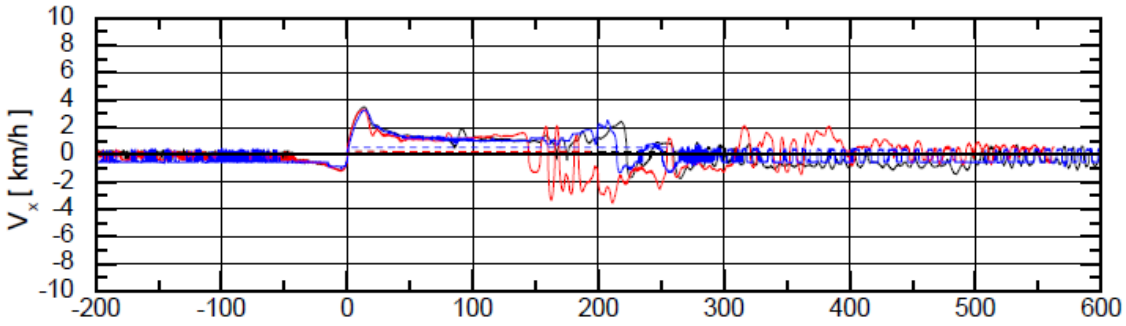

Figure 15: Example of velocity output of VBD experiments (h = 7.5 m, T = 4 m, V = 10 km/h)

2.6 Conclusions

From the literature research, the most important conclusions for this research are:

- Currently no methods (or models) exist which can calculate the flow field beneath vessels. Only formulations for a single maximum velocity value are available, and of these formulations the Modified Maynord equation (given by [2.22]) is preferred.
- The majority of the data sets similar to this research have only considered barges and only measured velocities in the sailing line. None of the previous experiments have measured transverse velocities (outside the centreline), thus the fanning out effect is not definitely proven. Nevertheless the data sets can be used to validate part of an eventual flow model.
- The flow field underneath sailing inland navigation vessels can be modelled with theoretical fluid mechanical topics. Especially boundary layer development and Couette flow seem to give promising leads. Physical model studies are necessary to investigate the similarity with these principles.
- As far as known, no research has been done on sailing vessels with small underkeel clearances. Some theoretical investigations have been made by Gourlay (2006), but there have been no experiments on this topic.
- Due to the passage of a vessel the shear stresses on the bed of the waterway increase significantly, and thus also the sediment transport and erosion increase. Experiments with moveable beds have shown the effect of the passing of a vessel on the bed, but due to the limited time period important bed scour is omitted. However, these experiments have been carried out with relatively large underkeel clearances, so the effect at small underkeel clearances still needs to be investigated.

3. Physical modelling

This chapter gives the setup of the physical model tests which were performed during this research. Attention is given to the scaling of the model, the flume setup, the conditions that need to be simulated and the determination of the experimental program.

3.1 Scaling laws

For modelling the reality to model circumstances, scale factors are applied. These give the ratio between the value of parameter X in model and reality, see [3.1].

$$n_X = \frac{X_{\text{reality}}}{X_{\text{model}}} \qquad [3.1]$$

For the scaling of prototype situations to model circumstances often dimensionless numbers are used. Dimensionless numbers give a ratio between different physical processes, and by requiring equality between model and prototype dimensionless numbers, the different physical processes keep the same ratio. Therefore, the scale factors of the dimensionless numbers are usually set at 1. The important dimensionless numbers here are the Froude, Reynolds and Shields number.

The most important processes are the water motions, the sediment transport and the boundary layers beneath the ship. For the project also the forces on the ship are of interest, therefore these must be modelled correctly as well. In this document however no attention is given to this, although it was included in the decision for the scaling of the experiments.

The scale factors of the gravitational constant (g), the viscosity (ν) and densities (ρ) are considered to be equal in model and reality, and are therefore set at unity: $n_g, n_\nu, n_\rho = 1$.

Water motions

Froude scaling

An important parameter for the correct scaling of water motions is the Froude number, given by [3.2]. It gives the ratio between the inertia of the water and the static weight of the water.

$$Fr = \frac{u}{\sqrt{g \cdot h}} \qquad [3.2]$$

For the correct scaling of the Froude number, the following scaling rule [3.3] should be applied.

$$n_{Fr} = \frac{n_u}{\sqrt{n_g \cdot n_h}} = \frac{n_u}{\sqrt{n_h}} = 1 \Rightarrow n_u = n_h^{0.5} \qquad [3.3]$$

This also means the time scale (see [3.4]) in the model will be different compared to reality.

$$n_t = \frac{n_L}{n_u} = \frac{n_L}{n_L^{0.5}} = n_L^{0.5} \qquad [3.4]$$

Reynolds scaling

The Reynolds number [3.5] gives the ratio between inertia forces and viscous forces. It is of importance for the characteristics of the flow (laminar or turbulent) and for instance for the ship's resistance.

$$Re = \frac{u \cdot L}{\nu} \quad [3.5]$$

Scaling results in the following scaling rule.

$$n_{Re} = \frac{n_u \cdot n_L}{n_\nu} = 1 \Rightarrow n_u = n_L^{-1} \quad [3.6]$$

It can be seen that this interferes with the Froude scaling rule. However, as long as the flow in the model is turbulent (high enough Reynolds numbers), not complying with the Reynolds scaling rule is not a problem. The drawback of not complying with the Reynolds scaling is that the ship resistance will increase in the model compared to the reality, since viscous resistance (relatively) increases. For self-propelling ships this is a problem, since in that case more power is needed to overcome this resistance. For this research the ship will be towed, so not problems with propulsion are expected.

Sediment transport

Shields scaling

The initiation of motion of sediment and the amount of transport can be expressed in a dimensionless parameter θ, called the Shields number, given by equation [3.7].

$$\theta = \frac{\tau_b}{(\rho_s - \rho_w) \cdot g \cdot d_{50}} \quad [3.7]$$

In which the bottom shear stress (τ_b) can be calculated by equation [3.8], the Chèzy coefficient (C) by formula [3.9], the roughness height k_S by [3.10] and the hydraulic radius R by [3.11].

$$\tau_b = \frac{g}{C^2} \cdot \rho_w \cdot u^2 \quad [3.8]$$

$$C = 5.75 \cdot \sqrt{g} \cdot \log\left(12 \cdot \frac{R}{k_s}\right) \quad [3.9]$$

$$k_S = 3 \cdot d_{90} \quad [3.10]$$

$$R = \frac{A_c}{P} = \frac{B \cdot h}{B + 2 \cdot h} \quad [3.11]$$

In the model, sediment transport is important, and should therefore be correctly scaled. Therefore, scaling on the Shields number is applied. The drawback of using the Shields number for scaling, is that the critical Shields number (θ_{cr}), indicating the beginning of movement, varies for different sediment sizes. As a result, when sediment is scaled on the Shields number, it should be checked if the scaled sediment has approximately the same critical Shields number as the prototype sediment. The scaling of Shields is given in [3.12] and [3.13], with applying Froude scaling for the velocity.

$$n_\theta = \frac{n_\tau}{n_\rho \cdot n_g \cdot n_d} = \frac{\frac{n_g}{n_C^2} \cdot n_\rho \cdot n_u^2}{n_\rho \cdot n_g \cdot n_d} = \frac{n_u^2}{n_C^2 \cdot n_d} = \frac{n_u^2}{\log^2\left(\frac{n_h}{n_d}\right) \cdot n_d} = 1 \quad [3.12]$$

$$n_\theta = \frac{n_u^2}{\log^2\left(\frac{n_h}{n_d}\right) n_d} = \frac{n_h}{\log^2\left(\frac{n_h}{n_d}\right) n_d} \Rightarrow \frac{n_h}{n_d} = \log^2\left(\frac{n_h}{n_d}\right) \Rightarrow \frac{n_h}{n_d} \approx 0.29 \Rightarrow n_d \approx \frac{n_h}{0.29} \quad [3.13]$$

Engelund-Hansen

Another possibility is to scale the sediment based on sediment transport. Here, the formula of Engelund-Hansen (1967) is used, described by [3.14], since it is relatively simple and does not require many variables. It is applicable for bed and suspended transport.

$$s = \frac{0.05 \cdot \overline{u}^{5}}{\sqrt{g} \cdot C^{3} \cdot \Delta^{2} \cdot d_{50}} \qquad [3.14]$$

Scaling sediment transport on the Engelund-Hansen formula, results in the following scaling law:

$$n_s = \frac{n_u^{\,5}}{n_C^{\,3} \cdot n_d} \qquad [3.15]$$

When Froude scaling of the velocity is applied (so $n_u=n_L^{0.5}$), and requiring that the volume of sediment transport in reality should be equal in model dimensions ($n_s=n_L^{\,2} / n_t$) gives:

$$\frac{n_L^{\,2}}{n_t} = n_L^{\,1.5} = n_L^{\,2.5} \cdot n_C^{\,-3} \cdot n_d^{\,-1} \Rightarrow n_L = n_C^{\,3} \cdot n_d = \log\left(\frac{n_L}{n_d}\right)^{3} \cdot n_d \Rightarrow \frac{n_L}{n_d} \approx 0.24 \qquad [3.16]$$

Boundary layers

According to theory, the following relations ([3.17] for laminar flow, [3.18] for turbulent flow) hold for the thickness of the boundary layer on a smooth flat plate.

$$\delta = 5\sqrt{\frac{\nu \cdot x}{u}} \qquad [3.17]$$

$$\delta = \frac{0.16 \cdot x}{Re_x^{\,1/7}} \qquad [3.18]$$

Then, for correct scaling the following rules should be applied:

Laminar flow: $$n_h = n_L^{\,0.5} n_u^{\,-0.5} = n_L^{\,0.5} n_h^{\,-0.25} \Rightarrow n_h = n_L^{\,0.4} \qquad [3.19]$$

Turbulent flow: $$n_h = \frac{n_L}{\left(n_u \cdot n_L\right)^{1/7}} = n_L^{\,6/7} n_h^{\,-1/14} \Rightarrow n_h = n_L^{\,0.8} \qquad [3.20]$$

It can be seen that these scaling laws do not comply with each other. In most of the cases however the flow will be turbulent, therefore scaling on a turbulent boundary layer will be applied.

Scaling choices

For a better substantiation of the scaling choices, reference is given to the work plan by Talmon et al. (2014). Here only the important decisions are given.

Length scale (horizontal)

Due to the dimensions of the available ship and the flume, it is decided to use a length scale of 30, or:

$$n_L = 30$$

Larger scales (up to 1:10) were possible, but gave problems with model ship availability, too large forces and stiffness of the construction. Smaller scales were also possible, but this resulted in problems with the measurement instruments.

Height scale (vertical)

For the height scale 2 choices are possible: a non-distorted scale ($n_h = n_L$) or a distorted scale ($n_h \neq n_L$).

The main advantage of a non-distorted scale is the geometric equality between model and reality, which results in easy translation to reality, but also gives a correct flow pattern and force distribution. However, the correct scaling of sediment becomes difficult, and the boundary layers on the ship and bed will be incorrect (relatively larger in model than in reality, see [3.19] and [3.20]).

For a distorted scale, it would be logical to scale on the correct modelling of the boundary layer. This results (for a turbulent boundary layer) in a height scale of approximately 15.

$$n_h = n_L^{0.8} = (30)^{0.8} \approx 15.2$$

The advantage of the distorted scale is mainly the correct scaling of the boundary layer, which is important for the influence on the flow beneath ships and the interaction on the bed. This also results in more room between ship and bed, and in better sediment scaling. The disadvantages are the difficult translation to reality since there is no geometric equality, as well as the incorrect force distribution on the ship and flow field.

It is chosen to apply a non-distorted model, despite of the disadvantages. This means $n_h = n_L$, or:

$$n_h = 30$$

The application of a non-distorted model has some advantages, especially with the boundary layers and the sediment. However, the main disadvantage is that the flow field will be completely different since the model is no longer geometrically equal, which also results in a different force distribution on the ship, which is not directly comparable to reality. Since both phenomena are not completely known now, and the goal of the research is to investigate the effects of sailing close to the bed on safety and navigability, the force field and the forces are deemed more important. Also these parameters (forces and velocities) are measured during the experiments, so it is important to correctly reproduce these compared to reality. Therefore, a non-distorted scale is chosen. The incorrect scaling of the boundary layers compared to reality hopefully can be shown correctly later on by means of a numerical model.

Velocity scaling

For the scaling of the velocity either Froude scaling ([3.3]) or Reynolds scaling ([3.6]) can be applied. It is chosen to scale with Froude, so the water movement around the ship is reproduced correctly. In the model the flow will still be in the turbulent regime (Re > 3000). However, this does mean that the viscous friction in het model is relatively higher than in reality, and also the boundary layer development (which for a larger part will be in the laminar regime, see § 2.3) will not be modelled correctly. Applying Froude scaling results in the following velocity scale:

$$n_u = n_h^{0.5} = (30)^{0.5} \approx 5.5$$

Sediment scaling

For the scaling of the sediment, sediment diameters from the Waal river are applied. According to Lenselink (2011) and Bots (2011), the sediment diameter d_{50} is approximately 1 mm in large parts of the Waal. Therefore d_{50} = 1 mm is used for the prototype situation.

For the scaling of the sediment, a choice can be made between scaling according to Shields or according to Engelund-Hansen. The difference between both methods, with n_L = 30, is very small:

Shields: $n_d = \frac{n_L}{0.29} = \frac{30}{0.29} \approx 103.4$; Engelund-Hansen: $n_d = \frac{n_L}{0.24} = \frac{30}{0.24} = 125$

As it turns out, both scaling methods result in far too small sediment diameters (less than 10 µm). Even if the roughness-scale is neglected in equations [3.13] and [3.15] (so n_C = 1, leading to $n_d = n_L$ = 30), the sediment is still too small, since the critical Shields-values with these sediment diameters are a lot higher than the critical Shields-value of the prototype sediment. This will result in a smaller sediment transport in the model compared to the reality. Therefore it is chosen to apply a sediment with d_{50} = 230 µm, which has approximately the same critical Shields-value as sediment with d_{50} = 1

mm. The sediment transport in the model is than still too low, approximately with a factor 11.7 (based on Engelund-Hansen), see [3.21].

$$\frac{n_{s,m}}{n_L^{\,2}\cdot n_t}=\frac{n_u^{\,5}\cdot\log\left(\frac{n_L}{n_d}\right)^{-3}\cdot n_d^{\,-1}}{n_L^{\,1.5}}=\frac{(30)^{2.5}\cdot\left|\log\left(\frac{30}{1/0.23}\right)^{-3}\right|\cdot\left(\frac{1}{0.23}\right)^{-1}}{30^{1.5}}\approx 11.7 \quad [3.21]$$

3.2 Facility, equipment and sediment

Flume

The experiments were carried out at Deltares, in the 'Water-Grond Goot'. This is a flume with a length of 50 m, a width of 2.4 m and a depth of 2 m, see Figure 16. At one end the flume is wider (5 m), which is used to damp the waves created by the start-up of the model ship.

Figure 16: Water-Grond Goot at Deltares

The flume is equipped with a (moving) measuring bridge and a towing facility (trolley). A model ship was hung in a frame beneath the trolley, which is connected to the moving measuring bridge. Due to the frame the model ship was fixed, which means it could not move vertically. In reality, ships will experience drawdown, which depends on (amongst others) sailing speed. For this research the drawdown is not relevant, but a fixed (although adjustable) underkeel clearance is, because it makes the interpretation of the results easier. Therefore it was simpler to fix the ship vertically.

Bottom

The flume was equipped with a false bottom, in order to be able to hide the equipment and cables for the measurement devices. This false bottom contained a section with sediments (moveable bed) to measure the impact of the flow beneath a ship on erosion/sedimentation patterns. The false bottom is also necessary because the flume needs a higher water level in order for the pumps to work correctly, so they can reach the necessary discharge for the required flow velocity during the experiments.

Therefore, a false bottom was created with plates, mounted on a wooden framework which in turn is fixed on Stelcon-plates, lying on concrete beams. Because of the availability of Stelcon-plates only 16 m in the flume could be heightened. The height of this construction is 0.835 m. This height was gradually achieved with a ramp (slope 1:5) on both sides. Due to flow transformations at the ramp (and at the constriction of the width) some distance is necessary to the measuring section. This gives the flow some time (and length) to adapt itself to the new situation.

The measuring section was 9 meter long and consists of a moveable bed (which was used in the experiments with sediments) of 6 m long and a part where all the measurement instruments are located. The devices are located on or near the sailing line of the vessel in order to derive a complete picture of the pressures and velocities beneath a sailing ship. The sediment section is placed before the measurement area, so return flow and ambient flow (which is directed opposite to the sailing direction) do not cause sediments to flow towards the measurement devices. The moveable bed was also used to create a dune profile for the experiments. The bottom was easy adjustable, since different bottom configurations (flat bed with/without sediment, dunes, sloping bed) were studied.

The design of the flume, with distances and instruments, can be found in Appendix A.

Ship

From previous experiments a model ship was already available at Deltares. This ship has a length of 3 m, a width of 0.56 m and a maximum draught of approximately 0.35 m. In order to simulate a conventional inland vessel, the bow of the model ship was modified. With a ship plan of a conventional inland vessel the bow, which was made of foam, was adapted. After the experiments with a conventional bow were done, the bow was adjusted to simulate a push-tow barge, see Figure 17. This bow was modelled after a Europa II-a barge. More information can be found in Appendix A.

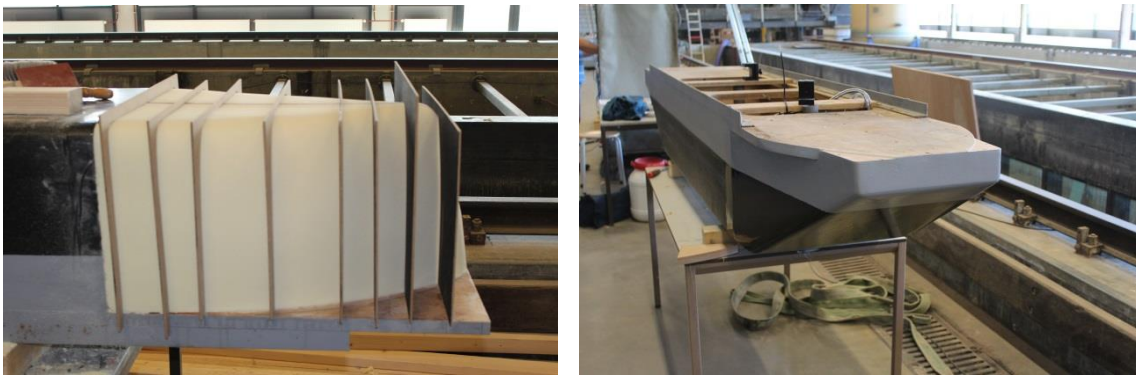

Figure 17: Model ship with conventional bow (left) and a barge bow (right)

As mentioned above, the ship was fixed in a frame. On the connection between the ship and the frame, two force meters measured the forces on the ship, in three directions. The difference between the force meters gives the momentum on the ship. Later on, these forces can be used to calculate the ship movements (not part of this research). Before each test the model ship was loaded with weights to counteract the water forces, so the forces on the ship before the experiments were nearly zero.

Although the ship is fixed vertically, the underkeel clearance is adjustable by two screw-threaded rods. These rods were fixed on the force meters, and by adjustable screw nuts on the rod the ship could be lowered or raised to obtain the required underkeel clearance. A ruler shows the actual underkeel-clearance, also see Figure 18.

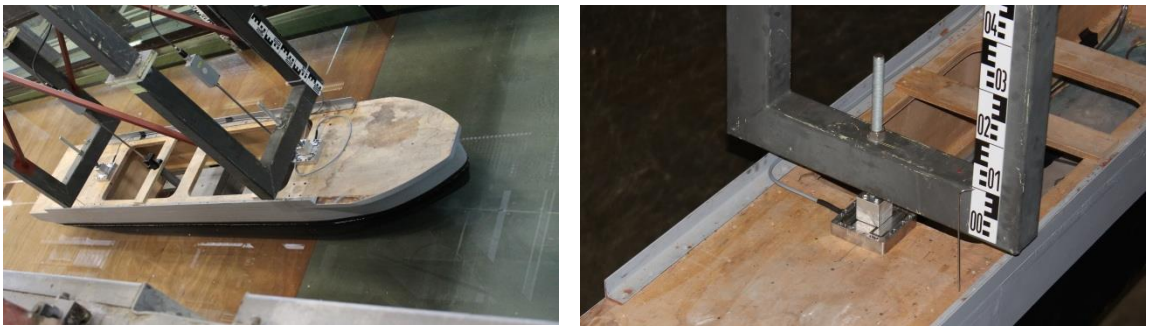

Figure 18: Model ship in frame (left), detail of force meter and ruler for underkeel clearance (right)

Instruments

Besides the force meters, the ship also is equipped with measurement instruments in the keel of the model ship. It contains two EMS-devices, which measured the velocity beneath the keel at two fixed distances from the bow. These EMS-devices were adjustable in height, so they could also be used to establish a vertical velocity profile. Furthermore, four PDCR-instruments measured the pressure at the keel, also at fixed distances from the bow. With a frequency of 30 Hz the measurements were saved at a computer on the moving measuring bridge.

In the false bottom also some measurement instruments were installed. Three specially made flat-headed EMS-devices measured the velocities at the bed, while six DP-cells measured the pressure differences compared to a reference level. One of these cells was placed outside the sailing area as a control device. Furthermore an extra EMS-device was placed in the flume to measure the ambient flow velocity. Two extra pressure sensors (one at the beginning, one at the end) measured the waterdepth and eventual waves created at the start-up of the model ship. All these instruments also measured with a frequency of 30 Hz. The measurements of the instruments in the flume were gathered by a computer besides the flume.

The data of the ship and the data of the flume were separately saved. To synchronize the signals two pulses were introduced at the beginning and the end of the measurement area. Once the measurement bridge passes these points, a pulse was send to both computers. Later on the data of both computers was synchronized by making sure the pulses overlap in time. This way, the exact position of the ship in the flume is deduced from the pulses and the sailing velocity.

More information about the placement of the instruments, and on the instruments itself, can be found in Appendix A.

Weir

To ensure a correct waterdepth and flow velocity in the flume, an adjustable weir was placed at the end of the flume. It is a sharp weir over the entire width of the flume, also known as a Rehbock-weir. The relation between water depth and discharge for a Rehbock-weir is given by [3.22], in which a is the height of the weir crest and h_k is the water depth in the flume above the weir crest.

$$Q = m \cdot \left(\frac{2}{3}\right)^{\frac{3}{2}} \cdot g^{\frac{1}{2}} \cdot B \cdot h_e^{3/2}$$

$$m = 1.045 + 0.141 \cdot \frac{h_e}{a} \qquad [3.22]$$

$$h_e = h_k + 0.0012$$

With these formulas the necessary weir heights can be calculated per water depth/flow velocity combination, since the discharge through the flume (and thus over the weir) is a function of the water depth and the flow velocity (and the fixed width). The weir was adjustable by placing/removing other beams on top of the weir, in order to reach the required weir height. Behind the weir two pumps pump the water back into the reservoir, so the water level behind the weir remains lower than the weir crest. For an impression, see Figure 19.

Figure 19: Weir and pumps before tests (left) and in action (right)

Sediments

For the moveable bed approximately 1.5 m^3 of sand was used. It consisted of quartz sand, with a d_{50} of approximately 230 µm. The sieve curve can be found in Appendix A.

During some experiments a small line with red sediment was laid in the flume. The goal of this line was to show the direction of sediment transport underneath a sailing vessel. Before this sediment could be used, it first had to be sieved, since it was too coarse. A sieve of 350 µm was applied, and the remnant of this sieve was used to create the red lines.

Wave reduction

Due to the start-up of the ship some initial waves were created in the flume. During the measuring this may lead to unwanted extra pressures or velocities after reflection of the waves at the end of the flume. To prevent this effect, wave damping was applied at the end of the flume. This also damped the waves after a run, in order to reduce the necessary waiting time between runs. Wave reduction was achieved by placing a screen at the sudden widening of the flume (to ensure a smooth transition and suppress the reflection of the translation waves), and by placing wave energy dissipation boxes (see Figure 20) over the entire width at the beginning of the flume. These boxes also reduced the turbulence of the water intake valve.

Figure 20: Wave reduction screen (right) and wave energy dissipation box (left)

More information on the design of the flume, the placement of the instruments, the measurement instruments and other model design aspects can be found in Appendix A.

3.3 Conditions to be simulated

River conditions

Rijkswaterstaat wants the experiments to cover a wide range of river circumstances. Therefore, the conditions on the Dutch rivers were translated to some dimensionless parameters, which needed to be covered during the experiments. The conditions on the Dutch rivers are given in Table 1, also see Sieben (2014).

River		Normative ship			Fairway				
		B_S [m]	L_S [m]	T [m]	B [m]	*fairway width [m]*	*Minimal draught [m]*	h [m]	U_0 [m/s]
Waal	general barges	22.8 22.9	135 193	4.5	260	150	2.80	5.0	1.1
Lek	general barges	22.8 22.9	135 116.5	3.5	150-230	80-130	3.15	5.3	0.3
Neder-Rijn	general barges	17.7 17.7	135 110	3.5	100-150	70-80	3.50	4.5	0.4
Boven-Merwede	general downbound upbound	23.5 34.4 22.9	200 153 229.5	3.5	450	200	4.50	6.0	0.6
Ijssel		12	110	3.5	70-180	40-60	2.5	4.0	0.7
Maas		17.5	193	3.0	50-140	46-130	3.0	3.0	0.2

Table 1: Order of magnitude parameters Dutch rivers

The following dimensionless parameters are introduced: the relative draught δ [3.23], the ship's relative cross-sectional area α [3.24] and the relative sailing speed β [3.25].

$$\delta = \frac{h}{T} \qquad [3.23]$$

$$\alpha = \frac{A_S}{A_C} = \frac{B_S / B}{\delta} \qquad [3.24]$$

$$\beta = \frac{V_S}{U_0} \qquad [3.25]$$

Since the ship was fixed during the experiments, and thus UKC is controlled, rather than the draught, the use of the parameter δ is not completely correct. Therefore a new parameter, the relative keel clearance γ, is introduced, see [3.26]. The relative keel clearance applies to a sailing ship (due to the squat of the vessel), while the relative draught applies to a ship that is at rest.

$$\gamma = \frac{h}{h - UKC} \qquad [3.26]$$

When applying a minimal underkeelclearance of 0.3 m (which is not uncommon for the Dutch rivers) and setting the maximum sailing speed $V_{S,max}$ at 90% of the limit velocity according to Schijf, the following values were obtained for the dimensionless parameters, see Table 2. For δ the fairway depth has been used, divided by the draught of a normative ship (except for the Maas, here the minimal UKC has been applied).

River	γ	δ	α	$V_{S,max}$	β
Waal	1.06	1.11	0.08	4.1	3.7
Lek	1.06	1.51	0.09 – 0.14	3.4 – 4.1	13.7
Neder-Rijn	1.07	1.29	0.11 – 0.17	3.0 – 3.6	9
Boven-Merwede	1.05	1.71	0.05 – 0.07	4.3 – 5.2	8.7
Ijssel	1.08	1.14	0.06 – 0.16	2.9 – 3.9	5.6
Maas	1.11	1.11	0.11 – 0.32	1.7 – 2.9	14.5

Table 2: Values of dimensionless parameters on Dutch rivers

As a result, Rijkswaterstaat requests the following range for the experiments:

- Relative keel clearance γ 1.4 – 1.02
- Relative sailing speed β 3.5 – 15

Flume conditions

In the flume the following parameters are fixed:

- Maximum discharge Q_{max} = 180 l/s
- Width flume B = 2.4 m
- Beam ship B_S = 0.56 m

On the other hand, the waterdepth and relative keel clearance can be varied:

- Waterdepth h 0.15 m, 0.20 m, 0.25 m, 0.30 m, 0.35 m, 0.40 m, 0.45 m and 0.50 m
- Relative keel clearance γ 1.4 , 1.3 , 1.2 , 1.1 , 1.05 , 1.03 and 1.02

Since the dimensions of the flume are fixed, the relative ship's cross-sectional area depends only on the relative keel clearance γ, see Table 3.

γ	**1.40**	**1.30**	**1.20**	**1.10**	**1.05**	**1.03**	**1.02**
α	0.17	0.18	0.19	0.21	0.22	0.23	0.23

Table 3: Relative ship's cross-sectional area

Maximum flow velocity

The maximum flow velocity in the flume depends on the possible discharge through the flume and the waterdepth. Since the maximum discharge is approximately 180 l/s, the maximum flow velocity depends only on the waterdepth, see Table 4.

h [m]	**0.15 m**	**0.20 m**	**0.25 m**	**0.30 m**	**0.35 m**	**0.40 m**	**0.45 m**	**0.50 m**
U_{max} *[m/s]*	0.50	0.38	0.30	0.25	0.21	0.19	0.17	0.15

Table 4: Maximum flow velocity in the flume

Maximum sailing velocity

The maximum absolute sailing velocity V_A (compared to the surrounding water, so not compared to the bed, see [3.27]) is set at 90% of the limit velocity according to Schijf (1949). The limit velocity varies with the waterdepth and the relative keel clearance, see Table 5.

$$V_A = V_S - U_0 \qquad [3.27]$$

	V_A [m/s]							
γ	**h =** *0.15 m*	*0.20 m*	*0.25 m*	*0.30 m*	*0.35 m*	*0.40 m*	*0.45 m*	*0.50 m*
1.40	0.57	0.65	0.73	0.80	0.86	0.92	0.98	1.03
1.30	0.55	0.63	0.71	0.77	0.83	0.89	0.95	1.00
1.20	0.53	0.61	0.68	0.74	0.80	0.86	0.91	0.96
1.10	0.50	0.58	0.65	0.71	0.77	0.82	0.87	0.92
1.05	0.49	0.56	0.63	0.69	0.75	0.80	0.85	0.89
1.03	0.48	0.56	0.62	0.68	0.74	0.79	0.84	0.88
1.02	0.48	0.55	0.62	0.68	0.73	0.78	0.83	0.88

Table 5: Maximum absolute sailing velocity in the flume (90% of limit velocity according to Schijf)

Maximum draught

The maximum (imposed) draught of the modelship is 0.35 m. However, at the bow the water will be 'pushed' up, causing the 'draught' at the bow T_{bow} to be higher than the imposed draught (which is equal to h – UKC). To prevent the model ship to take in water the draught at the bow needs to be lower than 0.35 m. The draught at the bow can be determined with the method of Bouwmeester (1977), which is able to calculate the headwater height (η) at the bow (see § 2.1). Then the draught at the bow, T_{bow} , is given by [3.28].

$$T_{bow} = T + \eta \qquad [3.28]$$

Applying this at different waterdepths and relative keel clearance, gives the results from Table 6. The configurations which are not possible due to the exceeding of the maximum draught are crossed out.

	T_{bow} [m]							
γ	**h =** *0.15 m*	*0.20 m*	*0.25 m*	*0.30 m*	*0.35 m*	*0.40 m*	*0.45 m*	*0.50 m*
1.40	0.12	0.15	0.19	0.23	0.27	0.31	0.35	~~0.38~~
1.30	0.12	0.17	0.21	0.25	0.29	0.33	~~0.37~~	~~0.41~~
1.20	0.13	0.18	0.22	0.27	0.31	~~0.36~~	~~0.40~~	~~0.45~~
1.10	0.15	0.20	0.24	0.29	0.34	~~0.39~~	~~0.44~~	~~0.49~~
1.05	0.15	0.21	0.26	0.31	~~0.36~~	~~0.41~~	~~0.46~~	~~0.51~~
1.03	0.16	0.21	0.26	0.31	~~0.37~~	~~0.42~~	~~0.47~~	~~0.52~~
1.02	0.16	0.21	0.26	0.32	~~0.37~~	~~0.42~~	~~0.48~~	~~0.53~~

Table 6: Draught at the bow at different waterdepths and relative keel clearances

Minimum keel clearance UKC

For the keel clearance there is actually no minimum, but at a certain low value doing measurements will be very difficult. It is decided that the minimum keel clearance may not be lower than 0.01 m (rounded up). This means the following configurations are not possible, see Table 7.

	UKC [m]							
γ	***h =*** *0.15 m*	*0.20 m*	*0.25 m*	*0.30 m*	*0.35 m*	*0.40 m*	*0.45 m*	*0.50 m*
1.40	0.04	0.06	0.07	0.09	0.10	0.11	0.13	0.14
1.30	0.03	0.05	0.06	0.07	0.08	0.09	0.10	0.12
1.20	0.03	0.03	0.04	0.05	0.06	0.07	0.08	0.08
1.10	0.01	0.02	0.02	0.03	0.03	0.04	0.04	0.05
1.05	0.01	0.01	0.01	0.01	0.02	0.02	0.02	0.02
1.03	~~0.00~~	0.01	0.01	0.01	0.01	0.01	0.01	0.01
1.02	~~0.00~~	~~0.00~~	~~0.00~~	0.01	0.01	0.01	0.01	0.01

Table 7: Keel clearances at different waterdepths and relative keel clearances

Choices experimental program

Based on Table 6 and Table 7, the following two waterdepths are chosen: 0.3 m and 0.2 m. The primary waterdepth is 0.3 m, since this is the only waterdepth at which the entire range of γ (1.4 to 1.02) can be chosen. Furthermore this is a good waterdepth compared to the draught of the modelship. For the second waterdepth 0.2 m is chosen, since for the diversity the waterdepth may not be too close to 0.3 m (so 0.25 m and 0.35 m drop out), and a waterdepth of 0.4 m has too few possible configurations with respect to the relative keel clearance γ.

When for the ratio sailing speed/flow velocity (β) the values 3.5, 7, 10.5 and 14 are used, the sailing speed V_S (compared to the bed) and the flow velocity U_0 can be calculated from the maximum absolute sailing speed V_A (which is compared to the surrounding water of the vessel), see [3.29] and [3.30].

$$V_S = \frac{V_A}{1+\frac{1}{\beta}} \qquad [3.29]$$

$$U_0 = \frac{V_S}{\beta} \qquad [3.30]$$

Table 8 (h = 0.3 m) and Table 9 (h = 0.2 m) show the sailing speeds and flow velocities at different relative sailing speeds β, as a function of the relative keel clearance γ.

					β = 3.5		β = 7		β = 10.5		β = 14	
γ	**α**	**V_A**	**T**	**UKC**	**V_S**	**U_0**	**V_S**	**U_0**	**V_S**	**U_0**	**V_S**	**U_0**
[-]	**[-]**	**[m/s]**	**[m]**	**[m]**	**[m/s]**	**[m/s]**	**[m/s]**	**[m/s]**	**[m/s]**	**[m/s]**	**[m/s]**	**[m/s]**
1.40	0.17	0.80	0.21	0.09	0.62	0.18	**0.70**	**0.10**	0.73	0.07	**0.75**	**0.05**
1.30	0.18	0.77	0.23	0.07	0.60	0.17	0.68	0.10	0.71	0.07	0.72	0.05
1.20	0.19	0.74	0.25	0.05	*0.58*	*0.17*	0.65	0.09	0.68	0.06	*0.69*	*0.05*
1.10	0.21	0.71	0.27	0.03	**0.55**	**0.16**	0.62	0.09	**0.65**	**0.06**	0.66	0.05
1.05	0.22	0.69	0.29	0.01	0.54	0.15	**0.60**	**0.09**	0.63	0.06	**0.65**	**0.05**
1.03	0.23	0.68	0.29	0.01	**0.53**	**0.15**	0.60	0.09	**0.62**	**0.06**	0.64	0.05
1.02	0.23	0.68	0.29	0.01	0.53	0.15	0.59	0.09	0.62	0.06	0.63	0.05

Table 8: Sailing speeds and flow velocities at 0.3 m

					β = 3.5		β = 7		β = 10.5		β = 14	
γ	**α**	**V_A**	**T**	**UKC**	**V_S**	**U_0**	**V_S**	**U_0**	**V_S**	**U_0**	**V_S**	**U_0**
[-]	**[-]**	**[m/s]**	**[m]**	**[m]**	**[m/s]**	**[m/s]**	**[m/s]**	**[m/s]**	**[m/s]**	**[m/s]**	**[m/s]**	**[m/s]**
1.40	0.17	0.65	0.14	0.06	*0.51*	*0.15*	0.57	0.08	0.60	0.06	*0.61*	*0.04*
1.30	0.18	0.63	0.15	0.05	0.49	0.14	0.55	0.08	0.58	0.05	0.59	0.04
1.20	0.19	0.61	0.17	0.03	0.47	0.13	*0.53*	*0.08*	*0.55*	*0.05*	0.57	0.04
1.10	0.21	0.58	0.18	0.02	0.45	0.13	*0.51*	*0.07*	0.53	0.05	*0.54*	*0.04*
1.05	0.22	0.56	0.19	0.01	*0.44*	*0.13*	0.49	0.07	*0.52*	*0.05*	0.53	0.04
1.03	0.23	0.56	0.19	0.01	0.43	0.12	0.49	0.07	0.51	0.05	0.52	0.04
~~*1.02*~~	~~0.23~~	~~0.55~~	~~0.20~~	~~0.00~~	~~0.43~~	~~0.12~~	~~0.49~~	~~0.07~~	~~0.51~~	~~0.05~~	~~0.52~~	~~0.04~~

Table 9: Sailing speeds and flow velocities at 0.2 m.

The experiments must cover the entire range of γ (1.4 – 1.02) and β (3.5 – 14). Because not all experiments can be carried out, it is chosen to use the following values for the different parameters:

- Relative keel clearance γ [-] 1.4 (1.2) 1.1 1.05 1.03
- Sailing speed V_S [m/s] 0.75 0.70 0.65 0.60 0.55 0.50 0.45 0.40 0.35
- Flow velocity U_0 [m/s] 0.15 0.10 0.05 0.00

These (round) values are chosen, since otherwise at each experiment a lot of testing and adjusting is necessary to reach the correct values of each parameter, leading to a lot of downtime. With these values a broad range can be achieved, as will be shown by the table with the experimental program.

In Table 8 and Table 9 the chosen experiments are graphically displayed. There are four **first priority experiments** (bold and underlined), four **second priority experiments** (bold) and ten *third priority experiments* (italic and underlined). The third priority experiments contain a few more experiments which are not listed in the table:

- Experiments without flow: these experiments were performed with still water, to determine the influence of the flow velocity.
- Experiments with fixed V_S, U_0 and β: these experiments give insight into the effect of the keel clearance, when all other parameters are fixed.
- Experiments with lower sailing speeds: to make sure not all experiments are performed at 90% of the limit velocity, some extra experiments with lower sailing speeds were done (one extra experiment per keel clearance).

All these extra experiments are done to validate and support eventual models.

3.4 Test configurations

The experimental program can be divided into 6 different parts:

1. Flat bed, no sediment: this part was about the measuring of pressures, velocities and forces in different situations. There is no moveable bed.
2. Flat bed, sediment: besides measuring pressures, velocities and forces, also the effects of the ship on the moveable bed were measured. With a profile tracker (Dutch: profielvolger) the bed was measured before and after experiments to measure these effects.
3. Dunes, sediment: this part was done to determine the consequences of river bed profiles on vessels. Once again the bed was measured before and after an experiment. Also the pressures and forces were measured to see whether there is a difference compared to a flat bed profile.
4. Sloping bed: in this part mainly the forces on the ship due to a sloping bed (perpendicular to the sailing direction) were measured. Also a pressure distribution beneath the ship could be measured. These experiments were performed without sediment.
5. Flat bed, no sediment, barge: the bow of the vessel was adapted to simulate a barge, to see the differences between barges and conventional cargo ships.
6. Flat bed, sediment, barge: the effects of a passing barge on a moveable bed were studied in this part of the experiments.

The first priority experiments were done in all experimental parts. The second priority experiments were done in parts 1, 2, 4 and 5. The third priority experiments were only done in part 1.

Before the definitive program started, experiments were carried out to determine the possible keel clearances during the experiments. Because of possible unwanted effects at small underkeel clearances, in part 1 the experiments began with a larger keel clearance (0.1 m). Gradually the keel clearance was lowered. When unwanted effects occur such as vibrations or too high forces the experiment was stopped. The results from these experiments determined the keel clearances.

Besides these experiments also some experiments with a drift angle (1° and 2°) were done. Since these are not of interest during this research, they will not be addressed furthermore.

The planned experiment program, with the priorities, can be found in Appendix B.

Each test without sediment (test 1 – 40 and 53 – 68) was performed with 4 runs, in order to average eventual turbulence (ensemble averaging). Otherwise it would be possible that the instruments would mainly measure turbulence. By applying averaging these effects can be reduced.

Extra configurations

During some of these tests (2, 4, 5, 8, 9, 19, 20 and 37) it was tried to also determine the vertical velocity profile. This was done by lowering the two EMS-probes in the model ship. These tests therefore had extra runs, one run extra per different EMS-probe height.

The tests with sediment were done just once. Before and after these tests the bed level was measured with the bottom follower. Some tests (46, 51 and 71) were performed with 10 runs. The bed level then also was measured after the 10^{th} run, to show the effect of multiple passages on the bed. In between these runs the bed was not repaired.

Furthermore during a few sediment tests a line of red sediment was deposited on the bed. The difference in the line before and after the run showed the direction of sediment transport beneath the ship. This was done during tests 43, 48, 51, 52, 70 and 71.

3.5 Limitations during experiments

Due to unexpected problems/conditions during the experiments, not all of the planned experiments could be executed as desired. The following are worth mentioning:

- During the first experiments, it turned out the minimal keel clearance of 0.01 m was not possible, since the modelship (and its instruments in the keel) would then scrape over the false bottom. Due to a seam in the flume, the bottom of the flume was not completely horizontal and flat, but had a very slight angle. As a result near the seam the false bottom was slightly curved, and the minimal safe possible UKC there was equal to 0.015 m at the measurement instruments. Therefore, all experiments with 0.01 m underkeel clearance were adapted: some were cancelled; others were executed with a UKC of 0.02 m or 0.015 m. This means the consequences of sailing with the smallest keel clearances could not be measured.
- At large underkeel clearances, the sediment was not/barely moving due to the passage of the vessel. This was especially true for the experiments with a flat sediment bed. As a result, it was decided that the bed after the tests with larger underkeel clearances (0.05 m and 0.09 m) were not measured, if there seemed to be no immediate effect on the bed. This means the effects of larger underkeel clearances on erosion of the river bed remains unclear. Also, at some experiments during the phase with the flat bed, first the bed was roughened (applying turbulence and higher flow velocities) by the creation of ripples before the tests were done, to ensure more sediment transport during the passing of the vessel.
- Between the rebuilding of the flume and ship from a sloping bed to the experiments with the barge, EMS 1 in the bottom was damaged somehow. During the experiments with the barge (tests 61 – 72) it didn't detect x-velocities anymore. Because this was a special EMS (with a flat head instead of a curved head) it couldn't be fixed within the time frame left for the experiments. Therefore, for these experiments no x-velocity data is available on 0.1 m distance from the sailing line. As a result the determination of the transversal velocity distribution profile for barges is less accurate (see § 5.4).
- Due to time limitations, not all barge experiments with sediment could be executed. The time limitation occurred due to problems with the profile tracker, during configuration 2 and 3 (see § 3.4). It was decided to cancel experiments 69 and 72, because only small erosion occurred with these experiments with a conventional bow, and because it was deemed more important to establish the flow field/forces with a sloping bed and with a barge.

3.6 Realized experiments

Because of the limitations, the finally realized experiments deviate on some points from the planned experiments. The planned experiments are given in Appendix B, while the realized experiments can be found in Table 10. The table also shows which tests were conducted with a vertical velocity profile measurement, bed profile measurement, red sediment or with a drift angle.

No.	Experiment part	h *[m]*	V_s *[m/s]*	U_0 *[m/s]*	UKC *[m]*	Runs	γ [-]	β [-]	Remarks
1	Flat bed, no sediment	0.30	0.75	-0.05	0.090	4	1.43	15.0	
2	Flat bed, no sediment	0.30	0.70	-0.10	0.090	8	1.43	7.0	(1)
3	Flat bed, no sediment	0.20	0.50	-0.15	0.060	4	1.43	3.3	
4	Flat bed, no sediment	0.20	0.60	-0.05	0.060	8	1.43	12.0	(1)
5	Flat bed, no sediment	0.30	0.70	-0.05	0.050	7	1.20	14.0	(1)
6	Flat bed, no sediment	0.30	0.60	-0.15	0.050	4	1.20	4.0	
7	Flat bed, no sediment	0.20	0.55	-0.05	0.033	4	1.20	11.0	
8	Flat bed, no sediment	0.20	0.50	-0.10	0.033	7	1.20	5.0	(1)
9	Flat bed, no sediment	0.30	0.55	-0.15	0.030	7	1.11	3.7	(1)
10	Flat bed, no sediment	0.30	0.65	-0.05	0.030	4	1.11	13.0	
11	Flat bed, no sediment	0.20	0.55	-0.05	0.020	4	1.11	11.0	
12	Flat bed, no sediment	0.20	0.45	-0.10	0.020	4	1.11	4.5	
13	Flat bed, no sediment	0.30	0.65	-0.05	0.015	4	1.05	13.0	
14	Flat bed, no sediment	0.30	0.60	-0.10	0.015	4	1.05	6.0	
15	Flat bed, no sediment	0.20	0.50	-0.05	0.015	4	1.08	10.0	
16	Flat bed, no sediment	0.20	0.45	-0.10	0.015	4	1.08	4.5	
17	Flat bed, no sediment	0.30	0.50	-0.15	0.015	4	1.05	3.3	
18	Flat bed, no sediment	0.30	0.60	-0.05	0.020	4	1.07	12.0	
19	Flat bed, no sediment	0.30	0.75	0.00	0.050	7	1.20	-	(1)
20	Flat bed, no sediment	0.30	0.50	0.00	0.050	7	1.20	-	(1)
21	Flat bed, no sediment	0.30	0.70	0.00	0.030	4	1.11	-	
22	Flat bed, no sediment	0.30	0.50	0.00	0.030	4	1.11	-	
23	Flat bed, no sediment	0.30	0.65	0.00	0.015	4	1.05	-	
24	Flat bed, no sediment	0.30	0.50	0.00	0.015	4	1.05	-	
25	Flat bed, no sediment	0.20	0.60	0.00	0.033	4	1.20	-	
26	Flat bed, no sediment	0.20	0.40	0.00	0.033	4	1.20	-	
27	Flat bed, no sediment	0.20	0.55	0.00	0.020	4	1.11	-	
28	Flat bed, no sediment	0.20	0.40	0.00	0.020	4	1.11	-	
29	Flat bed, no sediment	0.20	0.55	0.00	0.015	4	1.08	-	
31	Flat bed, no sediment	0.30	0.50	-0.05	0.090	4	1.43	10.0	
32	Flat bed, no sediment	0.30	0.50	-0.05	0.050	4	1.20	10.0	
33	Flat bed, no sediment	0.30	0.50	-0.05	0.030	4	1.11	10.0	
34	Flat bed, no sediment	0.30	0.50	-0.05	0.015	4	1.05	10.0	
35	Flat bed, no sediment	0.30	0.50	-0.05	0.020	4	1.07	10.0	
36	Flat bed, no sediment	0.30	0.45	-0.15	0.090	4	1.43	3.0	
37	Flat bed, no sediment	0.30	0.40	-0.05	0.050	7	1.20	8.0	(1)
38	Flat bed, no sediment	0.30	0.35	-0.05	0.030	4	1.11	7.0	
39	Flat bed, no sediment	0.30	0.40	-0.10	0.015	4	1.05	4.0	

No.	Experiment part	h *[m]*	V_s *[m/s]*	U_0 *[m/s]*	UKC *[m]*	Runs	γ [-]	β [-]	Remarks
40	Flat bed, no sediment	0.30	0.35	-0.05	0.015	4	1.05	7.0	
41	Flat bed, sediment	0.30	0.75	-0.05	0.090	1	1.43	15.0	
42	Flat bed, sediment	0.30	0.55	-0.15	0.030	1	1.11	3.7	(2)
43	Flat bed, sediment	0.30	0.55	-0.15	0.015	1	1.05	3.7	(2), (4)
44	Flat bed, sediment	0.30	0.65	-0.05	0.030	1	1.11	13.0	
45	Flat bed, sediment	0.30	0.65	-0.05	0.015	1	1.05	13.0	
46	Flat bed, sediment	0.30	0.60	-0.10	0.020	10	1.07	6.0	(3)
47	Flat bed, sediment	0.30	0.50	-0.15	0.012	1	1.04	3.3	(2)
48	Dunes, sediment	0.30	0.50	-0.15	0.020	1	1.07	3.3	(2), (4)
49	Dunes, sediment	0.30	0.70	-0.10	0.090	1	1.43	7.0	
50	Dunes, sediment	0.30	0.55	-0.15	0.030	1	1.11	3.7	(2)
51	Dunes, sediment	0.30	0.65	-0.15	0.010	10	1.03	4.3	(3), (4)
52	Dunes, sediment	0.30	0.60	-0.05	0.020	1	1.07	12.0	(4)
53	Sloping bed	0.30	0.75	-0.05	0.102	4	1.52	15.0	
54	Sloping bed	0.30	0.70	-0.10	0.102	4	1.52	7.0	
55	Sloping bed	0.30	0.55	-0.15	0.042	4	1.16	3.7	
56	Sloping bed	0.30	0.65	-0.05	0.042	4	1.16	13.0	
57	Sloping bed	0.30	0.65	-0.05	0.027	4	1.10	13.0	
58	Sloping bed	0.30	0.60	-0.10	0.027	4	1.10	6.0	
59	Sloping bed	0.30	0.50	-0.15	0.022	4	1.08	3.3	
60	Sloping bed	0.30	0.60	-0.05	0.022	4	1.08	12.0	
61	Flat bed, no sediment, barge	0.30	0.75	-0.05	0.090	4	1.43	15.0	
62	Flat bed, no sediment, barge	0.30	0.70	-0.10	0.090	4	1.43	7.0	
63	Flat bed, no sediment, barge	0.30	0.55	-0.15	0.030	4	1.11	3.7	
64	Flat bed, no sediment, barge	0.30	0.65	-0.05	0.030	4	1.11	13.0	
65	Flat bed, no sediment, barge	0.30	0.65	-0.05	0.015	4	1.05	13.0	
66	Flat bed, no sediment, barge	0.30	0.60	-0.10	0.015	4	1.05	6.0	
67	Flat bed, no sediment, barge	0.30	0.50	-0.15	0.015	4	1.05	3.3	
68	Flat bed, no sediment, barge	0.30	0.60	-0.05	0.020	4	1.07	12.0	
70	Flat bed, sediment, barge	0.30	0.55	-0.15	0.030	1	1.11	3.7	(2), (4)
71	Flat bed, sediment, barge	0.30	0.65	-0.15	0.015	10	1.05	4.3	(3), (4)
73	Flat bed, drift angle	0.30	0.60	-0.15	0.050	2	1.20	4.0	(5)
74	Flat bed, drift angle	0.30	0.60	-0.15	0.050	2	1.20	4.0	(6)
75	Flat bed, drift angle	0.30	0.55	-0.15	0.030	2	1.11	3.7	(5)
76	Flat bed, drift angle	0.30	0.55	-0.15	0.030	2	1.11	3.7	(6)
77	Flat bed, drift angle	0.30	0.65	-0.05	0.030	2	1.11	13.0	(5)
78	Flat bed, drift angle	0.30	0.65	-0.05	0.030	2	1.11	13.0	(6)
79	Flat bed, drift angle	0.30	0.75	-0.05	0.090	2	1.43	15.0	(5)
80	Flat bed, drift angle	0.30	0.75	-0.05	0.090	2	1.43	15.0	(6)
81	Flat bed, drift angle	0.30	0.65	-0.05	0.015	2	1.05	13.0	(5)
82	Flat bed, drift angle	0.30	0.65	-0.05	0.015	2	1.05	13.0	(6)
83	Flat bed, drift angle	0.30	0.60	-0.10	0.015	2	1.05	6.0	(5)
84	Flat bed, drift angle	0.30	0.60	-0.10	0.015	2	1.05	6.0	(6)

Table 10: Realized experiments

Remarks:

1. Vertical velocity profile measurement
2. Bed profile measurement
3. Bed profile measurement after run 1 and 10
4. Red sediment line applied during test
5. Drift angle 1°
6. Drift angle 2°

The experimental program is graphically displayed in Figure 21. This shows the range of values of γ and β that are covered with the experiments, as well as the approximate values on the Dutch rivers, as given by Rijkswaterstaat.

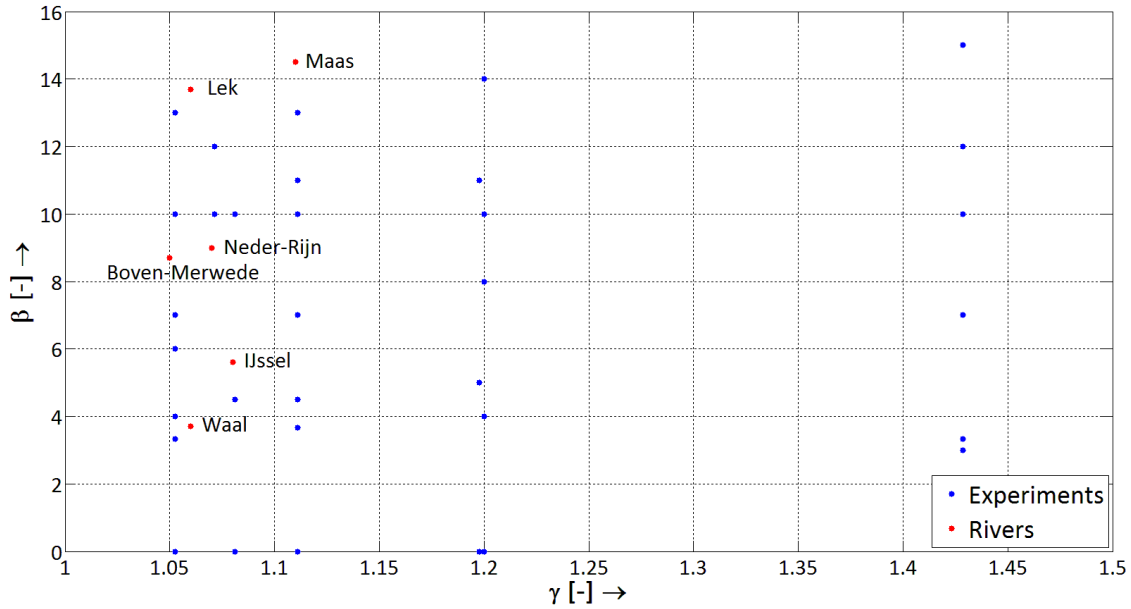

Figure 21: Range γ & β experiment program, including river values

4. Results of physical modelling

The aim of this chapter is to give an overview of the results of the model tests. First of all, the general flow field is described. Then the maximum occurring velocities will be analysed, and compared to the predictions of the current prediction methods. From this analysis a new prediction method for these maximum velocities is designed. Furthermore also the velocity distribution Is studied, as well as the qualitative aspects of the effects on the bed (erosion/sedimentation).

4.1 Data modification

Before the data of the experiments can be studied, some data modification was necessary. First of all, since there were two different stations where the measurements were collected, per run two data sets were available. In order to join them together into one dataset, the data of each station needs to be synchronized per run. Therefore, the data of both stations was shifted in such a way, that the pulses of both stations overlapped. This way the data is synchronized in time, so one dataset remains.

Secondly, ensemble averaging has been applied to join the different runs per experiment together. This has been done to cancel out turbulent fluctuations. Since there were only 4 runs per experiment, probably not all turbulent fluctuations will be cancelled out. To achieve that, a larger number of runs per experiment were necessary, which is very time-consuming. Although not all turbulent fluctuations are averaged out, the velocity profile obtained with ensemble averaging is more reliable.

Bed velocities

The zero-measurement of the EMS-devices in the bottom slowly shifts during the experiments. Therefore, each day the devices were calibrated on still water, to ensure a correct zero measurement. However, sometimes the calibration went difficult (when the devices had shifted too much), and as a result the measurement values of the EMS-devices at the start of the experiment needed to be checked. For EMS2 the measurements are shown in Figure 22. The velocity measurements (mean of measurements before the start of the ship) are given as a function of the ambient flow velocity.

It shows that especially for the experiments with 0 m/s and -0.10 m/s the measured velocities are incorrect. Therefore, a trendline is drawn through the measurements (disregarding the values for $U_0 \approx 0$). When the difference between the measured value and the trendline is more than 30%, the measurement values of that experiment are shifted towards the trendline. If the difference is less than 30% the measurements were not shifted, also see Figure 22.

This is done for all three EMS-devices, only in x-direction. (EMS1 and EMS3 have smaller differences).

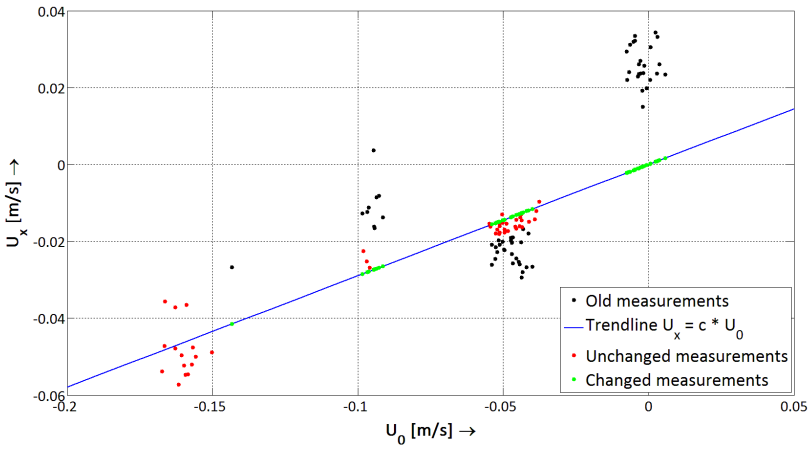

Figure 22: Bed velocity measurements before experiments for EMS2 and h = 0.30 m

Draught

Since the ship will be vertically fixed in the experiments, it will not experience squat. In reality however the ship will sink a little bit due to the water level depression around it. This water level depression is still present in the model when the ship is sailing. Therefore, the real draught in the model is lower than the draught which the (model) ship would have if it was lying still, see Figure 23.

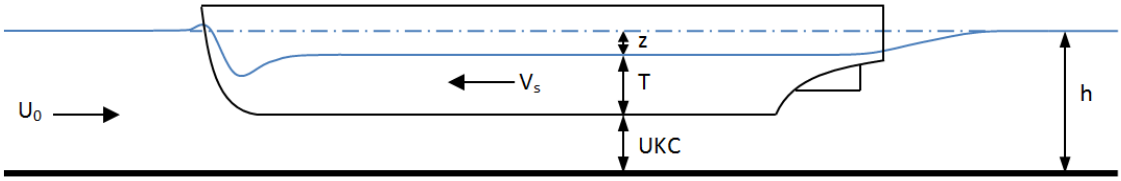

Figure 23: Vessel draught

The real draught in the model is:

$$T = h_0 - UKC - z \qquad [4.1]$$

In which the underkeel clearance (UKC) and the waterdepth (h_0) are fixed in the model, and the water level depression (z) is a function of sailing speed (V_S), channel cross-sectional area (A_C) and ship cross-sectional area (A_S). The water level depression will not be measured during the experiments, but may be estimated by the methods of Schijf and Bouwmeester. Another option is to predict the squat (S) of the vessel by means of the formulas of Barrass, Huuska or Römisch, and calculate the draught from there. Both methods require an iterative approach since the water level depression is a function of A_S, which depends again on the draught of the vessel. Therefore an initial draught will be assumed, after which the real draught will be determined by means of iteration on the water level depression (or the squat) and the draught. By applying this to all data, the draught per run is added to the data. Although the formula of Huuska is known to give better results, during the analysis of the results the method of Schijf is used to calculate the draught, since the method is also used for the determination of the return current.

Applying this to the realized experiments, the range of δ (h/T) turns out to be between 1.1 and 1.65. This is graphically displayed in Figure 24. The river values are obtained from Table 2. In this figure the range of the prediction methods has been graphically displayed at the top of the graph.

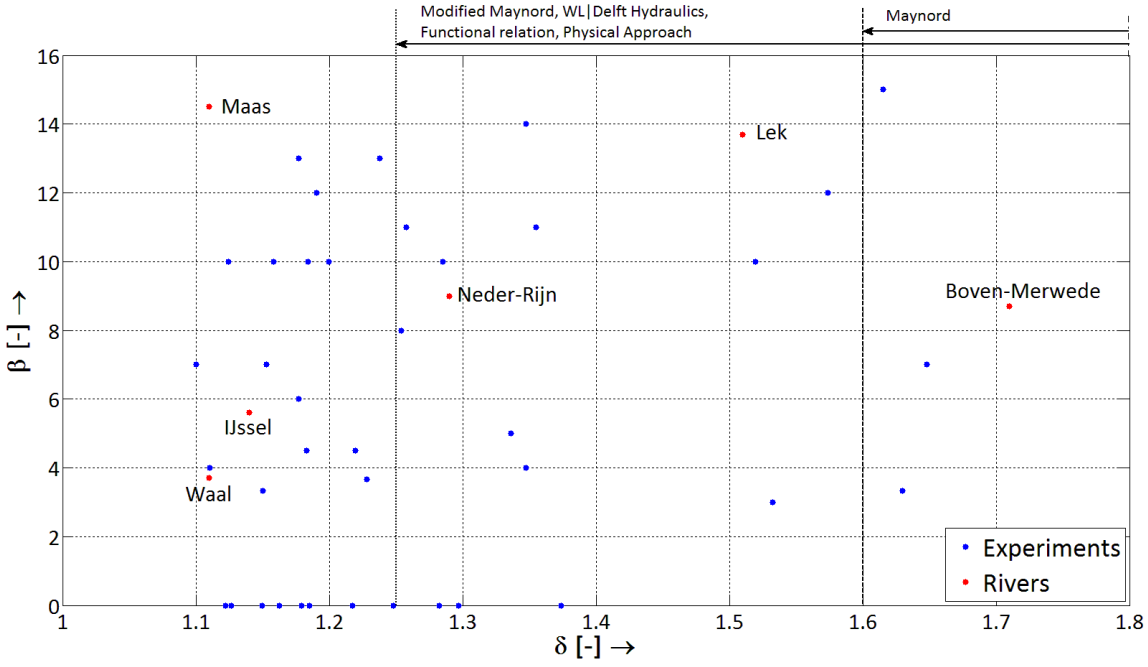

Figure 24: Range δ & β beta experiment program, including river values.

4.2 Qualitative flow description

Before the flow will be quantitatively analyzed, the flow is described with some simple graphs, to show the effect of the different parameters. This is done for both conventional vessels and barges.

Conventional vessel

Figure 25 and Figure 26 show the vector plots of the bottom EMS-devices of experiment 1 and 13. Note that the magnitude of the vectors may differ per graph, i.e. the magnitude of the vectors can't be compared per picture. The difference between these experiments is the keel clearance (0.09 m for experiment 1 and 0.015 m for experiment 13).

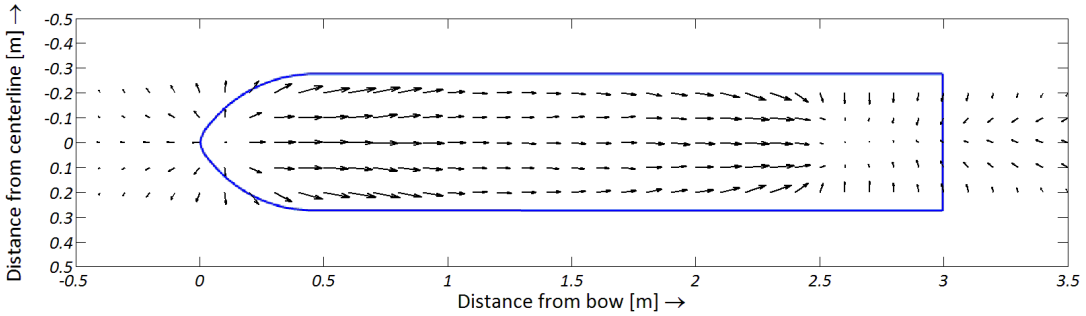

Figure 25: Vector plot of experiment 1 (V_S = 0.75 m/s, U_0 = -0.05 m/s, UKC = 0.09 m)

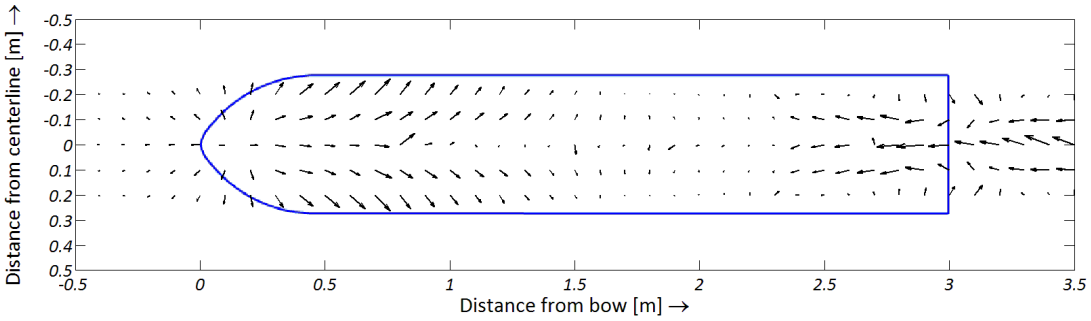

Figure 26: Vector plot of experiment 13 (V_S = 0.065 m/s, U_0 = -0.05 m/s, UKC = 0.015 m)

Two important differences can be distinguished between Figure 25 and Figure 26. First of all, the fanning-out effect is clearly visible in Figure 26. The flow tends to go sideways, out from under the keel. This is also visible, but far less pronounced, in Figure 25. Although the vector plots are only of the velocities at the bed (and therefore do not cover the entire distance between the bed and the keel of the ship), it seems the fanning-out effect increases with decreasing keel clearance.

The second important difference is in the through-flow beneath the keel. In Figure 25 the flow stays beneath the keel from bow to stern, although in the middle part the velocities somewhat decrease. However, at smaller underkeel clearance (Figure 26), there is almost no flow at the middle part of the ship; all flow is diverted to the sides of the vessel. It seems as if the boundary layers from the ship and the bed interact at this underkeel clearance. This is clearly not the case with an underkeel clearance of 0.09 m.

X-velocities

Figure 27 shows the x-velocities of the EMS-device in the sailing line of the vessel for different underkeel clearances. The x-coordinate is the distance along the ship from the bow of the ship.

As visible in Figure 27, there is a clear pattern in the velocities along the ship. Due to the approach of the vessel, the water before the bow of the ship is being 'pushed' forward, hence the increase in U_X. Immediately after passage of the bow the water is forced to go underneath the keel (or divert to the side), increasing the velocity underneath the bow. This leads to a maximum x-velocity approximately 0.4 m after passage of the bow. Due to a construction error in the model ship, the keel was

somewhat lower after 0.7 m, which led to higher velocities here (see Figure 27). In reality this is not expected since the keel usually is smooth, so this effect will not be taken into account furthermore.

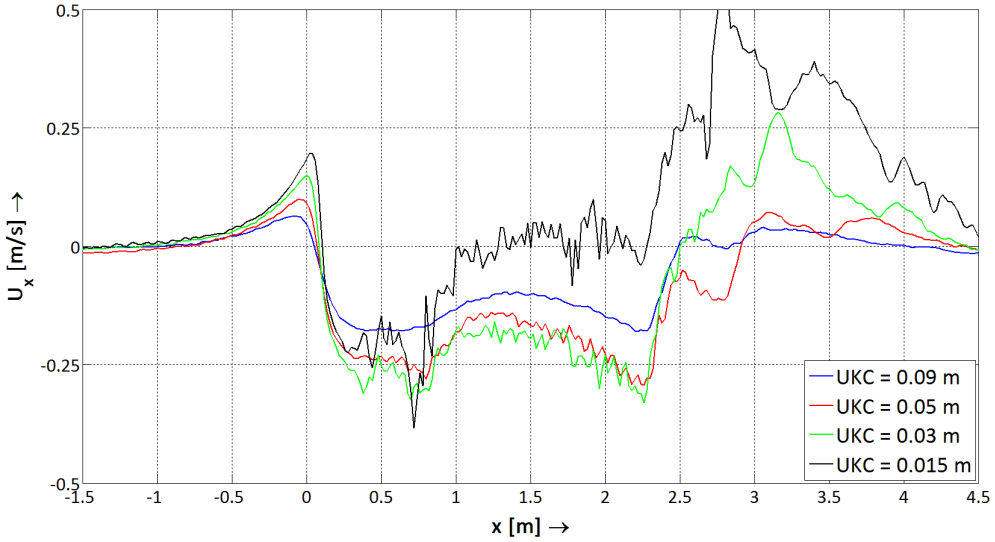

Figure 27: X-velocities of EMS2 for different UKC (with VS = 0.50 m/s, U_0 = -0.05 m/s, h=0.30 m)

After the maximum x-velocity has been reached, the velocity decreases again. After 1.5 m from the bow the x-velocity slightly increases again, before it drops when the keel clearance increases again around x = 2.3 m. In this region also the influence of the propeller becomes important (although not in the experiments, since no propeller was used). The flow reverses in this region, again following the ship (so positive values). These values increase with decreasing keel clearance.

Furthermore from Figure 27 it can be seen that a decreasing keel clearance results in higher flow velocities, although they seem to reduce again from approximately UKC = 0.03 m. Also, a decreasing keel clearance results in a faster velocity decrease after attaining the maximum x-velocity, and creates more turbulent fluctuations.

From Appendix C - Figure 1 it follows that the sailing speed V_S influences the amplitude of the x-velocity, not the trend. When the sailing speed is increased, the amplitude of the trend also increases.

At 2 points under the keel also a vertical profile is established, which is shown in more detail in § 4.5.

Y-velocities

Figure 28 shows the y-velocities of EMS3 (y = 0.2 m) for the same experiments as those in Figure 27.

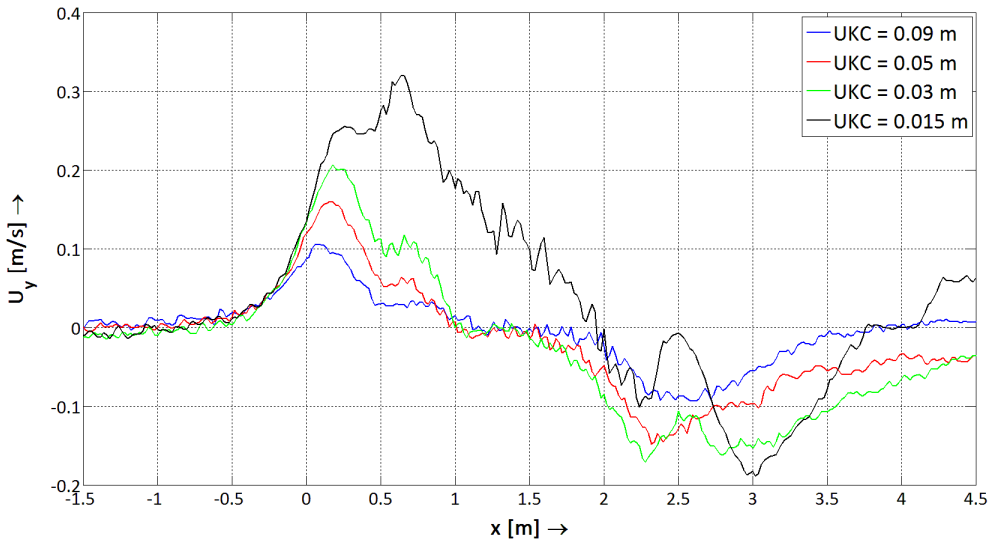

Figure 28: Y-velocities of EMS3 for different UKC (V_S = 0.50 m/s, U_0 = -0.05 m/s, h=0.30 m)

Figure 28 again shows a clear pattern, but now in y-velocities. The flow is diverted to the side of the vessel, even before the bow. The maximum y-velocity is reached at x ≈ 0.1 – 0.3 m. This coincides with the passing of the bow over EMS3, which means that the water that is pushed aside by the bow is responsible for this maximum y-velocity.

This maximum y-velocity depends on the underkeel clearance, and increases with decreasing keel clearance. After passage of the bow the y-velocity decreases but remains present, which proves the fanning-out effect beneath the hull. The fanning-out effect increases with decreasing keel clearance. Approximately halfway the ship, the flow reverses, and then water flows back underneath the ship. So here the fanning-out effect is reversed. This can be expected, since near the stern the keel clearance of the model ship increases.

However, for UKC = 0.015 m the maximum y-velocity is attained further away from the bow, near x = 0.6 m. This indicates that for very small underkeel clearances, the fanning-out effect is responsible for the largest y-velocities. With smaller underkeel clearances the fanning-out effect also occurs over a longer distance, so flow reversal happens further away from the bow.

Furthermore, Appendix C - Figure 2 shows that, as with x-velocities, the y-velocities increase with increasing sailing speed. Thus the sailing speed does not influence the trend, just the amplitude.

Barge

Figure 29 and Figure 30 show the vector plots of experiments 61 and 65, which have been carried out with a barge-type bow. Keep in mind that during these tests EMS1 (which was placed 0.1 m outside the centreline) broke down and did not register x-velocities correctly anymore. Therefore, the measurements of EMS1 are left out of these graphs. The contour of the ship is based on the intersection with the (still) water surface.

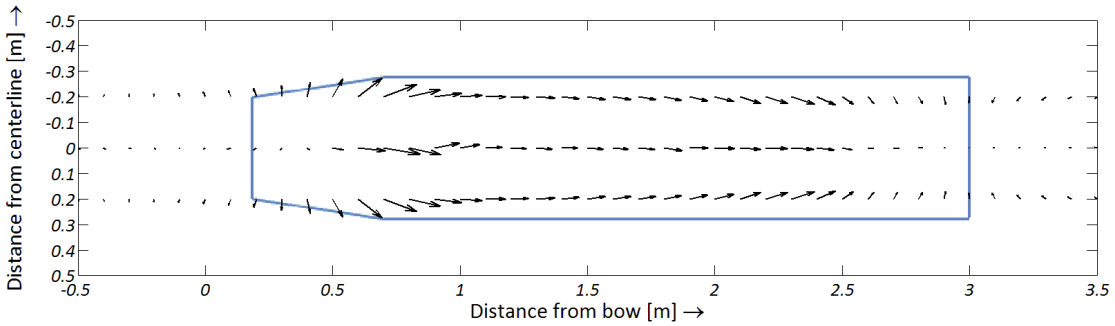

Figure 29: Vector plot of experiment 61 (V_S = 0.75 m/s, U_0 = -0.05 m/s, UKC = 0.09 m)

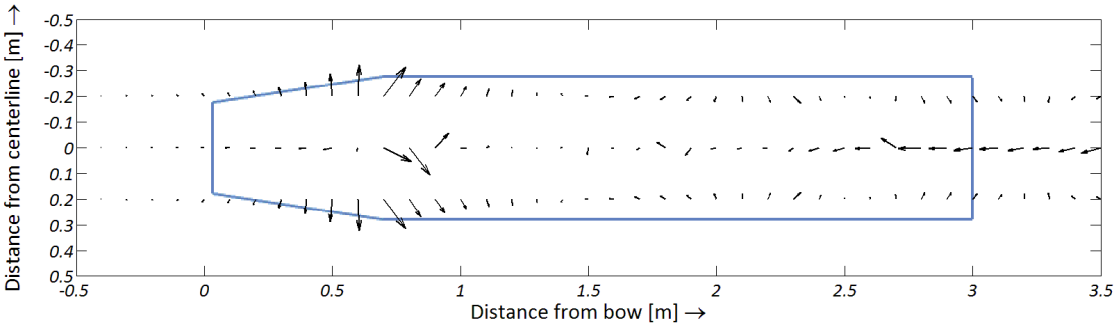

Figure 30: Vector plot of experiment 65 (V_S = 0.65 m/s, U_0 = -0.05 m/s, UKC = 0.015 m)

Figure 29 and Figure 30 show some similarity with Figure 25 and Figure 26, which were the vector plots for conventional ships. Again the flow is passing under the ship for a large underkeel clearance, while the flow seems to be obstructed with a small underkeel clearance. Due to this obstruction, the fanning-out effect is larger with smaller underkeel clearance.

However, there are also some differences: due to the bow shape the diversion of the flow occurs further away from the top of the bow. At the bow, the flow is forced downward, following the shape

of the bow, and then it is diverted to the sides. This means the largest y-velocities occur further away from the tip of the bow. Furthermore it seems that the flow is obstructed sooner (closer to the bow) compared to the conventional vessel.

X-velocities

Figure 31 shows the x-velocities for EMS2 during different experiments with barges. Before continuing it has to be pointed out that the peaks at x = 1.8 m are caused by interference between the EMS-devices in the bed and on the ship.

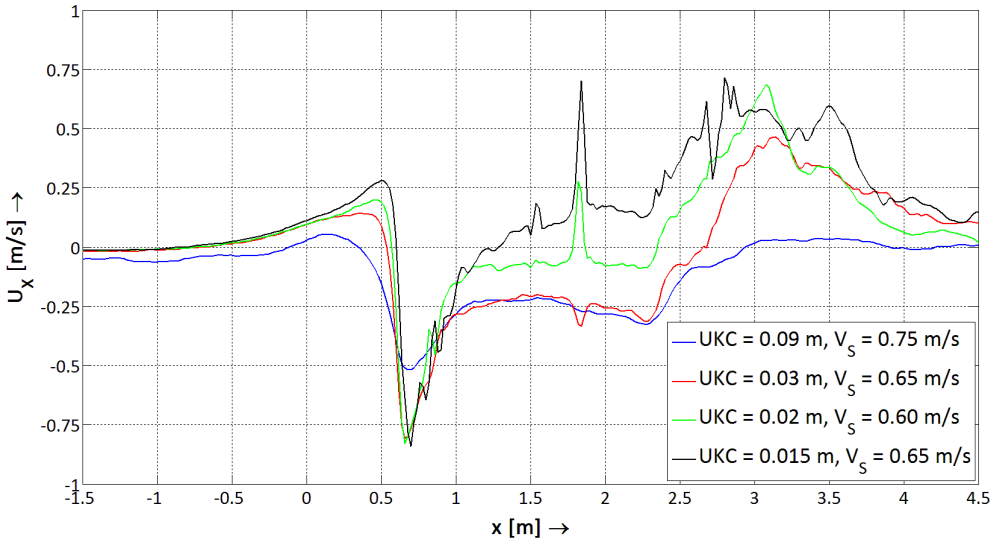

Figure 31: X-velocities for EMS2 for barge experiments (all with U_0 = -0.05 m/s and h = 0.30 m)

Figure 31 shows a clear velocity pattern. Immediately after the transition of the bow to the mid-ship (at x = 0.6 m) the maximum velocity is reached. The maximum velocity occurs always at the same point under the bow, independent of keel clearance or sailing velocity. This maximum velocity again increases with increasing keel clearance. After the maximum velocity is attained, the velocity decreases again. Compared to the velocity profile from a conventional vessel the velocity decreases more towards the stern. With conventional vessels the x-velocity around x = 2.3 m was approximately equal to the maximum velocity, now it is less. With keel clearances below 0.03 m the velocity decreases faster again, probably due to boundary layer interaction.

Y-velocities

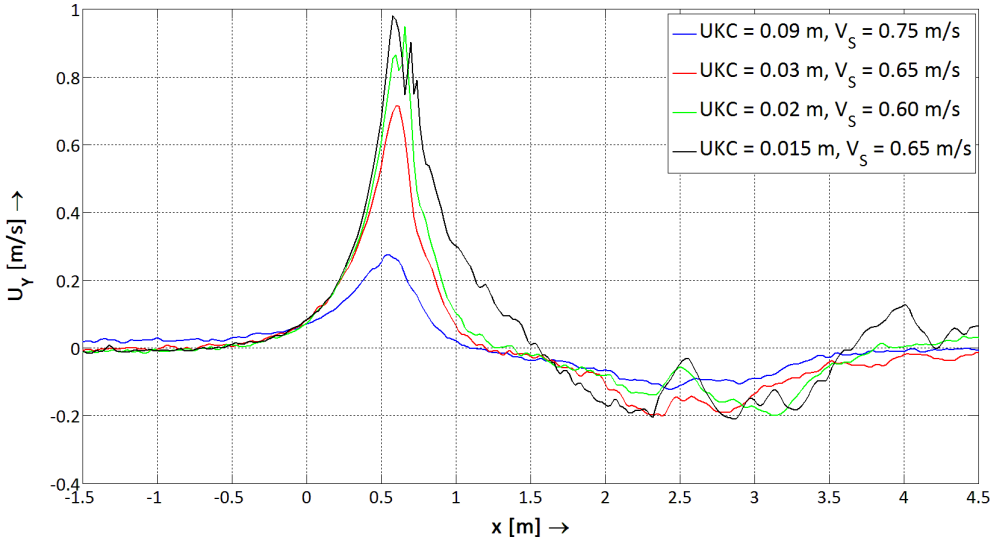

Figure 32: Y-velocities of EMS3 for barge experiments (all with U_0 = -0.05 m/s and h = 0.30 m)

Figure 32 shows the y-velocities underneath the keel at 0.2 m outside the sailing line. There is a clear peak, situated around x = 0.6 m, which coincides with the transition from bow to mid-ship. Apparently here the largest part of the flow is diverted to the sides. After this point, the y-velocity drops significantly, even reversing around x = 1.3 m for most cases. Only for UKC = 0.015 m there seems to be some fanning out underneath the bow, until the flow is blocked. After this point there is some fanning-in again towards the stern of the barge. This velocity profile is very different from the profile for conventional vessels (see Figure 28), especially in magnitude. The maximum occurring y-velocity is much higher for barges.

4.3 Existing prediction methods

For the comparison of different formulas or approaches, use is made of the R^2 and RMSE-parameter. The R^2-value (as calculated by [4.2]) indicates how good the data fits a model. It is a statistical measure of how well the model approximates the real data points. A perfect fit is realized when R^2 is equal to 1. The RMSE-value (as calculated by [4.3]) gives the mean (absolute) error of the data compared to the model. A RMSE of 0 means no errors.

$$R^2 = 1 - \frac{\sum_{i=1}^{n}\left(y_i - y_i\right)^2}{(n-1)\cdot \mathrm{var}\left(y_i\right)} \qquad [4.2]$$

$$RMSE = \sqrt{\frac{1}{n}\cdot\sum_{i=1}^{n}\left(y_i - y_i\right)^2} \qquad [4.3]$$

The comparison of the data to the prediction formulas can only be done for the maximum velocities, since the current methods can only predict maximum velocities beneath sailing vessels. For the comparison two maximum velocities are used: the maximum x-velocity and the maximum absolute (x, y) velocity. The methods are applied separately for conventional ship experiments and barges.

Conventional vessel

X-velocities

The results of the prediction methods, for x-velocities beneath conventional vessels, are given in Figure 33. The closer the points are to the black line, the better the prediction method is. This means the cluster of points of one method that lies closest to this line is the best prediction method.

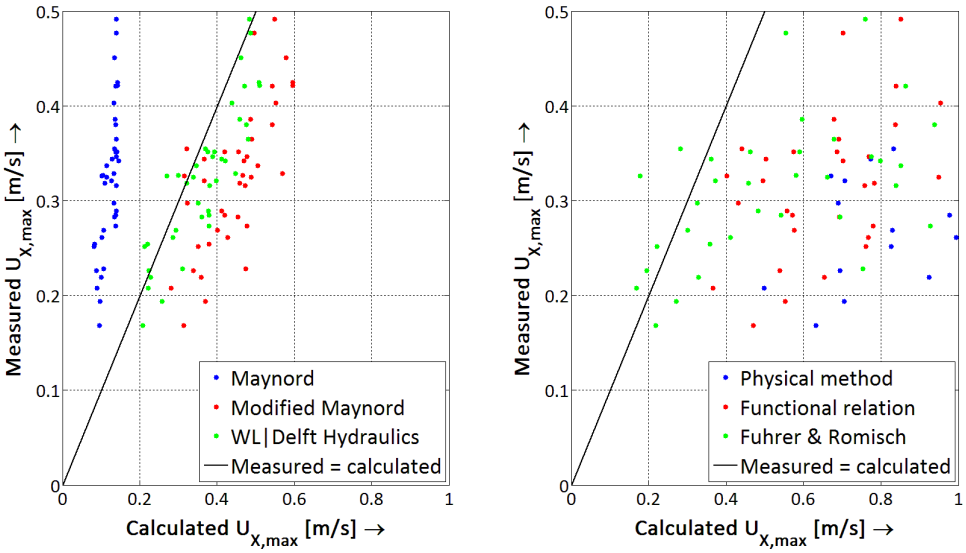

Figure 33: Results prediction formulas for experiments with conventional ships

As visible, not all formulas are equally accurate. Figure 33 (right) shows that both the physical approach and the functional relation considerably overestimate the maximum return current beneath the ship. The Führer & Römisch-equation has some good overlap with the measured data, but also shows values that deviate significantly from the measured data. The left graph of Figure 33 shows that the equation of Maynord underestimates the velocity. Both the Modified Maynord-equation and the WL|Delft Hydraulics formula correspond very well to the measured velocities. Modified Maynord slightly overestimates the flow velocity, and the WL|Delft Hydraulics formula seems to be the best fit for the model data. This is confirmed by the goodness of fit results in Table 11, where the WL|Delft Hydraulics formula clearly has the lowest R^2- and RMSE-value.

	X-velocity		Absolute velocity	
Method	R^2	*RMSE [m/s]*	R^2	*RMSE [m/s]*
Physical approach	-108.15	0.79	-212.66	1.51
Functional relation	-37.42	0.47	-126.68	1.17
Maynord	-6.69	0.21	-24.21	0.52
Modified Maynord	-2.23	0.14	-66.35	0.85
WL|Delft Hydraulics	0.36	0.06	-54.61	0.77
Führer & Römisch	-35.54	0.46	-116.59	1.12

Table 11: Goodness of fit prediction formulas for experiments with conventional ships

(X, Y)-velocities

In Table 11 also the goodness of fits are given when the prediction formulas are compared to the measured maximum absolute velocities. Now suddenly the formula of Maynord has the best fit, although the prediction is very poor and far from accurate. None of the methods give an accurate prediction. Compared to the prediction of maximum x-velocities, the prediction is far worse for absolute velocities. Apparently the prediction methods have been developed for x-velocities, rather than for absolute velocities.

Barges

X-velocities

When the prediction formulas are applied on the experiments with barges, Figure 34 is obtained.

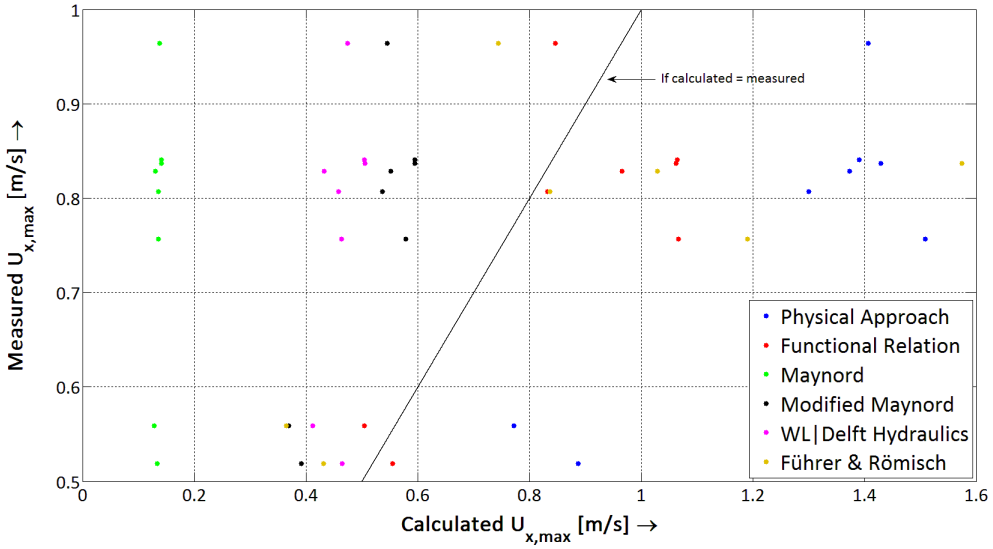

Figure 34: Results prediction formulas for experiments with barges

With barges larger x-velocities are measured at the bed, which leads to a different best prediction method. This can be seen in Figure 34 and Table 12, which gives the goodness of fit results of the prediction formulas for the barge experiments.

For barges the functional relation has the best goodness of fit and lowest RMSE, followed by the Modified Maynord equation and the WL|Delft Hydraulics formula. Compared to the conventional vessel experiments, the overall goodness of fit (of all formulas) is better, although the best goodness of fit is still achieved by the WL|Delft Hydraulics equation, applied to conventional ships. This is unexpected, since all methods have been developed for barges rather than for conventional ships, and they have been validated on experiments with barges, not with conventional vessels.

	X-velocity		Absolute velocity	
Method	R^2	*RMSE [m/s]*	R^2	*RMSE [m/s]*
Physical approach	-12.41	0.52	-54.60	2.35
Functional relation	-0.47	0.17	-37.54	1.96
Maynord	-19.77	0.64	-13.54	1.21
Modified Maynord	-2.30	0.26	-24.57	1.59
WL|Delft Hydraulics	-4.33	0.33	-22.41	1.52
Führer & Römisch	-8.99	0.45	-45.11	2.14

Table 12: Goodness of fit prediction formulas for experiments with barges

(X, Y)-velocities

The goodness of fits of the prediction formulas for the maximum absolute velocity is also given in Table 12. As with conventional vessels, the prediction is even worse, further reinforcing the claim that the prediction formulas are developed for x-velocities instead of absolute velocities.

Location maximum velocities

The locations under the ship where the maximum velocities occur depend on the type of ship and on the velocity type (x- or absolute velocity). The locations are given in Table 13.

		EMS 2	EMS 1	EMS 3
Method		*y = 0.00 m*	*y = 0.10 m*	*y = 0.20 m*
Conventional vessels	*X-velocity*	2/39	2/39	35/39
	Absolute velocity	0/39	2/39	37/39
Barges	*X-velocity*	8/8	0/8	0/8
	Absolute velocity	2/8	0/8	6/8

Table 13: Location of maximum velocities during experiments

For conventional vessels the maximum velocities occurred almost always at 0.2 m outside the sailing line. The bow shape forces the flow to the side, and then underneath the keel, resulting in larger flow velocities further away from the sailing line. For absolute velocities this effect is reinforced due to the influence of the fanning out.

For barges the largest x-velocity was always measured at the centreline of the ship. Due to the bow shape the flow is forced underneath the ship rather than to the sides. At the sides of the bow the flow is already diverted somewhat, leading to lower velocities further away from the sailing line. For absolute velocities the fanning-out effect becomes important again, leading to maximum velocities near the side of the barge (unless the fanning out effect is small due to large keel clearances, then the maximum absolute velocity is measured at the centreline).

The location where the maximum velocities occur is important, since the prediction formulas have been developed based on previous experiments, in which the velocity measurements were done in the sailing line of the ships (so at y = 0.00 m). However, for conventional vessels this is not the location of the maximum velocities, while for barges it is only the location for the maximum x-velocities. This could partly explain the differences between the prediction methods and the measurements. Comparison of the measured maximum x-velocities for conventional vessels at the centreline to the predicted values however results in even worse predictions (R^2 of for instance WL|Delft Hydraulics equation is -1.61 instead of 0.36). Therefore, it seems the current prediction methods do not accurately predict the maximum occurring velocities.

The approximate location of the maximum occurring velocities is graphically displayed in Figure 35.

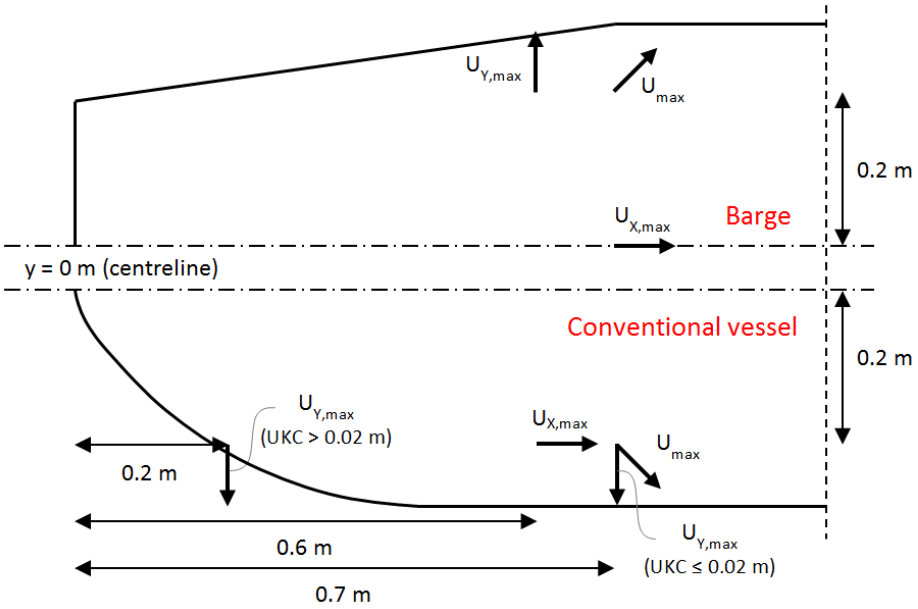

Figure 35: Approximate location of measured maximum velocities

Improvement of current prediction formulas

As shown above, the current prediction formulas are not able to predict the maximum x-velocities correctly. However, the methods of WL|Delft Hydraulics and Maynord (modified) (conventional vessels and barges) and the Functional Relation (barges) have shown to be acceptable. Therefore, the general form of these functions will be applied to the data from the experiments, and adapted with new coefficients. These coefficients can give insight into the dependence of the maximum x-velocity on the different parameters, and might also improve the application range of the formulas. Besides x-velocities, these methods are also adapted to predict maximum absolute velocities.

WL|Delft Hydraulics

The general WL|Delft Hydraulics equation is a linear relation between maximum velocity and return current, see [4.4]. In this formulation the return current U_R is calculated by the method of Schijf.

$$U_{X,max} = \alpha \cdot U_R \quad \text{or} \quad U_{max} = \alpha \cdot U_R \qquad [4.4]$$

Initially, experiments at WL|Delft Hydraulics (1984) showed that coefficient $\alpha \approx 1.5$ - 2. During their research, Stolker et al. (2006) proposed to change this to $\alpha \approx 1 - 5$. Finally, Lenselink (2011) found that $\alpha \approx 1.46$. For experiments with conventional ships a coefficient of 1.53 is found, see Figure 36.

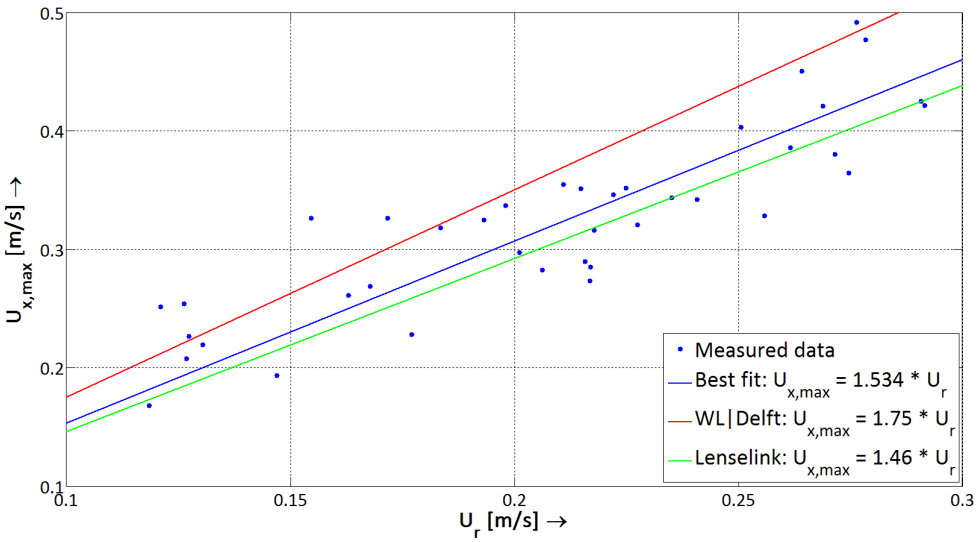

Figure 36: U_R versus $U_{x,max}$ for experiments with conventional ships

Table 14 shows the results of fitting the WL|Delft Hydraulics equation to the data, separately for conventional ships and barges, both for $U_{X,max}$ and U_{max}. The table also gives the minimum and maximum value for α (showing the bandwidth of the coefficients), as found by the experiments.

	Conventional ship		Barge	
Method	$U_{x,max}$	U_{max}	$U_{x,max}$	U_{max}
α	1.53	1.82	2.88	3.88
R^2	0.73	0.65	0.22	0.20
RMSE [m/s]	0.04	0.06	0.13	0.28
α (minimal)	1.26	1.41	1.95	1.98
α (maximal)	2.11	2.75	3.55	5.13

Table 14: Coefficients and goodness of fit for WL|Delft Hydraulics formula

This method seems reliable when using conventional ships (see R^2 and RMSE values), but less applicable for barges. This could also be due to the fact there were only 8 barge experiments, which is rather few for a good and accurate analysis.

The question remains whether the return current U_R indeed is a good parameter to base the maximum occurring velocity on. More discussion about this parameter will be given in § 4.4.

Maynord

The general form of the Maynord equation is given by [4.5]. The original equation of Maynord was later adapted (Modified Maynord) by Stolker et al. (2006) to improve the accuracy. Although the accuracy was improved, the predictions for the realized experiments are still very poor compared to the measured data. Therefore, a least-square fitting method with equation [4.5] on the experiment data is performed, leading to the results in Table 15.

$$\frac{U_{(X,)max}}{V_S - U_0} = \alpha \cdot \left(\frac{B_S}{h}\right)^{\beta} \cdot \left(\frac{T}{h}\right)^{\gamma} \qquad [4.5]$$

	Conventional ship		Barge	
Method	$U_{x,max}$	U_{max}	$U_{x,max}$	U_{max}
α	0.67	0.86	0.15	3.69
β	-0.07	0.13	3.73	-0.33
γ	0.74	1.77	1.59	3.25
R^2	0.73	0.73	0.76	0.89
RMSE [m/s]	0.04	0.05	0.07	0.10

Table 15: Coefficients and goodness of fit for equation of Maynord

In general it can be seen that coefficients α and γ are the most important for equation [4.5]. This can be explained by the fact that B_S/h is barely changed during the experiments. B_S was a fixed value, while only 2 waterdepths were used, resulting in just two B_S/h values. Therefore, the effect of this parameter remains relatively unknown, although it can be said that it is far less important than T/h (also see Stolker et al. (2006)).

The results with this equation are reasonable, but unfortunately the different coefficients are very different for each configuration. Therefore, the method is not very easy in use. In Appendix D an approach is given in which some coefficients are kept equal for different configurations, including the results of this approach. This approach significantly increases simplicity and still results in similar accuracy (slightly less accurate).

Functional relation

The functional relation is given by [4.6]. Results of the fitting are given in Table 16.

$$U_{(X,)max} = U_R \cdot \left(1 + \alpha\left(\frac{h-T}{h}\right)^{\beta} \cdot \left(\frac{V_S - U_0}{\sqrt{g \cdot (h-T)}}\right)^{\gamma} \cdot \left(\frac{A_C}{A_S}\right)^{\delta}\right) \qquad [4.6]$$

	Conventional ship		Barge	
Method	$U_{x,max}$	U_{max}	$U_{x,max}$	U_{max}
α	0.04	0.05	4.70	0.96
β	-0.60	-0.92	-1.13	-1.14
γ	0.98	0.15	-3.89	-0.60
δ	0.88	0.74	-1.68	-0.54
R^2	0.79	0.87	0.54	0.91
RMSE [m/s]	0.04	0.04	0.10	0.09

Table 16: Coefficients and goodness of fit for functional relation

For all configurations (ship type, U_{max} type) the functional relation gives more or less accurate results. However, when looking at the individual components, no clear pattern can be seen, just as with the method of Maynord. The coefficients vary significantly per configuration. In general it seems that (h-T)/h is more important than A_C/A_S, but again it must be noted that A_C/A_S is hardly changed during the experiment (fixed B and B_S).

As with the method of Maynord, Appendix D contains an approach for the functional relation in which some coefficients are kept equal. It reduces complexity almost without decreasing the accuracy. It also shows that the functional relation is more accurate than the equation of Maynord.

Conclusions

From the comparison with the current prediction methods, the following conclusions can be drawn:

- The current prediction methods have been developed for maximum x-velocities, rather than for maximum absolute velocities. By adapting the coefficients of the methods they can however also be used for predicting maximum absolute velocities (as done for the WL|Delft Hydraulics equation, the Maynord formula and the functional relation).
- The maximum absolute velocities were mainly found at the side of the ship, due to the fanning-out effect. For barges the maximum x-velocity is situated at the centreline of the barge, while for conventional vessels it mainly occurs near the side of the vessel.
- None of the current prediction methods are capable of accurately determining the maximum x-velocity beneath the bow with small underkeel clearances. This holds for both conventional ships and barges.
- Adaptation of the prediction methods by changing the coefficients is possible; however it does not lead to a clear relation between the maximum occurring velocity and the different parameters, since the coefficients vary significantly, dependent on ship and velocity type. This complexity can be reduced by requiring some coefficients to be equal, see Appendix D.
- It seems the most important parameters are the relative keel clearance (h/T or versions thereof) and a Froude number (based on values of coefficient γ of the functional relation).

From the adapted methods, the most accurate method is the functional relation, and it is best applied with the coefficients from Appendix D - Table 3. Unfortunately the method is complicated due to the amount of parameters and the required extra calculation on U_R. This last argument also applies to the WL|Delft Hydraulics equation. Therefore, when a simple and quick indication of the maximum occurring velocities is desired, it is advised to use the Maynord equation [4.5] with the coefficients as given by Appendix D - Table 1, which are also given in Table 17.

Velocity type	Ship type	α	β	γ	R^2	RMSE
$U_{X,max}$	Conventional	0.75	0	1.38	0.65	0.05 m/s
	Barge	1.50			0.66	0.08 m/s
U_{max}	Conventional	0.88	0.35	2.55	0.65	0.06 m/s
	Barge	2.10			0.86	0.12 m/s

Table 17: Advised coefficients for the Maynord equation

4.4 Dependency on parameters

Before trying to make a model for the velocities beneath sailing vessels, a clear understanding of the influences of the different parameters is necessary. Therefore, the maximum occurring x- and y-velocities will be studied. Later on, hopefully the entire flow field can be derived from these velocities. The analysis is only been done for conventional vessel experiments, since there are only 8 experiments with barges, which is very few to accurately base dependency on. Before analysing the influences of each parameter, it is wise to think about how the different parameters affect the maximum velocities.

Firstly, it must be stated that the occurring velocities underneath a vessel (including the maximum velocities) depend on other velocities. They depend either on a combination of sailing speed V_S and ambient flow velocity U_0 (as with the Maynord equation), or on the (one-dimensional, calculated) return current U_R (as for instance the WL|Delft Hydraulics equation).

The degree in which these velocities influence the velocity underneath the ship depends on:

- The proximity of the ship to the bed
- The size of the ship (determines the discharge that needs to be transported from the front of the ship to the stern due to the passing vessel)
- The bow shape (which influences the discharge being transported underneath the keel)
- The waterway dimensions (small channels have less cross-sectional area to transport these discharges, which results in higher velocities).

All these influences can be depicted by the parameters h, T or UKC, B_S and B, and coefficients to correct for the bow shape. A combination of these parameters will then determine the effect of V_S and U_0, or U_R, on the maximum occurring velocities. A large part of the analysis is given in Appendix E, only the most important conclusions and followed steps are given in this paragraph.

Maximum x-velocities

Based on V_S and U_0

First of all, the influence of the sailing speed and the flow velocity on the maximum x-velocity was studied. This is done by grouping the experiments with equal waterdepth, keel clearance and $V_S - U_0$ value (see Appendix E - Table 1). From this grouping, it can be concluded that the ambient flow velocity U_0 has a larger impact on the maximum x-velocity than the sailing speed V_S, since the maximum x-velocity increases with increasing U_0, when the absolute sailing velocity ($V_S - U_0$) is kept equal. This means the influence of V_S and U_0 on $U_{X,max}$ must be considered separately, rather than combined. Furthermore, a smaller underkeel clearance generally leads to a higher $U_{X,max}$ (disregarding the influence of V_S and U_0).

Since V_S and U_0 should be considered separately, function [4.7] is suggested to determine the maximum x-velocity. Coefficients α and β should then depend on h, UKC or T, B_S and possibly B.

$$U_{X,max} = \alpha \cdot V_S - \beta \cdot U_0 \qquad [4.7]$$

Analysis by grouping experiments with equal UKC and h (see Appendix E - Table 2), and then fitting these groups on equation [4.7], resulted in the following conclusions:

- The influence of U_0 on the maximum x-velocity is indeed larger than the influence of V_S, since for all data coefficient β is larger than coefficient α (see equation [4.7]).
- Coefficient α increases with decreasing keel clearance, and is approximately equal for equal values of UKC/h. However, when the ship is very close to the bed, coefficient α slightly decreases again. So the contribution of V_S depends on UKC/h or another version thereof.
- Coefficient β seems to depend only on the water depth, not on the underkeel clearance. Thus, the contribution of U_0 is not influenced by the underkeel clearance.
- The suggested function fits very well on the grouped data. For all groups $R^2 \geq 0.94$.

Besides a linear relation (see [4.7]), also a power function was investigated, as given by equation [4.8].

$$U_{X,max} = \alpha \cdot V_S^{\beta} - \gamma \cdot U_0^{\delta} \quad [4.8]$$

Although the goodness of fit (R^2 and RMSE) slightly increases, there is no clear relation anymore between the found values of coefficients α, β and the parameters (see Appendix E). Also, unit-wise a power relation does not make sense either, and therefore the linear approach is preferred.

Based on U_R

For the return current U_R, the same approach is applied: the experiments are grouped with equal UKC and h. A linear function is fitted on these groups, equal to the WL|Delft Hydraulics equation, see equation [4.4]. The resulting values for coefficient α can be found in Appendix E - Table 4. The coefficient α should now depend on h, UKC or T, B_S and B. However, from this table it can immediately be seen that the function is far less accurate than function [4.7] (compare R^2-values).

Besides the fact that a model based on U_R seems less accurate than a model based on V_S and U_0, also the use of the return current U_R might not be justified. It is logical that there is some agreement with the measurements, since the return current depends on V_S, U_0, T, h, A_C and A_S. However, it is obtained with a 1D-method (Schijf, Bouwmeester), which assumes the return current is equal over the entire channel cross-section. Already the implication of equation [4.4] shows that this is not the case, it is different dependent on the location. In reality only a specific part of the channel cross-section, around the ship, handles the return current, meaning the return current U_R is at least 2-dimensional. For extremely wide channels this results in a too small U_R, leading to a too small $U_{X,max}$.

Even when the channel dimensions are small (A_C / A_S ≈ 5), and remain approximately equal (like in the experiments), the range of coefficient α is still very large (see Table 14), where there seems to be little dependency on UKC or h (see Appendix E). A method base on U_R is still possible, but it will lead to errors, since there are already errors in the calculation of U_R. Therefore, this method will not be addressed further, even though it could give a quick indication of the expected maximum x-velocities.

Maximum y-velocities

For y-velocities the same procedure can be followed. Since U_Y will probably also depend on U_X, it might be expected that for $U_{Y,max}$ the best approach is also to use a linear formula on V_S and U_0, just as equation [4.7]. This results in equation [4.9].

$$U_{Y,max} = \alpha \cdot V_S - \beta \cdot U_0 \quad [4.9]$$

The experiments are grouped (on equal UKC and h) again and fitted onto equation [4.9]. The results are given in Appendix E - Table 5. The following conclusions can be drawn from this analysis:

- The suggested function again gives very good fits. Only for small underkeel clearances the goodness decreases.
- The influence of U_0 is still larger than the influence of V_S, although the difference is smaller.
- Both coefficients increase with decreasing keel clearance. This might be expected, since boundary layers on ship and bed will reduce the potential flowthrough area underneath the keel, which means water should be diverted to the side. This effect increases with smaller underkeel clearance (less/no flowthrough area), resulting in higher outward (y-) velocities.
- Coefficient α mainly depends on the underkeel clearance, and not very much on the water depth. The relation for coefficient β is more difficult to determine. It has some agreement with the values of h/UKC (or a version thereof), but the agreement is not very precise.

As with x-velocities, applying a power function or use U_R does not lead to better results.

Proposed prediction equations

In Appendix E the determination of the coefficients of equations [4.7] and [4.9] has been worked out further. As stated before, the contribution of U_0 on $U_{X,max}$ depended on h, and the contribution of V_S on $U_{Y,max}$ depended on UKC. However, unit-wise a dimensionless coefficient makes more sense. Therefore, also the ship's width B_S is used to create the dimensionless parameter h/B_S and UKC/B_S.

Since the width of the ship was not varied during the experiments, the question remains whether these parameters are correct or that another parameter (for instance L_S) should be used. Consequently, the proposed prediction equations are given by [4.10] for maximum x-velocities and [4.11] for y-velocities.

$$U_{X,max} = \alpha \cdot \left(\frac{h - UKC}{h} \right)^{\beta} \cdot V_S - \gamma \cdot \left(\frac{h}{B_S} \right)^{\delta} \cdot U_0 \qquad [4.10]$$

$$U_{Y,max} = \alpha \cdot \left(\frac{UKC}{B_S} \right)^{\beta} \cdot V_S - \gamma \cdot \left(\frac{h}{UKC} \right)^{\delta} \cdot U_0 \qquad [4.11]$$

The determination of the coefficients α – δ is given in § 5.2. Here also the equations are rewritten to use the draught T (of a still lying ship) rather than the underkeel clearance UKC during sailing, since the underkeel clearance is very difficult to predict correctly.

4.5 Velocity distribution

Besides looking at maximum velocities, also the distribution of the velocity beneath the ship is important. There are three directions: vertical, longitudinal and transverse. For the different distributions the shape of the model ship is of importance, see Figure 37 for a sketch of the model ship.

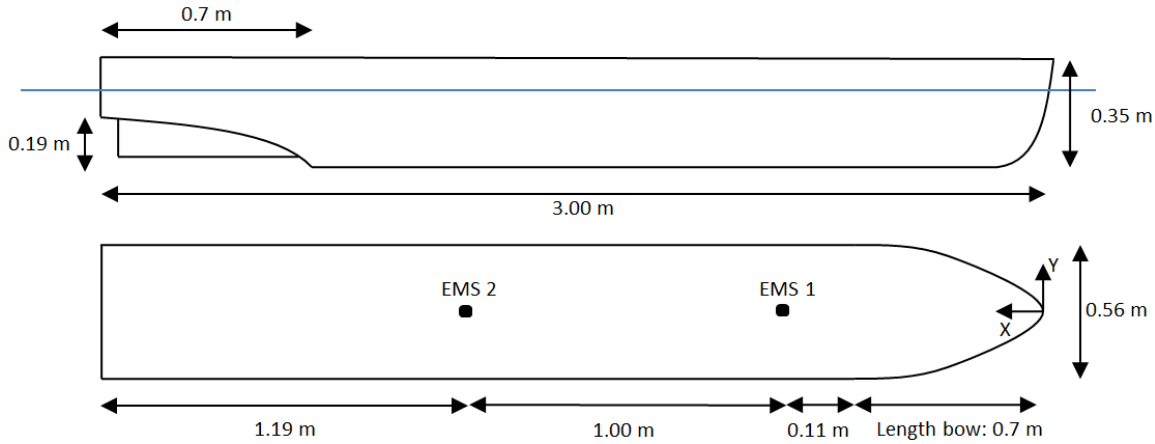

Figure 37: Shape of model ship with dimensions

Vertical distribution

By adjusting the EMS-devices in the ship, at some vertical points the velocity underneath the vessel could be measured. The distribution of some of these experiments is given in Figure 38. The distance to the bed has been made dimensionless by dividing through UKC. The velocity has been made dimensionless as well, by dividing through the sailing speed V_S. The graphs have been smoothened by applying a Piecewise Cubic Hermite Interpolating Polynomial over the data points.

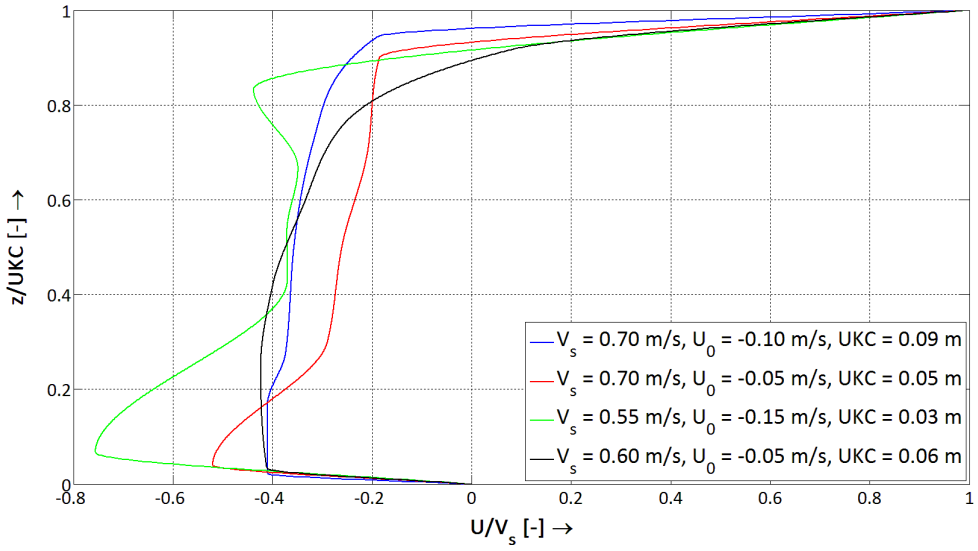

Figure 38: Vertical velocity distribution at EMS 1

In Figure 38 velocity profiles are found that resemble the turbulent Couette-Poiseuille flow with a positive pressure gradient (see Figure 12). Logically, the flow at the keel of the ship is equal to the ship's speed, while the flow at the bed is equal to zero. In almost all cases the maximum velocity is found near the bed, measured by the EMS-devices in the bottom. For smaller underkeel clearances the vertical distribution seems to bulge out near the bed and the keel, deviating from the turbulent Couette-Poiseuille flow profile. This could be due to a contraction effect at the bow (as with a underflow weir), forcing the flow mainly to the bed. This contraction effect is unproven so far.

Appendix C - Figure 3 shows the vertical distributions for one underkeelclearance. From the graph it becomes clear that higher flow velocities result in higher relative (U / V_S) velocities under the keel. The bulging out of the distribution near the bed is mainly caused by the ambient flow velocity, since the bulging out is far less prominent/absent when no ambient flow is present during the experiments.

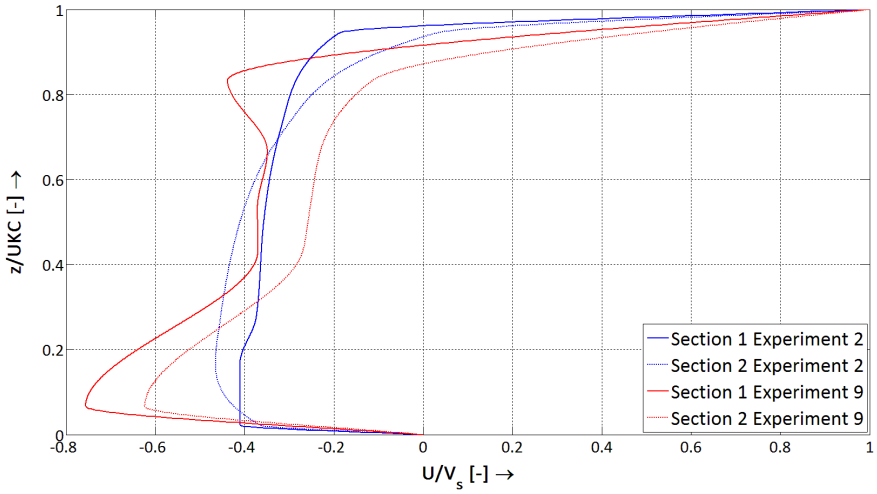

Figure 39: Vertical velocity distribution at EMS 1 and 2

Compared to the situation at EMS1, the flow velocities at EMS2 have decreased, see Figure 39. The overall shape of the distributions remains approximately equal, although the velocity profiles are somewhat smoother at EMS2 (further away from the bow). For experiment 9, which has an UKC of 0.03 m, mainly the amplitude of the velocity has decreased, proving the effect of fanning out (less velocity means a decreased discharge, so some flow must have diverted to the sides). For experiment 2, which has an UKC of 0.09 m, this effect is not visible.

The vertical velocity profile is not taken into account in the model development.

Longitudinal distribution

A first impression of the longitudinal distribution of velocities is already given in Figure 27. In order to retrieve the differences per experiment, the experiments are again grouped in sets with equal underkeel clearance and waterdepth. Since in these sets, only the sailing speed and ambient flow velocity will differ, a similar longitudinal distribution is expected. To investigate this similarity, all the velocity distributions will be divided by maximum value of the distribution (so by $U_{X,max}$ or $U_{Y,max}$).

X-velocities

For x-velocities at EMS2, the longitudinal distribution ratios of h = 0.30 m are given in Figure 40.

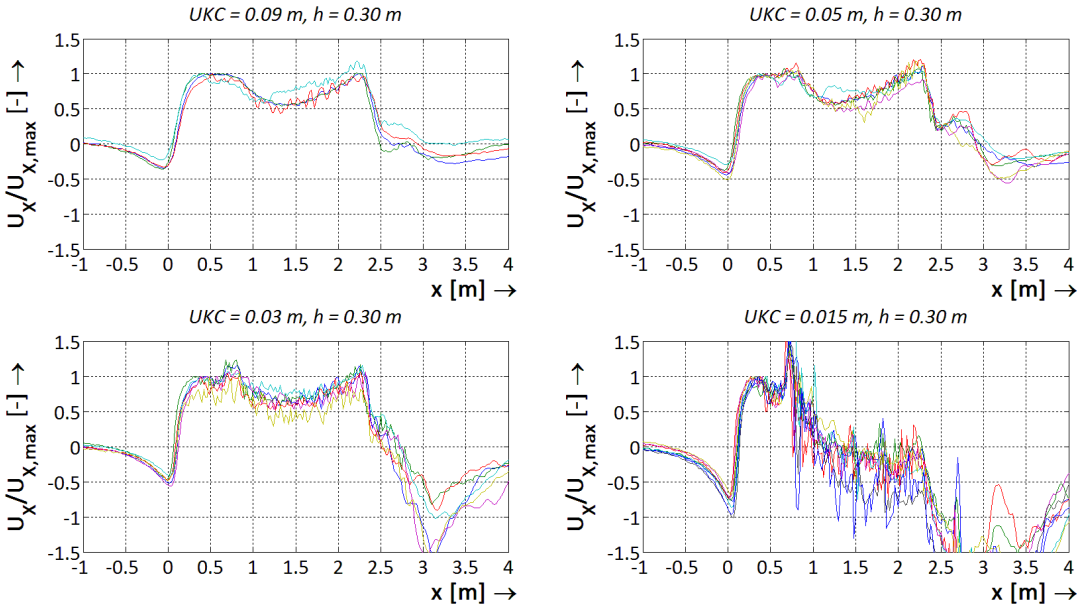

Figure 40: X-velocity distribution ratios of different experiment per situation (same UKC, h)

From Figure 40 it becomes clear that the velocity distribution ratios are indeed approximately similar for experiments with equal UKC and h. There are some small differences, but the general trend is similar. Turbulence effects result in a deviation from the general trend. This can be seen at the experiments with UKC = 0.015, here the bandwidth of the velocity distribution is wider because of the turbulence effects. Also the turbulence effects with all experiments increase after x = 2.3 m, which is at the start of the stern of the vessel. Here the keel clearances increase again (see Figure 37). In reality here also the influence of the propeller becomes very significant, which is not simulated during the experiments. Therefore, differences here will be neglected; this is out of the field of interest for this study.

Nevertheless the longitudinal distribution per situation (UKC, h) remains identical. Therefore, the mean trend of each situation is calculated and shown in Figure 41.

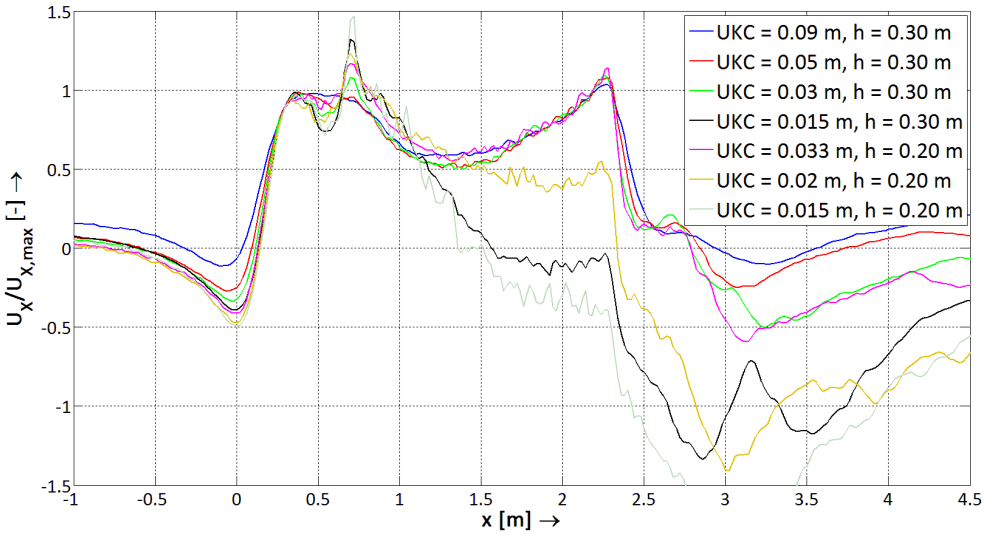

Figure 41: Mean x-velocity distribution ratios per different situation (same UKC, h) for EMS2

From Figure 41 two different distribution types can be distinguished. For the first distribution type, which holds for UKC ≥ 0.03 m, the x-velocity distribution ratios are approximately equal. There are some slight differences, especially at the ratios in front of the bow, and also during the passing of the stern. Beneath the vessel however the velocity ratios (U_X / $U_{X,max}$) are approximately equal. The peak at x ≈ 0.7 can be ascribed to the construction error in the model ship, in reality this extra peak will probably not occur and therefore it will be neglected.

These distributions (for UKC ≥ 0.03) also bear similarity to experiments performed by Lenselink (2011), see Appendix C - Figure 4. He performed calculations with DelKelv, a potential flow model, and obtained a similar velocity distribution under a barge (this velocity distribution is directly underneath the barge, so not close to the bed).

The second distribution type occurs for UKC ≤ 0.02 m. Here, the velocity distribution near the bow is similar to experiments with UKC ≥ 0.02 m, but at some point from the bow the distribution begins to deviate. This happens sooner for smaller underkeel clearances. Clearly, the effect of the proximity of the keel to the bed begins to play a role here. Since this effect occurs closer to the bow for smaller UKC, the boundary layers are clearly interacting in this region. Due to the interaction of the boundary layers, the actual flow area beneath the keel decreases, forcing the flow to divert to the sides, reducing the x-velocity at the bed. For smaller keel clearances this effect starts closer to the bow, since the boundary layer interaction occurs sooner. For the experiments with UKC = 0.015 m this is clearly visible, already after 1.5 m from the bow the velocity is approximately zero. After 2.3 m suddenly the flow reverses (or significantly decreases, for UKC ≥ 0.03 m), due to the increasing keel clearance here. Here also the boundary layer interaction ends.

Y-velocities

The same procedure can be applied to y-velocities. The velocity distributions of different experiments with equal conditions (h, UKC) are given in Appendix C - Figure 5. Just as with the x-velocities, the trends of the velocity distribution ratios are similar for experiments with equal UKC and h. Therefore, for y-velocities also the mean trend is calculated per situation, which results in Figure 42.

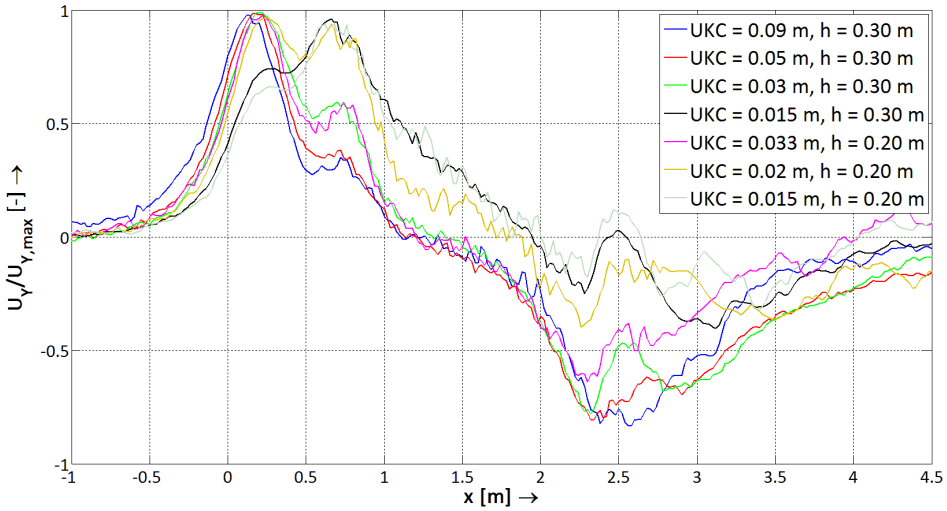

Figure 42: Mean y-velocity distribution ratios per different situation (same UKC, h) for EMS3

Here again there is a clear difference in the velocity ratio pattern for UKC ≥ 0.03 m and UKC ≤ 0.02 m. For UKC ≥ 0.03 m the highest y-velocity is recorded immediately after passage of the bow, due to the water that is being pushed aside by the bow. The water under the keel still flows aside till approximately 1.25 m after the bow, but the velocities are lower. After 1.25 m the flow reverses and now the water flows from the sides to underneath the vessel.

For UKC ≤ 0.02 m however, the maximum y-velocity is not recorded at the bow, but further away, under the keel. Now the fanning-out effect is the dominating phenomenon for the maximum occurring y-velocity. Also the flow reversal does not occur until x ≈ 2 m, and it is far less prominent than for UKC ≥ 0.03 m. This further proves the interaction of the boundary layers at these keel clearances. Due to this interaction the area between the keel and the bed is 'clogged', and therefore before the interaction occurs, the flow needs to be diverted to the sides (leading to higher y-velocities). The boundary layer interaction also prevents the inflow of large quantities of water after the flow reversal.

The derivation of prediction functions for the longitudinal x- and y-velocity is done in § 5.3.

Transverse distribution

Just as with the longitudinal distribution, the transversal distribution will be compared to the maximum occurring x- and y-velocity. This will result in formulations which show the maximum occurring x- and y-velocity dependent on the y-coordinate.

X-velocities

For the velocity distribution in transverse direction, there are just three data points available:

- In the sailing line of the ship (y = 0 m, EMS2)
- At y = 0.1 m (EMS1)
- At y = 0.2 m (EMS3)

For x-velocities, in general the maximum measured x-velocity was at y = 0.2 m (see § 4.3), and therefore the maximum x-velocities at y = 0 m and y = 0.1 m will be compared to that velocity. Analysis revealed no significant dependence on keel clearance, draught or water depth, thus a simple linear relation between $U_{X,max}$ and U_X (y = 0 m) or U_X (y = 0.1 m) is applied. The resulting graphs can be found in Appendix C - Figure 6 and Appendix C - Figure 7, and are summarised in Table 18.

y	-0.2 m	-0.1 m	0 m	0.1 m	0.2 m
Coefficient	1.00	0.87	0.84	0.87	1.00
R^2	1	0.88	0.77	0.88	1
RMSE [m/s]	0	0.03	0.03	0.03	0

Table 18: Coefficient transversal x-velocity distribution

Through this data a 2nd degree polynomial is drawn, resulting in equation [4.12].

$$\frac{U_{X,max}(y)}{U_{X,max}} = 4.14 \cdot y^2 + 0.83 \qquad [4.12]$$

This equation is valid at least for -0.2 m ≤ y ≤ 0.2 m. The question remains whether this still applies at for instance y = 0.28 m (which is directly underneath the side of the vessel), where extrapolation of equation [4.12] would lead to a maximum x-velocity (at y = B_S/2) of 1.14 times the measured maximum x-velocity. Unfortunately, no data is available outside y = 0.2 m to confirm the validity of this equation there. The transversal distribution is shown graphically in Figure 43.

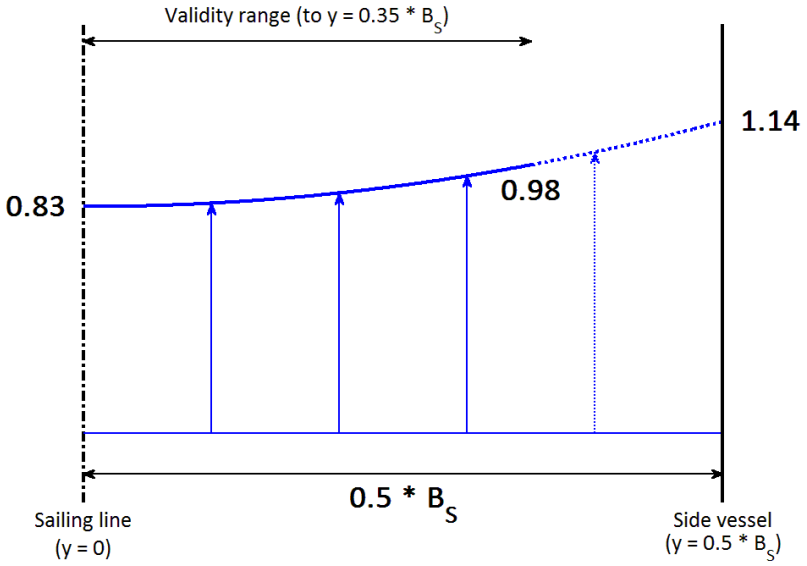

Figure 43: Transversal X-velocity distribution

Y-velocities

For the y-velocities also only three data points are available. Although the EMS-device recorded y-velocities at y = 0, in reality (without a cross-current) no y-velocity should be present here because of symmetry, only some fluctuations will occur due to turbulence. Therefore, the maximum y-velocity here will be set to 0 m/s (generally, the mean trend of the velocities measured here were also around 0 m/s). Once again the maximum measured y-velocities were at y = 0.2 m (so U_Y (y) / $U_{Y,max}$ = 1) , so the distribution will be defined by the value of U_Y (y) / $U_{Y,max}$ at y = 0.1 m. In comparison to x-velocities however, the distribution of y-velocity now depends on the keel clearance and water depth. Therefore, function [4.13] is suggested, in which coefficient α depends on UKC and h.

$$\frac{U_{Y,max}(y)}{U_{Y,max}} = \left(\frac{y}{0.2}\right)^{\alpha} \qquad [4.13]$$

This formula is chosen, such that it results in 0 for y = 0 m, and 1 for y = 0.2 m. The coefficient α depends on the keel clearance and water depth, see Table 19.

UKC	*0.09 m*	*0.05 m*	*0.03 m*	*0.015 m*	*0.033 m*	*0.02 m*	*0.015 m*
h	*0.30 m*	*0.30 m*	*0.30 m*	*0.30 m*	*0.20 m*	*0.20 m*	*0.20 m*
α	0.35	0.23	0.15	0.51	0.25	0.25	0.62

Table 19: Coefficients for transversal y-velocity distribution

Once again, from Table 19 it seems a logical fit is very difficult. There are fits possible for coefficient α, but these are very complex. Other formulations than [4.13], for instance with extra coefficients, have the disadvantage that they no longer result in U_Y (y) / $U_{Y,max}$ = 1 at y = 0.2 m.

From Figure 42 it was concluded that two different y-velocity distribution types are present, dependent on the keel clearance. Therefore it is not unlikely that the transversal y-velocity distribution also changes dependent on the UKC. Therefore, here two different transversal distributions are proposed, for UKC ≥ 0.03 m and UKC ≤ 0.02 m. Analysis of the data results in a coefficient α = 0.25 for UKC ≥ 0.03 m, and α = 0.5 (square root) for UKC ≤ 0.02 m. The hence obtained transversal y-velocity distributions are shown in Figure 44.

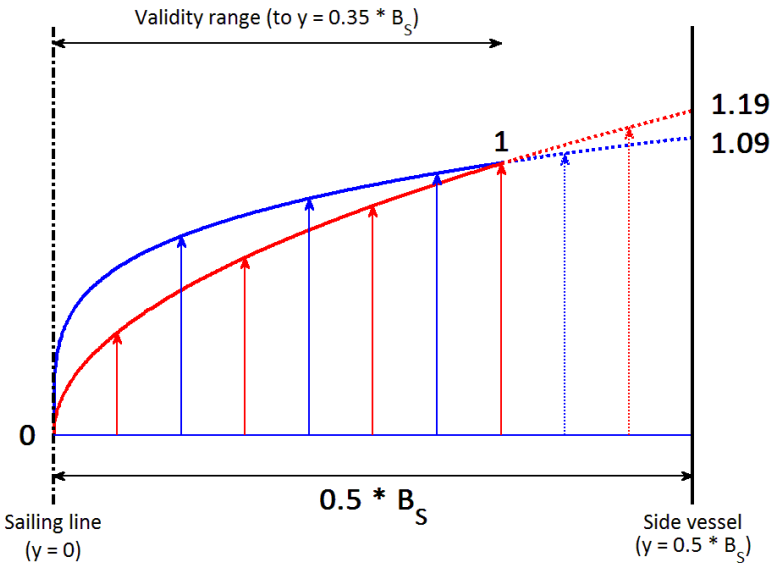

Figure 44: Transversal distribution y-velocities (blue for UKC ≥ 0.03 m, red for UKC ≤ 0.02 m)

Like with the x-velocity distribution, these equations hold for at least 0.2 m ≤ y ≤ 0.2 m. However, it might be expected that due to the fanning out of the flow, the y-velocities keep increasing under the keel, and that therefore the maximum y-velocities do indeed occur at y = 0.5 * B_S.

4.6 Erosion/sedimentation

During the experiments also some tests were performed with a mobile bed, i.e. a bed consisting of (non-cohesive) sediments. With a profile tracker the bed before and after passage of the vessel was measured. Three stages can be distinguished:

- Conventional vessel over a smooth bed
- Conventional vessel over dunes
- Barge over smooth bed

Conventional vessel with smooth bed

It proved difficult to achieve initiation of motion during these tests. Therefore, the bed was roughened before the experiments, which increased the possible achievement of initiation of motion. The bed was roughened by temporarily increasing the ambient flow velocity and by generating increased turbulence with flow obstruction objects.

Nevertheless, still only very little sediment transport is achieved with a conventional vessel. Only at smaller underkeel clearances a clear difference is observed in the bed before and after passage of the vessel. With UKC ≥ 0.03 m almost no changes are noticeable. Only with keel clearances smaller than 0.03 m changes are measured.

Figure 45 shows the erosion in cm (erosion is positive, deposition is negative) for experiment 47, in which the underkeel clearance was 0.012 m. This experiment consists of 1 vessel passage.

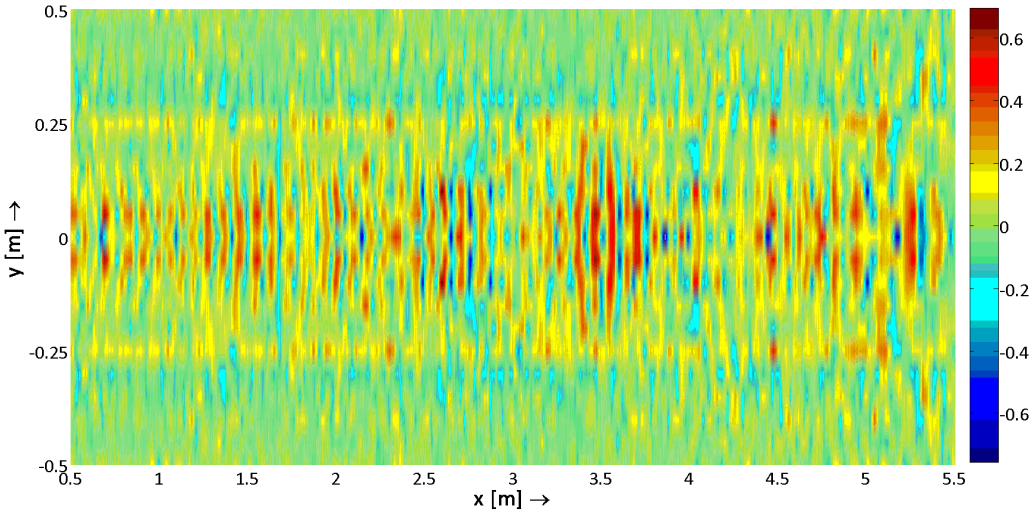

Figure 45: Erosion (in cm) after experiment 47

Figure 45 clearly shows that there is erosion/sedimentation on the path of the sailing vessel (the vessel passes between -0.28 m ≤ y ≤ 0.28 m). The following observations can be made:

- The main erosion of the bed happens near the centreline of the vessel. Here erosion occurs up to approximately 0.6 cm. Areas of erosion are followed by areas of deposition. This is because the sediment on top of ripples (closest to the keel) is eroded, and deposited in the troughs of the ripples. So, passage of a vessel flattens the bed. This can also be seen in Figure 46 (left picture).
- At the sides of the vessel (around y ≈ ± 0.28 m) the bed eroded approximately 0.2 cm. The fanning-out underneath the bow results in large velocities here, which leads to erosion near the side of the ship. The eroded sediment is deposited some distance from the side, which can be seen by the blue patches around y ≈ ± 0.30 m.

Figure 46: Erosion after experiments with flat bed and a conventional vessel

Figure 46 shows the erosion of the ripples (right side of left picture) and the pattern after 10 passages (right picture) during experiment 46. There is a clear path were the vessel has sailed. The ripples have flattened, especially in the centreline of the vessel. It also seems some sediment has deposited immediately near the side of the vessel. Appendix C - Figure 8 shows the measured erosion during this experiment.

The dispersion pattern of sediment due to the passing of a vessel is better shown with a red sediment line. Figure 47 shows the sediment movement when a conventional ship passes. The red sediment was laid from the sailing line of the vessel (y = 0 m, underside of line) to approximately y = 0.3 m (just more than 0.5 * B_S, top of line). The sailing direction is from left to right.

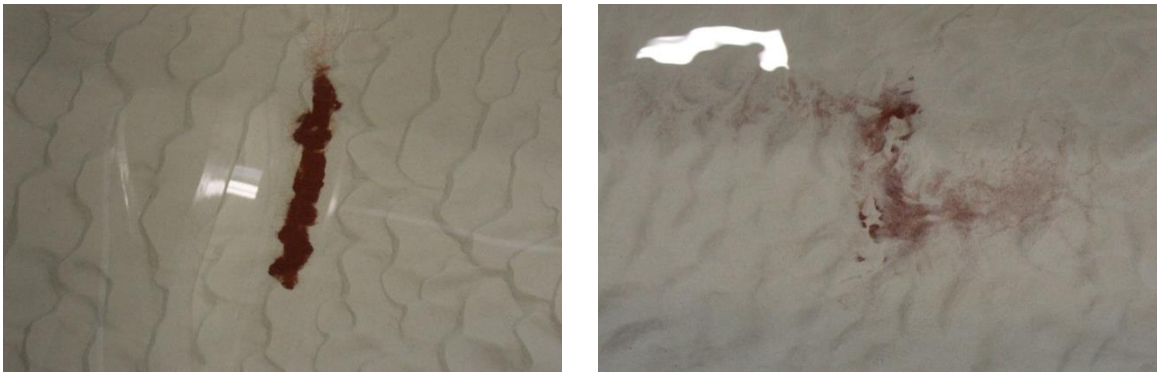

Figure 47: Sediment movement under conventional ship (left: before passage, right: after passage)

From Figure 46 two distinct movements can be distinguished:

- Near the centreline of the vessel the sediment movement is mainly in the sailing direction.
- At the side of the vessel the sediment is moving opposite to the sailing direction and also slightly sideways (away from the vessel).

These particular movements can be explained by the pick-up mechanisms of sediment. For sediment pick-up and thus erosion an important factor are the velocity gradients and turbulence, not just the velocity. Large turbulence intensity will lead to more sediment pick-up. Once the sediment is picked up, it will disperse with the reigning velocities. This also holds for the erosion due to the passing of a vessel. The largest turbulence can be found near the side of the vessel (transition of flow, rapid flow deceleration and thus turbulence generation) and near the stern. So here most sediment is picked up. The velocities here are directed opposite to the sailing direction and outward (side of the vessel) and in the sailing direction (near the stern). This explains the sediment movement from Figure 46. The large gradient at the bow does not lead to enormous sediment pick-up, since flow acceleration leads to less turbulence (see Schiereck et al. (2012)).

Although the different movements are clearly visible, the overall erosion for a conventional vessel on a flat bed is fairly limited; the velocity magnitudes are simply too low. Only at small UKC (≤ 0.02 m) the magnitudes and turbulence intensities become high enough to give substantial erosion.

Conventional vessel with dunes

When the experiments are carried out with dunes as a bedform, a much more mobile environment is created. When the vessel passes over the top of the dunes, clearly the top of the dune is eroding, depositing the picked up sediment in the trough of the dunes. This can be seen in Figure 48, which shows the erosion (in cm) of experiment 51, after 10 passages of the vessel.

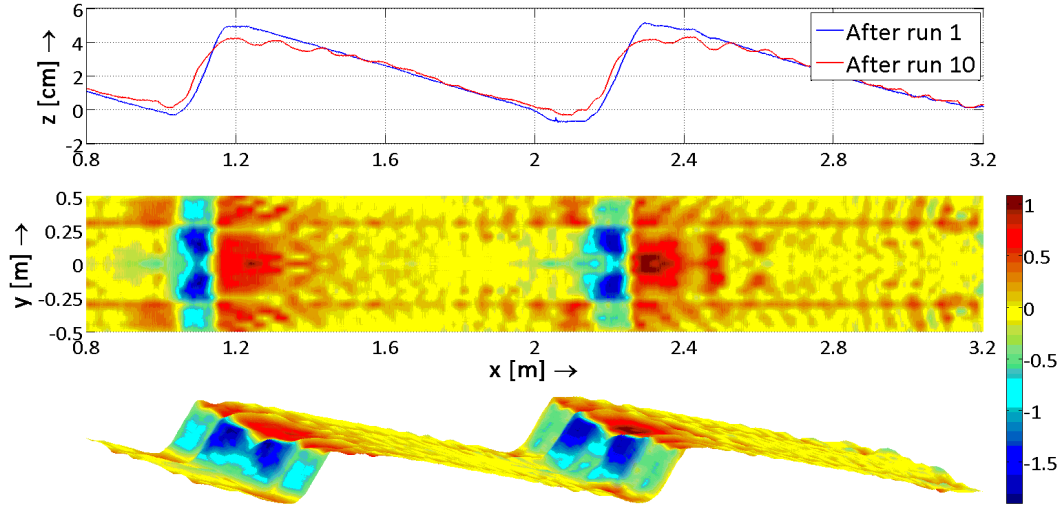

Figure 48: Erosion (in cm) after run 10 of experiment 51

Figure 48 clearly shows the erosion on top of the dune, were the vessel is passing. This erosion is up to 1.2 cm after 10 runs. The eroded sediment is deposited in the through of the dune. The passing of the vessel reduces the bed form, making the profile smoother, and the actual water depth greater (since the dune top is reduced by approximately 1 cm). This means the underkeel clearance (for the same ship with the same draught) will increase, and the effect of the passing of the vessel on the bed will decrease.

The sudden increase in erosion compared to a flat bed is caused by the clear separation point at the top of the dune. When a ship passes over, this creates turbulent fluctuations at the dunes topes which picks up the sediment and deposits them in the trough. This is also clearly visible in the movies from experiments 49-52. This process does not only occur underneath the bow (although the effect is the strongest here), but also alongside the ship due to the increase in flow velocity by the return current. The stills in Appendix C - Figure 10 also show this effect.

This erosion already occurs at larger underkeel clearances, although the effect here is minimal. Also the turbulence near the stern still is an important factor for erosion, as well as the turbulence created near the sides of the vessel.

Figure 49: Sediment movement under conventional vessel with dunes (Experiment 51 run 1)

Applying a red sediment line (from -0.4 m ≤ y ≤ 0.4 m) atop a dune also shows the erosion at the top of the dune and the deposition in the trough, see Figure 49. Furthermore, Figure 50 shows the dunes before experiment 51, and Figure 51 shows the consequences of 10 vessel passages over these dunes.

Figure 50: Dunes before experiment 51

Figure 51: Dunes after experiment 51 run 10

The erosion/deposition development during this experiment can be seen in Appendix C - Figure 9, which shows 4 different cross-sections (dune tops and troughs) before the experiment, after run 1 and after run 10.

Barge with smooth bed

For barges with a smooth bed, the picture is somewhat different, see Figure 52. This is after 10 passages of a barge over a smooth bed. There is some clear erosion visible, up to 0.5 cm underneath the barge. However, the greatest erosion is measured next to the barge. Apparently the water flowing besides the vessel has such a great velocity and turbulence intensity, that the erosion is very large here, up to 1 cm. This is probably due to the fanning out near the bow of the barge.

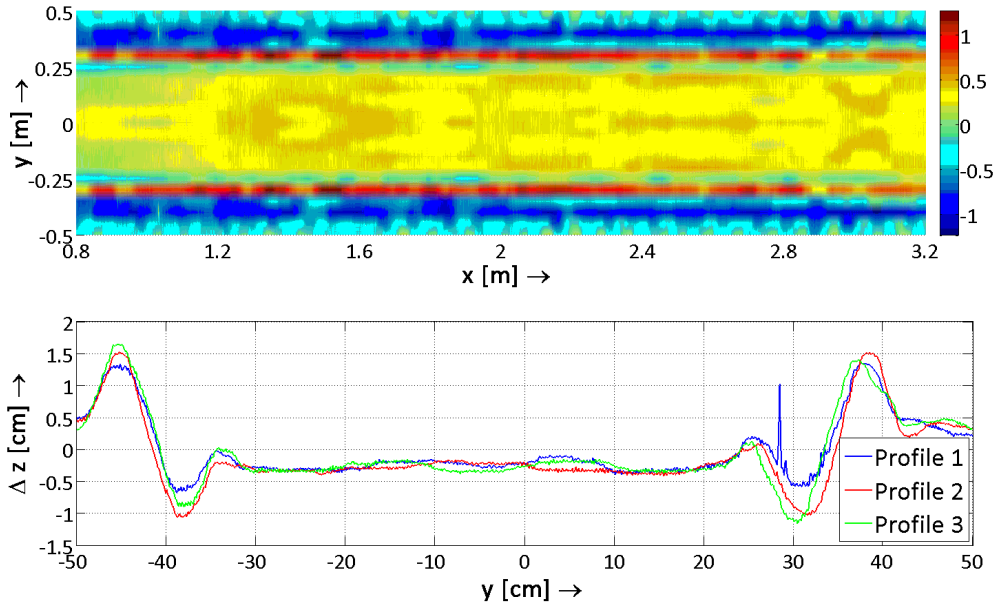

Figure 52: Erosion (in cm) after run 10 of experiment 71 (UKC = 0.015 m)

The lower graph of Figure 52 shows three cross-sectional erosion/deposition curves, which are similar to each other. In the middle part there is some erosion in the sailing path of the vessel,

approximately 0.3 cm. Most erosion occurred immediately next to the vessel, at y = 0.3 m. This is also visible in the top figure. The erosion here is approximately 1 cm. This is in agreement with earlier observations: due to turbulent fluctuations and large velocity gradients here the sediment is picked-up most easily. The velocity then transports the sediment away. Due to the fanning out the velocity is aimed away from the vessel here, resulting in a large deposition (up to 1.5 cm) on some distance beside the vessel, see Figure 52.

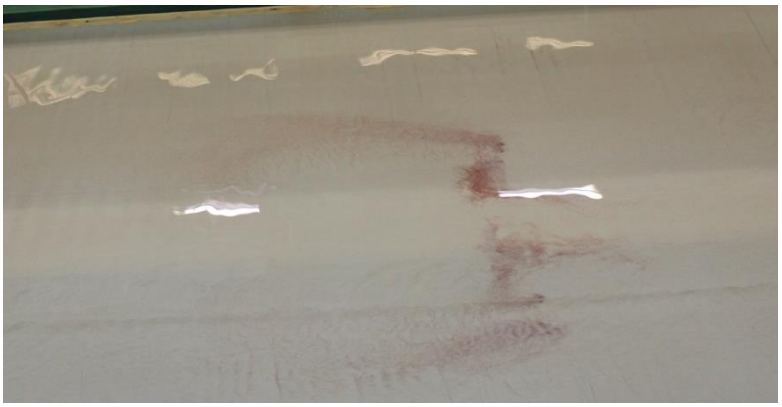

Figure 53: Sediment movement after passage of a barge (Experiment 71 run 1)

Figure 53 again shows the sediment movement direction, but now underneath a barge. The red line was laid from -0.4 m ≤ y ≤ 0.4 m. In general the movement seems the same as with conventional vessels, but there are a few differences:

- The sediment near the side of the barge has been spread over a larger area. Clearly the velocities are higher (as was already shown in § 4.2), and the picked up sediment is deposited over a larger area.
- In the sailing line of the barge there is a small area where no red sediment is present anymore. This is at the place where the highest x-velocities are measured. The velocity directly after the bow apparently is high enough to immediately erode this sediment away.

The resulting bed profile after 10 runs (Experiment 71) is given in Figure 54. The passing of the vessel is clearly visible. Although only two experiment with barges have been performed, the increase in velocity (also see § 4.2) and turbulence results in more erosion than with conventional vessels. Therefore it may be expected that the effect of a passing barge on the bed will be noticeable with a larger underkeel clearance already. Unfortunately no tests with underkeel clearances larger than 0.03 m were done with barges.

Figure 54: Bed profile after experiment 71 run 10

Conclusions

From the figures and explanations above the following can be concluded:

- Not necessarily only high velocities lead to erosion, also turbulent fluctuations and large velocity gradients are important for the pick-up of sediment underneath sailing vessels.
- Sailing barges induce larger velocities and fluctuations on the bed than conventional vessels, and this results in more erosion (compare Figure 52 with Appendix C - Figure 8). Conventional vessels need very small underkeel clearances to have some effect (UKC ≤ 0.02 m), while for barges the effect is still noticeable with underkeel clearances of at least 0.03 m (maybe even higher UKC, but no experiments were done with larger underkeel clearances). This can be rewritten to the following effective underkeel clearances for eroding bed material:

  Conventional vessels: $\frac{h}{h-UKC} \leq 1.07$; Barges: $\frac{h}{h-UKC} \leq 1.1$
- The highest sediment transport does not occur underneath the keel, but immediately beside the keel (for both barges and conventional vessels). The fanning-out effect results in high y-velocities underneath the keel, while immediately next to the ship the flow velocity is limited. The outflow of water from underneath the keel induces large velocity gradients and fluctuations here, which transports the sediment away from the keel.
- Sharp bed forms induce turbulence (due to clear flow separation points where the sediment is easily picked up) underneath the keel and therewith increases the erosion. In reality the bed forms (especially dunes) will be less sharp, partly counteracting this effect. However, also with simple ripples it was observed that the bed forms were flattened by the passing of the vessel. The picked up sediment was deposited in the troughs, reducing the bed forms and thus slightly increasing the navigable depth.
- Although no quantitative results are shown, it can be seen that sailing close to the bed will induce erosion of the bed, especially with bed forms, which will be flattened. Therefore, sailing inland navigation vessels (especially barges) can be used to flatten very local shallows, which would increase the navigable depth. From the experiments it seems the effectiveness can be significant. 10 passages of a conventional vessel reduced the dune top with 25% of its original height, see Figure 49. With a barge this probably would have been even higher. The true effectiveness remains unknown, extra analysis or computer models are necessary to investigate this.

Remarks

It must be noted that the experiments were conducted without propeller action. The outflow of propellers is an important (sometimes even governing) factor for erosion of the bed, especially when the ship sails very close to the bed. Since this was not considered here, in reality the erosion in the path of the vessel (‘under the propeller’) will be larger.

The translation of the bed measurements to reality is complicated. Due to some problems with the measurement device (see § 4.7) the accuracy of the measurements is questionable. Furthermore, in § 3.1 it was shown that the sediment transport was a factor 11.7 too low. However, simply applying this factor on the erosion depth is probably not correct, since with an increasing erosion depth also the velocities and fluctuations decrease (distance to the keel of the ship increases), which will lead to less erosion. Probably the best way to interpret the bed change is comparing them to the underkeel clearance or the water depth.

For a better indication of the erosion process, reference is made to the different movies and photos of the erosion tests, which were used for the qualitative analysis.

4.7 Discussion on measurements

Although the data set allows for an extensive and thorough analysis, some aspects of the measurements need to be used with caution. Therefore some remarks on the measurements are necessary, which are addressed here:

- There are only 8 experiments with barges, which is a bit low for a proper analysis. This is circumvented by basing new formulations on the data from the experiments with conventional ships, and then adapting them (see § 5.3) to the situation with barges. Also a lot of validation data is available for barges (see § 5.5), which helps improve the accuracy of a new formulation. Nevertheless, more experiments are helpful to give a better analysis.
- During the experiments the ship's width B_S and channel width B could not be changed. Therefore all experiments have been executed with equal B and B_S (and thus with only a small range of A_S and A_C). Consequently the influence of these parameters remains uncertain.
- For the vertical velocity distribution, at some points the EMS in the ship was very close to the bed. The question remains whether the measurement here is still accurate, or that the measurements here need to be modified. EMS-devices are usually not used this close to the bottom. Since the EMS-devices in the ship are only used for the (qualitative description of) vertical velocity distribution, in this study no extra attention is given to this. Furthermore, spikes occurred in the measurements when the EMS in the ship moved over the EMS in the bed (with small keel clearances), due to magnetic interaction. An example is the spike at x = 0.8 m for UKC = 0.02 m in Figure 41. During the analysis these spikes are ignored, and therefore the consequences of this effect are minimal.
- The model ship had a small construction error, which had some effects on the measurements. At approximately x = 0.7 m, at the transition from the bow of the ship (made of foam) to the mid-section of the ship (made of wood), there was a hump downward; both parts did not align perfectly. As a result, the keel clearance slightly drops after this point, and the flow was 'forced' down, leading to a small increase in flow velocities at the bed. This is visible in various graphs showing the longitudinal distribution. This effect increases with decreasing keel clearance. During the analysis these effects are ignored, which occur approximately between x = 0.6 m and x = 1.0 m.
- Furthermore, it must be noted that the bow of the barge has been simplified compared to reality (see Appendix A). Probably with this bow shape even more water is forced beneath the keel, although the effect will not be very large.
- With decreasing underkeel clearance, the turbulence intensity beneath the keel increases. This occurs especially when UKC ≤ 0.02 m (see for example Figure 41). Since the turbulent fluctuations increase, also the deviations from the mean increase. As a result, the model data has a larger spread, and therefore the prediction methods drop in accuracy. This leads to a slightly worse prediction and thus to a lower R^2 and higher RMSE for small underkeel clearances. Despite this decrease in accuracy, the prediction capabilities remain quite good for small underkeel clearances (see § 5.2).
- During the experiments with sediment, there were some problems with the measurement of the bed profile. Due to problems with the accuracy of the profile tracker (and vibration of the needle) and unexplainable differences between measurements done before and after tests with a night in between, not all measurement are usable. Whether the data is therefore usable for a quantitative analysis remains to be seen. Since here only a qualitative analysis is done, this is not a problem. For future research with this data and translation of the erosion results to reality caution is necessary.

All these remarks do not mean that the data set is not usable, just that caution is necessary when using the data set: one needs to be aware of the specific circumstances during the experiments. In fact, when these remarks are kept in mind, a very good analysis is possible, as is already demonstrated in this chapter.

5. Model development

The goal of this chapter is to design an empirical flow model, which is able to predict the flow field directly above the bed, beneath a sailing inland navigation vessel. First, this flow model is developed for conventional vessels. Then the model is adapted, to predict the flow field underneath barges. This order has been chosen, since there were more experiments with conventional vessels than with barges. Finally, it is tried to validate the models with results from previous experiments.

5.1 Set-up of the flow model

The set-up to predict the flow field underneath sailing inland navigation vessels is as follows:

1. Determine the maximum flow velocities occurring beneath the keel, for the x- and y-direction.
2. Determine the maximum velocity distribution ratios in transverse direction for $U_{X,max}$ and $U_{Y,max}$.
3. Determine the longitudinal distribution ratio.
4. Combining 1 – 3 should lead to a complete picture of the flow field beneath a sailing vessel.

Currently in all analysis the underkeel clearance is used, since these were fixed during the experiments. However, in reality the underkeel clearance is rarely known and used. Therefore a formulation based on the draught is preferable. This may lead to a worse prediction, but does not require extra computations to determine the squat/drawdown of the vessel. During the model development both options (formulation on UKC, formulation on T) will be given. The formulation on the draught T is based on a still lying ship, while the formulation on the underkeel clearance UKC is based on a sailing ship. This means the only difference is the drawdown z, and that the parameter UKC can be replaced by $h_0 - T - z$.

In § 4.5 it is furthermore shown that there seems to be two different flow types, dependent on the underkeel clearance. For UKC ≤ 0.02 m the boundary layers are interacting, leading to different velocity distributions, and also slightly different maximum flow velocities. To counteract these effects, the model can be separated in two parts: one part for UKC ≥ 0.03, and one part for UKC ≤ 0.02 m. Where the exact transition point is (between 0.02 m and 0.03 m) for the different models is unknown at this moment. The advantage of this approach is that it delivers two more precise prediction methods, since clearly different phenomena are important in these different parts. The disadvantage however is that it leads to a more complex model, while the increase in accuracy might not be very high. It is decided to give general formulations where possible (for instance at the maximum flow velocities), and a separated version where necessary (for instance y-velocity distribution). For the maximum flow velocities furthermore the results of the least-square error computations will be given for the separated models.

For the model the transition point between the different situations lies between 0.02 ≤ UKC ≤ 0.03. In reality however it will depend on the ship's length also, since the length mainly determines whether the boundary layers will interact and 'clog' the flow beneath the keel. Therefore, the transition point is made dimensionless by dividing through the length between perpendiculars, L_{PP}. For the model ship this value is approximately 3 m, but here 2.3 m is used, since after x = 2.3 m the keel clearance was already increasing, so no boundary layer interaction occurred here. This results in the following situations:

$$\frac{L_{PP}}{UKC} \leq 77 \text{ (no interaction)}; \quad \frac{L_{PP}}{UKC} \geq 115 \text{ (interaction)}$$

In reality it is more complex, since the boundary layer development also depends on the roughness of the surface and the flow velocities. Unfortunately the exact transition point for interaction is unknown. More experiments or calculations on boundary layers are necessary to exactly determine the transition point.

When applying formulations on the draught, the transition point is not that easy to determine, since only the draught does not give information on the underkeel clearance. For the data from the experiments (in which the draught is calculated from the UKC by means of the method of Schijf), the approximate relation between the keel clearance and the draught can be found, see Figure 55.

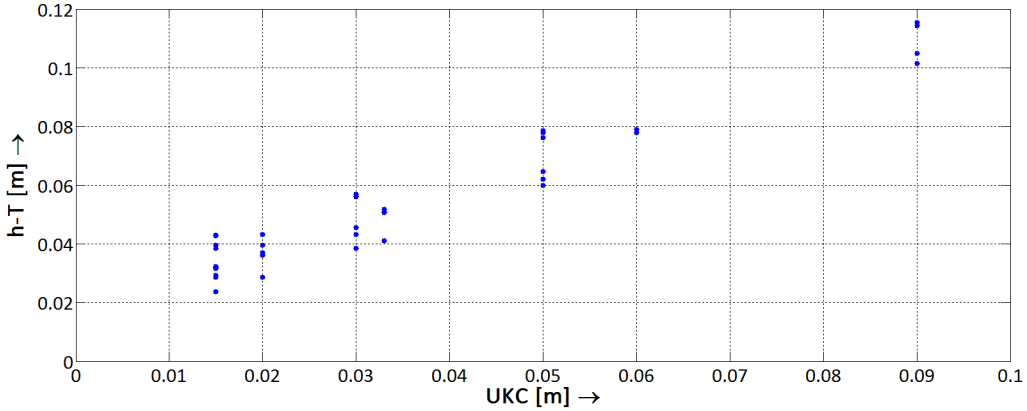

Figure 55: UKC vs. h – T of experiment data

It turns out that when the UKC ≤ 0.02 m, the difference between the water depth and the draught is approximately 0.04 m. This results in the following transition point:

$$\frac{L_{PP}}{h-T} \leq 58 \text{ (no interaction)};\ \frac{L_{PP}}{h-T} > 58 \text{ (interaction)}$$

5.2 Maximum flow velocities

For the maximum flow velocity formulations, per velocity type (x, y or absolute) the influence of each parameter is given in graphs. In these graphs, one parameter (UKC, h or B_S) has been changed, while the others remained equal. The reference scenario consists of the following values:

$$V_s = 4 \text{ m/s};\ \ U_0 = -1 \text{ m/s};\ \ \text{UKC} = 1 \text{ m};\ \ h = 5 \text{ m};\ \ B_s = 12 \text{ m}$$

Figure 35 already showed the approximate location of the different maximum velocities. There are three different maximum velocities:

- Maximum x-velocities ($U_{X,max}$), which gives the maximum velocity underneath the keel, opposite to the sailing direction.
- Maximum y-velocities ($U_{Y,max}$), which gives the maximum velocity underneath the keel, perpendicular to the sailing direction.
- Maximum absolute velocities (U_{max}), which gives the maximum absolute velocity underneath the keel, without regarding the direction, as a combination of x- and y-velocities (but not a combination of the maximum x- and y-velocity, since these occur at different locations).

Besides these velocities, two additional velocities are introduced in § 5.3:

- Maximum bow x-velocity ($U_{X,bow,max}$), which gives the maximum x-velocity in sailing direction, just before passage of the bow (due to the pushing forward of water by the bow).
- Maximum stern x-velocity (U_{stern}), which gives the maximum x-velocity near the stern, just before the propellers, in the centerline of the vessel. This stern velocity is sometimes even higher than $U_{X,max}$.

X-velocities

For the prediction of the maximum occurring x-velocities beneath the keel, in § 4.4 equation [5.1] has been found, in which the coefficient α, β, γ and δ will be determined by a least-squares method on the data set of the experiments. The values of these coefficients can be seen as the influence of the bow shape on the velocities beneath the ship. When this equation is adapted to the draught T rather than the underkeel clearance UKC, equation [5.2] is obtained.

$$U_{X,max} = \alpha \cdot \left(\frac{h}{h - UKC} \right)^{\beta} \cdot V_S - \gamma \cdot \left(\frac{h}{B_S} \right)^{\delta} \cdot U_0 \qquad [5.1]$$

$$U_{X,max} = \alpha \cdot \left(\frac{h}{T} \right)^{\beta} \cdot V_S - \gamma \cdot \left(\frac{h}{B_S} \right)^{\delta} \cdot U_0 \qquad [5.2]$$

Results for all methods (separated/general models, based on T or UKC) are given in Table 20.

	All UKC		**L_{PP} / UKC ≤ 77**		**L_{PP} / UKC ≥ 115**	
	Based on UKC	*Based on T*	*Based on UKC*	*Based on T*	*Based on UKC*	*Based on T*
α	0.59	0.63	0.63	0.67	0.54	0.52
β	-1.46	-1.18	-1.74	-1.36	-0.51	-0.02
γ	1.48	1.40	1.46	1.37	1.68	1.85
δ	0.36	0.27	0.33	0.25	0.48	0.59
R^2	0.94	0.91	0.96	0.92	0.93	0.94
RMSE	0.02	0.02	0.02	0.02	0.02	0.02

Table 20: Formulations for maximum x-velocity

When applying different formulations for L_{PP} / UKC ≤ 77 and L_{PP} / UKC ≥ 115, the goodness of fit and therewith the prediction capabilities of the maximum x-velocity indeed increase. However, this does lead to numerous formulations with different coefficients, decreasing the simplicity of a possible prediction method. Also, since the maximum x-velocity occurs right after passage of the bow, and thus well before there is any possible boundary layer interaction, it is expected that the influence of this interaction on the maximum x-velocity is minimal. Therefore it is decided to use a general formulation, applicable to both situations.

In order to arrive at a more general expression, first of all coefficients γ and δ are fixed. Although they change somewhat over the different model possibilities, they should stay equal since no influence of T and UKC is present. To prevent random numbers, the coefficients are fixed at γ = 1.5 and δ = 1/3.

Applying this to the formulations for all underkeel clearances, the formulations [5.3] and [5.4] are obtained for predicting the maximum x-velocities.

$$U_{X,max} = 0.6 \cdot \left(\frac{h - UKC}{h} \right)^{3/2} \cdot V_S - \frac{3}{2} \cdot \left(\frac{h}{B_S} \right)^{\frac{1}{3}} \cdot U_0 \qquad [5.3]$$

$$U_{X,max} = 0.6 \cdot \left(\frac{T}{h} \right)^{1.2} \cdot V_S - \frac{3}{2} \cdot \left(\frac{h}{B_S} \right)^{\frac{1}{3}} \cdot U_0 \qquad [5.4]$$

The influence of each parameter is given in Figure 56, while the goodness of fit is given in Table 23.

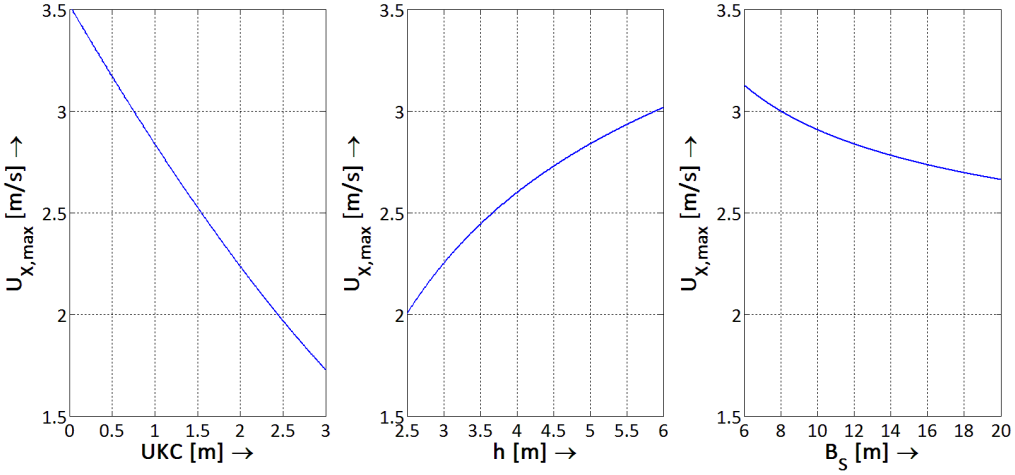

Figure 56: Influence of different parameters on maximum x-velocity

It must be noted that the maximum x-velocities were always taken near the bow. In some cases the x-velocity near the stern (around x ≈ 2.3 m) is equal or higher than this velocity. Since the difference with the velocity near the bow is very small in these cases (max. 10% of $U_{X,max}$), this difference is ignored.

Y-velocities

From § 4.4 it became clear that, for determining the maximum y-velocities, it was more difficult to find a clear relation between the weights for V_S and U_0 and the different parameters. The best relation was found based on UKC, but this leads to an error in dimensions. Therefore, UKC is divided by B_S to introduce a new dimensionless parameter. The ship's width B_S should be important for the maximum y-velocity, since a wider ship introduces a higher discharge beneath the keel. Since the area at the side of the ship, where this discharge can flow through during the fanning out, does not increase, an increase in B_S should lead to a higher maximum y-velocity. Therefore the following equation [5.5] to calculate $U_{Y,max}$ is suggested. Adapting equation [5.5] to the draught T results in equation [5.6].

$$U_{Y,max} = \alpha \cdot \left(\frac{UKC}{B_S}\right)^{\beta} \cdot V_S - \gamma \cdot \left(\frac{h}{UKC}\right)^{\delta} \cdot U_0 \qquad [5.5]$$

$$U_{Y,max} = \alpha \cdot \left(\frac{h-T}{B_S}\right)^{\beta} \cdot V_S - \gamma \cdot \left(\frac{h}{h-T}\right)^{\delta} \cdot U_0 \qquad [5.6]$$

Applying these formulas as was done with the x-velocities, results in the coefficients from Table 21.

	All UKC		**L_{PP} / UKC ≤ 77**		**L_{PP} / UKC ≥ 115**	
	Based on UKC	*Based on T*	*Based on UKC*	*Based on T*	*Based on UKC*	*Based on T*
α	0.04	0.05	0.08	0.07	0.02	0.29
β	-0.74	-0.82	-0.50	-0.64	-0.93	-0.21
γ	0.20	0.12	0.09	0.10	0.15	0.15
δ	0.53	1.11	0.86	1.12	0.65	0.99
R^2	0.94	0.78	0.98	0.87	0.89	0.59
RMSE	0.023	0.046	0.006	0.017	0.028	0.054

Table 21: Formulations for maximum y-velocities

As with the x-velocities, applying different formulations for UKC ≥ 0.03 and UKC ≤ 0.02 result in better predictions. This is expected, since the y-velocity is influenced by the possible interaction of boundary layers of ship and bed. Due to boundary layer interaction, the area underneath the hull will become 'clogged', which means the discharge underneath the keel needs to be diverted to the sides.

This means an increase in y-velocity. When the boundary layers do not interact, the flow will not be clogged, leading to smaller y-velocities (less fanning out). This can also be seen in the differences in Figure 28.

Therefore, the following general expressions, [5.7] and [5.8], are suggested. The coefficients of these equations deviate from the coefficients in Table 21, since otherwise the goodness of fit of these equations for UKC ≥ 0.03 m and UKC ≤ 0.02 m are too far apart. The goal is to apply the general expressions on both situations.

$$U_{Y,max} = 0.04 \cdot \left(\frac{B_S}{UKC}\right)^{\frac{3}{4}} \cdot V_S - 0.2 \cdot \sqrt{\left(\frac{h}{UKC}\right)} \cdot U_0 \qquad [5.7]$$

$$U_{Y,max} = 0.06 \cdot \left(\frac{B_S}{h-T}\right)^{\frac{3}{4}} \cdot V_S - 0.15 \cdot \left(\frac{h}{h-T}\right) \cdot U_0 \qquad [5.8]$$

The influence of each parameter is given in Figure 57, while the goodness of fit is given in Table 23.

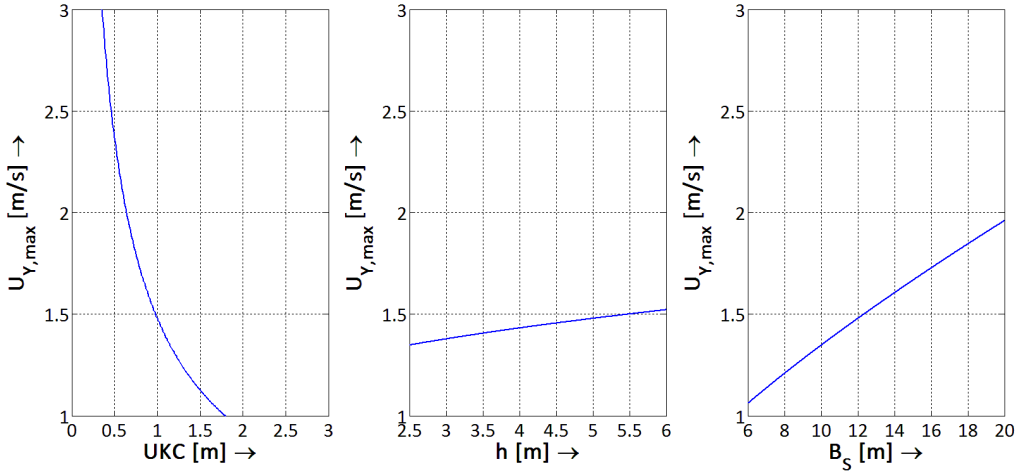

Figure 57: Influence of different parameters on maximum y-velocity

X,Y-velocities (absolute velocities)

Besides x- and y-velocities also absolute velocities can be calculated. For determining the flow field this might not be extremely important (these are based on x- and y-velocities), but for a quick indication of the maximum occurring velocities they are. It is found that the best fit is found by basing the weights (dimensionless coefficients) of V_S and U_0 on UKC/B_S and h/UKC. This results in equation [5.9].

$$U_{max} = \alpha \cdot \left(\frac{UKC}{B_S}\right)^{\beta} \cdot V_S - \gamma \cdot \left(\frac{h}{UKC}\right)^{\delta} \cdot U_0 \qquad [5.9]$$

For the prediction of the maximum absolute velocity based on the draught, equation [5.9] is adapted to equation [5.10]. The coefficients of these equations, with their goodness of fit, are given in Table 22.

$$U_{max} = \alpha \cdot \left(\frac{h-T}{B_S}\right)^{\beta} \cdot V_S - \gamma \cdot \left(\frac{h}{h-T}\right)^{\delta} \cdot U_0 \qquad [5.10]$$

	All UKC		L_{PP} / UKC ≤ 77		L_{PP} / UKC ≥ 115	
	Based on UKC	*Based on T*	*Based on UKC*	*Based on T*	*Based on UKC*	*Based on T*
α	0.18	0.20	0.22	0.27	0.10	0.99
β	-0.39	-0.43	-0.31	-0.27	-0.56	0.12
γ	0.65	0.42	0.48	0.34	0.47	0.24
δ	0.29	0.70	0.47	0.87	0.38	0.90
R^2	0.97	0.86	0.96	0.90	0.97	0.89
RMSE	0.02	0.04	0.02	0.03	0.02	0.03

Table 22: Formulations for maximum absolute (x,y) velocities

The general expressions are somewhat different than the coefficients found in Table 22. Once again, they are based on creating similar goodness of fits for both situations (UKC ≥ 0.03 m and UKC ≤ 0.02 m), and on the application of 'round' numbers for the powers. They are given by equation [5.11] (based on UKC) and equation [5.12] (based on the draught T).

$$U_{max} = 0.22 \cdot \left(\frac{B_S}{UKC}\right)^{\frac{1}{3}} \cdot V_S - 0.6 \cdot \left(\frac{h}{UKC}\right)^{\frac{1}{3}} \cdot U_0 \qquad [5.11]$$

$$U_{max} = 0.32 \cdot \left(\frac{B_S}{h-T}\right)^{\frac{1}{4}} \cdot V_S - 0.36 \cdot \left(\frac{h}{h-T}\right)^{\frac{3}{4}} \cdot U_0 \qquad [5.12]$$

The influence of each parameter is given in Figure 58, while the goodness of fit is given in Table 23.

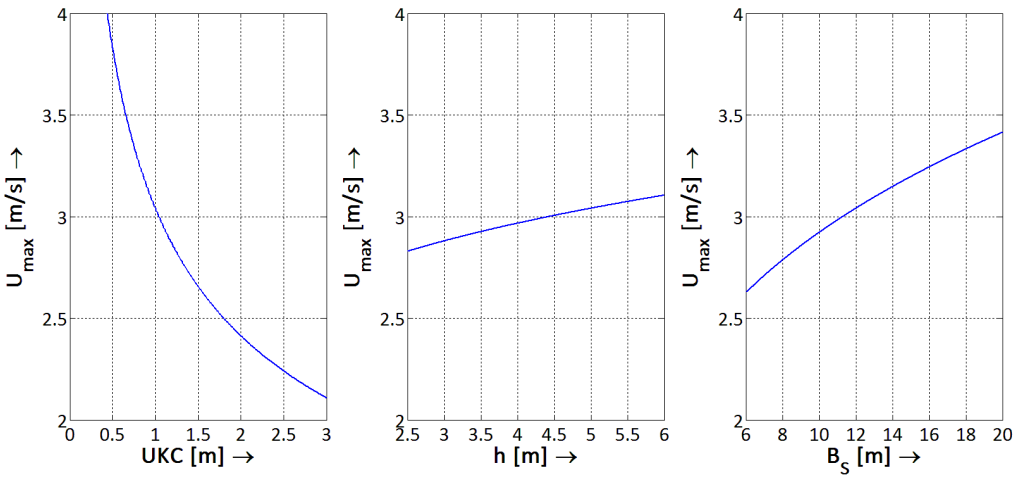

Figure 58: Influence of different parameters on maximum absolute velocity

Conclusions

Table 23 contains the goodness of fits for the different maximum velocity formulas. The predictions are quite good, especially when the underkeel clearance is used. In general the expressions for the draught have a worse prediction, although the prediction is still accurate. Unfortunately in many occasions only the draught is known. It can also be seen that the prediction for smaller keel clearances is less accurate than for higher keel clearances, probably due to the larger turbulence fluctuations. Nevertheless the equations are usable for both situations.

	$U_{X,max}$		$U_{Y,max}$		U_{max}	
	UKC [5.3]	*T* [5.4]	*UKC* [5.7]	*T* [5.8]	*UKC* [5.11]	*T* [5.12]
R^2	0.94	0.89	0.94	0.77	0.96	0.82
RMSE [m/s]	0.02	0.03	0.02	0.05	0.02	0.04
R^2 *(UKC ≥ 0.03 m)*	0.96	0.88	0.94	0.62	0.94	0.77
R^2 *(UKC < 0.03 m)*	0.89	0.89	0.84	0.45	0.85	0.72

Table 23: Goodness of fit for the different velocity formulations

5.3 Velocity distribution

Transversal distribution

In § 4.5 function [4.12] was found for the transversal distribution of maximum x-velocities. This function however does not take the width of the ship into account, and very wide ships will therefore have enormous predicted x-velocities, which will not occur in reality. The function therefore has to be scaled, which is done by making it dimensionless through B_S. This results in equation [5.13].

$$\frac{U_{X,max}(y)}{U_{X,max}} = 1.25 \cdot \left(\frac{y}{B_s}\right)^2 + 0.83 \qquad [5.13]$$

For the transversal distribution of maximum y-velocities, the same procedure is followed. Rewriting formula [4.13] then results in equation [5.14].

$$\frac{U_{Y,max}(y)}{U_{Y,max}} = \left(8 \cdot \left(\frac{y}{B_s}\right)^2\right)^{\frac{1}{8}} \quad \text{for } \frac{L_{PP}}{UKC} \leq 77$$
$$\frac{U_{Y,max}(y)}{U_{Y,max}} = \left(8 \cdot \left(\frac{y}{B_s}\right)^2\right)^{\frac{1}{4}} \quad \text{for } \frac{L_{PP}}{UKC} \geq 115 \qquad [5.14]$$

With these formulations, the transversal distribution of the maximum velocities can be calculated. This means that, for a given y-coordinate underneath the ship, the maximum x- and y-velocity in the longitudinal cross-section with coordinate y can be calculated, compared to the overall maximum x- and y-velocity. Both formulations ([5.13] and [5.14]) hold at least for $-0.35*B_S \leq y \leq 0.35*B_S$. Outside this zone no measurements were done so the validity of these equations is questionable there. The distributions have already been graphically given in § 4.5. Their goodness of fit is given in Table 24.

Prediction equation	$U_{X,max}$ (y)	$U_{Y,max}$ (y)
R^2	0.49	0.96
RMSE	0.071	0.068

Table 24: Goodness of fit for the transversal distribution functions of maximum flow velocities

Longitudinal distribution

Although the research into a prediction for the longitudinal velocity profile is easier compared to the transversal distribution due to the presence of the three EMS-devices (which result in three clear longitudinal velocity profiles), the making of such a prediction function is very difficult. The longitudinal velocity profile depends on a lot of factors: the fanning out (or fanning in later on, see Figure 28), keel clearances, bow and keel shapes, boundary layers, etc.

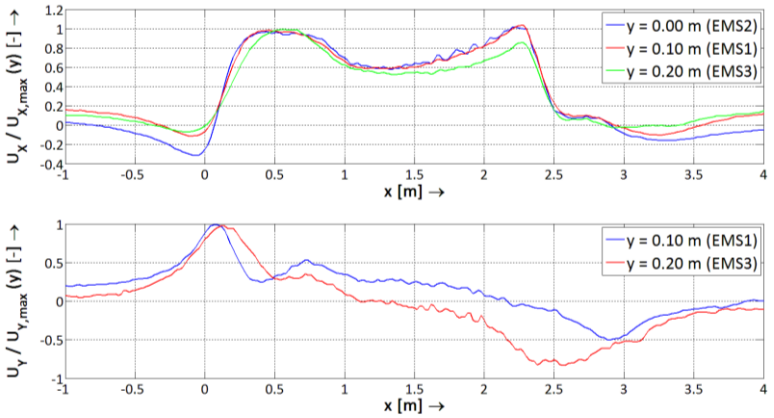

Figure 59: Different longitudinal distributions for UKC = 0.09 m and h = 0.30 m

Furthermore it is also dependent on the y-coordinate, as is visible from Figure 59. There is a clear difference in the distributions, dependent on y-coordinate, both for x- and y-velocities. As a result, it is difficult to predict these distributions accurately.

A computer model is preferable for the computation of these distributions. In § 4.5 it was already shown that the potential flow model KelDelv is able to simulate the velocity distribution under the hull of a ship. The use of potential flow models (or other models) in general should lead to better results. However, since the set-up of this research is to deliver a simple model, extensive use of difficult theories or models is undesirable. This leaves only very simple, but rather inaccurate methods. To predict the x- and y-velocity distribution, use can be made of polynomials, sum of sinuses or a rational approach. However, all methods require at least a 6^{th} degree approach, which is not very robust. Unfortunately other methods require heavy computation and complex formulations, so there is no other option. The analysis is given in Appendix F, only the most important conclusions are given here:

- It is very difficult to develop an empirical relation for the longitudinal velocity profile. Appendix F contains an empirical formulation for $L_{PP} / (h - T) \leq 58$, with a correction factor for $L_{PP} / (h - T) > 58$.
- The developed functions are very unstable (small changes in coefficients result in large deviations) and the coefficients are in no way related to the parameters. It is not recommended to use these functions; instead it is recommended to apply computer models.

For smaller underkeel clearances, perhaps a model based on boundary layers is fruitful. A quick analysis of the boundary layer development along the hull of the passing vessel results in Figure 60 and Figure 61. The boundary layers have been calculated with equations [2.31] and [2.32]. The knick in the lines is caused by the transition from laminar to turbulent boundary layer flow.

Figure 60 shows the boundary layer development with an underkeel clearance of 0.015 m. It can be seen that the boundary layer on the passing vessel reaches the bed at approximately 1.6 m from the bow, which is similar to location of the flow reversal in Figure 41. This could mean a model with inclusion of boundary layer development can result in a good approximation of the flow field with small UKC.

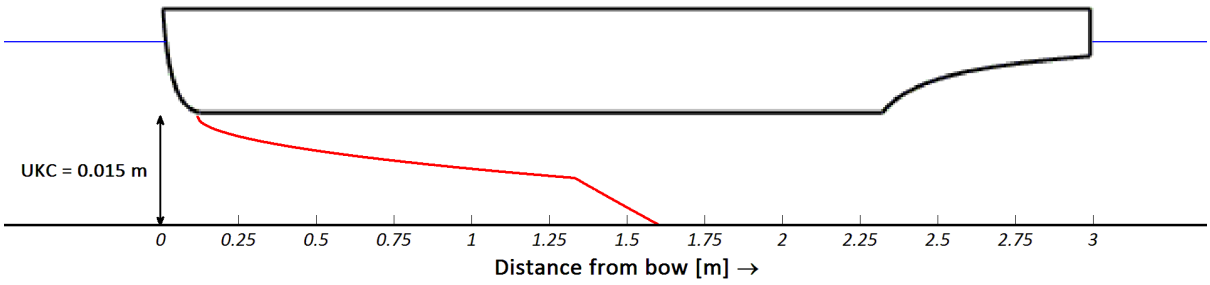

Figure 60: Boundary layer development on ship's keel for experiment 13 (UKC = 0.015 m)

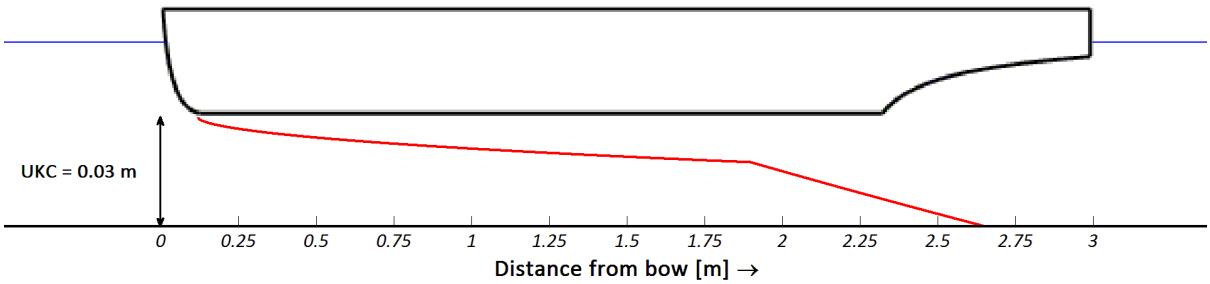

Figure 61: Boundary layer development on ship's keel for experiment 38 (UKC = 0.03 m)

For Figure 61 the boundary layer of the ship does not reach the bed before x = 2.3 m, which means the flow will not be blocked underneath the keel (since from there on the keel clearance increases again), as was earlier found for UKC ≥ 0.03 m. Although this quick analysis does not mean a good velocity profile could be obtained with this approach, it does show that the flow reversal and clogging of the flow underneath the keel is indeed due to boundary layer interaction at the bed.

Characteristic points

Since it proves difficult to predict longitudinal velocity profiles, a few extra points in the distribution which can be predicted accurately will give additional information about the flow field underneath the keel. In the longitudinal x-velocity profile of Figure 41 three characteristic points can be found, and the exact location of these characteristic points is shown in Appendix C - Figure 11:

- Around x ≈ 0 m: this is the x-velocity directly before the bow.
- Around x ≈ 0.5 m: Here the maximum x-velocity underneath the bow is reached. The maximum x-velocity is already ascertained and can be predicted by formula [5.3] or [5.4].
- Around x ≈ 2.2 m: here again approximately the maximum x-velocity is reached. From now on this will be called the stern velocity.

Bow velocity (around x = 0 m)

Analysis revealed the bow velocity depends on the keel clearance. With increasing keel clearance, the velocity in front of the bow (in comparison to the maximum x-velocity) decreases. This can be expected: with increasing keel clearance the distance from the bed towards the water volume that is 'pushed' forward by the ship increases, reducing the influence on the water motion at the bed.

It is possible to make a dimensionless parameter through for instance the water depth h or the beam's width B_S. However, this does not lead to better results. Additional research will be necessary to investigate these parameters. Therefore, for now a fit based on only the underkeel clearance is suggested, based on equation [5.15].

$$\frac{U_{X,bow,max}}{U_{X,max}} = \alpha \cdot UKC^{\beta} \qquad [5.15]$$

As it turns out, the bow velocity depends on the inverse of the square root of the UKC, while coefficient α is a function of cross-direction y. The largest bow velocity is measured at y = 0, so directly in the sailing line of the vessel. Going towards the sides of the vessel, the bow velocity decreases. This is expected, since there the ability of the flow to divert to the sides is greater, reducing the x-velocity. Analysis results in equation [5.16]. It is important to realize that this equation is based on $U_{X,max}$ (y), so dependent on the y-coordinate (thus not the overall maximum x-velocity).

$$\frac{U_{X,bow,max}(y)}{U_{X,max}(y)} = \frac{\left(\sqrt{0.04 \cdot \left(\frac{y}{B_S}\right)^2} - 0.1\right)}{\sqrt{UKC}} \qquad [5.16]$$

The goodness of this fit is equal to R^2 = 0.93, with a RMSE of 0.054. When applying this formulation, in combination with equation [5.13], and assuming $U_{X,bow}$ (0) = 1, the velocity distribution from Figure 62 is obtained. It turns out the x-velocity in front of the bow is nearly linear with the distance from the sailing line. In reality it may be expected that near y = 0 the gradient of the velocity ($\partial U_X/\partial y$) should be zero to guarantee a smooth function. This is not taken into account here. When equation [5.16] is adapted to include the draught T, formulation [5.17] is obtained.

$$\frac{U_{X,bow,max}(y)}{U_{X,max}(y)} = \frac{\left(\sqrt{0.07 \cdot \left(\frac{y}{B_S}\right)^2} - 0.13\right)}{\sqrt{h-T}} \qquad [5.17]$$

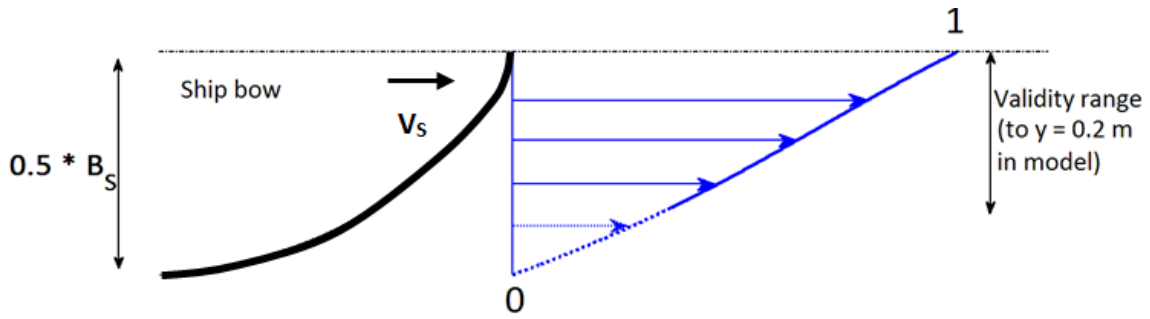

Figure 62: X-velocity distribution at x = 0 (U_{Bow})

Stern velocity (around x = 2.2 m)

In Appendix F it is shown that the correction factor for the longitudinal x-velocity distribution depends on the stern velocity. In many circumstances this velocity is the 2nd highest x-velocity underneath the barge, and thus important for the flow field and eventual erosion. From Figure 41 it is visible that there are two possible scenarios:

1. The underkeel clearance is higher than (or equal to) 0.03 m. In this case the stern velocity is approximately equal to the maximum occurring x-velocity.
2. The underkeel clearance is smaller than 0.03 m. Now the boundary layers interact between the bow and the stern, leading to smaller x-velocities near the stern.

This means that the stern velocity is mainly dependent on the underkeelclearance. Analysis for UKC ≤ 0.03 m revealed the following function for the stern velocity, see [5.18].

$$\frac{U_{stern,max}}{U_{x,max}} = 1 \quad \text{for UKC} \geq 0.03$$

$$\frac{U_{stern,max}}{U_{x,max}} = 1 - 0.08 \cdot \left(\frac{L_{PP}}{UKC} - 77.5 \right)^{\frac{2}{3}} \quad \text{for UKC} < 0.03 \text{ m} \qquad [5.18]$$

Rewriting formula [5.18] to contain the draught T rather than the underkeel clearance, gives relation [5.19], which is graphically displayed in Figure 63.

$$\frac{U_{stern,max}}{U_{x,max}} = 1 \quad \text{for} \quad \frac{L_{PP}}{h-T} \leq 58$$

$$\frac{U_{stern,max}}{U_{x,max}} = 1 - 0.1 \cdot \left(\frac{L_{PP}}{h-T} - 58 \right)^{\frac{2}{3}} \quad \text{for} \quad \frac{L_{PP}}{h-T} > 58 \qquad [5.19]$$

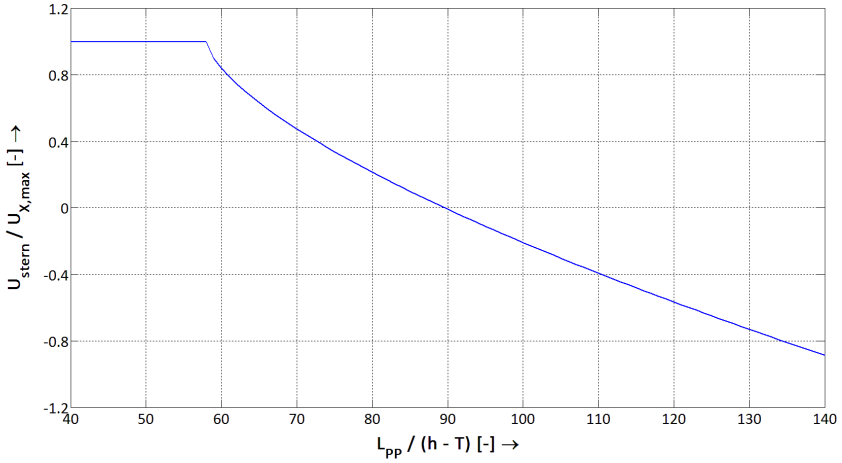

Figure 63: Stern velocity (as a function of L_{PP} / (h - T) and $U_{X,max}$)

5.4 Barge model

Now that the model for conventional inland vessels is finished, the same approach is applied to the barge experiments. For the barge model unfortunately only 8 experiments are available, of which only 3 experiments have a keel clearance lower than 0.03 m. Therefore it is decided to only make general equations based on UKC and T, without looking at separate models for L_{PP} / UKC ≤ 77 and L_{PP} / UKC ≥ 115. It is necessary to use a different model for barges, because the equations for conventional vessels do not give good predictions with the data of the barge experiments, as is visible from Table 25.

	$U_{X,max}$		$U_{Y,max}$		U_{max}	
	UKC [5.3]	*T* [5.4]	*UKC* [5.7]	*T* [5.8]	*UKC* [5.11]	*T* [5.12]
R^2	-5.82	-6.81	-1.18	-1.53	-2.36	-2.85
RMSE [m/s]	0.37	0.39	0.46	0.65	0.58	0.62

Table 25: Goodness of fit when data of barges is applied to the conventional vessel equations

Maximum velocities

X-velocities

The place where the maximum x-velocity occurs under a barge is different from place under the conventional ships. Now the maximum velocity occurs in the sailing line of the vessel, not near the sides.

For the x-velocities also equations [5.1] and [5.2] are used, resulting in formulations [5.20] and [5.21].

$$U_{X,max} = 1.4 \cdot \left(\frac{h - UKC}{h} \right)^{5/2} \cdot V_S - 1.7 \cdot \left(\frac{h}{B_S} \right)^{\frac{1}{3}} \cdot U_0 \qquad [5.20]$$

$$U_{X,max} = 1.7 \cdot \left(\frac{T}{h} \right)^{2.2} \cdot V_S - 1.7 \cdot \left(\frac{h}{B_S} \right)^{\frac{1}{3}} \cdot U_0 \qquad [5.21]$$

Y-velocities

Using equations [5.5] and [5.6] on the experiments with barges, results in the following equations:

$$U_{Y,max} = 0.1 \cdot \left(\frac{B_S}{UKC} \right)^{\frac{3}{4}} \cdot V_S - 0.72 \cdot \sqrt{\left(\frac{h}{UKC} \right)} \cdot U_0 \qquad [5.22]$$

$$U_{Y,max} = 0.03 \cdot \left(\frac{B_S}{h - T} \right)^{\frac{3}{2}} \cdot V_S - 0.17 \cdot \left(\frac{h}{h - T} \right)^{\frac{3}{2}} \cdot U_0 \qquad [5.23]$$

X,Y-velocities (absolute velocities)

For the maximum absolute velocities the placement is usually (6/8 experiments) again at the sides (EMS3, 0.2 m outside the sailing line), rather than in the middle. Only the experiments with high underkeel clearance (and thus small y-velocities) have their maximum velocity in the sailing line of the vessel. Applying equations [5.9] and [5.10] on the experiment data of the barges result in [5.24] and [5.25].

$$U_{max} = 0.29 \cdot \sqrt{\left(\frac{B_S}{UKC} \right)} \cdot V_S - 0.65 \cdot \sqrt{\left(\frac{h}{UKC} \right)} \cdot U_0 \qquad [5.24]$$

$$U_{max} = 0.07 \cdot \left(\frac{B_S}{h-T} \right)^{\frac{5}{4}} \cdot V_S - 1.6 \cdot \left(\frac{h}{h-T} \right)^{\frac{1}{4}} \cdot U_0 \qquad [5.25]$$

All coefficients and goodness of fits of the formulations for maximum velocities for barges are given in Table 26.

	X-velocities		**Y-velocities**		**Absolute velocities**	
	Based on UKC	*Based on T*	*Based on UKC*	*Based on T*	*Based on UKC*	*Based on T*
α	1.4	1.7	0.1	0.03	0.29	0.07
β	2.5	2.2	0.75	1.5	0.5	1.25
γ	1.7	1.7	0.72	0.17	0.65	1.6
δ	0.33	0.33	0.5	1.5	0.5	0.25
R^2	0.72	0.75	0.88	0.90	0.89	0.93
RMSE	0.07	0.07	0.14	0.13	0.11	0.09

Table 26: Coefficients and goodness of fit for maximum velocity formulations for barges

Remarks

- Since there were only a few experiments with barges, the found coefficients for equations [5.20] - [5.25] may not be the correct coefficients. These coefficients approximately give the best fit, but there may be other coefficients which also give a good prediction. For equation [5.23] for instance, using α = 0.1, β = 1, γ = 0.07 and δ = 2 results in a R^2-value of 0.86 and a RMSE of 0.151, which is only slightly worse than the results with the before found coefficients. This means the prediction of velocities for barges is uncertain at the moment.
- Strangely, the formulations on the draught T are now better than the formulations based on UKC. This is unexpected, since the actual underkeel clearance while sailing determines the flow field and the maximum velocities, not the draught.
- The equations for barges have far larger errors (RMSE) than the equations for conventional ships. This has two reasons: first of all the occurring velocities are higher, which in general leads to higher prediction errors. Furthermore, the lack of barge data probably makes the developed equations less accurate. More data is necessary to improve the accuracy.

During the validation of the models an attempt will be made to improve the current equations.

Transversal distribution

For the transversal distribution the same functions are applied as for conventional vessels, only with different coefficients. For the transversal distribution of maximum x-velocities, unfortunately there are only two data points, since the x-velocity measurements of EMS1 (0.1 m outside sailing line) are not available because the EMS-device broke down (only for x-velocities). Therefore, it is chosen to only change the coefficient in front of (y / B_S). Since the maximum x-velocity is now measured in the sailing line, equation [5.26] gives the y-distribution of maximum x-velocity.

$$\frac{U_{X,max}(y)}{U_{X,max}} = 1 - 1.25 \cdot \left(\frac{y}{B_S} \right)^2 \qquad [5.26]$$

The validity of this equation is questionable, due to the fact that it is based on only two data points. If it is valid, it is applicable to at least $-0.35 * B_S \leq y \leq 0.35 * B_S$. Outside this area (up till $0.5 * B_S$) no measurements were made.

For the transversal distribution of y-velocity luckily three data points are available (EMS1 still measured y-velocities). Analysis and fitting of the data resulted in equation [5.27] for the y-distribution of maximum y-velocity.

$$\frac{U_{Y,max}(y)}{U_{Y,max}} = \left(8 \cdot \left(\frac{y}{B_S} \right)^2 \right)^{\frac{3}{4}} \qquad [5.27]$$

This formula is also valid for at least $-0.35*B_S \leq y \leq 0.35*B_S$. The distributions are given in Figure 64 (left: x-velocities, right: y-velocities). For comparison the transversal distribution of conventional vessels are given in Figure 65. It is important to note that these distributions are based on a $U_{X,max}$ or $U_{Y,max}$ with a value of 1. So the graphs below show the ratio to this value as a function of distance from the centreline, they can't be used to compare different velocity magnitudes.

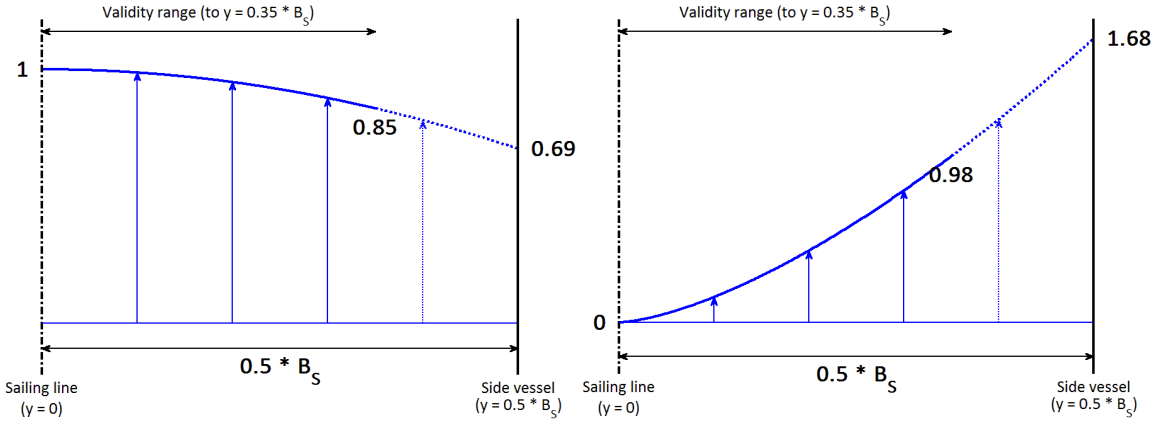

Figure 64: Transversal distribution for barges (left: x-velocities, right: y-velocities)

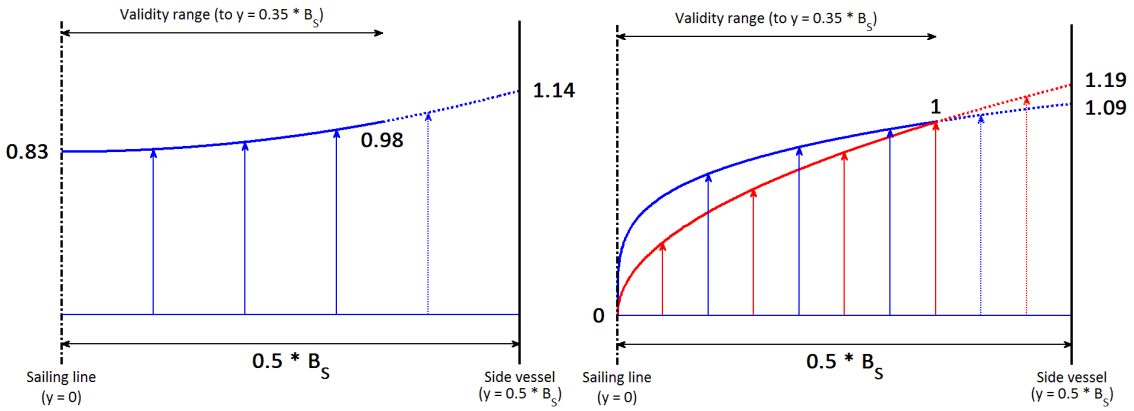

Figure 65: Transversal distribution conventional vessel (left: x-velocities, right: y-velocities)

Longitudinal distribution

Due to the fact that only 8 experiments were done with barges, and the prediction of a longitudinal velocity distribution under the keel is very difficult (see Appendix F), it is decided not to make a prediction function for the longitudinal velocity distribution under barges. As discussed before, computer models should be used or made to determine these distributions. The general trend on the longitudinal distributions is already given in § 4.2. Some extra remarks are given in Appendix F.

5.5 Model validation

For the validation three data sets from previous experiments are available:

- WL|Delft Hydraulics (1984)
- Maynord (1990)
- VBD (2003)

Unfortunately, the data of VBD is only available on graphs, and therefore the maximum velocities had to be estimated from these graphs. Furthermore, the data sets of WL|Delft Hydraulics and Maynord only give the maximum occurring velocity in the centreline of the vessel. The velocities are measured with a micro-mill (WL), an ADV (Maynord) and a dynamic pitot tube (VBD). This means the

maximum occurring velocity is the absolute velocity (independent of direction) for WL and Maynord, but VBD only measured the x-velocity. Since the velocity for these experiments is measured in the sailing line of the vessel, for the validation of the model the maximum x-velocity in the centreline is used.

For the experiments with conventional ships almost no data sets exist to validate the model. The available data sets mainly use barges, only in the data set of WL|Delft Hydraulics there are a few (12) experiments with conventional vessels. This is unfortunate, since with this research it is vice versa: there are more experiments with conventional vessels than with barges. Therefore, the formulation for conventional vessels is validated, while the formulation for barges is adapted based on the outcome of the validation.

Conventional vessel

During the experiments of WL|Delft Hydraulics two types of 'conventional' vessels were used: the Rijn-Herne-Channel (RHK) ship 'Adriaan', and the research vessel 'Rixt'. Both ships are used in 6 experiments. Of these vessels the RHK-ship is a real conventional vessel, while the 'Rixt' has a somewhat different keel shape (and also less draught), and is thus less useful for the validation. More information can be found in WL|Delft Hydraulics (1987). Application of equation [5.4] on the experiment data, results in Figure 66. For completeness also the current experiments are added. The goodness of fits is given in Table 27.

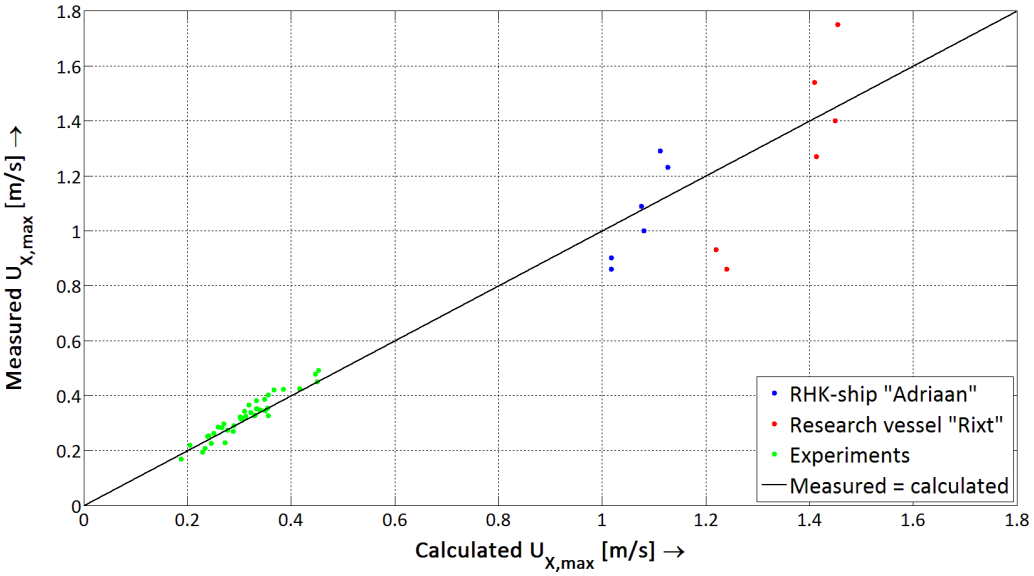

Figure 66: Validation conventional vessels

Experiments	All (RHK + Rixt)	RHK-ship 'Adriaan'	Research vessel 'Rixt'	Own experiments
R^2	0.51	0.42	0.41	0.89
RMSE [m/s]	0.19	0.12	0.24	0.03

Table 27: Goodness of fits of equation [5.4] *on other experiments*

As visible in Figure 66, there are some differences between the calculated and measured values of the maximum velocity for the experiments from WL|Delft Hydraulics. This is also shown by the goodness of fit for all experiments (which is without the experiments from this research), and the RMSE (which is approximately 20 % of the measured values!). However, the greatest deviations from the measured values are found with the research vessel 'Rixt' (see Table 27), which isn't an actual conventional inland navigation vessel (see WL|Delft Hydraulics (1984)). The error with the RHK-ship is far less; the RMSE is approximately 10% of the measured values. This is quite accurate, considering the fact that during these experiments the ship was not sailing very close to the bed (h/T = 2), while equation [5.4] has been designed with experiments in which h/T ≤ 1.4. Unfortunately, the RHK-ship only has 6 experiments, which influences the R^2-value negatively, and this value is therefore not a good indicator for the goodness of fit.

When the prediction results of equation [5.4] are compared to the prediction results of the Modified Maynord equation (recommended by Stolker et al. (2006)) and the WL|Delft Hydraulics equation (best prediction according to Table 11), Figure 67 and Table 28 are obtained. The prediction capabilities of these methods on the current experiments are already given in Table 12.

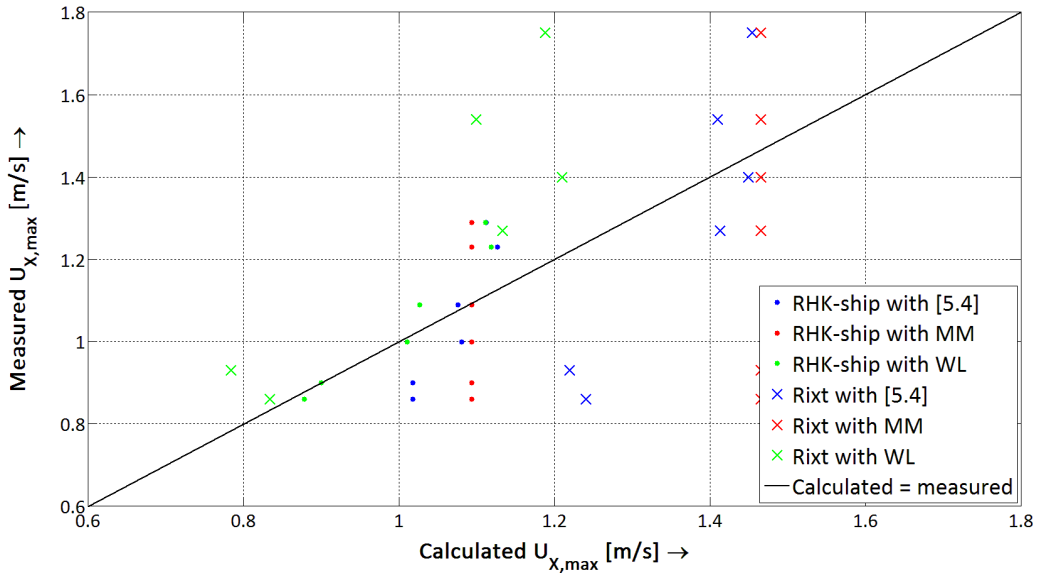

Figure 67: Validation other methods

Method	All (RHK + Rixt)		RHK-ship 'Adriaan'		Research vessel 'Rixt'	
	R^2	*RMSE [m/s]*	R^2	*RMSE [m/s]*	R^2	*RMSE [m/s]*
Equation [5.4]	0.51	0.19	0.42	0.12	0.41	0.24
Modified Maynord	-0.03	0.28	-0.04	0.16	-0.30	0.36
WL|Delft Hydraulics	0.30	0.23	0.68	0.09	0.02	0.31

Table 28: Goodness of fit of other methods on conventional vessel data

From Table 28 it can be seen that equation [5.4] is overall the best prediction method. However, for just the experiments with the RHK-ship the WL|Delft Hydraulics equation has a better prediction. The prediction for the current experiments is far worse however (R^2 = 0.36 compared to R^2 = 0.89 for equation [5.4]). The modified Maynord formula does not give an accurate prediction at all. Therefore, it can be concluded that equation [5.4] is the preferred method of calculating the maximum (x-) velocity underneath conventional vessels, and its prediction capabilities are good, especially when ships are sailing close to the bed (h/T < 1.4).

Barges

For barges there are more validation experiments available. The data set of Maynord consists of 19 experiments, WL|Delft Hydraulics has 27 experiments with barges, and there are 26 experiments from the VBD data set. Together with the 8 experiments from this research, there are 80 experiments. When equation [5.21] is used, Figure 68 is obtained. The goodness of fits for each data set is given in Table 29.

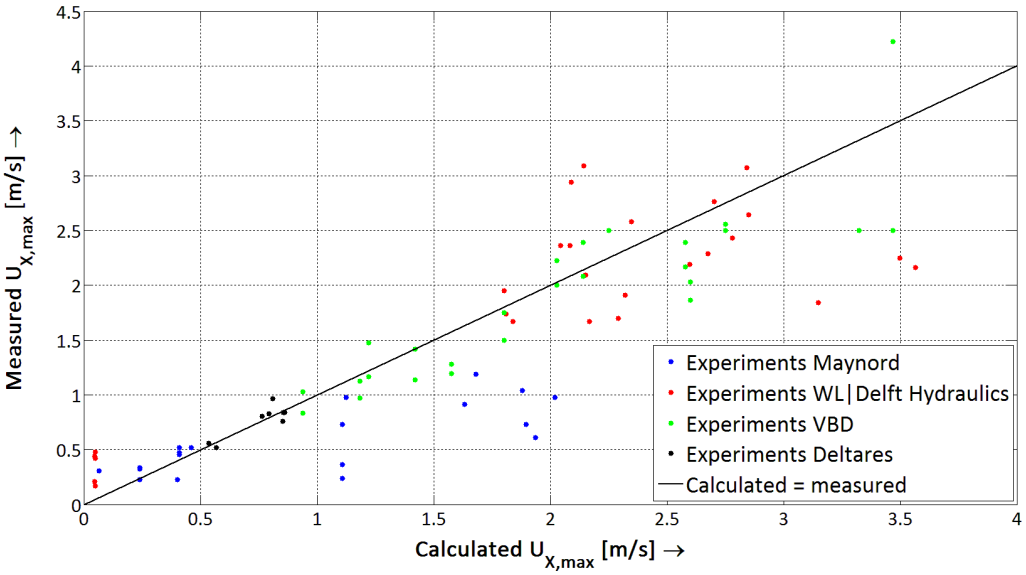

Figure 68: Validation barges

Experiments	All	Maynord	WL|DH	VBD	Deltares
R^2	0.68	-3.29	0.59	0.71	0.75
RMSE [m/s]	0.50	0.62	0.58	0.40	0.07

Table 29: Validation equation [5.21] for *different barge experiments*

As visible from Table 29 and Figure 68, the predicted values deviate significantly from the measured values. The results of the experiments of Deltares (on which the equation is based) give a good prediction, just as the results from VBD. For the experiments of WL|Delft Hydraulics the results are better than for the experiments of Maynord, although the results of WL also have some large deviations. The overall goodness of fit is reasonable, but from Figure 68 it can be clearly seen that a better relation is possible.

Therefore, an improved equation is made, based on all experiments. Since only the experiments from this research contained an ambient flow velocity U_0 (all other experiments have been carried out with U_0 = 0 m/s), it is chosen to keep this part of the improved equation equal to equation [5.21]. So only the coefficients for the influence of V_S change. The resulting function is given by [5.28].

$$U_{X,max} = 1.36 \cdot \left(\frac{T}{h}\right)^2 \cdot V_S - 1.7 \cdot \left(\frac{h}{B_S}\right)^{\frac{1}{3}} \cdot U_0 \qquad [5.28]$$

The prediction results for the different experiments are given in Figure 69 and Table 30.

Experiments	All	Maynord	WL|DH	VBD	Deltares
R^2	0.76	-1.76	0.69	0.75	0.07
RMSE [m/s]	0.44	0.50	0.51	0.37	0.14

Table 30: Validation improved equation [5.28] *for different barge experiments*

The results are better than with the original equation ([5.21]), which is also shown by the R^2-value (0.76) and the RMSE of 0.44 m/s. In fact, for all experiment sets (except the research experiments) the goodness increases. Therefore, equation [5.28] is preferred for calculating the maximum x-velocity underneath barges.

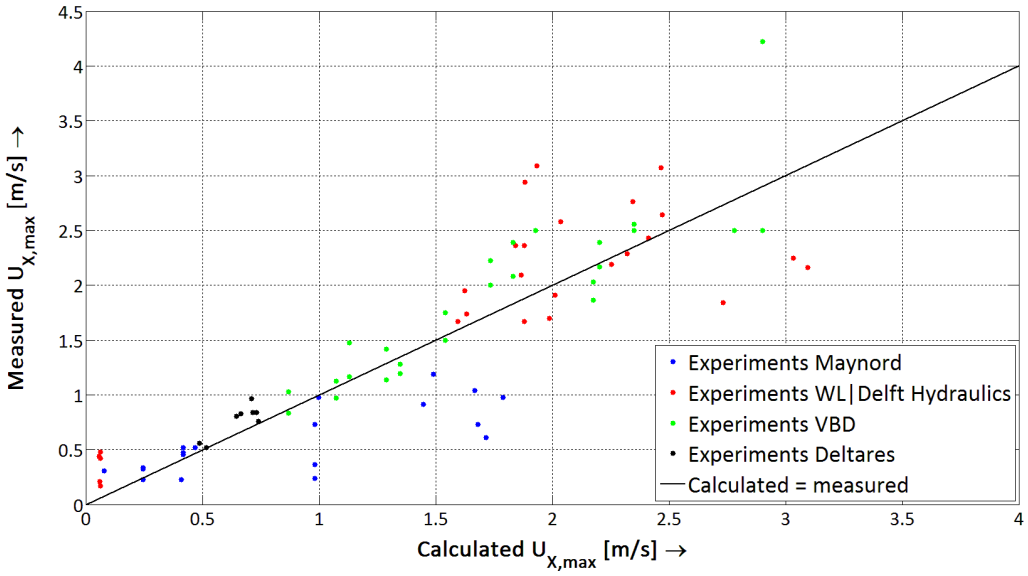

Figure 69: Validation for barges, based on equation [5.28]

Stolker et al. (2006) found the best function to predict the maximum occurring velocity underneath barges was the Modified Maynord equation (see equation [2.22]). When this equation is applied on the same data, it is found that R^2 = 0.77 and the RMSE = 0.43 m/s. This means the newly found prediction formula [5.28] is approximately equally good as the Modified Maynord approach, which can be seen in Figure 70. As visible, the differences are negligible. This could be expected, since the coefficients of the Modified Maynord (1.07 and 1.81) are quite similar to the coefficients from equation [5.28] (1.36 and 2).

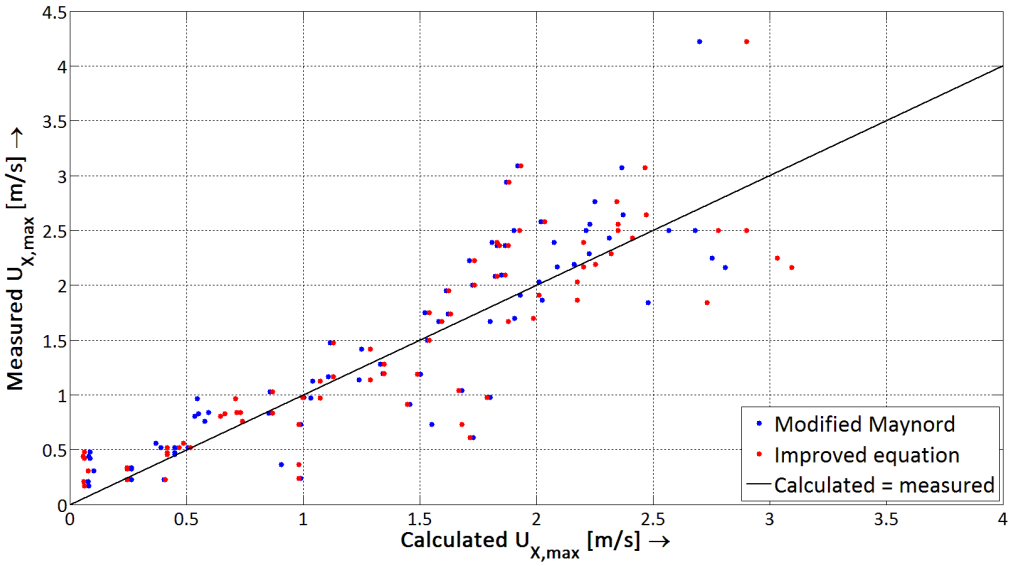

Figure 70: Differences between equation [5.28] *and the Modified Maynord equation*

Conclusions

Unfortunately the lack of data (especially about the y-velocities underneath sailing vessels) does not allow for validation of all predictive relations. The only available data is for maximum velocities in the sailing line of the vessel. This means only the equations on the maximum x-velocity can be validated.

During the validation of conventional vessels, it was found that equation [5.4] gives a good prediction of the maximum x-velocities, much better than the other existing methods, which have been

designed for barges. It can be concluded that equation [5.4] is a good predictor for conventional vessels.

For barges, the predictive relation was given by equation [5.21]. However, this relation was based on just 8 experiments. During the validation the equation was adapted (by including experiments of VBD, Maynord and WL|Delft Hydraulics). This resulted in equation [5.28], which showed a good accuracy with the data. However, this does result in a worse agreement with the measurements from this research (see Table 30). Compared to the Modified Maynord approach, equation [5.28] gives similar results.

Remarks

Although the validation showed that the agreement between the designed predictive relations and the measurements from other experiments were reasonable, some remarks are in order. The data from other experiments were differently obtained, which could explain part of the deviations.

During the experiments of WL|Delft Hydraulics micro mills were applied to capture the velocity beneath the vessel. These were fixed in the sailing line of the ship and measured absolute velocities, which is already a difference with the basis of the designed equations, which were based on x-velocities. Furthermore, according to WL|Delft Hydraulics (1984) the micro mills were placed at 1.25 m above the bed (prototype value, with a water depth of 6 m), while in the current experiments the EMS-devices measured velocities at the bed. This could explain part of the differences between measurement and calculations. In § 4.5 it was shown that the maximum velocity in the vertical was near the bed. This means the measured velocities of the WL|Delft Hydraulics experiments would be higher near the bed, which corresponds to the generally higher calculated maximum velocities (see Figure 68). This effect is partly reduced however, since absolute velocities are measured, possibly leading to higher measured velocities than the real x-velocity.

During the experiments of Maynord a Nixon propeller meter was used (see Maynord (1990)), which could not measure direction. Just as with the WL|Delft Hydraulics experiments this means eventual y-velocity fluctuations are part of the maximum measured velocities. Here however the results are compared with the maximum x-velocity, without y-velocity fluctuations. Strangely enough the calculated values are still higher than the measured velocities (see Figure 68). The meter was placed at 2 ft. above the bed, with water depths of 15 and 30 ft. (prototype situations), which translates to approximately 0.04 and 0.02 m above the bed in the current experiments. This is also quite far above the bed, which might explain a part of the difference with the predicted velocities.

The data points from the VBD experiments had to be read from graphs, with an error margin of approximately 0.1 m/s. They were measured with pitot tubes, situated 0.014 m above the bed during the experiments. This is already quite close to the bed, and results in x-velocities, without y-fluctuations. As a result, the experiment data is similar to the current experiments, and this can also be seen in the validation. The values of the VBD experiments cluster around the line in Figure 68. Nevertheless, it can be seen that there are some deviations.

The lack of experiments for conventional vessels makes it difficult to validate the equation for the maximum x-velocity. More data is necessary to validate (or improve) the current function.

The data from previous experiments only gives a single value per experiment; unfortunately they do not give information about x- and y-distributions or x- and y-velocities. From the different sources some graphs are available, but not exact data on velocities. This means the other developed equations can’t be validated at this moment. On the other hand this shows the uniqueness of this data set.

Despite all these drawbacks and remarks, the validation shows the validity of the developed maximum x-velocity equations. More validation is recommended however, possibly the data of the Julianakanaal tests can be used for this, which have been carried out by Deltares in the summer of 2014.

6. Conclusions and recommendations

The goal of this research was **to develop an analytical model which is able to predict the flow velocities between the keel of an inland navigation vessel, sailing at small underkeel clearance, and the bed of the waterway.**

In addition the research questions, which were defined to obtain this goal, are as follows:

- What are the governing parameters that determine the flow beneath a sailing vessel?
- How do the governing parameters influence the flow field beneath a sailing vessel?
- On what properties does the fanning out effect depend, and how does it influence the flow field?
- What happens with the flow beneath vessels at very small underkeel clearances?
- What is the influence of the flow beneath sailing vessels on erosion of the bed?

In order to present a prediction model and answer the research questions a physical model study has been carried out at Deltares. The setup of the physical model study was based on literature research and the governing conditions on Dutch rivers. During the experiments flow velocities, pressures and forces were measured. In total 84 experiments have been performed with a (length) scale of 30. The experiments gave insight into the flow field and the erosion of bed material, and enabled to develop empirical formulas for the flow velocities. The results are presented in § 6.1, and recommendations for future research on this topic are given in § 6.2.

6.1 Conclusions

In the following answers are given to the research questions. Conclusions/answers are organized into:

- Flow description (types of flow and fanning-out effect)
- Influence of different parameters on flow underneath the keel
- Erosion of bed material
- Empirical flow model
- Use of prediction methods

Flow description

Types of flow

Two distinct types of flow can be distinguished underneath the keel of sailing ships. Which type of flow occurs, depends on the development of the boundary layers of ship and bed. If these boundary layers interact ('touch'), the flow beneath the keel is obstructed, leading to a completely different flow situation than when the boundary layers do not interact. A simple threshold for this boundary layer interaction has been derived; interaction occurs for approximately $L_{PP} / (h - T) > 58$ (in which L_{PP} is the ship length, T is the draught and h is the water depth). In that case the flow will be obstructed at some point beneath the keel. This results in small velocities at the bed or even flow in the sailing direction for smaller underkeel clearances. Between this point and the bow all flow must be diverted to the sides, which is called the fanning-out effect. This leads to large velocities near the sides of the keel. After the point of boundary layer interaction, there is only limited flow underneath the keel.

When the boundary layers do not interact ($L_{PP} / (h - T) \leq 58$) the flow is not obstructed completely, leading to only small fanning-out of the flow. As a result, the velocities after passage of the bow somewhat decrease, but later on (near the stern) they increase again due to some fanning in.

In reality, the best way to calculate whether the boundary layers interact is to actually calculate the boundary layer thickness and the actual underkeel clearance.

Fanning out-effect

The experiments have clearly proven the fanning-out effect underneath the keel of a ship. With decreasing keel clearance this effect (the discharge) increases, since the effective flow area reduces (due to boundary layer development) more rapidly. This leads to higher transverse velocities with decreasing underkeel clearances. The velocities also increase with the width of the ship, because a larger discharge needs to be diverted to the sides, while the area of possible outflow (UKC · L_{PP}) does not increase.

However, it is also observed that near the stern of the vessel there seems to be fanning-in: the flow goes from besides the vessel underneath the stern. In reality this effect might be even larger due to the suction effects of the ship's propellers.

Influence of parameters on the flow underneath the keel

As expected, the sailing speed and ambient flow velocity positively influence the flow underneath the keel (increase in V_S or U_0 leads to an increase in flow underneath the ship). The ambient flow velocity U_0 has a larger impact on the velocities than the sailing speed V_S. The degree in which the ambient flow velocity and the sailing speed influence the flow is determined by the bow shape, the (relative) underkeel clearance and the ship's width.

The bow shape is the most important influence, which can be seen by the different results for conventional vessels and barges. The bow shape influences the amount of water which is forced underneath the ship, and thus the velocities. The occurring velocities for barges are approximately 2 times higher than for conventional ships.

Secondly, the actual distance between the ship's keel and the bed is also very important. With decreasing underkeel clearance, the velocity on the bed beneath the ship increases. However, for very small keel clearances boundary layer interaction 'blocks' the area underneath the keel, which reduces the velocities near the stern of the vessel.

The ship's width influences mainly the fanning-out effect. When the ship's width increases, the total discharge under the keel increases, while the outflow area (UKC · L_{PP}) remains equal. This results in an increase in transverse velocity. However, it should be noted that due to the fixed dimensions of the flume and the ship, the influence of these dimensions on the flow field underneath the ship could not be ascertained. As a result, their effect is not included in the empirical formulations.

Erosion of bed material

Erosion of bed material was clearly observed during the experiments. The pick-up of sediment underneath the keel of inland navigation vessels is determined by velocity gradients and turbulence fluctuations. Most sediment transport does not occur underneath the bow (where x-velocities are the highest), but immediately alongside the vessel. Smaller underkeel clearances result in increased turbulence, and thus more erosion. Barges induce higher velocities than conventional vessels, which in turn lead to more erosion. Especially with bed forms erosion due to the passing of a vessel is clearly visible: the bed forms flatten due to erosion at the tops and deposition in the troughs. For the removal of small shallows this might be an interesting effect, although small underkeel clearances are needed, as well as multiple passages of vessels (preferably barges).

Empirical flow model

An empirical flow model has been developed to predict the flow velocities at the bed underneath conventional inland ships and barges. The model is based on the maximum velocities in the sailing and transverse direction. The model can also compute the maximum velocity distribution perpendicular to the sailing direction (over the width of the ship), and the maximum velocity distribution in the longitudinal direction. By combining these functions the complete flow field (magnitude and direction) underneath the keel can be computed.

For conventional vessels, with a more streamlined bow, the maximum velocity underneath the keel almost always occurs near the edge of the keel, both for x- and y-velocities, as well as absolute velocities. The maximum x-velocity and absolute velocity occur approximately at a distance of

$0.2 \cdot L_{PP}$ from the bow. For barges the maximum x-velocity occurs immediately after the bow, in the centerline of the vessel. With a large underkeel clearance, the effect of the fanning out is very small, and thus also the maximum absolute velocity is located here. For smaller underkeel clearances the maximum absolute velocity is located right after passage of the bow, near the side of the keel. This is also where the highest y-velocities are recorded.

The application range for the empirical flow model is restricted to the experimental range: $1.1 \leq h/T \leq 1.7$. It is recommended to use the model based on the underkeel clearance UKC. Furthermore, the model is more accurate for conventional vessels than for barges, because the number of experiments carried out with barges was very limited.

Maximum flow velocities

Equations have been developed for the maximum flow velocities in different directions, see § 5.2 for more detailed information. Here only the formula for the maximum absolute velocity (U_{max}) is given:

$$U_{max} = 0.32 \cdot \left(\frac{B_S}{h-T} \right)^{\frac{1}{4}} \cdot V_S - 0.36 \cdot \left(\frac{h}{h-T} \right)^{\frac{3}{4}} \cdot U_0 \qquad [6.1]$$

In which: V_S = sailing speed [m/s] U_0 = ambient flow velocity [m/s]
B_S = ship's width [m] T = draught [m]

The maximum velocity equations are restricted to $-0.35 \cdot B_S \leq y \leq 0.35 \cdot B_S$, in which $y = 0$ at the centerline of the vessel. Probably larger velocities may be found outside this region. This is unknown however, since no measurements were done in this area.

The barge model uses the same functions as the model for the conventional vessels, only with different coefficients (see § 5.4). Due to the small amount of barge experiments, these prediction functions are less accurate. They could not be improved further since no other data sets are available, only the maximum occurring x-velocity prediction function was improved during the validation.

Velocity distributions

The transversal distribution functions predict the maximum occurring x- and y-velocities for a specific y-coordinate as a function of the maximum flow velocities. The functions are at least valid for $-0.35 \cdot B_S \leq y \leq 0.35 \cdot B_S$. Unfortunately finding prediction functions for the longitudinal distribution was difficult and resulted in highly empirical formulas. It is not recommended to use these longitudinal distribution functions, since there are not very robust.

Validation

Validation of the empirical flow model was done with three other data sets, but unfortunately only data on the maximum x-velocities was available. For conventional vessels only 6 experiments are available. The RMSE for the predictions of the maximum x-velocities are approximately equal to 10% of the measured values, meaning the model predicts the maximum x-velocity fairly good.

For the barge model more data (with respect to maximum x-velocities) was present, but validation showed that the prediction function for barges is less accurate. Adapting the equation to fit the validation data resulted in a slight improvement, but still the RMSE is in the order of 20% of the maximum velocity, which is quite a large deviation. However, compared with the predictions of the Modified Maynord approach, identified by Stolker et al. (2006) as the best prediction method for maximum velocities underneath the ship's keel, the errors are equally large.

Use of prediction methods

For conventional vessels, it has been shown that of all previous prediction methods only the WL|Delft Hydraulics equation gives reasonable results. However, the newly developed method gives much better results, and is therefore preferred. The new method does not only provide maximum x-velocities, but also y-velocities and transversal distributions of velocities. Although a further check of the validity of some of these equations is required, the method is much more enhanced than the previous methods.

For barges the optimized new equation for the maximum velocity in the sailing direction is approximately equally good as the Modified Maynord equation. However, this method only gives the maximum x-velocity, while the newly developed method also gives insight into the other occurring velocities underneath the keel. These other equations need to be used with care, since validation is not yet possible due to the lack of data sets. Nevertheless, the insight into the flow field beneath the keel is significantly improved by the developed method.

6.2 Recommendations

Based on the research, the following recommendations are given to improve the knowledge with respect to flow beneath sailing inland vessels:

- The most important recommendation is to make a computer model which is able to simulate the flow field beneath vessels, particularly when sailing with small underkeel clearances. The experimental results of this study can be used to validate the numerical model. With a CFD-model the most important physical processes can be simulated. With the help of such a computer model, research can be done into:
    - Ship movements and navigability
    - Influence of different bed forms on the ship's behavior
    - Erosion/sedimentation due to the passing of a vessel by coupling the flow model to an erosion/sedimentation model.
- The current empirical model requires more validation to improve the accuracy. Only the maximum x-velocity equations have been validated at this moment due to the lack other data sets. Therefore it is recommended to search for extra data sets, carry out more experiments, or use a numerical model (which has to be developed yet). During this study, also prototype tests were performed in the Julianakanaal in the Netherlands. Results from this research can be used for validation/improvement of the model, which is highly recommended.
- Some parameters were not varied during the experiments, although they may play an important role in the flow field underneath the ship. Therefore, it is recommended to investigate the effects (on the flow) of these parameters:
    - Ship's width B_S
        - influences the fanning-out effect
    - Ship's length L_{PP}
        - influences the total thickness of the boundary layer on the hull
    - Cross-sectional area A_C
        - influences the available area for the return flow adjacent to the ship, and thus probably also the discharge underneath the ship's keel
    - Roughness of the ship's keel
        - influences the development of the boundary layer

  The majority of these parameters are not included in the empirical formulations now. Their effect can be investigated by means of new experiments, or by a newly developed computer model.
- A good prediction model has been developed for the conventional inland vessels, but the model for barges is still inaccurate. It is highly recommended to improve this model, because the interaction between barges and the river bed is stronger than for conventional vessels. Perhaps the results of the Julianakanaal tests can be used or an eventual computer model.
- It is established that for small underkeel clearances the boundary layer development plays an important role on the flow field. Interaction with the bed results in a flow blockage underneath the ship. Also other phenomena, such as Couette flow, keel roughness and potential flow are important in this respect. These phenomena should be implemented in the model to increase the theoretical basis of the developed empirical model. However, this requires more research into these phenomena, as well as the effects on the bed.

References

Blaauw, H.G. and Knaap, F.M.C. van der, 1983 *Prediction of squat of ships sailing in restricted water*, Publication no. 302, WL|Delft Hydraulics, Delft

Bots, H.C.G., 2011 *Efficient maintenance of the Dutch fairways*, MSc thesis, TU Delft, Delft

Bouwmeester, J., Kaa, E.J. van de, Nuhoff, H.A. and Orden, R.G.J. van, 1977 *Recent studies on push-towing as a base for dimensioning waterways*, WL|Delft Hydraulics, Delft

Gourlay, T., 2006 *Flow beneath a ship at small underkeel clearance*, Journal of Ship Research, Vol. 50, No. 3, pp. 250-258

Ijsebaert, T., 2010 *Integral Design of Work Channels and Basins for the Execution of Dredging Projects*, MSc thesis, TU Delft, Delft

Jansen, P.P. and Schijf, J.B., 1953 *Paper presented at the XVIIIth International PIANC Congress*, 18th International PIANC Congress, Rome, Italy

Lenselink, R.J., 2011 *Interaction between loaded barges and bed material*, MSc thesis, TU Delft, Delft

Lundbladh, A. and Johansson, A.V., 1991 *Direct simulation of turbulent spots in plane Couette flow*, Journal of Fluid Mechanics, Vol. 229

Maynord, S.T., 1990 *Velocities induced by commercial navigation*, Department of the Army Corps of Engineers, Technical report HL-90-15, Louisville, USA

Maynord, S.T., 2000 *Physical Forces near Commercial Tows*, Department of the Army Corps of Engineers, ENV report 19, Louisville, USA

PIANC and IAPH, 1997 *Approach channels – a guide for design*, Final report of Working group no. 30, PIANC, Brussels, Belgium

Port of Rotterdam, 2012 *Modal split containers 2009 - 2012*, Port of Rotterdam, Rotterdam

Rodríguez, J.F., Admiraal, D.M., López, F and Garciá, M.H., 2002 *Unsteady bed shear stresses induced by navigation: laboratory observations*, Journal of Hydraulic Engineering, Vol. 128, No. 5, pp. 515-526

Schiereck, G.J. and Verhagen, H.J., 2012 *Introduction to bed, bank and shore protection*, Lecture notes CIE4310, 2nd edition, VSSD, Delft

Schijf, J.B., 1949 *Paper presented at the XVIIth International PIANC Congress*, 17th International PIANC Congress, Lisbon, Portugal

Schlichting, H., 1968 *Boundary-Layer Theory*, 6th edition, McGraw-Hill, New York, USA

Shields, A., 1936 *Application of similarity principles and turbulence research to bed-load movement*, Preussischen Versuchsanhalt fur Wasserbau und Schiffbau, Berlin, Germany

Sieben, A, 2014 *Ship parameters fairways* (in Dutch), memo RWS

Stolker, C. and Verheij, H.J., 2006 *Ship-induced water motions beneath the ship's hull*, 31th International Navigation Congress PIANC, Estoril, Portugal

Talmon, A. and Verheij, H.J., 2014 *Memo aan RWS*, concept KPP 2014 Vlot en veilig gebruik vaarwegen, Deltares, Delft

Tillmark, N. and Alfredsson, P.H., 1992 *Experiments on transition in plane Couette flow*, Journal of Fluid Mechanics, Vol. 235, pp. 89-102

Uijttewaal, W., 2013 *Lecture notes Turbulence in Hydraulics*, Lecture notes CIE5312, TU Delft, Delft

VBD, 2003 *Introduction of enlarged four barge units on the Rhine*, VBD-report 1713, Versuchsanstalt für Binnenschiffbau e.V., Duisburg, Germany

Verheij, H.J., Stolker, C. and Schwanenberg, D., 2004 *Flow velocities beneath a ship's keel and their effect on bed material*, WL|Delft Hydraulics, Delft

Verheij, H.J., Stolker, C. and Groenveld, R., 2008 *Inland Waterways – Ports, waterways and inland navigation*, Lecture notes CT4330, VSSD, Delft

Vriend, H.J. de, Havinga, H, Visser, P.J., Wang, Z.B., 2010 *River Engineering*, lecture notes CIE4345, TU Delft, Delft

WL| Delft Hydraulics, 1984 *Erosion of cross-sections of navigation channels: setup physical model water movement due to navigation* (in Dutch), report model research M1115 part 3b, WL|Delft Hydraulics, Delft

WL| Delft Hydraulics, 1986 *Erosion of cross-sections of navigation channels: return flow, water motions and stability* (in Dutch), report model research M1115 part 10b, WL|Delft Hydraulics, Delft

WL| Delft Hydraulics, 1987 *Erosion of cross-sections of navigation channels: systematic test serie of water motions by three different types of inland navigation vessels* (in Dutch), report model research M1115 part 4, WL|Delft Hydraulics, Delft

White, F.M., 2008 *Fluid mechanics*, 6th edition, McGraw-Hill, New York

List of figures

List of tables

Appendices

Appendix A – Design experiments

Design flume

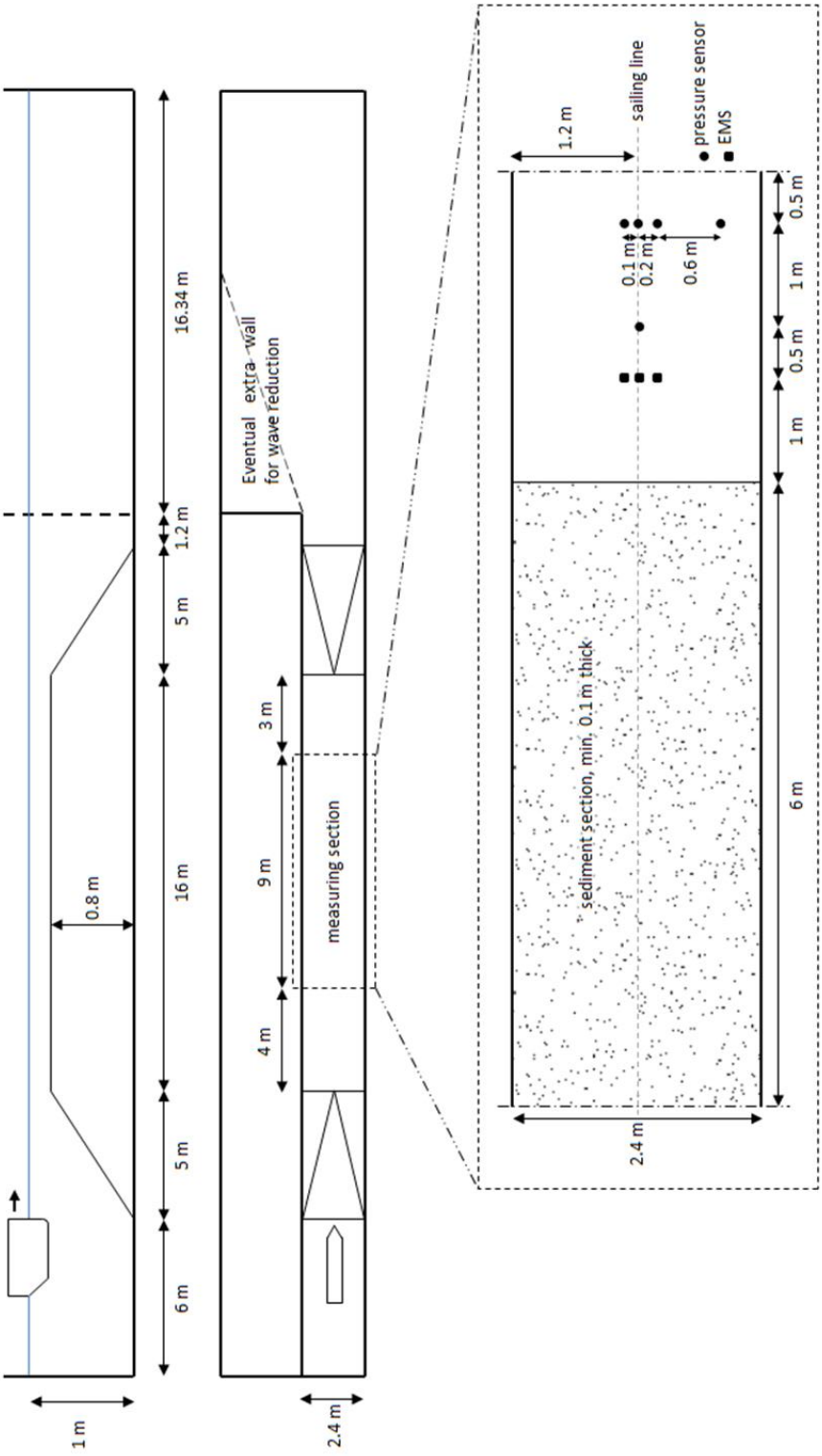

Appendix A - Figure 1: Design flume

Appendix A - Figure 1 gives the design of the flume with all distances and placement of the measurements. For more information about the design of the flume, see the work plan by Talmon et al. (2014). Additional information on measurement instruments can be obtained via Deltares.

Placement instruments flume

After installation of all the measurement devices, the exact position in the flume has been measured. The results are given in Appendix A - Table 1, while Appendix A - Figure 2 shows the general overview of the location of the instruments.

Device	X	Y	Z	Remarks
EMS 1	11,000 m	1,302 m	0,000 m	
EMS 2	11,000 m	1,203 m	0,000 m	
EMS 3	11,000 m	1,001 m	0,000 m	
EMS 4	5,027 m	0,217 m	0,170 m	After test 40: x=3.61 m y=0.213 m
DP 1	11,500 m	1,205 m	-0,016 m	
DP 2	12,542 m	1,2995 m	-0,017 m	
DP 3	12,542 m	1,201 m	-0,018 m	
DP 4	12,542 m	1,001 m	-0,017 m	
DP 5	12,542 m	0,602 m	-0,016 m	
Pressure sensor start	0,955 m	0,250 m	0,0135 m	
Pressure sensor end	14,930 m	0,250 m	0,0135 m	
Pulse 1	4,022 m	-	-	X-value is bow of ship
Pulse 2	15,993 m	-	-	X-value is bow of ship

Appendix A - Table 1: Placement (x, y and z-coordinate) of measurement instruments in the flume

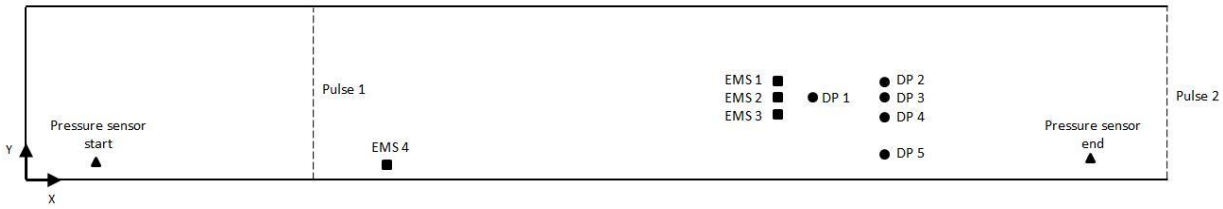

Appendix A - Figure 2: Location of different measurement instruments

Placement instruments ship

For the instruments in the ship the same procedure has been followed, see Appendix A - Table 2 and Appendix A - Figure 3.

Device	X	Y	Z	Remarks
Force meter 1	0,7085 m	0	-	
Force meter 2	2,2935 m	0	-	
PDCR 1	0,735 m	0	-	
PDCR 2	0,985 m	0	-	Broken during some of the tests before being replaced
PDCR 3	1,485 m	0	-	
PDCR 4	2,253 m	0	-	
EMS 1	0,809 m	0	-	
EMS 2	1,809 m	0	-	

Appendix A - Table 2: Placement (x and y-coordinate) of measurement instruments in the flume

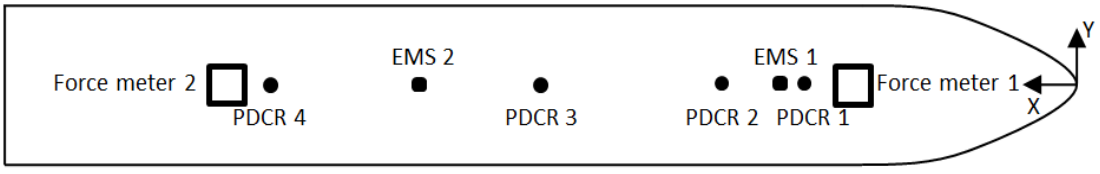

Appendix A - Figure 3: Location of different measurement instruments in ship

Measurement instruments

EMS

The electromagnetic velocity meter (EMS) is a device which measures velocities in x- and y-direction. The device creates a magnetic field, through which the water flows. This will create a potential difference, proportional to the velocity of the flow. The measurement area had a diameter of approximately 55 mm, with a thickness of 5 mm, directly underneath the electrodes in the probe's head. During the experiments two different type of EMS-devices have been used.

- Traditional EMS-device (E-30 probe): with a slightly curved head. These probes were used in the ship and for the determination of the ambient flow velocity (EMS4).
- Adapted EMS-device: these EMS-devices were specially made with a flat head to fit into the bottom without disturbing the flow (EMS 1 – 3).

The devices can measure velocities up to 2.5 m/s in all directions. The output signal is a 0-10 V signal (after amplification) which is converted to a velocity by means of a P-EMS control-unit. Appendix A - Figure 4 shows the electrodes on the EMS-head (left) and the entire probe (EMS4) in the flume (right). More information on EMS-devices can be found in Uijttewaal (2013) or via Deltares.

Appendix A - Figure 4: EMS-probe head with electrodes (left) and EMS-30 probe in flume (right)

DP-cells

DP-cells are pressure sensors. In the false bottom 5 of these cells are installed. They exist of two small open channels with a membrane in between. One channel is connected to a reference pressure, while the other channel is in contact with the flume (situated in the bottom, aimed upward). In this part the pressure continuously changes, dependent on the situation in the flume directly above the device. The difference in pressure between the flume and the reference pressure results in a curvature of the membrane.

The exact curvature of the membrane is measured, which results in an output signal after amplification of 0-10 V. The installed DP-cells could measure pressures up to 60 mbar. All DP-cells were connected to the same reference pressure. Since the vertical placement of each DP-cell was not exactly equal (see Appendix A - Table 1), the reference pressure is compared to DP-cell 1.

Appendix A - Figure 5 shows a DP-cell.

Appendix A - Figure 5: DP-cell

PDCR

A PDCR is a sensitive pressure meter, which were mounted in the keel of the ship to measure the pressures here. The PDCR's uses during the experiments were able to measure pressures up to 125 mbar, and gave an output signal (after amplification of the signal) of 0-10 V. A problem with the PDCR's was the fact that they were not completely waterproof. Although the ship was almost waterproof, at the place where the PDCR's were mounted some water could flow in. Therefore adhesive waterproof clay was used here, which severely diminished water inflow. Nevertheless, during some tests a PDCR (PDCR 2) was broken due to water damage. Later on, this device was replaced.

Force meters

The force meters were installed on the ship, between the ship itself and the frame. It consists of a hard steel casing, in which a sensitive core measures all forces with strain gauges. The hard steel casing was screwed onto the ship, and the sensitive core (also with hard casing) was attached to the screw-threaded rods. When a force is exercised on the ship, the strain gauges are stretched, which is measures. For all directions (x,y and z) different strain gauges are present, which results in different signals for each direction. After amplification through a signal amplifier (like with the rest of the instruments (except the EMS)), an output signal of 0-10 V is obtained. The force meters were capable of measuring forces up to 100 kg (980 N) in all directions. Differences in measurement between the two force meters will result in moments on the ship (pitch and yaw).

Profile tracker (provo)

The profile tracker, also known as the provo, is capable of measuring bed levels. It consists of a long pole with a probe, attached to a station. The probe measures conductivity of the water and in a way can sense the presence of the bed. When the bed level drops, the conductivity will increase and the station lowers the pole until the conductivity decreases again due to the presence of the bed. If the bed level increases, the conductivity will decrease and the station raises the pole. In this way the profile is followed when the provo is towed over the bed. The exact height of the needle of the pole is measured by the station, which results in the bed levels. During the experiments with sediment the bed profile was measured in longitudinal direction from 0 – 0.5 m outside the sailing line, with an interval of 0.05 m. Also some transversal profiles were measured:

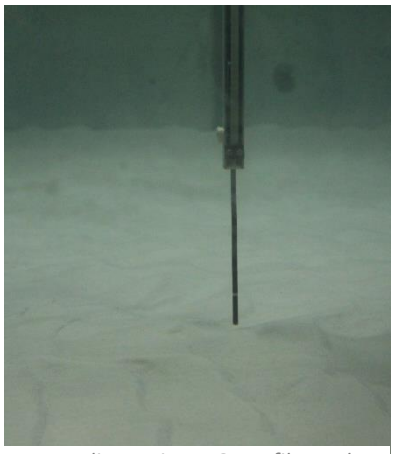

Appendix A - Figure 6: Profile tracker

- For flat sediment beds: at 1.76, 3.07 and 4.49 m from the start of the sediment bed.
- For experiment 51: at 2.15, 2.25, 3.42 and 3.52 m from the start of the sediment bed.
- For experiment 48 and 50: at 2.29, 2.39, 3.48 and 3.58 m from the start of the sediment bed.

There were some problems with the provo. First of all it had the tendency to vibrate, which resulted in poor measurements. To counteract this, the speed in which the provo was towed over the bed had to be reduced, which increased measurement time significantly. Also, there were differences in measurements between morning and midday, probably due to suspended concentrations and water temperature. This means some measurements are difficult to compare and only a quantitative comparison can be made.

Measurement stations

All output signals from the measurement devices were collected at two different stations. One station was situated next to the flume, here all data from the devices in the flume was collected. The other station was situated on the moving bridge, and here all data from the ship was collected. At these stations the signals were converted to actual pressures/velocities/etc, with a sampling frequency of 30 Hz (all devices). Later on, the data from the stations could be merged by using two

pulse signals at specific locations in the flume. These pulses were collected in both stations, so later on the data of the stations could be combined. Appendix A - Figure 7 shows the set-up of both stations.

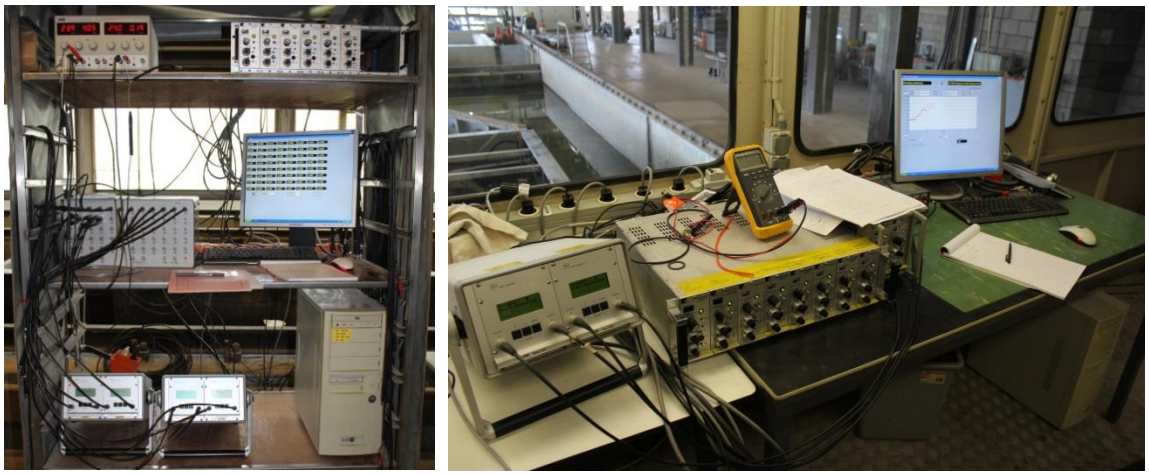

Appendix A - Figure 7: Measurement station of flume (left) and moving bridge (right)

Ship design

The general ship design is given by Appendix A - Figure 8. The model ship was already available from a previous experiment, only the bow had to be modified. The total length of the ship is 3 m. The bow (first 0.7 m) was made of foam, while the midship section was a wooden box. The stern (last 0.7 m) again consisted of foam. The whole ship was covered with a layer of epoxy, smoothing the keel and strengthening the foam.

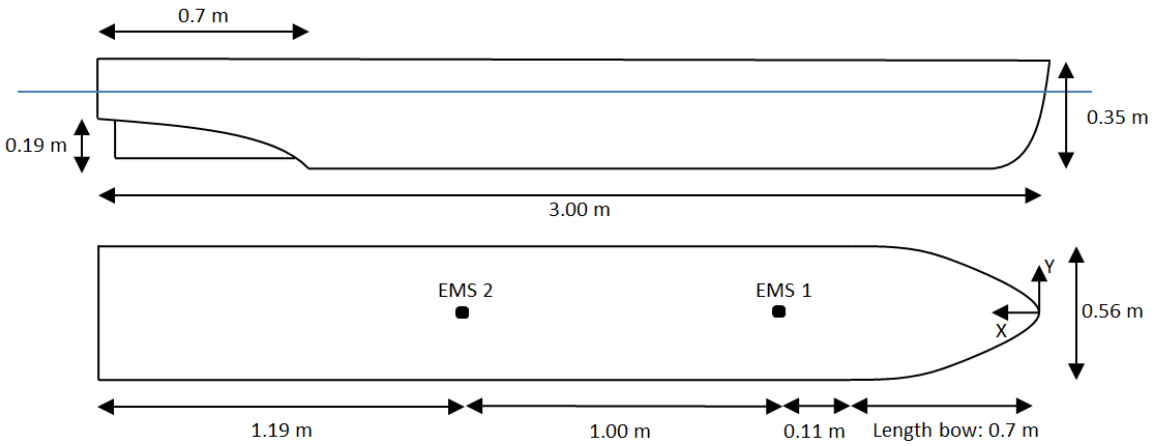

Appendix A - Figure 8: Design ship

Conventional inland vessel bow

For the conventional inland vessel bow a replica of a ship from H.J. de Koning-Gans has been used. It is a typical inland motor vessel, with a blunt bow and a flat keel. The frame plan of the bow is given in Appendix A - Figure 9 (left). The water line is taken to be at the top of these frame lines. In reality this is approximately 3.5 m, in the model this is equal to 0.23 m, with a ship's width B_S of 0.56 m. The individual frames have a spacing in the model of 25 cm (as if the model ship had been 5 m long), since the length of the model ship was too short compared to reality. Otherwise the bow would have been far too blunt. The bow was constructed from foam by hand (see Appendix A - Figure 9 (right)).

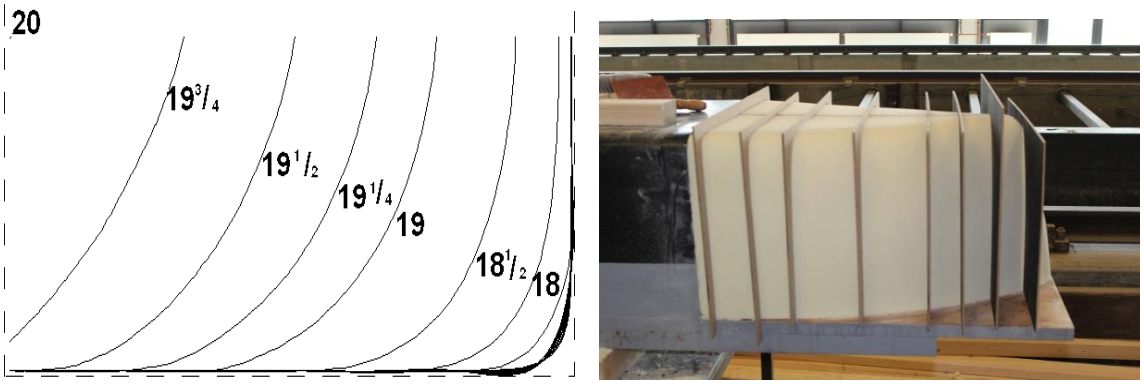

Appendix A - Figure 9: Bow of conventional inland vessel (left: frame plan, right: construction)

Push-tow barge bow

For the design of the bow of a push-tow barge an Europa-IIa barge has been used. The ship plan of such a barge can be found in M1115-IV (WL|Delft Hydraulics (1986)), figure 3. This plan has been simplified, to be able to quickly adapt the bow. Without simplifications, the adjustment of the bow would have taken too much time. The design of the bow can be found in Appendix A - Figure 11. The bow was made of wood, constructing it with foam would have taken too much time. Due to the simplification it could very well be that more flow is forced underneath the keel than with an actual barge, although the difference will not be very large. This must be remembered when using the data from these experiments. The constructed bow can be seen in Appendix A - Figure 10.

Appendix A - Figure 10: Constructed barge bow

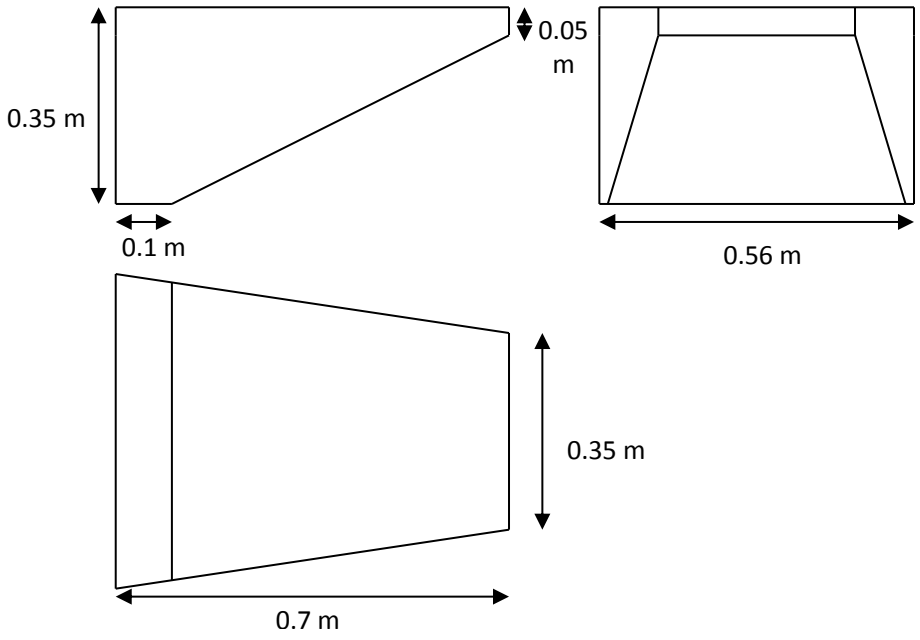

Appendix A - Figure 11: Design bow of push-tow barge

Bottom configurations

During the experiments four different bottom configurations are used. All will be discussed here shortly.

Flat bed, no sediment

The first tests with the conventional vessel and with the barge are performed with a flat bed without sediment, see Appendix A - Figure 12 (left). During these tests the velocity and pressure distributions, as well as the forces are accurately measured. These experiments were done with 4 runs, to cancel out turbulence as much as possible, and thus hopefully obtaining a clear velocity/pressure distribution.

Unfortunately due to a seam in the flume, the bed was not entirely level, but it was slightly higher near the start of the flume (top side in Appendix A - Figure 12). Therefore the experiments with the smallest keel clearance (0.01 m) could not be done.

Appendix A - Figure 12: Flat bed without sediment (left) and with sediment (right)

Flat bed, sediment

The flat bed was constructed in such a way, that some of the bottom plates could be lowered, allowing for an area of 6 m long where sediment could be placed. Over this entire stretch sediment was laid, with a thickness of approximately 0.08 m. This can be seen in Appendix A - Figure 12 (right). When the ship sails over the sediment bed, sediment is picked-up and eroded away. The sediment container in the bottom was made watertight, so no sediment could drain away somewhere else.

Sediment, dunes

A few experiments with the conventional vessel where also performed with dunes rather than a flat sediment bed. 5 dunes were constructed in the flume with dimensions as in Appendix A - Figure 14. The ship approaches at the steep side (so from right to left in Appendix A - Figure 14). After each bed measurement the dunes were restored again for the next experiment. Water levels were compared to the bottom of the flume, while the UKC now was compared to the top of the dunes. This means the draught decreased during these experiments. Appendix A - Figure 13 shows the constructed dunes in the flume.

Appendix A - Figure 13: Constructed dunes in the flume

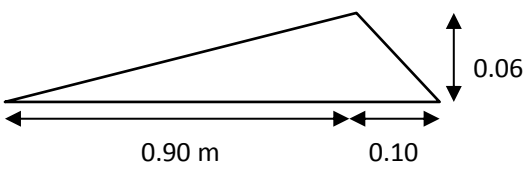

Appendix A - Figure 14: Dimensions dunes

Sloping bed

With some experiments with the conventional vessel a sloping bed was applied. All bottom plates were lifted on one end of the flume, creating a transversal slope on the bottom. This is visible in Appendix A - Figure 15. The aim was to create a slope of 1:25, after construction the slope turned out to be 1:24. During these tests especially the forces measured on the ship were important. The underkeel clearance is compared to the sailing line of the ship. In Appendix A - Figure 15 there is also clearly a gap visible between the false bottom and the ascending ramp. This was not a problem at the start of the flume, but it was at the end of the flume (since water flowed opposite to the sailing direction). Therefore here an extra plate was mounted between the ramp and the bottom, allowing for a smooth transition and thus limited flow disturbance.

Appendix A - Figure 15: Sloping bed

Drift angles

A few experiments have been conducted with a drift angle, either of 1° or 2°. For these experiments first the centre of gravity of the model ship was determined. It was found to be at approximately 1.86 m from the bow. Applying the drift angles resulted in the deviations from the original sailing line, see Appendix A - Figure 16. The frame with the ship was then rotated around the centre of gravity until these deviations were obtained.

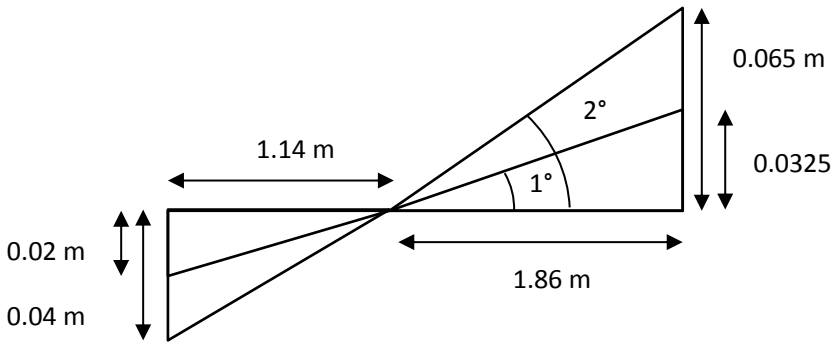

Appendix A - Figure 16: Deviations from sailing line with drift angles

Sieve curve sediment

The sediment which is used during the experiments has the following composition, see Appendix A - Table 3. This results in the sieve curve from Appendix A - Figure 17. From this sieve curve it can be found that d_{50} = 230 µm and a d_{90} of approximately 290 µm.

Sieve [µm]	Weight empty [g]	Weight after sieving [g]	Weight on sieve [g]	Weight cumulative [g]	Percentage Cumulative [%]	Throughfall Cumulative [%]
450	208.21	208.63	0.42	0.42	0.07	99.93
355	195.16	200.66	5.50	5.92	1.05	98.95
300	195.08	220.67	25.59	31.51	5.61	94.39
250	203.05	338.86	135.81	167.32	29.81	70.19
212	188.86	380.84	191.98	359.30	64.02	35.98
180	183.27	310.11	126.84	486.14	86.62	13.38
150	178.22	240.84	62.62	548.76	97.77	2.23
125	192.76	203.13	10.37	559.13	99.62	0.38
106	174.57	175.79	1.22	560.35	99.84	0.16
90	173.97	174.61	0.64	560.99	99.95	0.05
rest	266.83	267.10	0.27	561.26	100.00	0.00

Appendix A - Table 3: Sediment composition after sieving

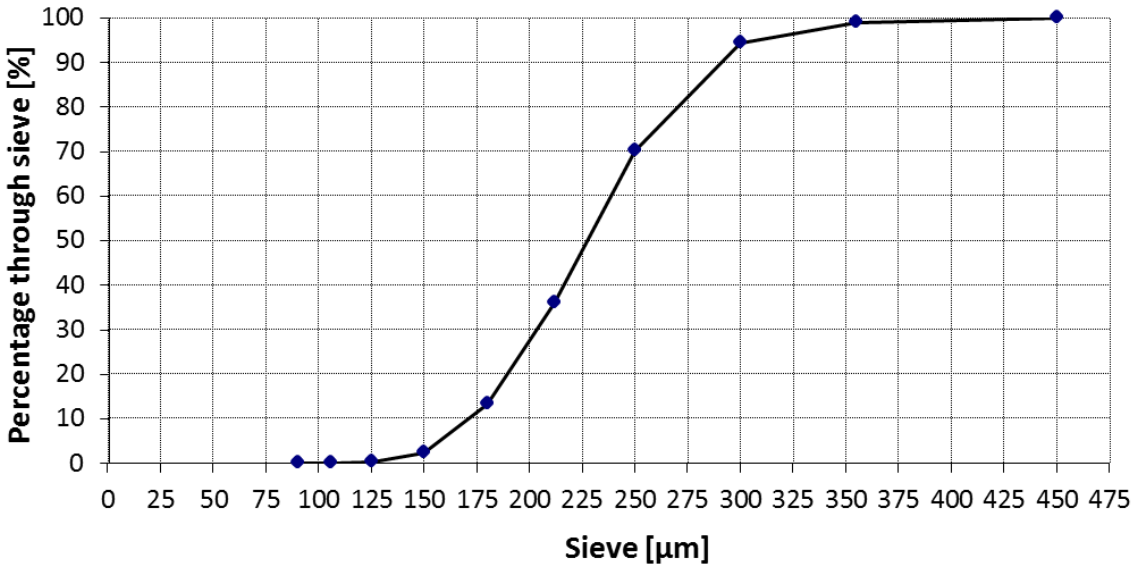

Appendix A - Figure 17: Sieve curve of sediment

Appendix B - Planned experiments

No.	Priority	Experiment part	h [m]	V_s [m/s]	U_0 [m/s]	UKC [m]	γ [-]	β [-]
0	1	Flat bed, no sediment	0.30	0.65	-0.10	vary	-	6.5
1	1	Flat bed, no sediment	0.30	0.75	-0.05	0.090	1.43	15.0
2	1	Flat bed, no sediment	0.30	0.70	-0.10	0.090	1.43	7.0
3	1	Flat bed, no sediment	0.20	0.50	-0.15	0.060	1.43	3.3
4	1	Flat bed, no sediment	0.20	0.60	-0.05	0.060	1.43	12.0
5	1	Flat bed, no sediment	0.30	0.70	-0.05	0.050	1.20	14.0
6	1	Flat bed, no sediment	0.30	0.60	-0.15	0.050	1.20	4.0
7	1	Flat bed, no sediment	0.20	0.55	-0.05	0.033	1.20	11.0
8	1	Flat bed, no sediment	0.20	0.50	-0.10	0.033	1.20	5.0
9	1	Flat bed, no sediment	0.30	0.55	-0.15	0.030	1.11	3.7
10	1	Flat bed, no sediment	0.30	0.65	-0.05	0.030	1.11	13.0
11	1	Flat bed, no sediment	0.20	0.55	-0.05	0.020	1.11	11.0
12	1	Flat bed, no sediment	0.20	0.45	-0.10	0.020	1.11	4.5
13	1	Flat bed, no sediment	0.30	0.65	-0.05	0.015	1.05	13.0
14	1	Flat bed, no sediment	0.30	0.60	-0.10	0.015	1.05	6.0
15	1	Flat bed, no sediment	0.20	0.50	-0.05	0.010	1.05	10.0
16	1	Flat bed, no sediment	0.20	0.45	-0.10	0.010	1.05	4.5
17	1	Flat bed, no sediment	0.30	0.50	-0.15	0.010	1.03	3.3
18	1	Flat bed, no sediment	0.30	0.60	-0.05	0.010	1.03	12.0
19	2	Flat bed, no sediment	0.30	0.75	0.00	0.050	1.20	-
20	2	Flat bed, no sediment	0.30	0.50	0.00	0.050	1.20	-
21	2	Flat bed, no sediment	0.30	0.70	0.00	0.030	1.11	-
22	2	Flat bed, no sediment	0.30	0.50	0.00	0.030	1.11	-
23	2	Flat bed, no sediment	0.30	0.65	0.00	0.015	1.05	-
24	2	Flat bed, no sediment	0.30	0.50	0.00	0.015	1.05	-
25	2	Flat bed, no sediment	0.20	0.60	0.00	0.033	1.20	-
26	2	Flat bed, no sediment	0.20	0.40	0.00	0.033	1.20	-
27	2	Flat bed, no sediment	0.20	0.55	0.00	0.020	1.11	-
28	2	Flat bed, no sediment	0.20	0.40	0.00	0.020	1.11	-
29	2	Flat bed, no sediment	0.20	0.55	0.00	0.010	1.05	-
30	2	Flat bed, no sediment	0.20	0.40	0.00	0.010	1.05	-
31	2	Flat bed, no sediment	0.30	0.50	-0.05	0.090	1.43	10.0
32	2	Flat bed, no sediment	0.30	0.50	-0.05	0.050	1.20	10.0
33	2	Flat bed, no sediment	0.30	0.50	-0.05	0.030	1.11	10.0
34	2	Flat bed, no sediment	0.30	0.50	-0.05	0.015	1.05	10.0
35	2	Flat bed, no sediment	0.30	0.50	-0.05	0.010	1.03	10.0
36	1	Flat bed, no sediment	0.30	0.45	-0.15	0.090	1.43	3.0
37	1	Flat bed, no sediment	0.30	0.40	-0.05	0.050	1.20	8.0
38	1	Flat bed, no sediment	0.30	0.35	-0.05	0.030	1.11	7.0
39	1	Flat bed, no sediment	0.30	0.40	-0.10	0.015	1.05	4.0
40	1	Flat bed, no sediment	0.30	0.35	-0.05	0.010	1.03	7.0
41	1	Flat bed, sediment	0.30	0.75	-0.05	0.090	1.43	15.0

No.	Priority	Experiment part	h [m]	V_S [m/s]	U_0 [m/s]	UKC [m]	γ [-]	β [-]
42	2	Flat bed, sediment	0.30	0.70	-0.10	0.090	1.43	7.0
43	1	Flat bed, sediment	0.30	0.55	-0.15	0.030	1.11	3.7
44	2	Flat bed, sediment	0.30	0.65	-0.05	0.030	1.11	13.0
45	1	Flat bed, sediment	0.30	0.65	-0.05	0.015	1.05	13.0
46	2	Flat bed, sediment	0.30	0.60	-0.10	0.015	1.05	6.0
47	2	Flat bed, sediment	0.30	0.50	-0.15	0.010	1.03	3.3
48	1	Flat bed, sediment	0.30	0.60	-0.05	0.010	1.03	12.0
49	2	Dunes, sediment	0.30	0.70	-0.10	0.090	1.43	7.0
50	1	Dunes, sediment	0.30	0.55	-0.15	0.030	1.11	3.7
51	2	Dunes, sediment	0.30	0.65	-0.05	0.015	1.05	13.0
52	1	Dunes, sediment	0.30	0.60	-0.05	0.010	1.03	12.0
53	1	Sloping bed	0.30	0.75	-0.05	0.102	1.43	15.0
54	1	Sloping bed	0.30	0.70	-0.10	0.102	1.43	7.0
55	1	Sloping bed	0.30	0.55	-0.15	0.042	1.11	3.7
56	1	Sloping bed	0.30	0.65	-0.05	0.042	1.11	13.0
57	1	Sloping bed	0.30	0.65	-0.05	0.027	1.05	13.0
58	1	Sloping bed	0.30	0.60	-0.10	0.027	1.05	6.0
59	1	Sloping bed	0.30	0.50	-0.15	0.022	1.03	3.3
60	1	Sloping bed	0.30	0.60	-0.05	0.022	1.03	12.0
61	1	Flat bed, no sediment, barge	0.30	0.75	-0.05	0.090	1.43	15.0
62	2	Flat bed, no sediment, barge	0.30	0.70	-0.10	0.090	1.43	7.0
63	1	Flat bed, no sediment, barge	0.30	0.55	-0.15	0.030	1.11	3.7
64	2	Flat bed, no sediment, barge	0.30	0.65	-0.05	0.030	1.11	13.0
65	1	Flat bed, no sediment, barge	0.30	0.65	-0.05	0.015	1.05	13.0
66	2	Flat bed, no sediment, barge	0.30	0.60	-0.10	0.015	1.05	6.0
67	2	Flat bed, no sediment, barge	0.30	0.50	-0.15	0.010	1.03	3.3
68	1	Flat bed, no sediment, barge	0.30	0.60	-0.05	0.010	1.03	12.0
69	3	Flat bed, sediment, barge	0.30	0.70	-0.10	0.090	1.43	7.0
70	2	Flat bed, sediment, barge	0.30	0.55	-0.15	0.030	1.11	3.7
71	2	Flat bed, sediment, barge	0.30	0.65	-0.05	0.015	1.05	13.0
72	3	Flat bed, sediment, barge	0.30	0.60	-0.05	0.010	1.03	12.0

Appendix C - Graphs and figures

This appendix gives extra graphs and figures for the substantiation of theory, results and equations.

Chapter 4

4.2 Qualitative flow description

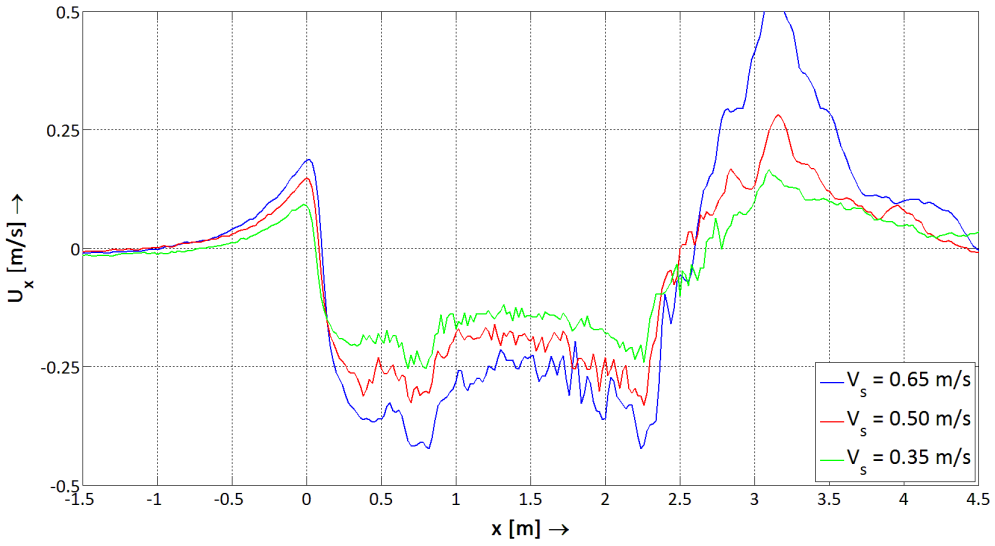

Appendix C - Figure 1: X-velocities of EMS2 for different V_S (with U_0 = -0.05 m/s, h = 0.30 m and UKC = 0.03 m)

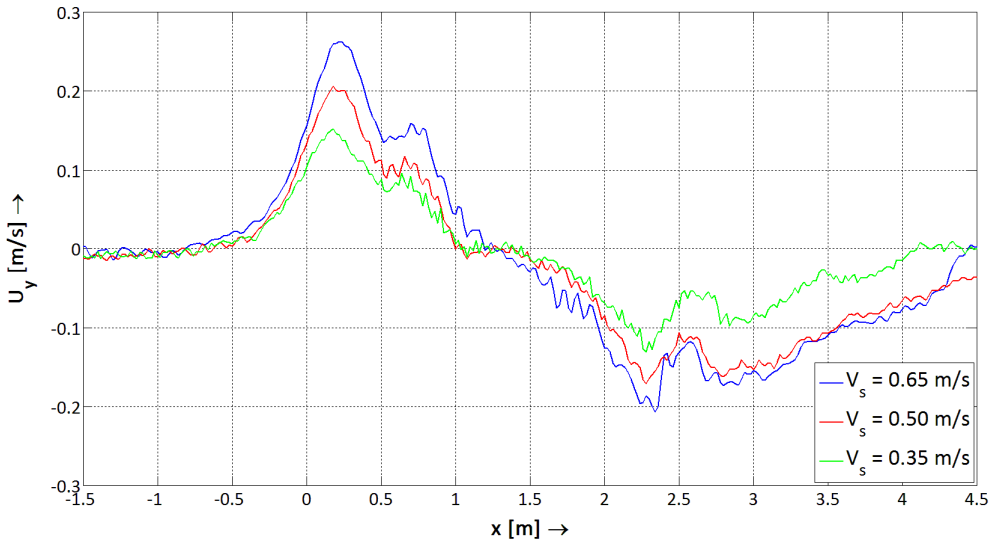

Appendix C - Figure 2: Y-velocities for EMS3 for different V_S (with U_0 = -0.05 m/s, h = 0.30 m and UKC = 0.03 m)

4.5 Velocity distribution

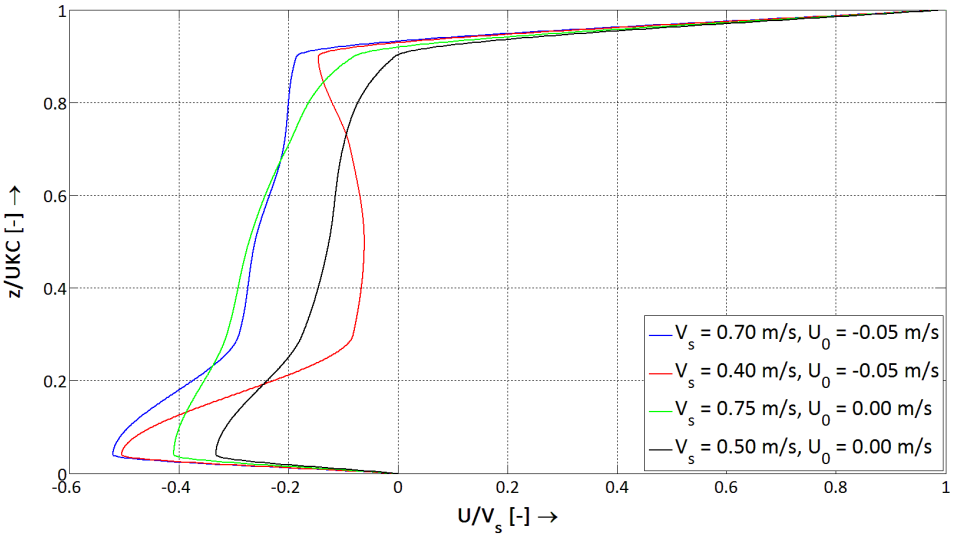

Appendix C - Figure 3: Vertical velocity distribution at EMS 1 for UKC = 0.05 m

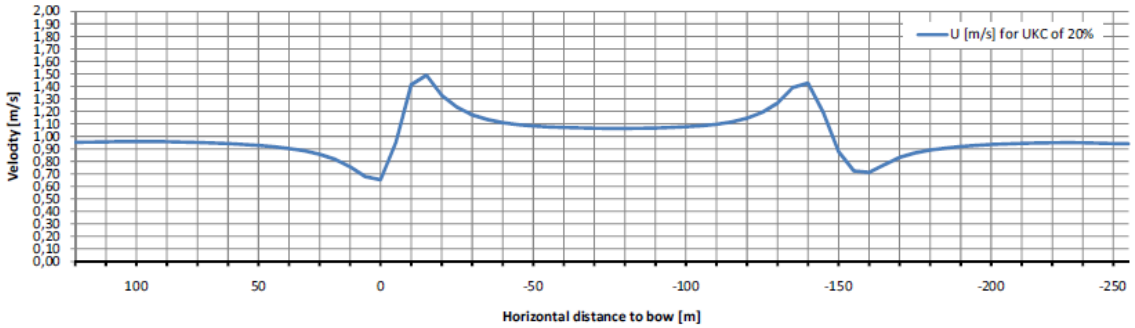

Appendix C - Figure 4: Result experiment Lenselink (2011) with DelKelv (source: Lenselink (2011))

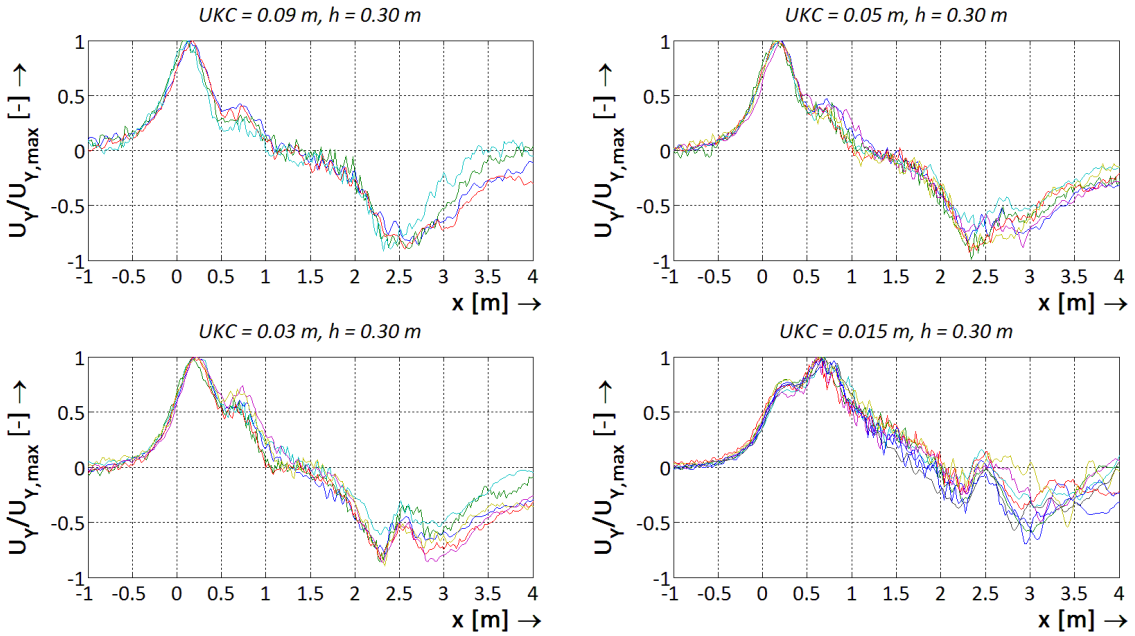

Appendix C - Figure 5: Y-velocity distribution of different experiments per situations (same UKC, h)

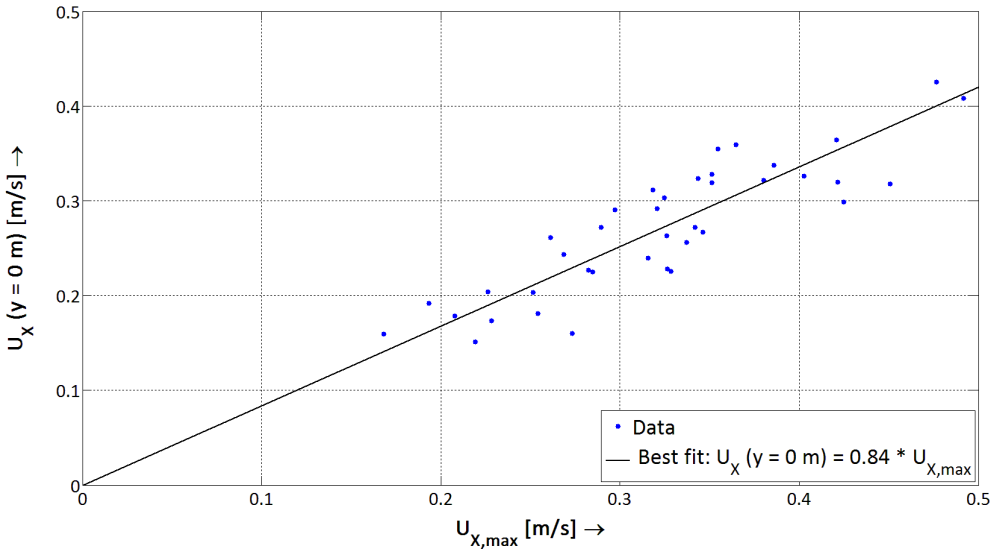

Appendix C - Figure 6: Maximum x-velocity at y = 0 m compared to $U_{X,max}$

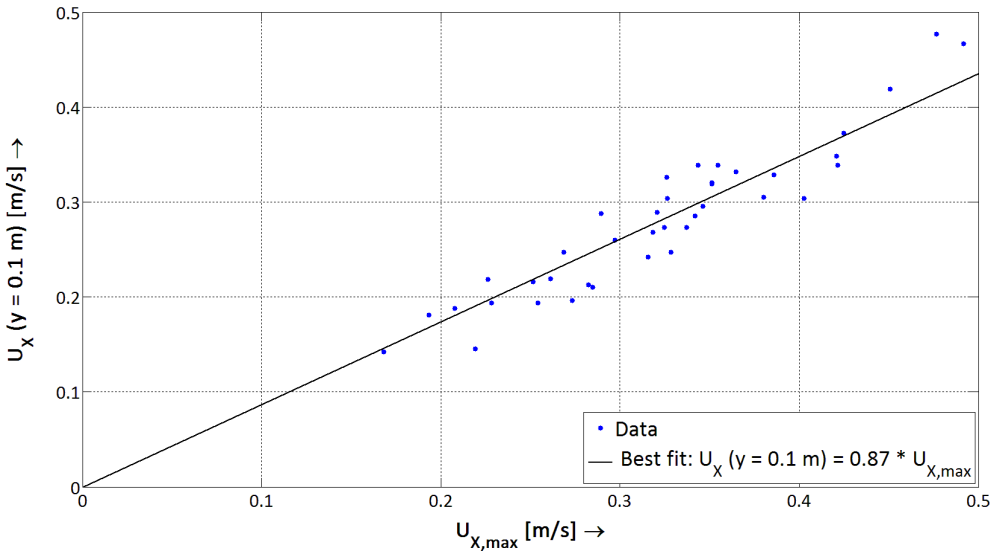

Appendix C - Figure 7: Maximum x-velocity at y = 0.1 m compared to $U_{X,max}$

4.6 Erosion/sedimentation

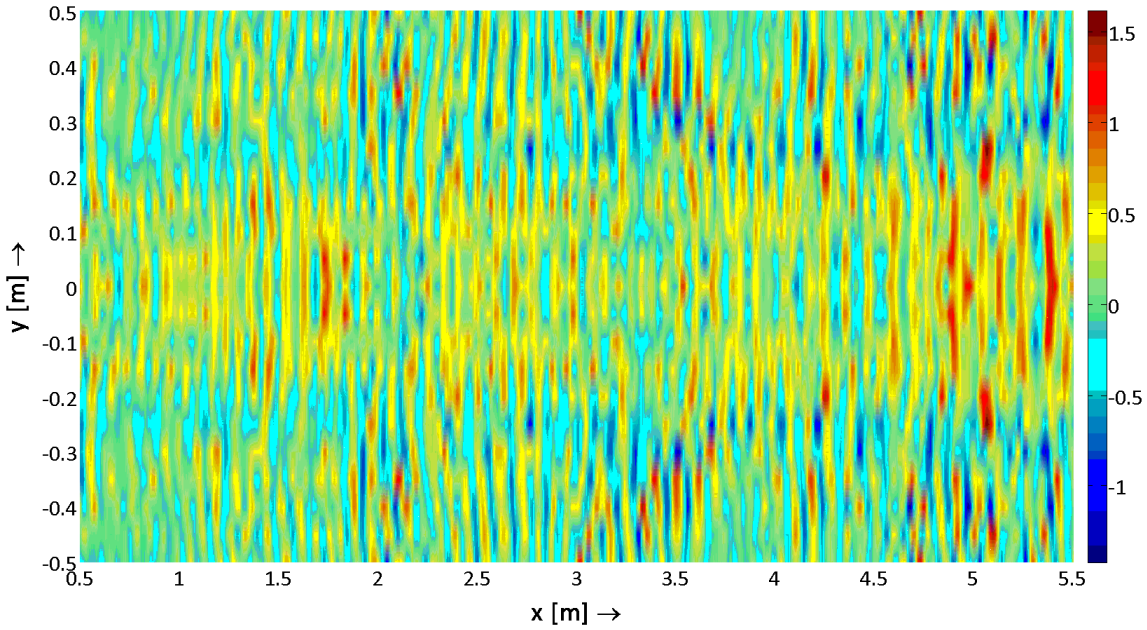

Appendix C - Figure 8: Erosion (in cm) after experiment 46 run 10

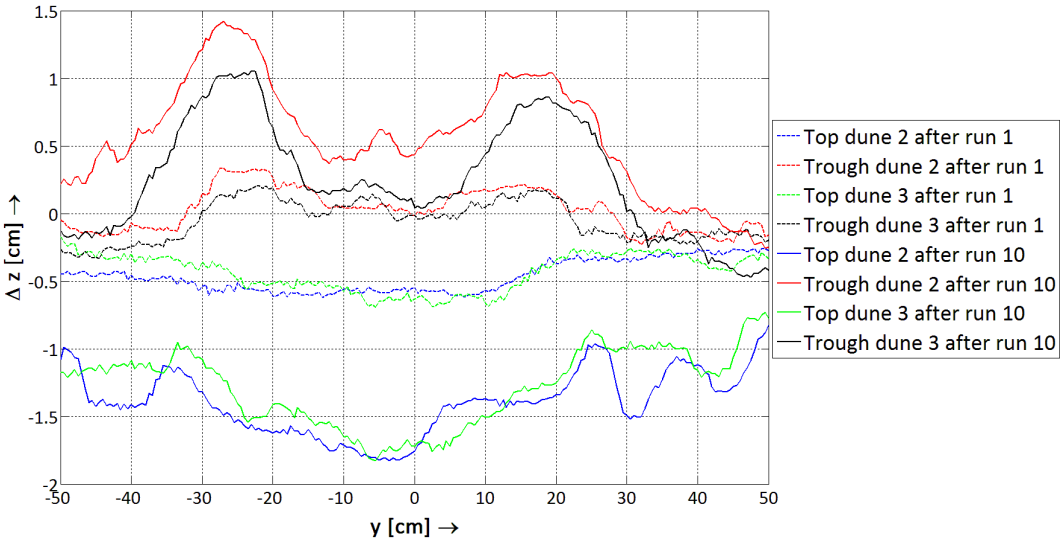

Appendix C - Figure 9: Bed level change (in cm) during experiment 51 at 4 different cross-sections

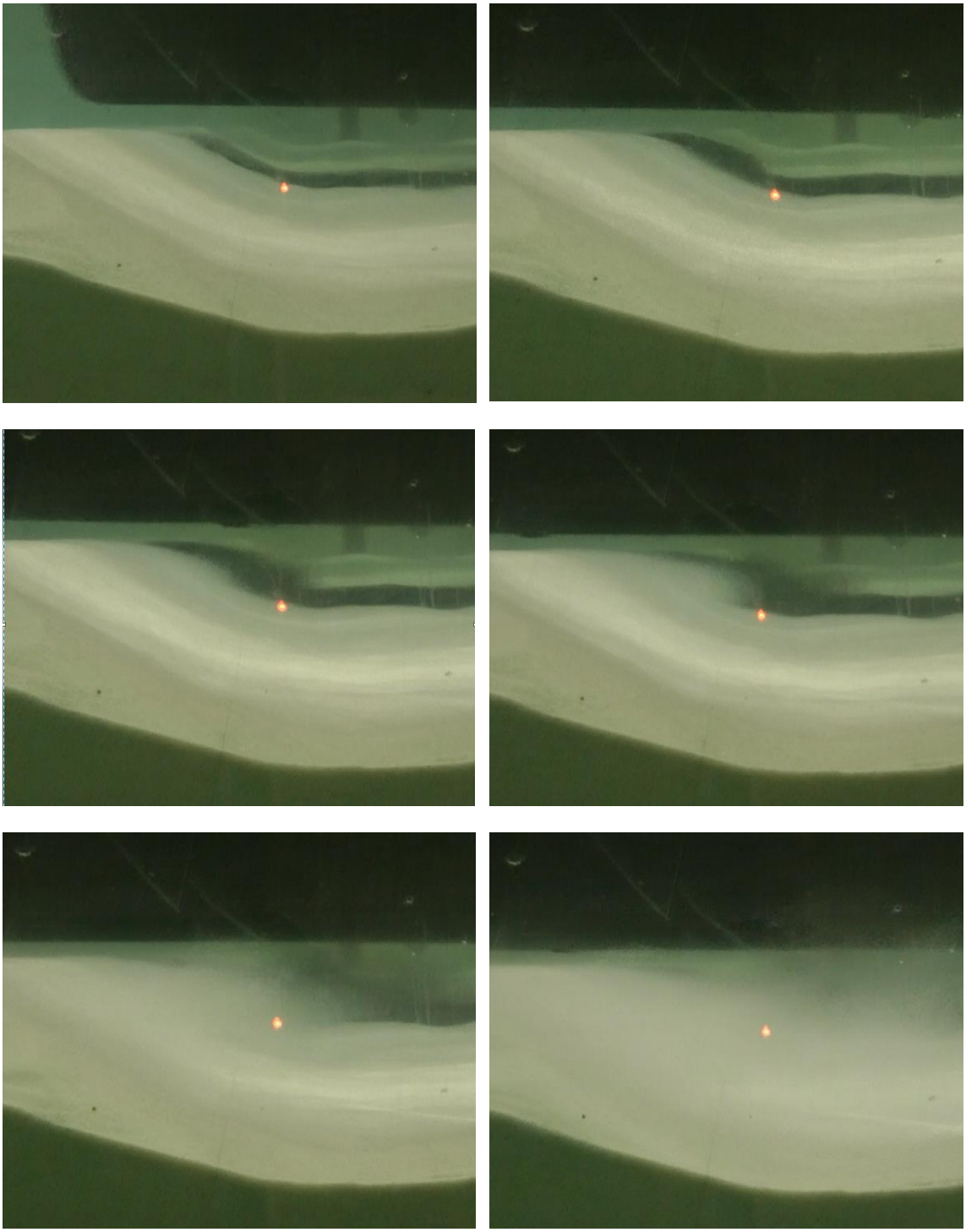

Appendix C - Figure 10: Stills from experiment 51 run 6

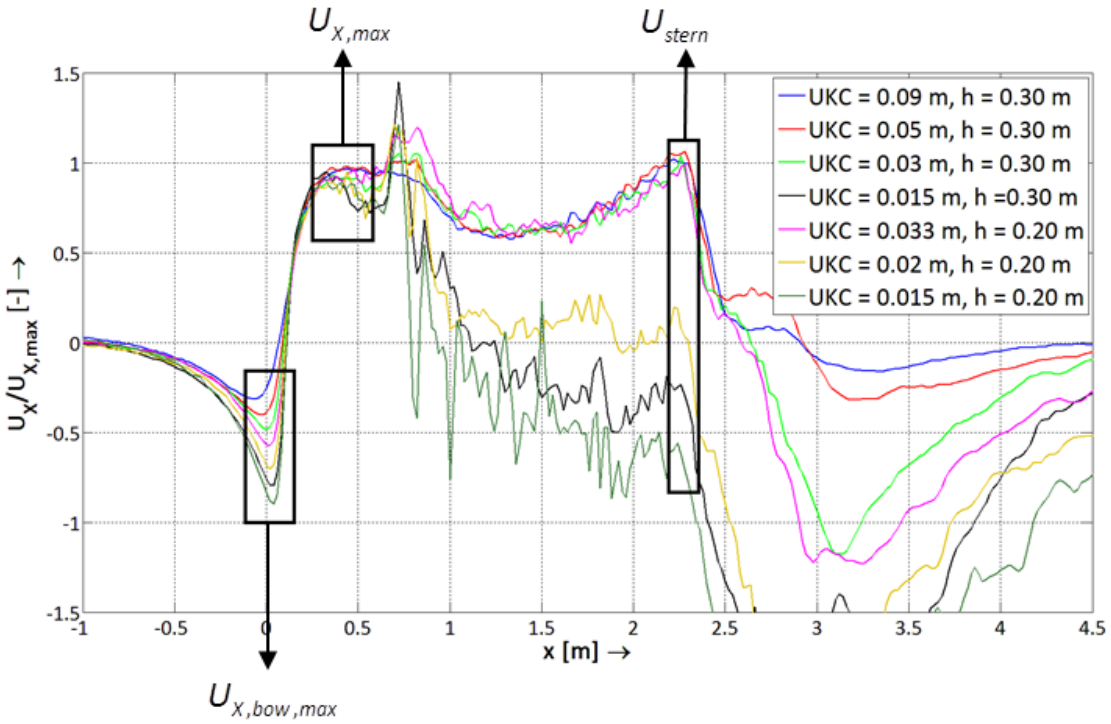

Appendix C - Figure 11: Location of different velocities

Appendix D - Adaptations current prediction methods

Since the adaptation of Maynords equation and the Functional relation in § 4.3 resulted in very different coefficients per situation (ship type, max. velocity type), it was difficult to discover the influence of the different parameters, and thus determine the best method to calculate the maximum velocities.

Therefore in this appendix another approach is applied: despite of the type of ship (conventional or barge) or maximum velocity ($U_{X,max}$ or U_{max}), some coefficients are required to be equal, while other coefficients may vary. This will increase the simplicity and results in a clearer understanding of the influence of each parameter. This is done for the equation of Maynord and the Functional relation.

Finally it must be mentioned that this appendix is just showing a new approach, with the results. More analysis is always possible but is not considered useful at this moment. Perhaps in the future, with more data and potential computer models, this analysis can be expanded.

Equation of Maynord

The equation of Maynord is given by formula [D.1]. In § 4.3 all coefficients (α, β and γ) were varied per different configuration. Now, coefficients β and γ are kept equal for different configurations, while coefficient α may still vary. Two different options are applied:

- Independent of ship type
- Independent of maximum velocity type

$$\frac{U_{max}}{V_s - U_0} = \alpha \cdot \left(\frac{B_s}{h}\right)^{\beta} \cdot \left(\frac{T}{h}\right)^{\gamma} \qquad [D.1]$$

The coefficients are determined based on a least squares method, in which the error is now a combination of the errors of the different configurations (ship type/maximum velocity type). Despite of the different amount of experiments for some configurations, no weighing on these errors is done.

Independent of ship type

When the maximum velocity as predicted by Maynord is considered independent of the type of the ship, β and γ will only vary per maximum velocity type, while α will still vary per ship type. The results are given in Appendix D - Table 1.

Velocity type	Ship type	α	β	γ	R^2	RMSE
$U_{X,max}$	Conventional	0.75	0	1.38	0.65	0.05 m/s
	Barge	1.50			0.66	0.08 m/s
U_{max}	Conventional	0.88	0.35	2.55	0.65	0.06 m/s
	Barge	2.10			0.86	0.12 m/s

Appendix D - Table 1: Coefficients and goodness of fit for equation of Maynord per velocity type, with equal coefficients β and γ

Independent of maximum velocity type

Considering the maximum velocity formulations independent on the maximum velocity type ($U_{X,max}$ and U_{max}), means the coefficients β and γ will only vary per ship type. Results are shown in

Ship type	Velocity type	α	β	γ	R^2	RMSE
Conventional	$U_{X,max}$	0.71	0.05	1.28	0.67	0.04 m/s
	U_{max}	0.84			0.71	0.06 m/s
Barge	$U_{X,max}$	0.76	1.47	2.55	0.54	0.10 m/s
	U_{max}	1.05			0.86	0.12 m/s

Appendix D - Table 2: Coefficients and goodness of fit for equation of Maynord per ship type, with equal coefficients β and γ

Functional relation

The same approach can be applied to the Functional relation, which is given by formula [D.2]. Now, coefficients β, γ and δ are kept equal for different configurations, while coefficient α may still vary. Again two different options are applied:

- Independent of ship type
- Independent of maximum velocity type

$$U_{max} = U_R \cdot \left(1 + \alpha \left(\frac{h-T}{h} \right)^{\beta} \cdot \left(\frac{V_S - U_0}{\sqrt{g \cdot (h-T)}} \right)^{\gamma} \cdot \left(\frac{A_C}{A_S} \right)^{\delta} \right) \qquad [D.2]$$

Independent of ship type

When the prediction of the maximum velocity is regarded independent of the ship type, coefficients β, γ and δ will only vary with the formulations for $U_{X,max}$ and U_{max}. The results are given in Appendix D - Table 3.

Velocity type	Ship type	α	β	γ	δ	R^2	RMSE
$U_{X,max}$	Conventional	0.27	-0.66	-1.28	-0.36	0.75	0.04 m/s
	Barge	1.09				0.67	0.08 m/s
U_{max}	Conventional	0.26	-0.88	0.20	-0.22	0.86	0.04 m/s
	Barge	0.91				0.90	0.10 m/s

Appendix D - Table 3: Coefficients and goodness of fit for Functional relation with equal coefficients β, γ and δ

Independent of maximum velocity type

Considering the maximum velocity formulations independent on the maximum velocity type ($U_{X,max}$ and U_{max}), means the coefficients β and γ will only vary per ship type. Results are shown in Appendix D - Table 4.

Ship type	Velocity type	α	β	γ	δ	R^2	RMSE
Conventional	$U_{X,max}$	0.12	-0.70	-0.31	0.15	0.70	0.04 m/s
	U_{max}	0.19				0.85	0.04 m/s
Barge	$U_{X,max}$	0.64	-1.21	-1.65	-0.65	0.48	0.10 m/s
	U_{max}	1.03				0.89	0.11 m/s

Appendix D - Table 4: Coefficients and goodness of fit for Functional relation per ship type, with equal β, γ and δ

Conclusions

Based on the R^2 and RMSE-values from the tables above, the functional relation is more accurate in predicting the maximum occurring velocities, whether it is x-velocities or absolute velocities. This is independent of the ship type. However, it must be noted that the functional relation is more complex, since it has more parameters and also uses the return current velocity U_R (as calculated by Schijf). This requires extra computation on this velocity, while this parameter is also somewhat arbitrary as depicted in § 4.4. In short, the Functional relation has a better prediction capability but with increased complexity.

When looking at the different options, it seems the formulations independent of ship type (so different maximum velocity type formulations, and only parameter α is different per ship type) are a little bit more accurate than the formulations independent of maximum velocity type. It must be admitted that the predictions for conventional vessels are slightly lower, but the predictions for barges are much better. This means the coefficients from Appendix D - Table 1 and Appendix D - Table 3 should be used for predicting maximum flow velocities.

The advantage of this approach is that the different parameters and its coefficients now are linked in different configurations, which was not the case in Table 15 and Table 16. Although this slightly decreases the accuracy (compare R^2-values), it reduces complexity enormously, and gives better insight into the dependence on different parameters. This was much more difficult with the coefficients from Table 15 and Table 16.

Appendix E - Dependence on parameters

This appendix gives a more detailed analysis of the dependence of the maximum velocity on the different parameters. The most important conclusions are given in § 4.4.

$U_{X,max}$ velocities

Sailing speed (V_S) and ambient flow velocity (U_0)

First of all, the influence of the sailing speed and the flow velocity will be studied. This will be done by grouping the experiments with equal waterdepth, keel clearance and $V_S - U_0$ value. The results can be found in Appendix E - Table 1.

UKC	h	$V_S - U_0$	V_S	U_0	$U_{x,max}$	x	y
			0.75 m/s	0.00 m/s	0.36 m/s	0.60 m	0.20 m
0.05 m	0.30 m	0.75 m/s	0.70 m/s	- 0.05 m/s	0.39 m/s	0.58 m	0.20 m
			0.60 m/s	- 0.15 m/s	0.48 m/s	0.40 m	0.10 m
			0.70 m/s	0.00 m/s	0.38 m/s	0.60 m	0.20 m
0.03 m	0.30 m	0.70 m/s	0.65 m/s	- 0.05 m/s	0.42 m/s	0.60 m	0.20 m
			0.55 m/s	- 0.15 m/s	0.49 m/s	0.60 m	0.20 m
			0.60 m/s	0.00 m/s	0.28 m/s	0.56 m	0.20 m
0.033 m	0.20 m	0.60 m/s	0.55 m/s	- 0.05 m/s	0.29 m/s	0.60 m	0.20 m
			0.50 m/s	-0.10 m/s	0.35 m/s	0.58 m	0.20 m
			0.55 m/s	0.00 m/s	0.27 m/s	0.50 m	0.20 m
0.015 m	0.20 m	0.55 m/s	0.50 m/s	-0.05 m/s	0.32 m/s	0.54 m	0.20 m
			0.45 m/s	-0.10 m/s	0.35 m/s	0.58 m	0.20 m

Appendix E - Table 1: Influence of sailing speed and ambient flow velocity on maximum x-velocity

From Appendix E - Table 1 the following can be concluded:

- The ambient flow velocity U_0 has a larger impact on $U_{x,max}$ than the sailing speed V_S
- A smaller underkeel clearance leads to a higher $U_{X,max}$ (see difference at UKC = 0.05 and UKC = 0.03), although at some point (close to the bed) the effect reverses (see UKC = 0.033 m and UKC = 0.015 m, although this could also be due to the lower $V_S - U_0$ value).

In order to quantify the effect of V_S and U_0 on $U_{X,max}$, new groups are made with equal keel clearance and water depth. Each group has been fitted on function [E.1], the results can be found in Appendix E - Table 2, while Appendix E - Figure 1 shows the result for UKC = 0.03 m and h = 0.30 m.

$$U_{X,max} = \alpha \cdot V_S - \beta \cdot U_0 \qquad [E.1]$$

UKC	h	h/UKC	# experiments	α	β	R^2	RMSE
0.09 m	*0.30 m*	3.33	4	0.3602	0.998	0.97	0.013
0.05 m	*0.30 m*	6	6	0.4462	1.257	0.95	0.026
0.03 m	*0.30 m*	10	6	0.5305	1.248	0.99	0.008
0.015 m	*0.30 m*	20	8	0.5121	1.278	0.94	0.022
0.033 m	*0.20 m*	6	4	0.4428	1.069	0.97	0.017
0.02 m	*0.20 m*	10	4	0.5180	1.026	0.99	0.008
0.015 m	*0.20 m*	13.33	3	0.4884	1.144	0.97	0.009

Appendix E - Table 2: Fitting results for linear function on V_S and U_0

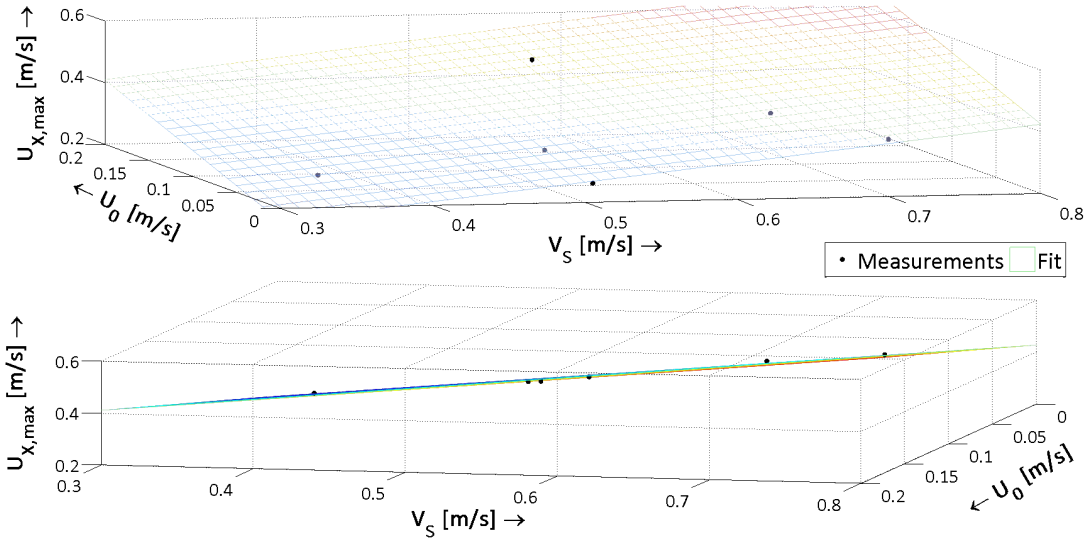

Appendix E - Figure 1: Linear fitting result for UKC = 0.03 m and h = 0.30 m

The following can be concluded:

- The ambient flow velocity is indeed more important than the sailing speed.
- For h = 0.30 m it seems that coefficient β is approximately 1.25. This does not hold for UKC = 0.09 m, but this could very well be due to the small number of experiments. Changing β to 1.25 for UKC = 0.09 m results in α = 0.3272, with an R^2 of 0.90, which is still acceptable.
- As a result, it seems that the underkeel clearance has no influence on the contribution of U_0, but it does have an influence on α, and thus on the contribution of V_S. A decrease in keel clearance leads to an increase in α, until somewhere between 0.015 and 0.03 m, then α decreases again.
- Coefficient α is approximately equal for same values of UKC/h, compare the results for h = 0.30 m with the results from h = 0.20 m. The discrepancy at 0.015 m can be explained by the lack of data points here.
- Coefficient β depends mainly on the waterdepth, and does not vary significantly with different underkeel clearances (the difference at h = 0.20 m/s could also be due to the lack of data points).

Besides a linear relation, also a power function can be investigated, see equation [E.2].

$$U_{X,max} = \alpha \cdot V_S^{\beta} - \gamma \cdot U_0^{\delta} \qquad [E.2]$$

However, this function is only relevant for configurations with more than 4 data points, otherwise a perfect fit will be found (4 relations, 4 coefficients), which is not realistic. The results for the 3 remaining configurations can be found in Appendix E - Table 3.

UKC	h	h/UKC	# experiments	α	β	γ	δ	R^2	RMSE
0.05 m	*0.30 m*	6	6	0.5408	1.503	1.120	0.8803	0.99	0.008
0.03 m	*0.30 m*	10	6	0.5463	1.088	1.072	0.9038	0.99	0.009
0.015 m	*0.30 m*	20	8	0.5208	1.221	0.658	0.6028	0.97	0.017

Appendix E - Table 3: Fitting results for power function on V_S and U_0

From Appendix E - Table 3 it can be seen that the results are improving (lower RMSE and higher R^2), however, there seems to be no clear relation between the coefficients anymore. Furthermore, unit-wise this power relation does not make sense either. Therefore, the linear approach is preferred, since it also gives good results.

Return current velocity

For the return current U_R the same approach is applied. A linear function is used, just as the WL|Delft Hydraulics equation, on different groups with equal UKC and h. When comparing the goodness of fit with the results from V_S and U_0 however, the results are less accurate, see Appendix E - Figure 2.

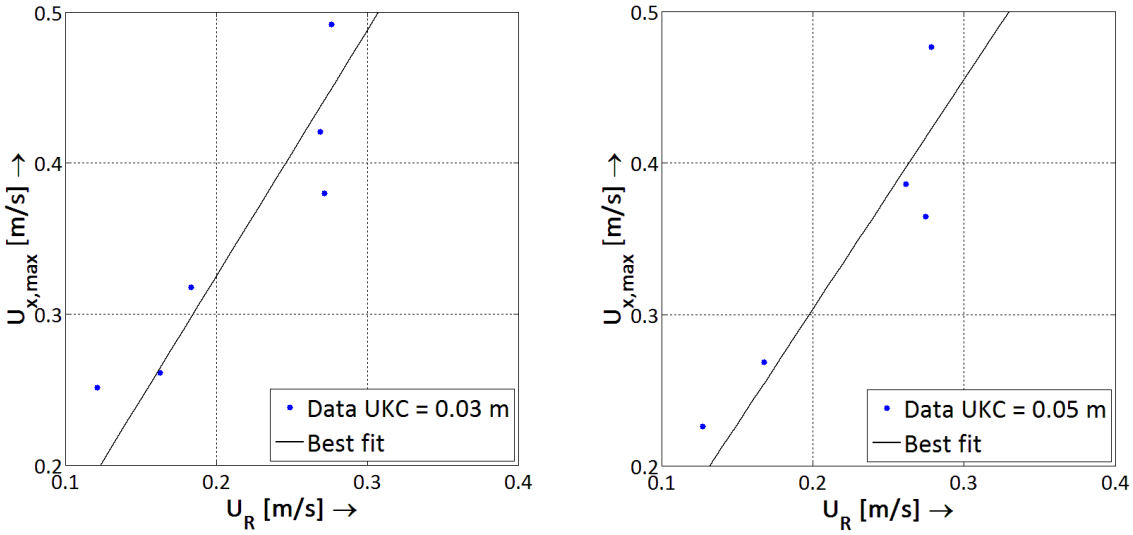

Appendix E - Figure 2: Linear data fitting on U_R (h = 0.30 m)

From this graph, it can immediately be seen that the linear function does not fit as accurate as with the dependency on V_S and U_0. There is definitely some agreement, which can be expected since the return current also depends on V_S and U_0. However, the data points are far more scattered, and also a power function will not suffice. The results of the linear fitting can be found in Appendix E - Table 4.

UKC	h	h/UKC	# experiments	α	R^2	RMSE
0.09 m	*0.30 m*	3.33	4	1.567	0.22	0.055
0.05 m	*0.30 m*	6	6	1.518	0.86	0.040
0.03 m	*0.30 m*	10	6	1.627	0.79	0.043
0.015 m	*0.30 m*	20	8	1.532	0.61	0.051
0.033 m	*0.20 m*	6	4	1.410	0.90	0.025
0.02 m	*0.20 m*	10	4	1.495	0.78	0.029
0.015 m	*0.30 m*	13.33	3	1.425	0.18	0.033

Appendix E - Table 4: Fitting results for a linear function on U_R

$U_{Y,max}$ velocities

For y-velocities the same procedure can be followed. Since U_Y will probably also depend on U_X, it might be expected that for $U_{Y,max}$ the best approach is also to use a linear formula on V_S and U_0, just as equation **[4.7]**. The coefficients and the goodness of fit can be found in Appendix E - Table 5.

UKC	h	h/UKC	# experiments	α	β	R^2	RMSE
0.09 m	*0.30 m*	3.33	4	0.1934	0.221	0.99	0.001
0.05 m	*0.30 m*	6	6	0.2734	0.449	0.99	0.003
0.03 m	*0.30 m*	10	6	0.3483	0.601	0.99	0.003
0.015 m	*0.30 m*	20	8	0.5851	0.992	0.87	0.028
0.033 m	*0.20 m*	6	4	0.3070	0.614	0.99	0.003
0.02 m	*0.20 m*	10	4	0.3918	0.709	0.99	0.006
0.015 m	*0.20 m*	13.33	3	0.6657	0.769	0.32	0.021

Appendix E - Table 5: Fitting results ($U_{Y,max}$) for a linear function on V_S and U_0

As with x-velocities, applying a power function here does not result in better goodness of fits (R^2-values of 0.58 - 0.99, and RMSE of 0.002 - 0.05), neither does using the return current U_R with a linear function (R^2-values of 0.28 - 0.91, and RMSE of 0.014 - 0.047).

From Appendix E - Table 5 again some conclusions can be drawn:

- Again the linear function on V_S and U_0 gives rather good fits. Only for very small underkeel clearances the goodness of fit decreases.
- Both coefficient α and β increase with decreasing underkeel clearance. This is expected, since smaller keel clearances should result in larger outward velocities, because at some point the boundary layers on both ship and bed will interact, resulting in a 'closed' area between ship and bed. Therefore, water flowing underneath the bow need to be directed to the sides of the keel. With smaller keel clearances this effect will occur closer to the bow, resulting in larger outward (y-) velocities.
- Both α and β depend both on the keel clearance and the water depth, in contrast to $U_{X,max}$, although the values for α at h/UKC = 6 and h/UKC = 10 are somewhat similar. Probably the influence of the water depth is marginal here.

Coefficient determination

From the linear fitting functions above, the coefficients are given in Appendix E - Table 6. The β-coefficient for $U_{X,max}$ has been adapted, since it seemed that they were independent of the underkeelclearance. As a result, also some of the α-values have slightly changed. Furthermore, the parameter γ is defined according to [E.3].

$$\gamma = \frac{h}{h - UKC} \qquad [E.3]$$

			$U_{X,max}$		$U_{Y,max}$	
UKC	**h**	**h/(h-UKC)**	α_X	β_X	α_Y	β_Y
0.09 m	*0.30 m*	1.42	0.33	1.25	0.19	0.22
0.05 m	*0.30 m*	1.20	0.45	1.25	0.27	0.45
0.03 m	*0.30 m*	1.11	0.53	1.25	0.35	0.60
0.015 m	*0.30 m*	1.05	0.51	1.25	0.59	0.99
0.033 m	*0.20 m*	1.20	0.44	1.07	0.31	0.61
0.02 m	*0.20 m*	1.11	0.51	1.07	0.39	0.71
0.015 m	*0.20 m*	1.08	0.50	1.07	0.67	0.77

Appendix E - Table 6: Coefficients of linear fitting of $U_{X,max}$ and $U_{Y,max}$

Parameter β_X does not depend on UKC (and thus probably not on T), so it should depend on the water depth h and the shape of the bow. However, unit-wise a dimensionless coefficient should make more sense. Therefore, also the ship's width B_S is used to create a dimensionless parameter h/B_S . The width is used, since it is expected that the width also influences the value of the coefficient. With a wide ship, the discharge underneath the ship has a larger flow area, resulting in smaller velocities. This should result in a small β_X. However, it may also be expected that the discharge underneath a wide ship increases, since a larger part of the water before the bow will go underneath the ship. The power coefficient will determine the most dominant process. This dimensionless parameter is also used in the formula of Maynord. Analysis results in equation [E.4].

$$\beta_x = 1.59 \cdot \left(\frac{h}{B_s} \right)^{0.38} \qquad [E.4]$$

Since the ship's width was not varied during the experiments, the validity of this equation is questionable.

Coefficient α_X seems to depend only on the earlier defined parameter γ. Also, it seems that when γ is approximately smaller than 1.10, α_X is suddenly decreasing, probably due to boundary layer interaction. When this effect is neglected, the following fit [E.5] can be found.

$$\alpha_x = 0.58 \cdot \left(\frac{h - UKC}{h} \right)^{1.48} \qquad [E.5]$$

This gives a goodness of fit of 0.89 (R^2) and a RMSE of 0.026. However, this means that values of γ around 1.10 are underestimated, while values lower than 1.10 are overestimated. Therefore, when values of $\gamma \leq 1.10$ are neglected, the new formulation for α_X becomes:

$$\alpha_X = 0.64 \cdot \left(\frac{h - UKC}{h} \right)^{1.91} \quad [E.6]$$

This equation results in an R^2 of 0.99 and a RMSE of 0.008 for α_X. Unfortunately only two data points remain for $\gamma < 1.10$, so no good relation can be found here.

For coefficient α_Y no immediate clear relation can be found. It does not completely depend on parameter γ, although it seems to increase with increasing UKC. Analysis results in equation [E.7].

$$\alpha_Y = 0.025 \cdot UKC^{-0.76} \quad [E.7]$$

This equation has a goodness of fit of 0.91 (R^2). However, unit-wise this relation does not make any sense. Since the dimensions of the ship were not changed during the experiments, it might be that a combination with B_S or L_S results in a good fit with a dimensionless parameter. Another approach is to use the parameter γ. This gives a far less good fit (R^2 = 0.77, RMSE = 0.092), but does make more sense unit-wise. The relation is given by [E.8].

$$\alpha_Y = 0.79 \cdot \left(\frac{h - UKC}{h} \right)^{5.37} \quad [E.8]$$

For coefficient β_Y approximately the same holds as for α_Y. Now however the best fit is obtained by using parameter γ. This results in the following equation, see [E.9].

$$\beta_Y = 1.17 \cdot \left(\frac{h - UKC}{h} \right)^{4.74} \quad [E.9]$$

This formula gives a R^2 of 0.91 and a (rather large) RMSE of 0.082. A fit on UKC is also possible, but this gives a slightly less good result, and also gives incorrect units. However, with incorporation of B_S or L_S a dimensionless parameter can be formed. However, the effect of these parameters remains unknown at this moment.

Finally, it must be pointed out that, due to the fixed values of B and B_S, the parameter γ could also be described as A_C/A_S or something thereof. When this is applied to the determination of the coefficients, equal goodness of fits are found, only with different factors. It might very well be that in reality parameter γ should be changed to A_C/A_S. It is also possible that rather than h-UKC the draught T should be used. The influence of the draught shall be investigated in § 5.2.

Appendix F - Longitudinal velocity distribution

This appendix gives a more detailed analysis of the longitudinal velocity distribution of the empirical flow model. The most important conclusions are given in § 5.3.

Conventional vessels

It was shown in § 5.3 that the velocity distribution was dependent on the y-coordinate of the longitudinal cross-section. Making a model, dependent on the y-coordinate would be vary laborious work and is therefore not applied here. It is decided to only simulate one distribution per velocity direction. For the x-velocity this is the distribution at y = 0.00 m, since it is almost equal to the distribution at y = 0.10 m. For the y-velocity the distribution at y = 0.20 m is chosen, since this distribution has higher maximum velocities.

X-velocities

For x-velocities a 6^{th} degree polynomial is applied between x = 0 m (bow) and x = 2.25 m (start of stern). After 2.3 m the stern of the vessel begins and the keel clearance increases (see Figure 37). Here also the turbulence increases, and in reality the influence of the propeller will start to dominate. As visible from Figure 41, the longitudinal distribution is similar for all experiments with UKC ≥ 0.03 m. Therefore, the longitudinal distribution prediction for these situations is taken equal, and given by equation [F.1].

$$\frac{U_X(x)}{U_{X,max}(x)} = -0.6x^6 + 5x^5 - 16.5x^4 + 27.5x^3 - 23.9x^2 + 9.63x - 0.46 \qquad [F.1]$$

Formula [F.1] holds for L_{PP} / (h - T) ≤ 58 and is a rather peculiar formulation, which is the great drawback of this method. Even changing the coefficients slightly will result in a totally different, and thus wrong, prediction. For now there is however no other option. The result is given in Appendix F - Figure 1.

This equation however is now only applicable with an L_{PP} of 2.3 m. Adaptation of this formulation can be done to include this parameter, and thus other ship lengths, which results in equation [F.2].

$$\frac{U_X(x)}{U_{X,max}(x)} = 30 \cdot \left(-15\left(\frac{x}{L_{pp}}\right)^6 + 40.83\left(\frac{x}{L_{pp}}\right)^5 - 44.67\left(\frac{x}{L_{pp}}\right)^4 + 25\left(\frac{x}{L_{pp}}\right)^3 - 7.35\left(\frac{x}{L_{pp}}\right)^2 + \left(\frac{x}{L_{pp}}\right) \right) - 0.5 \qquad [F.2]$$

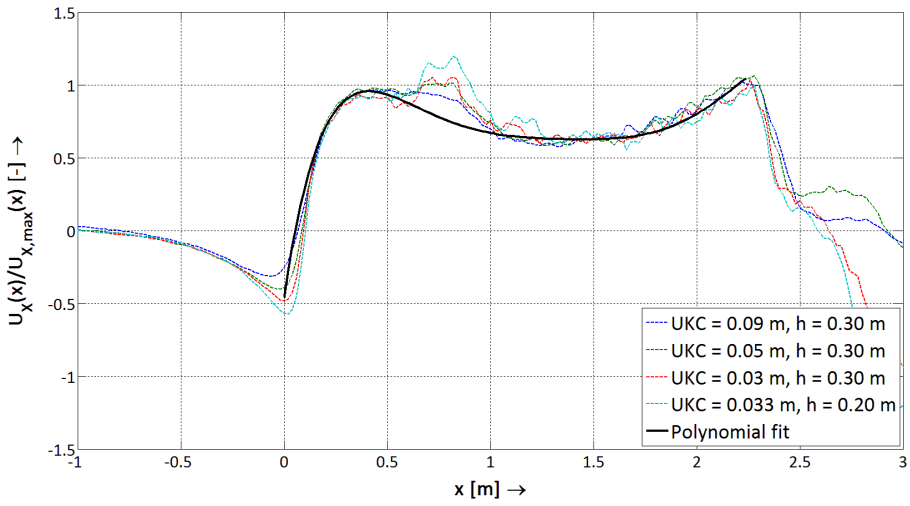

Appendix F - Figure 1: Prediction of longitudinal x-velocity distribution for L_{PP} / (h – T) ≤ 58

For the velocity profile when L_{PP} / (h - T) ≥ 58, a new polynomial can be formed. However, the profile now is different dependent on the keel clearance. Therefore it is chosen to use equation [F.2] and apply a correction factor on this equation. The correction factor is given by

$$Corr = a \cdot \left(e^{-\left(\frac{x-0.25}{b}\right)^2} - 1 \right) + 1 \qquad [F.3]$$

In which coefficient a is equal to (1 – U_{Stern}), in which U_{Stern} is the stern velocity (see next paragraph). Coefficient b depends on the underkeel clearance, and can be approximated by function [F.4].

$$b = 0.09 \cdot \sqrt{\frac{L_{PP}}{UKC} - 77} \qquad [F.4]$$

Rewriting of functions [F.3] and [F.4] in terms of draught T, dependent on the length of the vessel, results in equation [F.5]. Application of this formulation results in Appendix F - Figure 2.

$$Corr = \left(1 - U_{Stern}\right) \cdot \left(e^b - 1\right) + 1; \quad \text{with b} = -\left(\frac{2.3 \cdot \frac{x}{L_{PP}} - 0.25}{0.1 \cdot \sqrt{\frac{L_{PP}}{h-T} - 58}} \right)^2 \qquad [F.5]$$

Both equation [F.2] and [F.5] are valid for 0 ≤ x / L_{PP} ≤ 1.

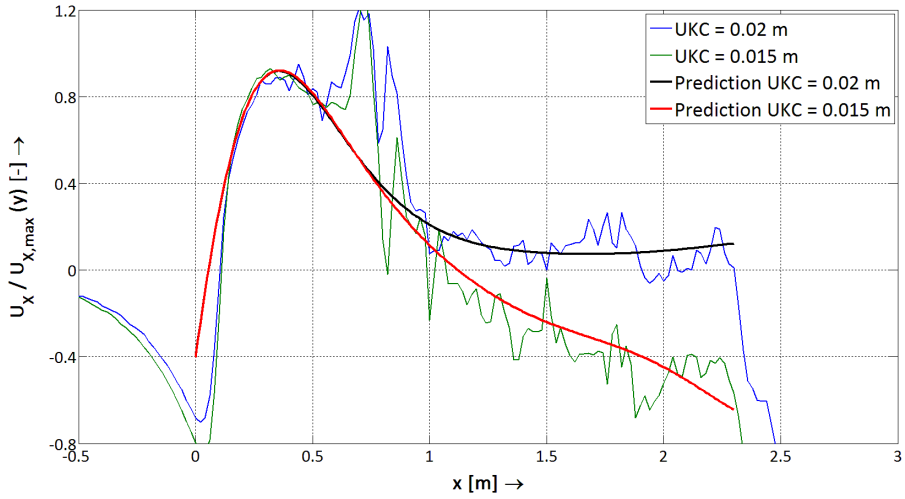

Appendix F - Figure 2: Prediction of longitudinal x-velocity for L_{PP} / (h - T) > 58

Y-velocities

For the y-velocities approximately the same story holds, only now no good fit can be obtained with a polynomial. Furthermore, the y-velocity distribution is somewhat smoother and the prediction formula is therefore applied on -1 m ≤ x ≤ 3 m (or -1/3 ≥ x / L_{PP} ≥ 1). Since no good fit can be obtained with a polynomial, a rational function is applied. There are different functions for L_{PP} / (h - T) ≤ 58 and L_{PP} / (h - T) > 58, which are given by equation [F.6]. The distribution ratios and there predictions are given in Appendix F - Figure 3 and Appendix F - Figure 4.

$$\frac{U_Y(x)}{U_{Y,max}(x)} = \frac{-0.5\left(\frac{x}{L_{PP}}\right)^3 - 0.15\left(\frac{x}{L_{PP}}\right)^2 + 0.07\left(\frac{x}{L_{PP}}\right) + 0.05}{10\left(\frac{x}{L_{PP}}\right)^4 - 16.5\left(\frac{x}{L_{PP}}\right)^3 + 8.3\left(\frac{x}{L_{PP}}\right)^2 - 8\left(\frac{x}{L_{PP}}\right) + 0.075} \quad \text{for } \frac{L_{PP}}{h-T} \le 58$$

[F.6]

$$\frac{U_Y(x)}{U_{Y,max}(x)} = \frac{-3.2\left(\frac{x}{L_{PP}}\right)^5 + 1.5\left(\frac{x}{L_{PP}}\right)^4 + 0.53\left(\frac{x}{L_{PP}}\right)^3 - 0.08\left(\frac{x}{L_{PP}}\right)^2 - 0.02\left(\frac{x}{L_{PP}}\right) + 0.037}{10\left(\frac{x}{L_{PP}}\right)^4 - 5.6\left(\frac{x}{L_{PP}}\right)^3 + 1.36\left(\frac{x}{L_{PP}}\right)^2 - 0.163\left(\frac{x}{L_{PP}}\right) + 0.0093} \quad \text{for} \quad \frac{L_{PP}}{h-T} > 58$$

[F.7]

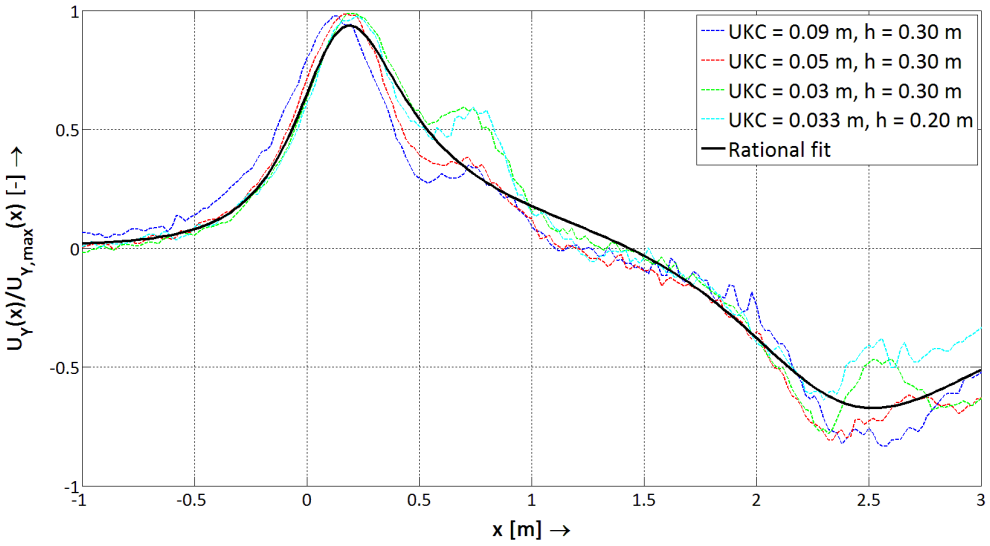

Appendix F - Figure 3: Prediction of longitudinal y-velocity for L_{PP} / (h - T) ≤ 58

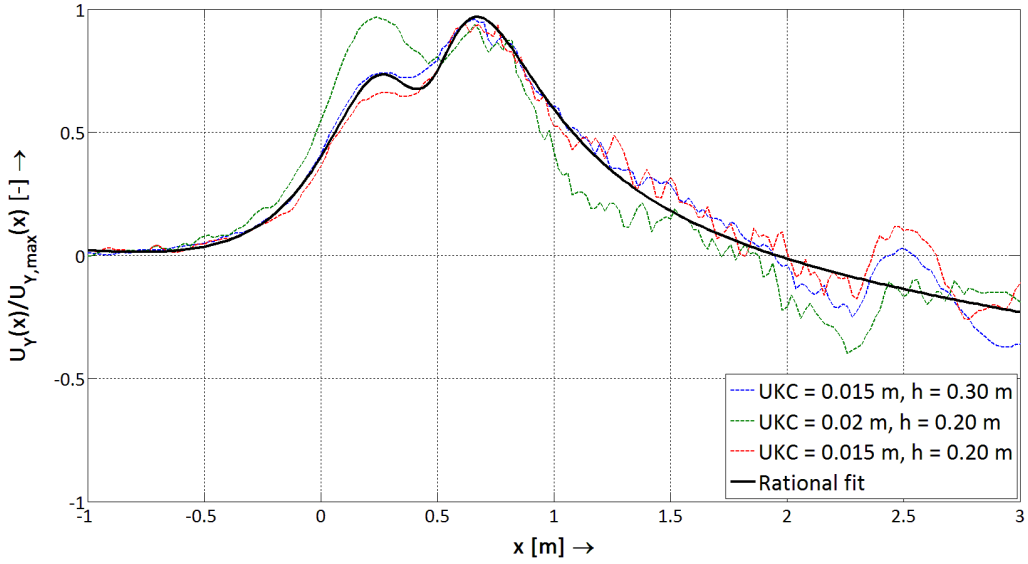

Appendix F - Figure 4: Prediction of longitudinal y-velocity for L_{PP} / (h - T) > 58)

Conclusions

The found longitudinal prediction formulations for both directions have some major drawbacks:

- The coefficients and functions are not based on parameters. They are simply a result of fixing the longitudinal distribution to the distance from the bow. It might very well be that a different keel shape will result in different coefficients.
- The coefficients are very sensitive. Changing them only slightly will result in a totally different distribution (hence also the small coefficients, they can't be ignored). This means the approach is not robust.

- For smaller keel clearances, the longitudinal velocity profile is deviating significantly. It is difficult to model this correctly. For instance for the y-velocity distribution, at some point the fanning out becomes dominant over the displacement due to the bow (see Appendix F - Figure 4). Therefore the found distribution will vary with the keel clearance, which is not correctly modelled now.
- For x-velocity distributions, it is currently not possible to predict the distribution in front of the bow, or near the stern. Especially when the correction factor (for smaller keel clearances) is applied, the distribution deviates significantly from the real distribution.

In general it can be said that it is very difficult to find an empirical formulation for the distribution in longitudinal direction. Only complex, but very undesirable and unstable functions can be found, with no direct relation to physics and no clear background. Therefore, it is better to use models for the calculation of the longitudinal distribution. For smaller keel clearances (UKC < 0.03 m) perhaps a model based on boundary layers can be fruitful. When the exact position of boundary layer interaction (and thus flow blockage), the rest of the profile can be determined from this point (point of flow reversal, or U_X / $U_{X,max}$). This is not researched here further.

Barges

Due to the lack of barge experiments, it is not tried to empirically derive expressions for the longitudinal velocity profile. Only the main differences compared to conventional vessels are given.

X-velocities

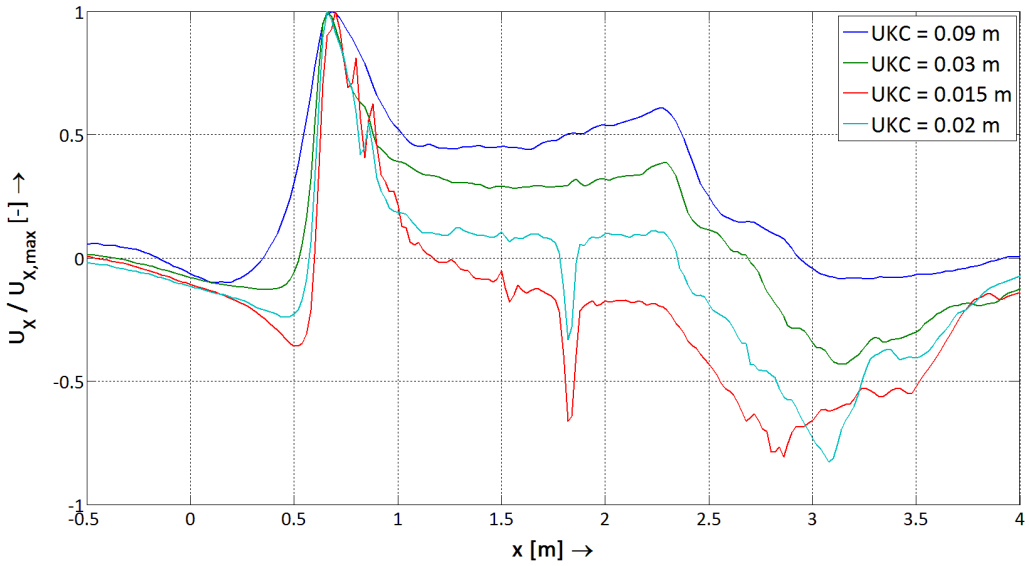

Appendix F - Figure 5: Longitudinal distribution of x-velocities underneath a barge (EMS2, y = 0.0 m)

Compared to the x-velocity distribution of conventional vessels (see Figure 41), three important differences can be distinguished (note: the peak near x = 1.8 m is interference with the ship's EMS):

- The maximum bow velocity does occur farther away, since the bow is much longer in the design of the model barge. The end of the bow is now near x = 0.6 m, resulting in a maximum bow velocity near x = 0.5 m.
- The maximum stern velocity is not approximately equal to the maximum velocity near the bow, as was the case for the conventional vessel with UKC ≥ 0.03 m. This could be explained due to the fact that the maximum occurring x-velocities for barges are much higher than for conventional vessels. This means a larger peak near the bow and thus (since velocities are compared to this peak) a smaller ratio near the stern.
- Already at UKC = 0.03 m the ratio from the bow to the stern is different from UKC = 0.09 m. Since this effect did not occur for the conventional vessels, it is probably not due to the boundary layers (otherwise it would also have occurred there). Probably also the higher velocities with barges is the cause, which increase significantly with smaller underkeel

clearances. For example, with UKC = 0.09 m the maximum occurring x-velocity is approximately 0.5 m/s in the experiments, while it is approximately 0.9 m/s for UKC = 0.03 m.

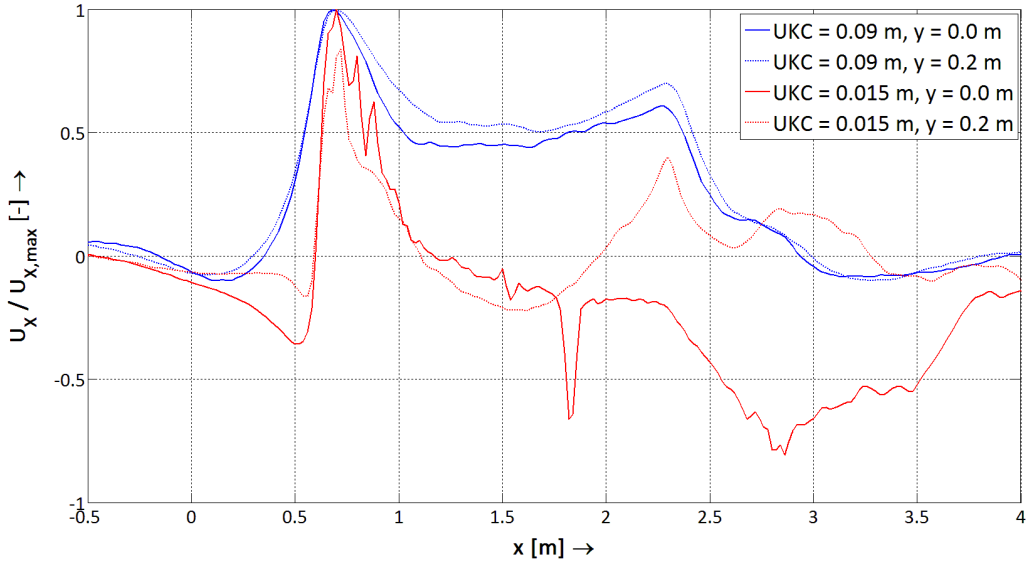

Appendix F - Figure 6: Differences in longitudinal distribution of x-velocity at different transversal positions

Appendix F - Figure 6 shows the differences between x-velocities at y = 0 m and y = 0.2 m. For larger keelclearances there are only small differences, but for smaller keel clearances the difference is more prominent. Although the general trend in from the bow to the middle of the vessel is similar (apart from a smaller bow velocity), after that the difference is significant. For y = 0.2 m the velocity increases again (even changes direction) after x = 1.5 m, while this is not the case for the x-velocity in the sailing line. This means the water must be fanning in (so from the side to underneath the barge) again here, leading to a positive ratio. This effect does not reach the centreline of the vessel.

Y-velocities

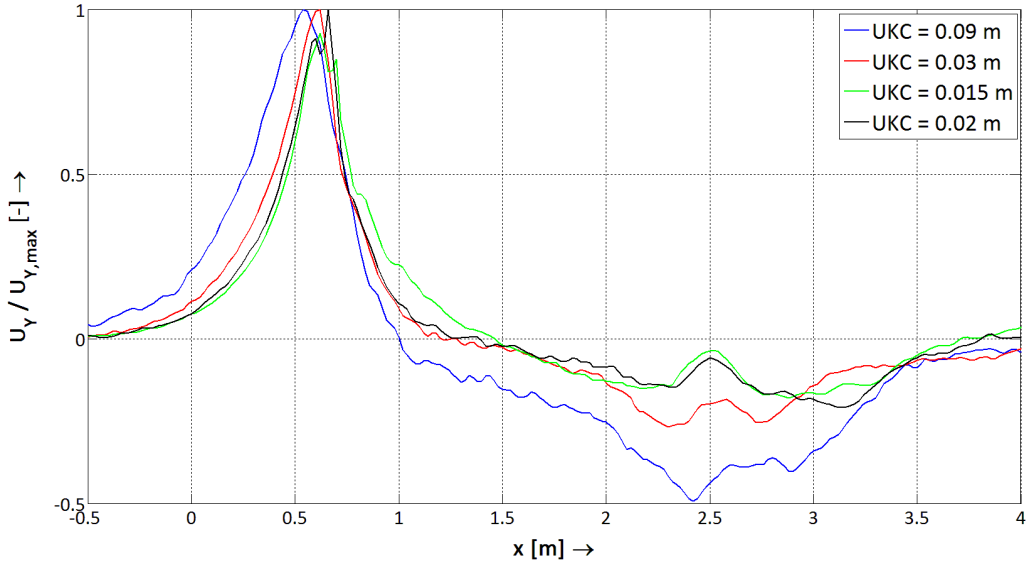

Appendix F - Figure 7: Longitudinal distribution of y-velocities underneath a barge (EMS3, y = 0.2 m)

Appendix F - Figure 7 gives the longitudinal distribution of y-velocities. Again there are some differences with the distribution for conventional vessels (compare to Figure 42). Now there is only one large peak for all experiments, near x = 0.6 m. This is at the end of the bow, which means the y-velocities mainly occur here, and not underneath the ship. After his peak the flow direction reverses, which means that the flow in now fanning in, rather than fanning out. All experiments show the same trend, there is no difference (only in magnitude) for large or small underkeel clearances.